

NORTHWESTERN UNIVERSITY

Toxicity Mediated by Seed-Dependent Off-Target Effects in RNA Interference

A DISSERTATION

SUBMITTED TO THE GRADUATE SCHOOL  
IN PARTIAL FULLFILLMENT OF THE REQUIREMENTS

for the degree

DOCTOR OF PHILOSOPHY

Field of Driskill Graduate Training Program in Life Sciences

By  
William Putzbach

Evanston, IL

June 2018

© Copyright by William Putzbach 2018

All Rights Reserved

**Abstract:**

Post-transcriptional gene silencing (PTGS) and, more specifically, RNA interference (RNAi) include the processes by which a small double-stranded RNA, 19 to 22 nucleotides (nts) long, negatively regulates the expression and/or translatability of a target RNA, which harbors reverse complementarity to that small RNA, by recruiting the so-called RNA-Induced Silencing Complex (RISC). Scientists can “knock down” or deplete a specific RNA by introducing small interfering RNA (siRNA) duplexes that are fully complementary to a region within the intended target. However, targeting can occur with complementarity of as little as six bps between an siRNA’s so-called seed sequence and a mRNA’s 3’ Untranslated Region (UTR). This seed-based targeting produces off-target effects (OTEs) in RNAi experiments, which result from unintended target RNAs, which harbor complementarity to the siRNA’s seed sequence, being downregulated. Whereas scientists can accurately predict the cellular effects of a *specific* and potent siRNA, provided the function of its intended target is understood, the phenotypic changes associated with seed-based OTEs (sOTEs) cannot be as easily predicted because these changes depend on the net outcome of a promiscuous six nt seed sequence that simultaneously, and to varying degrees of efficiency, targets up to hundreds of genes harboring, by chance, a compatible target site.

Non-overlapping siRNAs that specifically and potently target the same gene would be predicted to evoke the same phenotypic change, provided the intended target performs an overt function. However, non-overlapping siRNAs with different seed sequences, even those designed to target a common gene, would also be predicted to evoke different sOTEs because of differences in off-target profiles. However, this presented work shows this is not always the case.

Indeed, over 80% of commercially available siRNAs and short hairpin (sh)RNAs derived from CD95/CD95L mRNA sequences are toxic to cancer cells in the absence of the intended target site in these two genes, demonstrating this toxicity is independent of knocking down CD95 or CD95L and likely results from repression of other genes through seed-based targeting. This was confirmed by assessing the toxicity and functionality of chemically-modified and chimeric siRNAs. An shRNA lethality screen composed of every shRNA that can be derived from these two genes and an unrelated control gene, Venus, showed toxic sequences are enriched in certain regions including the Open Reading Frame (ORF) and the 3' UTR of CD95L and CD95, respectively.

These nonredundant CD95/CD95L-derived si/shRNAs all induce a novel form of cancer cell death, with distinct biochemical and morphological features best described as simultaneous activation of multiple death pathways. Interestingly, these toxic si/shRNAs, which do not share sequence homology in their seed regions, all *preferentially* downregulate mRNAs from the same cohort of survival genes, which initiates a unique sOTE coined Death Induced by Survival Gene Elimination (DISE). Toxicity positively correlates with the GC content of an siRNA's seed sequence, and Dicer and Drosha knock-out cells display hypersensitivity. Together, these results reveal a subset of non-overlapping seed sequences embedded in the mRNAs of CD95 and CD95L that share certain characteristics and are highly toxic to cancer cells through the same sOTE mechanism of DISE.

The abundance of toxic shRNA sequences derived from the CD95L ORF, as identified in the screen, suggested the full-length mRNA may exhibit functionality independent of its role in translating for CD95L protein. Indeed, expression of wild type (WT) CD95L and CD95L mutants

that do not produce full-length apoptosis-inducing proteins are toxic to cells, even those harboring homozygous deletion of the CD95 gene. Global downregulation of survival genes occurs during overexpression—similar to DISE. Small RNA fragments derived from CD95L ORF mRNA associated with the RISC in cells overexpressing CD95L cDNA were also detected. These results show that expression of certain mRNAs, in this case CD95L, may produce small guide RNAs that evoke a specific cellular response through RNAi. The Peter lab is currently investigating how mRNAs (e.g. CD95/CD95L) may evoke DISE as a conserved cell-autonomous tumor surveillance system.

**Acknowledgements:**

My deepest gratitude to my advisor and friend Marcus Peter. Exploring this complex and wonderful world requires an experienced guide, who is a skilled practitioner and teacher of the scientific process. All my current and future successes are directly the result of his patient tutelage.

My sincerest thanks to my lab mates Quan Gao, Monal Patel, Andrea Murmann, Calvin Law, Qadir Syed, Brian Bridgeman, and Ashley Haluck-Kangas for their friendship and considerable assistance in this project. Without them, I would not be preparing this thesis right now.

All my love and respect to my wife Danielle. As difficult as it was for me to devote nearly a fifth of my life to this pursuit, I realize this is a life I share with her. We put our lives on hold for me to achieve this degree no matter how stressful and dark things got, and I will be forever thankful and devoted to her. Without her, I have nothing. Finally, words cannot express what the support of my family means to me. Someday, I will have children of my own and know what it means to raise them right to be thoughtful and loving, regardless of the state of things, only to let them free to explore the world on their own. Only then, will I understand the sacrifice they made for me. I shudder to think what my future would hold without the Mom and Dad God blessed me with.

**List of Abbreviations:**

AEBSF, 4-(2-Amino-Ethyl) Benzene-Sulfonyl Fluoride hydrochloride;

AICD, Activation-Induced Cell Death;

APAF1, Apoptotic Protease Activating Factor 1;

bp, base pair;

CRISPR, Clustered Regularly Interspaced Short Palindromic Repeats;

DGCR8, DiGeorge Syndrome Critical Region Gene 8;

DISC, Death Inducing Signaling Complex;

DISE, Death Induced by Survival gene Elimination;

Dox, Doxycycline;

ds, double stranded;

DsiRNA, Dicer substrate siRNA;

DTT, 1,4-Di-Thio-Threitol;

ERK, Extracellular signal-Regulated Kinase;

FADD, Fas-Associated protein with Death Domain;

FBL, Feedback loop;

FFL, Feedforward loop;

FitC, Fluorescein Iso-Thio-Cyanate;

GO, Gene Ontology;

GRN, Gene Regulatory Network;

GW182, Glycine-Tryptophan Protein Of 182 KDa;

HuR, Hu-Antigen R;

JNK, c-Jun N-terminal Kinases;

KEGG, Kyoto Encyclopedia of Genes and Genomes;

KCTC, Korean Collection for Type Cultures;

MAPK, Mitogen-Activated Protein Kinase;

MCL-1, Myeloid Cell Leukemia sequence-1;

MID, Middle domain;

miRNA, microRNA;

MOI, Multiplicity Of Infection;

MOMP, Mitochondrial Outer Membrane Permeabilization;

NF- $\kappa$ B, Nuclear Factor kappa-light-chain-enhancer of activated B cells;

nt, nucleotide;

ORF, Open Reading Frame;

OTE, Off-Target Effect;

PABP, Poly(A)-Binding Proteins;

PARN, Poly-A-specific Ribo-Nuclease;

PAZ, Piwi/Argonaute/Zwille;

PI, Propidium Iodide;

PIWI, P-element Induced Wimpy testis;

PMSF, Phenyl-Methyl-Sulfonyl Fluoride;

PTGS, Post-Transcriptional Gene Silencing;

RBP, RNA-Binding Proteins;

RISC, RNA Induced Silencing Complex;



RNAi, RNA Interference;

rRNA, ribosomal RNA;

RTK, Receptor Tyrosine Kinase;

RT-qPCR, Reverse Transcription quantitative PCR;

SDS, Sodium Dodecyl Sulfate;

shRNA, short hairpin RNA;

siRNA, short interfering RNA;

snoRNA, small nucleolar RNA;

snoRNP, snoRNA Ribo-Nucleoprotein;

sOTE, seed-based Off-Target Effect;

ss, single stranded;

t-Bid, truncated Bid;

TF, Transcription Factor;

TI, Toxicity Index;

TLDA, Taqman Low Density Array;

TNFL, Tumor Necrosis Factor Ligand;

TNFR, Tumor Necrosis Factor Receptor;

TRBP, HIV-1 TAR RNA Binding Protein;

TRC, The RNAi Consortium;

tRNA, transfer RNA;

UTR, Untranslated Region;

WT, Wild Type;

**Dedication:**

I dedicate this work to my loved ones and all aspiring scientists, who hold seeking objective truth as their highest contribution to humanity.

## Table of Contents

<b>Copyright</b> .....	2
<b>Abstract</b> .....	3-5
<b>Acknowledgements</b> .....	6
<b>Abbreviations</b> .....	7-9
<b>Dedication</b> .....	10
<b>Table of Contents</b> .....	11-15
<b>List of Figures and Tables</b> .....	16-19
<b>Chapter 1: Introduction</b>	
Components of RNAi .....	20-26
Basis of Seed-Dependent Targeting .....	26-30
Off-Target Effects in RNAi .....	30-38
Non-Canonical Sources of Guide RNAs .....	38-43
CD95 and CD95L .....	43-46
Central Hypothesis and Rationale .....	47
Summary and Significance .....	48-49
<b>Chapter 2: Materials and Methods</b>	
Reagents and Antibodies .....	49-50
Acquired Cell Lines .....	50-51
Generation of Lentiviral and Retroviral Plasmid Constructs .....	51-53

Generation of Stable Over-Expressing Cells .....	53-55
Generation of Deletion and Knock Out Clones with CRISPR .....	55-59
Assessing Toxicity of Over-Expressing CD95L cDNAs .....	59-60
Knock Down of CD95 and CD95L with shRNAs .....	60-62
Dox-Induced shRNA Knock Down .....	62
Transfection with Short Oligonucleotides .....	62-64
Treatment with Recombinant CD95L Protein .....	65
Reverse Transcription Quantitative PCR .....	65-68
Western Blot Analysis .....	68
CD95 Surface Staining .....	69
Cell Death Quantification with PI Staining .....	69
Assessing Cell Growth and Fluorescence Over Time .....	69-70
RNA-Seq Analysis to Find Deregulated Genes Upon Toxic shRNA or CD95L Expression.	70-74
Conversion of shL3 and shR6 to siRNAs .....	75
Purification of Flag-GST-T6B Peptide .....	76-77
Pull-Down of Human AGO2 in HCT116 and Drosha <sup>-/-</sup> Cells .....	77
Pull-Down of Loaded RISC and RNA-Seq of Unbound and Bound Small RNAs .....	78-80
Construction and Functional Validation of pTIP-shRNA Libraries .....	80-82
Lethality Screen with pTIP-shRNA Libraries .....	82-85
Arrayed siRNA Screen .....	85-86
Assigning a Toxicity Score to Every miRNA .....	87
Identification of Survival and Nonsurvival Gene Sets .....	87

	13
The Toxicity Index (TI) and GC Content Analysis .....	87-88
Sylamer Analysis .....	88-89
Statistical Analyses .....	89-90
Treatment of Outliers and Research Integrity .....	91
Data Availability .....	91

**Chapter 3: Many si/shRNAs can Kill Cancer Cells by Targeting Multiple Survival Genes through an Off-Target Mechanism**

Introduction .....	92-93
Results .....	93-133
<i>si/shRNAs Kill Cells in the Absence of the Targeted Site</i> .....	93-104
<i>Involvement of Canonical RNAi</i> .....	104-109
<i>Toxic si/shRNAs Cause Downregulation of Survival Genes</i> .....	109-117
<i>Toxic si/shRNAs Target Survival Genes in their 3'UTR</i> .....	117-122
<i>Identification of Toxic shRNAs in the CD95L and CD95 mRNAs</i> .....	123-129
<i>Predicting shRNA Toxicity - the Toxicity Index (TI) and GC Content</i> .....	129-133
Discussion .....	133-139
<i>DISE Represents a Specific Form of RNAi sOTE</i> .....	133-135
<i>What are the Requirements for an si/shRNA to Induce DISE?</i> .....	135-136
<i>DISE is Caused by Loading of the Guide Strand of Toxic si/shRNAs into the RISC</i> ....	136-137
<i>DISE has Features of the RNAi OTE Previously Reported</i> .....	137
<i>The Role of Dicer in DISE</i> .....	137
<i>Open questions regarding the relevance of DISE</i> .....	138-139

<i>A Model for why DISE Preferentially Kills Cancer Cells</i> .....	139
Tables for Chapter 3.....	140-169

#### **Chapter 4: CD95L mRNA is Toxic to Cells**

Introduction .....	169-170
Results.....	170-185
<i>Expression of CD95L cDNA is Toxic in the Absence of Apoptosis</i> .....	170-175
<i>Over-Expression of CD95L cDNA may Kill Cells through RNAi</i> .....	175-179
<i>CD95L ORF is Degraded into Small RNA Fragments that are then Loaded into the RISC.</i>	179-181
<i>The Degradation of CD95L mRNA is Independent of Dicer and May be Determined by its Secondary Structure</i> .....	181-183
<i>Puromycin Does Not Kill Cells Because of Differences in Viral Titer</i> .....	183-184
<i>Stabilization of CD95L Expression Enhances Toxicity</i> .....	184
<i>Apoptosis-Independent Toxicity of CD95L Over-Expression Depends on AGO2</i> .....	185
Discussion .....	185-188

#### **Chapter 5: Discussion**

DISE was Discovered through a Unique sOTE.....	188-193
Basis of Preferential Survival Gene Targeting/Downregulation: Gene Regulatory Network..	194-201
Basis of Preferential Survival Gene Targeting/Downregulation: Seed Base Composition.	201-202

DISE as a Driver of miRNA Evolution .....	202-204
Relationship between DISE and miRNAs in Cancer .....	204-206
DISE-Inducing Guide RNAs Derived from CD95L mRNAs.....	206-209
Evolution of Guide RNAs Derived from mRNAs.....	209-212
Donor Genes as Sources of DISE-Inducing Guide RNAs.....	212-214
<b>References</b> .....	215-258
<b>Vita</b> .....	259-261

### List of Figures and Tables:

Figure 1.1 – Timeline of RNAi discoveries.....	20
Figure 1.2 – Exogenous and endogenous RNAi pathways in humans .....	23
Figure 1.3 – Types of targeting in RNAi .....	26
Figure 1.4 – Sources of guide RNAs in humans.....	38
Figure 1.5 – Signaling downstream of CD95 stimulation .....	44
Figure 3.1 – The majority of siRNAs and shRNAs targeting CD95L or CD95 are toxic.....	94
Figure 3.2 – Toxicity of si/shRNAs is dose dependent .....	96
Figure 3.3 – Exogenous CD95L or CD95 proteins do not protect cells from toxicity of CD95L/CD95-derived shRNAs .....	98
Figure 3.4 – Membrane-bound CD95L does not protect against toxicity of CD95L-derived shRNA .....	99
Figure 3.5 – CD95 and CD95L derived si/shRNAs kill cells in the absence of the targeted sites in CD95 or CD95L .....	101-102
Figure 3.6 – Sanger sequencing confirms successful deletion of si/shRNA target sites .....	102
Figure 3.7 – Knock Out of CD95 in HeyA8 cells .....	104
Figure 3.8 – Toxicity of CD95L-derived siRNAs involves canonical RNAi activity.....	105-106
Figure 3.9 – Knock down mediated by siL3 can be inhibited with addition of competing siRNA .....	107
Figure 3.10 – Toxic shRNAs derived from CD95 and CD95L cause downregulation of critical survival genes .....	110-111



Figure 3.11 – Down-regulation of critical survival genes after treatment with CD95 and CD95L-derived shRNAs and siRNAs .....	112-113
Figure 3.12 – Characterization of the six genes downregulated in shL3 and shR6 treated cells and found to be critical survival genes in lethality screens .....	114
Figure 3.13 – Histones are downregulated in all forms of DISE but are not the most highly expressed genes in cells .....	116
Figure 3.14 – DISE inducing si/shRNAs target critical survival genes through RNAi .....	118
Figure 3.15 – Sylamer analysis using ORF sequences .....	119
Figure 3.16 – Quantification of the mature shRNA forms .....	120
Figure 3.17 – Identification of seed matches targeted by shL1 and siL3 .....	121
Figure 3.18 – Activity to knockdown CD95 does not determine shRNA toxicity .....	122
Figure 3.19 – Identifying all toxic shRNAs derived from CD95L and CD95 .....	124
Figure 3.20 – Toxicity and RNAi of individual shRNA pools .....	126
Figure 3.21 – Toxicity of individual pTIP-shRNA in 293T and HCT116 cells .....	127
Figure 3.22 – Fold change in shRNA representation after infection of NB7 cells and after treatment with Dox .....	128
Figure 3.23 – <i>In silico</i> prediction of DISE activity tracks with experimentally determined toxicity of shRNAs .....	130
Figure 3.24 – DISE does not just target all highly expressed genes .....	132
Table 3.1.1 – Alignment-based analysis: all genes with a padj <0.05, >1.5 downregulated, and base mean expression >2000 .....	140-141

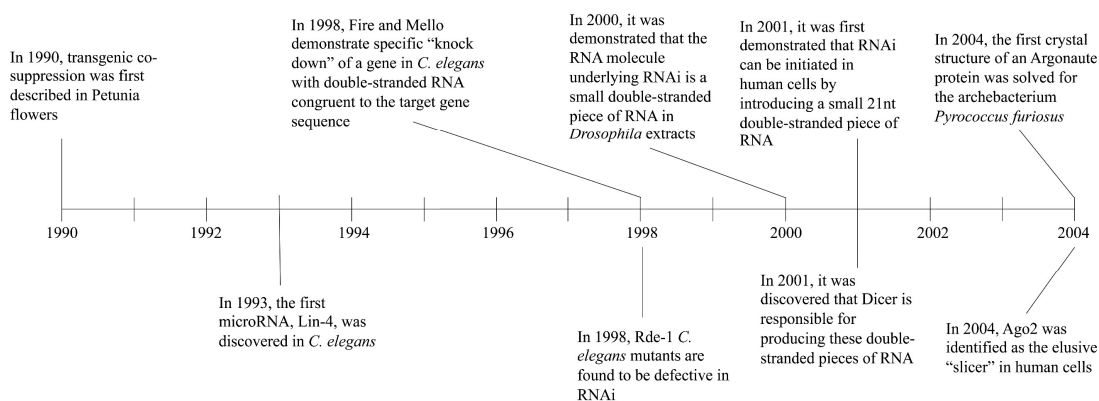
Table 3.1.2 – Alignment-based analysis: all genes with a padj <0.05, >1.5 upregulated, and base mean expression >2000 .....	142
Table 3.1.3 – Read-based analysis: all genes with a variation <2 per duplicate and >1.5 downregulated.....	143-144
Table 3.1.4 – Read-based analysis: all genes with a variation <2 per duplicate and >1.5 upregulated .....	145
Table 3.2 – Survival and non-survival gene sets used.....	146-154
Table 3.3 – Toxicity of shRNAs in the CD95 and CD95L screens .....	155-163
Table 3.4 – 8mer toxicity index of all shRNAs in screen .....	164-169
Figure 4.1 – Over-expression of CD95L is toxic independently of apoptosis .....	171
Figure 4.2 – Expression of CD95LMUT and CD95LMUTNP does not induce cell death with morphology of apoptosis .....	172
Figure 4.3 – CD95L is toxic to MCF-7 cells lacking the entire CD95 gene .....	174
Figure 4.4 – Toxic small RNAs are generated in cells expressing CD95L mRNA and loaded into the RISC .....	176
Figure 4.5 – Pull-down efficiency of human AGO2 in HCT116 versus Drosha <sup>-/-</sup> cells.....	177
Figure 4.6 – The entire CD95L mRNA gives rise to small RNAs that bind to the RISC .....	180
Figure 4.7 – Maximal CD95L mRNA toxicity requires full-length wild type sequence and is independent of Dicer .....	182
Figure 4.8 – CD95L mRNA toxicity is not the result of puromycin on cells with different levels of lentiviral infection .....	183

Figure 4.9 – Co-expression of CD95 cDNA stabilizes expression of transgenic CD95L and enhances toxicity .....	184
Figure 4.10 – Knock Down of AGO2 expression attenuates toxicity evoked by CD95L over-expression in CD95 deficient cells .....	185
Figure 5.1 – DISE is distinct from conventional seed-based off-target effect .....	189
Figure 5.2 – Lack of seed match conservation in DISE targets .....	190
Figure 5.3 – RNAi seed-based repression of genes embedded in feedforward and feedback loops composed of TFs and miRNAs.....	195
Figure 5.4 – Nucleotide and evolutionary characteristics of toxic seed sequences .....	203
Figure 5.5 – Triggering DISE <i>in vivo</i> .....	213

## Chapter 1: Introduction

### Components of RNAi

RNAi is a form of PTGS that represses expression of target RNAs that harbor reverse complementary to a RISC-associated small (19 to 22 nts) guide RNA. Hybridization between the guide RNA strand and the target recruits the RISC, which directly cleaves the target RNA or recruits additional factors that lead to its deadenylation/degradation or translational repression if the target is a mRNA. Although RNAi traditionally only refers to RISC-mediated target RNA cleavage, the term “RNAi” will be used when referring to all forms of PTGS mediated by the RISC, as this work does not focus on the effector phase of RNAi.



**Figure 1.1 – Timeline of RNAi discoveries.** Timeline showing the major discoveries in the RNAi field, which elucidated the small RNA guide responsible for targeting specificity and the enzymes involved in the RNAi pathway.

RNAi was first described in *Petunia* flowers in 1990 by the Jorgensen group (see **Figure 1.1** for timeline of RNAi discoveries)<sup>1</sup>. The investigators attempted to enhance the coloration of the flowers by over-expressing the enzyme chalcone synthase. In contrast to their expectations, transgenic expression reduced flower coloration, with some flowers losing color altogether, and reduced expression of the enzyme’s mRNA. This kind of transgenic RNAi was later shown to also

occur in fungi and animals<sup>2,3</sup>, and in 1998, Fire and Mello discovered introducing double stranded (ds)RNA was sufficient to repress expression of homologous mRNA in *C. elegans*<sup>4</sup>. Later biochemical studies in *Drosophila* extracts by Hannon's group suggested a ribonucleolytic "slicer" associates with small dsRNA intermediates to direct RNAi against homologous targets<sup>5</sup>. Bartel's group used a similar system to show dsRNAs are processed into smaller 21 to 23 bp dsRNA segments that somehow induce cleavage of a target mRNA directly in the center of the homologous region<sup>6</sup>; the investigators also showed dissociation of the small dsRNA intermediate produced single stranded (ss)RNA that could still evoke target cleavage<sup>6</sup>, consistent with hybridization between a single stranded guide RNA and a target RNA as the basis of specificity in RNAi. In 2001, Bernstein *et al.* found the endoribonuclease III enzyme Dicer was responsible for processing dsRNA into smaller dsRNA intermediates<sup>7</sup>, and in 2004, guided by previous studies of plants and animals with loss-of-function mutations that are defective in RNAi<sup>8-11</sup>, Joshua-Tor's group solved the first Argonaute crystal structure in the archebacterium *Pyrococcus furiosus*, whose active domain resembled that of RNase H and also contained a groove capable of housing a small single stranded guide RNA hybridized to its target RNA<sup>12</sup>. The placement of the active domain predicted cleavage should happen in the center of the duplexed region of the target RNA<sup>12</sup>, consistent with Bartel group's observations in *Drosophila* extracts<sup>6</sup>. In the same year, the human Argonaute paralog AGO2 was shown to possess guide RNA-directed slicer activity<sup>13</sup>. Thus, Argonautes were found to be the principle enzymatic components of the RISC.

Instead of using long dsRNAs like in the seminal RNAi studies, scientists, today, use short siRNAs fully homologous to the RNA of their gene-of-interest to achieve targeted knock down. The first siRNAs were implemented by Tuschl's group in 2001 in *Drosophila* extracts<sup>14</sup> and human

cells<sup>15</sup> and mimic the small dsRNAs produced after Dicer processing that get directly loaded into Argonaute to prime the RISC for targeted RNAi. Many groups also make liberal use of short hairpin (sh)RNAs, which produce a mature siRNA upon Dicer cleavage and are readily amenable to artificial viral-mediated delivery since the shRNA is transcribed as a single RNA strand<sup>16-20</sup> (reviewed in <sup>21</sup>).

Although RNAi can be directed using exogenous dsRNA reagents, it has been long-known multicellular organisms use small endogenous dsRNAs to repress expression of genes that harbor complementary target sites. The first microRNA (miRNA), *lin-4*, was discovered in 1993 and shown to regulate the larvae-to-adult transition in *C. elegans* by repressing expression of *lin-14* through base-pairing between the miRNA and target<sup>22</sup>. Today, over 250 annotated miRNA loci in *C. elegans* and approximately 1,900 in humans are catalogued in the public database miRbase version 22 (<http://www.mirbase.org/>)<sup>23,24</sup>, although stricter structural criteria proposed by Fromm *et al.* suggests only about 16% of annotated metazoan miRNA loci produce functioning miRNAs<sup>25</sup>. These miRNAs control everything from proliferation<sup>26-30</sup> and apoptosis<sup>31-34</sup> to differentiation<sup>35-38</sup> and development<sup>21,39-41</sup> by directing RNAi-based gene regulation. It is estimated over 60% of all human genes are conserved targets of at least one miRNA<sup>42</sup>.

Although miRNAs and artificial si/shRNAs come from endogenous and exogenous sources, respectively, both interact with common processing and effector components of RNAi (**Figure 1.2**). For a miRNA, the RNAi pathway begins in the nucleus with transcription of a miRNA precursor called the primary miRNA typically from a polymerase II promoter<sup>43</sup>. Human primary miRNA transcripts may be hundreds of nts in length and mono- or polycistronic<sup>44-46</sup>. These transcripts contain the core miRNA secondary structure—a short hairpin with a stem region

of about 33 to 35 base pairs (bps) that contains variable bulges/mismatches and flanking 5' and 3' single RNA strands at the basal ss-dsRNA junction opposite to the apical loop<sup>44,47-49</sup>. The 5' half of the stem that precedes the loop is referred to as the 5p arm, and the following half, after the loop, is the 3p arm. Artificial shRNAs can be delivered via engineered lentivirus and are usually transcribed from polymerase III promoters<sup>16-20</sup> and do not contain bulges or mismatches in the stem nor any extended ssRNA at the 5' or 3' termini<sup>16-20</sup>.

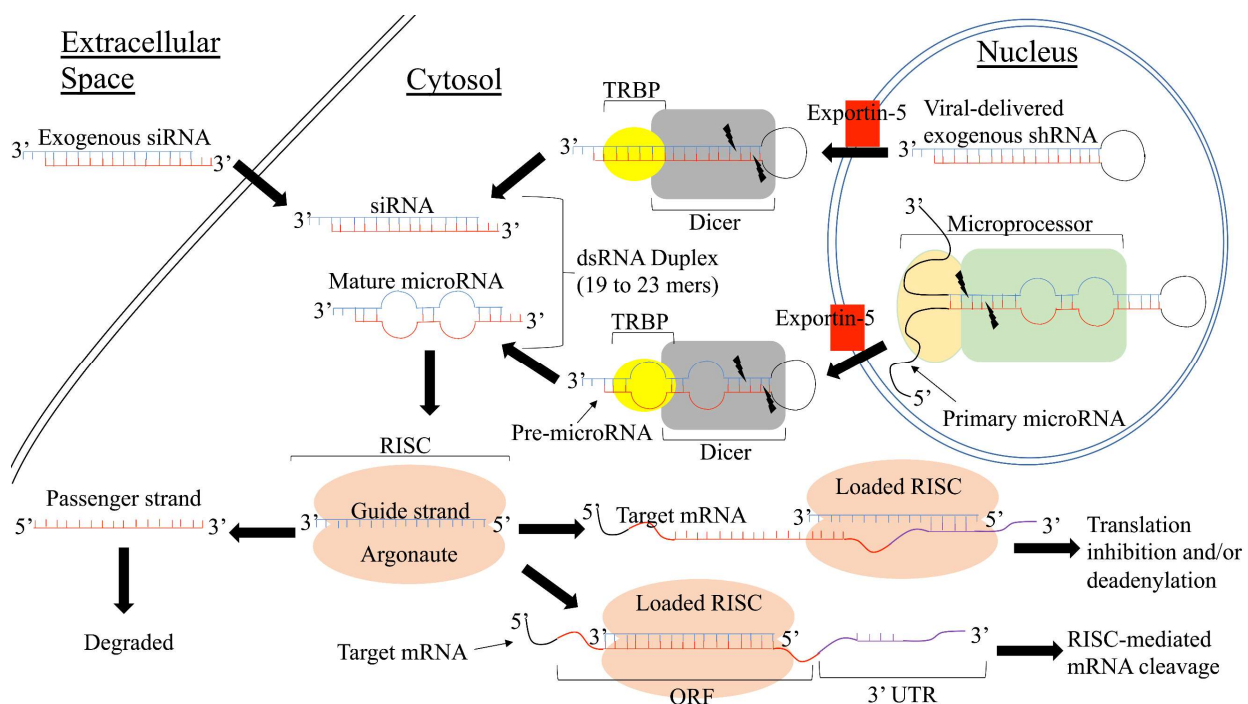


**Figure 1.2 – Exogenous and endogenous RNAi pathways in humans.** Schematic depicting how artificial exogenous shRNAs and endogenous miRNAs, after processing by the Microprocessor and/or Dicer, and exogenous siRNAs give rise to mature dsRNA duplexes that can evoke cleavage-dependent and independent RNAi of a target mRNA.

Primary miRNAs are first processed by the Microprocessor complex<sup>50</sup>, which is comprised of the endoribonuclease III enzyme Drosha<sup>46</sup> and the dsRNA-binding protein DiGeorge Syndrome Critical Region Gene 8 (DGCR8)<sup>49</sup>. Drosha contains two tandem RNase III domains that each coordinate  $Mg^{2+}$  to catalyze phosphodiester hydrolysis of each RNA strand in the stem region of the miRNA<sup>48,51</sup>. DGCR8 contains two dsRNA-binding domains that, in conjunction with Drosha,

recognize the primary miRNA structure and position/orient Drosha correctly<sup>52-56</sup>, so cleavage occurs about 11 bps from the basal ss-dsRNA junction<sup>49</sup>. Besides secondary structure, many primary miRNAs are also recognized by several primary sequence features such as a basal UG motif, a UGU motif in the loop region, and a CNNC motif downstream of the hairpin structure<sup>57</sup>. Microprocessor cleavage eliminates the primary miRNA's basal ss-dsRNA junction along with the flanking ssRNA regions, leaving behind only the core miRNA hairpin—comprised of a shorter stem region (composed of the 5p and 3p arms), the loop region, and a 3' dinucleotide overhang at the terminus—called the pre-miRNA<sup>48</sup>.

Both newly-transcribed shRNAs and processed pre-miRNAs are exported from the nucleus to the cytoplasm by Exportin-5<sup>58,59</sup>, although knock out of this protein shows additional mechanisms of export must also exist<sup>60</sup>. Once in the cytoplasm, another endoribonuclease III enzyme, Dicer, in conjunction with the dsRNA-binding HIV-1 TAR RNA binding protein (TRBP), processes them further, along with other dsRNA duplexes<sup>7,61-68</sup>. The Piwi/Argonaute/Zwille (PAZ) domain of Dicer binds and recognizes the 3' dinucleotide overhang of potential substrates<sup>69</sup>. The distance between the PAZ domain and its tandem RNase III domains corresponds to the length of its dsRNA products<sup>62,70</sup>. Dicer positions its RNase III domains a fixed distance from its substrate's terminal 5' phosphate/3' dinucleotide overhang because the relative position of the PAZ domain and the RNase III domains is predetermined; this produces a mature dsRNA duplex product of ~ 22 bps with 3' dinucleotide overhangs at each end<sup>62,70,71</sup>. In the case of shRNAs and pre-miRNAs, the site of Dicer cleavage is also influenced by the presence of bulges/mismatches in the stem and the position of the apical loop<sup>72</sup>.



Mature dsRNA duplexes are then loaded into Argonaute proteins to form the RISC<sup>73-76</sup>, with the assistance of Hsc70/Hsp90 proteins in human cells<sup>77</sup>. Once loaded, the passenger strand is ejected/degraded, while the guide strand remains associated with the RISC<sup>78,79</sup>. Argonautes contain a PAZ and Middle domain (MID) that interact with the dinucleotide overhang at the 3' terminus through phosphate-ribose backbone interactions<sup>80</sup> and the terminal 5' monophosphate and nucleobase moiety<sup>81</sup>, respectively. Argonaute forms a bilobal structure, and the guide strand lies in a basic channel between the two lobes, allowing it to form bp interactions with target RNAs<sup>76,82</sup>.

Much of our understanding of Argonaute slicing activity has come from crystal structures of *Thermus thermophilus* Argonaute. Extensive base pairing causes the PAZ domain to release the 3' terminus of the guide strand, permitting the guide strand/target RNA duplex to assume its natural A-form structure<sup>71,83</sup>. This causes a conformational shift in Argonaute's P-element Induced Wimpy testis (PIWI) domain, which induces formation of a catalytic tetrad at the active site<sup>71,79</sup>, characteristic of RNase H motifs<sup>12,84</sup>. This tetrad coordinates Mg<sup>2+</sup> and enables PIWI to cleave target RNAs<sup>12,13,71,84</sup>. The structural underpinnings for human AGO2 slicer activity are slightly different. The catalytic tetrad is already assembled at the active site in guide RNA-bound AGO2 even in the absence of the target RNA. However, the catalytic Mg<sup>2+</sup> is stabilized in an inactive position through interaction with a main chain Val residue. It is believed extensive guide RNA/target hybridization and accompanying conformational changes exchanges Val for the catalytic Asp-669 residue as the fourth participant in coordinating Mg<sup>2+</sup>. This exchange is predicted to shift the Mg<sup>2+</sup> about 1.5 Å to its active position, which induces target cleavage<sup>85</sup>.

In humans, only AGO2's PIWI domain possesses slicer activity<sup>13,73,75</sup>, whereas AGOs1, 3, and 4 do not<sup>13,86,87</sup>. Nevertheless, Argonautes can still execute RNAi through slicer-independent mechanisms like deadenylation/degradation or translational repression via interaction with Glycine-Tryptophan Protein Of 182 KDa (GW182)<sup>73,88,89</sup>. The RISC-bound GW182 recruits repressive factors like deadenylation enzymes and mRNA decapping complexes<sup>88,90-94</sup> and also binds Poly(A)-Binding Proteins (PABPs)<sup>90</sup>, thereby displacing other PABP-binding factors needed for mRNA stabilization and translation<sup>95,96</sup> (reviewed in <sup>97</sup>).

### Basis of Seed-Dependent Targeting

Less extensive base pairing between a guide RNA (guide strand of the 19 to 23 bp dsRNA that gets incorporated into the RISC; **Figure 1.3A**) and a target mRNA can evoke non-cleavage modes of RNAi<sup>98-104</sup>. Although artificial si/shRNAs are usually designed with 100% reverse complementarity to their intended targets, cleavage-independent RNAi can be initiated with as

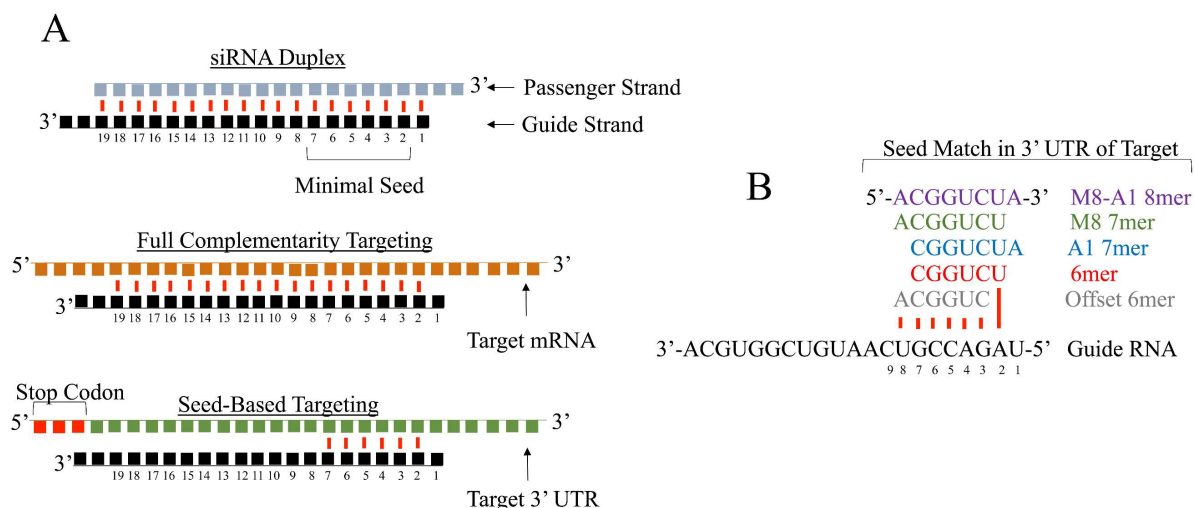


**Figure 1.3 – Types of targeting in RNAi.** (A) The structure of a typical siRNA duplex, a guide RNA targeting a mRNA through full complementarity, and a guide RNA targeting a mRNA through a 6mer seed match in the 3' UTR. (B) The five different types of contiguous seed matches. Figure adapted from Nielsen *et al*<sup>105</sup> and Kamola *et al*<sup>106</sup>.

little as six bps between a guide RNA's so-called seed sequence (positions two to seven/eight) and the target RNA (**Figure 1.3A**)<sup>101,107-109</sup>. This seed-based targeting is restricted to binding sites located in the 3' UTR<sup>110-112</sup>, whereas full-complementary binding sites can initiate RNAi whether located in the ORF or UTR regions of an mRNA<sup>113</sup>. One possible explanation for this is the lower occupancy of traversing ribosomes in the 3' UTR versus the ORF<sup>114</sup>.

Most metazoan miRNAs utilize seed-based targeting to regulate gene expression<sup>101,115-123</sup>, which is consistent with crystal structures showing the only region of the guide RNA in complex with Argonaute exposed to the solvent and ready to interact with a target are the nucleobases of the seed sequence<sup>73,75,85</sup>. Many miRNA target sites are characterized by a sharp peak in conservation *only* in the seed match region (sequence that hybridizes to the guide RNA's seed sequence). Outside this region, conservation can drop exponentially<sup>101</sup>. The most conserved region of a metazoan miRNA is the 5' half of the guide strand arm, which contains the seed<sup>115</sup>. Furthermore, deep sequencing of RNAs associated with immunoprecipitated RISC reveals enrichment of target RNAs with seed matches corresponding to co-purified miRNA guide strands<sup>116-117</sup>. The importance of the seed sequence in targeting is also highlighted by the observation that mismatches between the guide strand and target in the non-seed region is permissive to RNAi, whereas mismatches in the seed match region are not tolerated well<sup>98,124</sup>. In fact, mismatches near the 3' end of the guide RNA/strand (the non-seed region) can enhance miRNA-mediated RNAi<sup>125</sup>. Finally, microarray data show introduction of RNAi reagents (e.g. mi/si/shRNAs) downregulates targets with seed matches in their 3' UTRs<sup>104,108,109,126,127</sup>.

Although base pairing between the guide RNA's seed and the target RNA requires minimal conformational changes in the RISC<sup>73,75,83,85</sup>, less extensive hybridization would also presumably

increase the rate of RISC dissociation from the target. Indeed, association and dissociation between a miRNA-loaded RISC and its target is nearly instantaneous<sup>128</sup>. However, Wee *et al.* showed the overall affinity between guide-loaded mouse AGO2 and its target is comparable whether base-pairing is 100% or restricted to just the seed match region, suggesting Argonautes participating in miRNA-based targeting would acquire little to no advantage from extensive guide RNA/target hybridization<sup>122</sup>. In fact, full complementarity between the guide RNA and target can destabilize the RISC, promoting release of the guide RNA. Interestingly, introduction of mismatches at the non-seed 3' half of the guide RNA attenuates this and actually enhances seed-based RNAi<sup>119</sup>. Additionally, guide RNA loaded-RISC are already primed for seed-based RNAi even before binding to the target, as the majority of Argonautes are bound to guide RNAs—exemplified by a binding affinity of nearly 1 nM for human AGO2-guide RNA complexes<sup>129</sup>—and display a five to eight-fold increase in affinity for GW182 versus unbound Argonautes<sup>130</sup>. Taken together, these studies show seed-based targeting can operate efficiently, despite minimal base-pairing between the guide RNA and target.

Since seed-based targeting is dependent on a minimum of six contiguous bps (**Figure 1.3B**), guide RNAs can regulate many targets simultaneously. Based on conservation of seed matches in 3' UTRs, there are potentially hundreds of mRNA targets per miRNA<sup>42,101</sup>. Of course, not all these conserved sites lead to equal repression. Indeed, most miRNA target prediction algorithms incorporate both sequence/structural parameters and conservation when compiling the prediction score for a putative miRNA target<sup>131-133</sup>.

The type of seed match critically determines the ability of a guide RNA to repress the target. There are generally five types of seed matches, all with at least six contiguous nts that

hybridize with the guide RNA's seed sequence (see **Figure 1.3B** for depiction of seed match types). In order of increasing effectivity, the five types are offset 6mer, canonical 6mer, A1 7mer, M8 7mer, M8-A1 8mer<sup>42,105,118</sup>. Generally, adding an additional contiguous bp lowers the binding energy and enhances repressibility. Addition of an adenosine adjacent in the seed match and opposite to position one of the guide RNA does as well. Interestingly, crystal structures of Argonaute in complex with a guide RNA and target show position one of the guide is unavailable for target interaction<sup>83</sup> and that an adenosine on the target strand opposite to this position directly interacts with Argonaute<sup>134</sup>, contributing to its repressive potential. Deep sequencing of target RNAs bound to RISC reveals the occurrence of offset 6mer seed matches, which mediate repression slightly less well than canonical 6mer seed matches<sup>42</sup>. Metazoan miRNAs can supplement seed-based interaction with additional base-pairing between the 3' half of the guide RNA and the target<sup>135,136</sup>, which is consistent with structural models of human AGO2 showing initial hybridization in the seed region causes conformational changes that exposes nts 13 to 16 of the guide RNA for further target recognition<sup>85</sup>.

The base composition of the seed match is also important, with a higher GC content contributing to RNAi by making the interaction between the guide RNA's seed and the target's seed match more energetically favorable<sup>137,138</sup>. In contrast, AU-richness surrounding the core seed match site positively correlates with repressibility by reducing impeding secondary structure<sup>118,139</sup>. This is particularly interesting as overlap between miRNA sites and binding sites for other non-AGO RNA-binding proteins (RBPs) can impede RNAi<sup>140-144</sup>, which suggests an energetically favorable environment for RBP binding may actually work against RISC binding. RBPs can either enable or repress RNAi through cooperative interactions or competition for the site<sup>145-147</sup>.

The position of the seed match target site is also important. Effective target sites are typically located at least 15 nts away from the stop codon and away from the center of the 3' UTR<sup>118</sup>. Additionally, longer 3' UTRs seem to inhibit RNAi even if a seed match is present, presumably through constraining non-specific secondary structure<sup>148</sup>.

### **Off-Target Effects in RNAi**

Exogenous RNAi was revolutionary at the time of its discovery and continues to be the “work horse” today in biology labs to suppress gene function because it enables scientists to *specifically* knock down expression of their gene-of-interest, making reverse genetic study of any gene possible so long as the sequence is known. Forward genetic studies were also revolutionized, as the synthesis and implementation of sequence-based reagents like si/shRNAs, is readily amenable to screening formats. Despite these benefits, exogenous RNAi does have a major caveat—off-target effects (OTEs).

In the context of RNAi, OTEs are defined as the responses evoked by the exogenous si/shRNA that are independent of knocking down the target the reagent was designed against (referred to as the on-target). There are three major types of RNAi OTEs: (1) unintended immune response to dsRNA, (2) saturation of the RNAi machinery, and (3) sequence-based OTEs. This work will briefly describe the first two and focus on the latter, as sequence-based OTEs comprise the major part of this thesis.

It has been known for a long time that introducing exogenous dsRNAs, including siRNAs, can evoke an immune response OTE by stimulating an interferon response<sup>149-152</sup>. The receptors responsible for detecting pathogenic dsRNA products are Protein Kinase R<sup>150,153</sup> and Toll-Like

Receptors<sup>152,154-157</sup>. These sensors can also be triggered by exogenous RNAi reagents. Although the features of dsRNA that trigger these receptors are not completely understood, there seems to be a preference for uridine-guanosine-rich motifs<sup>149,155</sup>. Using RNAi reagents that lack these motifs or substituting uridines with 2' deoxyuridine or thymidine mitigates immune OTEs<sup>158-160</sup>, as does certain chemical modification of the ribose-phosphate backbone<sup>161</sup>.

Saturating the endogenous RNAi pathway machinery with exogenous RNAi reagents also induces OTEs by competing with endogenous miRNAs. A seminal study by Grim *et al.* demonstrated *in vivo* delivery of shRNAs caused major liver toxicity in mice by saturating Exportin-5<sup>162</sup>; this phenotype has also been described by others<sup>163,164</sup>. Besides inducing toxicity, exogenous siRNAs can perturb tissue-specific gene expression regulated by miRNAs through saturation of the miRNA machinery<sup>165</sup>. Indeed, transfection of exogenous siRNAs can compete with endogenous miRNAs, thereby increasing the expression of mRNAs harboring endogenous miRNA sites through de-repression<sup>127,166</sup>. This kind of OTE can usually be dealt with by lowering the amount of si/shRNA introduced into cells<sup>162,166</sup>.

The third type of OTE is mediated by the guide RNA recruiting the RISC to an unintended target (i.e. the off-target) through sequence homology and can be divided into two categories.

The first category consists of targeting genes that have a high degree of homology to the gene-of-interest in the region being targeted by the guide RNA. Obviously, the guide RNA cannot distinguish between the on-target (intended target) and the off-target if the binding site has congruent sequences. This kind of sequence-based OTE is easily dealt with by performing a BLAST search for the siRNA sequence<sup>167</sup>.

The second category is the more common seed-based OTE (sOTE). In this case, off-targets are repressed due to the seed-based targeting discussed in the previous section. In 2003, Jackson *et al.* used microarray-based transcript profiling to show that global changes in mRNA expression occur following transfection with an siRNA<sup>168</sup>. The downregulated transcripts' 3' UTRs were enriched in sequences that had as few as 11 tandem nts of reverse complementary to the 5' half of the siRNA guide strand. Further work by Jackson *et al.* and follow-up studies revealed exogenous si/shRNAs are perfectly capable of miRNA-like targeting through interaction between their seed sequence and the 3' UTRs of potential off-targets<sup>108,126,138,169</sup>.

Numerous strategies seek to mitigate sOTEs, including the use of multiple si/shRNAs targeting the same gene-of-interest to validate results, as well as reconstituting cells with mutant on-target cDNAs that harbor silent mutations at the si/shRNA target site to “rescue” the cells from the phenotypic changes that occur when that si/shRNA is introduced (reviewed in<sup>170</sup>). Incorporating locked nucleic acids or 2'-O-methylated ribose within the siRNA guide strand's seed sequence seems to mitigate sOTEs<sup>171,172</sup>, purportedly by hindering seed interaction with off-targets<sup>173</sup>. In addition, algorithms design si/shRNAs with lower GC content (~30 to 50%) in the seed sequence to make the interaction between the guide RNA's seed sequence and off-target's seed match less stable<sup>138,174,175</sup>.

Compounding the challenge of mitigating sOTEs is the fact that an si/shRNA can produce multiple guide strands with different seed sequences, thereby expanding the number of potential off-targets<sup>176,177</sup>. Because siRNAs (and mature miRNAs) are composed of two RNA strands, it follows that there exist two potential seed sequences: one on the intended guide strand and one on the passenger strand. Fortunately, preferential loading of the intended guide strand can be



accomplished by establishing thermodynamic asymmetry at the termini of an siRNA<sup>178,179</sup>. Specifically, placing an adenosine or uridine at the 5' end and a guanosine or cytosine at the 3' end of the intended guide strand favors its incorporation in the RISC<sup>167,180</sup>. Indeed, structural examination shows that human AGO2 favors incorporation of the strand with an unstable 5' end through two sensor regions that interact with the 5' phosphate and nucleobase of the intended guide strand<sup>181</sup>. Imprecise Dicer cleavage of shRNAs and pre-miRNAs can also produce different mature siRNAs with shifted seed sequences<sup>72,182</sup>, thereby expanding the number of seed sequences available to repress off-targets. Placing the intended cleavage site two bps from the apical loop makes Dicer cleavage more precise<sup>72</sup>. Indeed, nearly a third of all endogenous human miRNAs share this feature to ensure homogenous Dicer cleavage<sup>72</sup>.

Although miRNA-mediated gene regulation and sOTEs are both manifestations of seed-dependent targeting and therefore are influenced by the parameters mentioned in the previous section, only miRNA targeting is a naturally selected process, as evidenced by conservation of miRNAs<sup>47,183-186</sup> and their functions<sup>187,188</sup> and target seed match sites<sup>42,101,132</sup>. Selection can preserve the interaction between a miRNA and an individual mRNA target<sup>189-193</sup> and/or between a miRNA and its targeted gene network<sup>187,188,194,195</sup>, allowing miRNAs to efficiently repress specific functional cohorts of genes to regulate cellular processes<sup>196-201</sup>. Conversely, evolution can eliminate miRNA target sites from certain classes of genes<sup>200-203</sup>. As shown in *Drosophila*, these so-called anti-targets are enriched amongst housekeeping genes<sup>201</sup>, as targeting these genes with miRNAs are not conducive to life.

In contrast to phenotypes evoked and/or maintained by miRNAs, sOTEs are triggered by artificial si/shRNAs designed to target a gene with complete complementarity but whose seed

sequence has corresponding seed matches scattered throughout the transcriptome in the absence of selective pressure. As mentioned previously, functional seed matches are generally found in the 3' UTR of an mRNA. The 3' UTR sequences are, overall, the least conserved region of a mature mRNA—with the exception of intermittent conserved RNP binding sites (e.g. miRNA and Hu-Antigen R or HuR protein binding sites) and so-called hyper-conserved elements<sup>101,142,145,204,205</sup> located in this region—and have a nucleotide mutation rate similar to that of synonymous mutations<sup>206,207</sup>. The lack of conservation is indicative of genetic drift constantly randomizing the sequences of 3' UTRs by chance mutations. Therefore, all possible sequence permutations equivalent in size to a functional seed match ( $4^6$  for 6mers and  $4^7$  for 7mers), except those corresponding to conserved seed match sites targeted by miRNAs or those embedded in a conserved 3' UTR sequence element, would manifest in genes' 3' UTRs at random and presumably not be enriched in any specific family or cohort of genes such as Gene Ontology (GO) or Kyoto Encyclopedia of Genes and Genomes (KEGG) gene sets—even amongst genes that descended from a common ancestral gene (provided enough time has passed for 3' UTR divergence to occur by genetic drift) or are part of a common pathway or regulatory network. In other words, any given sequence of appropriate size and *not* representing or is part of any conserved RNP binding sites preserved by nature for participating in any functional or regulatory role could permit an siRNA to target gene cohorts more or less at random through seed-based off-targeting by acting as a complementary seed match<sup>208,209</sup>.

This makes *in silico* seed match target searches a poor predictor of sOTEs because non-selected seed matches, for the most part, will be scattered across many functionally-unrelated genes, thereby obfuscating any overt concerted targeting bias against a specific gene cohort that

might result in a distinct phenotypic change. This is especially true of cellular changes evoked by seed-based targeting—which are determined by the *collective* and *simultaneous* repression of hundreds of off-target genes harboring seed matches—since repression of any single mRNA is highly variable (not all seed matches confer consistent repressibility) and generally mild<sup>112</sup>.

Although mild, this repression is not *negligible*. Indeed, some groups are now using sOTE information to their advantage when analyzing large RNAi-based screens<sup>210,211</sup>. For example, Myeloid Cell Leukemia Sequence-1 (MCL-1) was identified as a contributor to ABT-737 resistance in small cell lung cancer based on predicted seed matches to sensitizing siRNAs in an arrayed screen, which were not even designed to target MCL-1<sup>212</sup>. Algorithms such as PheLim incorporate both the intended on-target and potential seed-dependent off-target repertoires of thousands of RNAi reagents used in forward genetics screens to more accurately identify candidate genes than other analysis techniques that assume the only targets of an RNAi reagent is the intended on-target<sup>211</sup>. This is only possible because seed-based RNAi can repress a gene enough to execute at least a partial knock down. Nevertheless, the effect of fully knocking down a gene can be extrapolated by seed-based repression only when *many* si/shRNAs—as those from an RNAi-based screen—with and without corresponding seed matches within the candidate gene-of-interest are included to enhance the sensitivity of the analysis, since the potency of seed-based off-targeting is much lower than that of full complementary on-targeting. The successful implementation of this strategy in RNAi-based screens does not imply that the dominant sOTE triggered by any *individual* siRNA can be any more easily predicted, since it is the composite net result of many “partial knock down” events that occur through seed-based off-targeting interacting amongst each other. In other words, the mild phenotypic change evoked by an siRNA partially

knocking down a candidate gene through seed-based off-targeting may not correspond to the dominant overall sOTE evoked by that siRNA repressing its entire off-target repertoire.

Although sOTE prediction would be difficult for siRNAs that target nonconserved seed match sequences scattered randomly throughout the transcriptome, this may not be the case for si/shRNAs harboring seed sequences congruent to miRNAs that exhibit a high degree of functional and/or target site conservation, as evolution has maintained and optimized these specific seed sequence-target network interactions to perform a specific biological role. These si/shRNAs might evoke sOTEs that are similar to the cellular responses triggered by the miRNAs with the congruent seed sequence. However, differences between exogenous siRNAs and endogenous miRNAs, such as cellular concentration and method of delivery, and competition between siRNAs and miRNAs for the RISC<sup>127</sup> will make this difficult to demonstrate.

Now, the probability an si/shRNA will evoke any particular sOTE by chance presumably increases as the number of predicted target genes harboring seed matches increases since a broader target profile has a higher chance of encompassing any given gene cohort(s)—including those whose repression evokes the sOTE in question. This would mean the capacity of an si/shRNA to evoke an sOTE could be predicted simply by the number of genes with seed matches. However, this relationship has limited predictive value for two reasons: (1) The si/shRNAs with broad seed-based target profiles would evoke multiple sOTEs simultaneously, not just the sOTE being investigated/predicted, as multiple different gene cohorts would be repressed concurrently. (2) As the number of target genes with seed matches increases, the repression of any individual target conferred by the corresponding siRNA would lessen since there is less guide RNA available to mediate RNAi for any single mRNA<sup>213</sup>. In this way, exogenous si/shRNAs that repress many off-

targets through seed-based RNAi would not necessarily produce an overt and predictable sOTE because the targeting is diluted.

However, there are several pieces of evidence suggesting seed-based off-targeting by exogenous si/shRNAs, even with different seed sequences, can evoke a predictable and specific sOTE by preferentially targeting certain cohorts of genes. First, the genomic distribution of base composition is not random, and therefore, the distribution of potential seed matches is biased. Although the statistical significance is disputed by several reports, it seems housekeeping genes are abundant in GC-rich isochore regions of the genome and have 3' UTR sequences with higher GC content<sup>214-216</sup>, which are presumably enriched in GC-rich seed matches. Second, housekeeping and proliferative genes in dividing cells and tissue-specific genes in differentiated cells have shorter 3' UTRs, likely to eliminate repressive seed match sites to endogenous miRNAs<sup>203,217-220</sup>. However, longer 3' UTRs can also inhibit seed-based RNAi, possibly through steric hindrance<sup>148,220</sup>; therefore, these genes with shortened 3' UTRs may become predisposed to seed-based off-targeting, provided an exogenous seed match remains intact. Third, genes depleted in endogenous miRNA sites (known as anti-targets) are enriched amongst certain Gene Ontology (GO) cohorts, including some involved in basic cell maintenance processes (as well as tissue-specific activities)<sup>200-203</sup>. Interestingly, genes harboring seed matches to transfected siRNAs in their 3' UTRs are less repressed when endogenous miRNA sites are also present versus absent<sup>127</sup>. Although competition between the exogenous siRNAs and endogenous miRNAs may partially explain this, the enhanced repressibility of genes depleted in miRNA sites can also be explained by a lack participation of these genes in stabilizing miRNA-mediated gene regulatory motifs that

would otherwise counterbalance seed-based targeting by a siRNA (see **Chapter 5: Basis of Preferential Survival Gene Targeting/Downregulation: Gene Regulatory Network**).

Together, these studies suggest si/shRNAs with GC-rich seed sequences, independent of the actual sequence, may exhibit targeting bias toward housekeeping or proliferative genes. However, virtually no reports exist exploring whether seed-based targeting by nonredundant exogenous si/shRNAs can evoke a specific and recurring uniform biological outcome or sOTE.

### Non-Canonical Sources of Guide RNAs

The most abundant source of RISC-bound small RNAs in mammals are *canonical* miRNAs, which account for about 96% of all miRNAs<sup>60</sup>; their processing into mature miRNAs

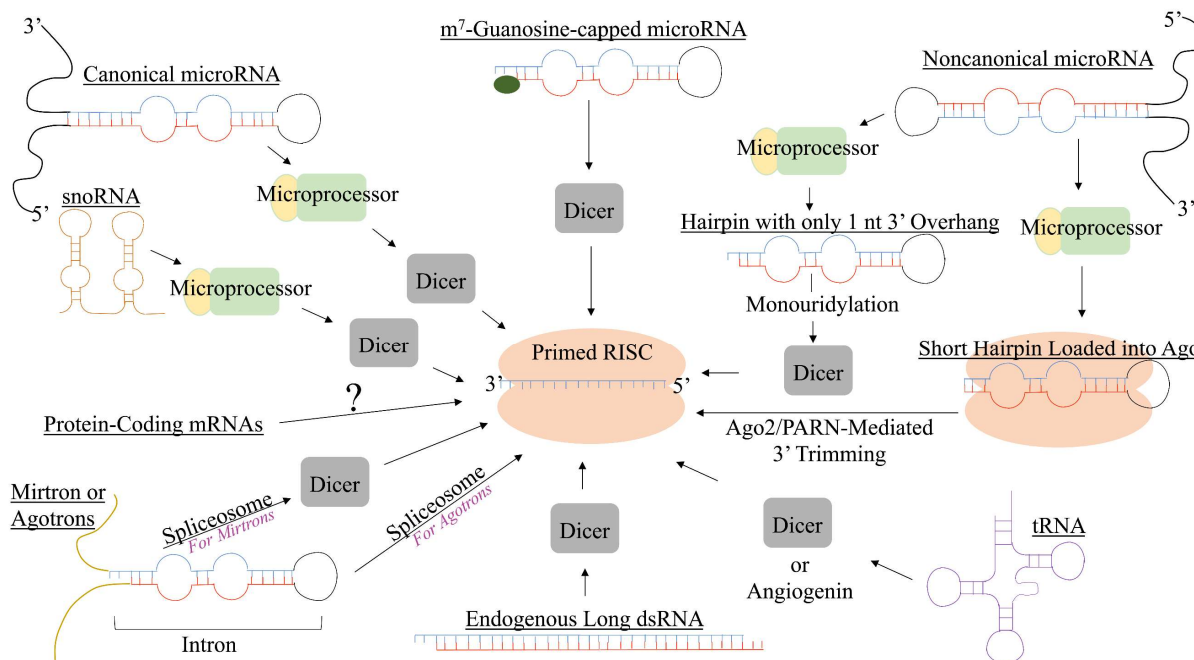


**Figure 1.4 – Sources of guide RNAs in humans.** Schematic showing the various sources of guide RNAs in humans and the processing components that produce them.

follows the steps outlined in **Figure 1.2**. There are also multiple examples of non-canonical miRNAs, whose processing is independent of Drosha and/or Dicer or undergo atypical processing

(**Figure 1.4**), as highlighted by deep sequencing data gathered from Drosha and Dicer knock out cells generated by Narry Kim's group<sup>60</sup>.

Members of the vertebrate let-7 family and human miRNA-105b undergo atypical Drosha processing, which produces a 1 nt overhang at the 3' terminus that needs to be monouridinylated before Dicer processing<sup>221</sup>. The m<sup>7</sup>-guanosine capped miRNAs, like human miRNA-320a, are transcribed as minimal shRNA sequences with no extended flanking 5' or 3' single stranded ends, which negates the need for Drosha processing<sup>222-224</sup>. The pre-miRNA of miRNA-451a is loaded directly into Argonaute following Drosha-mediated cleavage but requires further processing by human AGO2's slicer and AGO-associated Poly-A-specific RiboNuclease (PARN) to produce the final guide strand<sup>225</sup>. So-called mirtrons are miRNAs that are imbedded in introns and released as pre-miRNAs through the action of the spliceosome and Dicer but independently of Drosha<sup>226-229</sup>.

There are also so-called agotrons (**Figure 1.4**), which are similar to mirtrons except there are no prior processing steps before incorporation into the RISC. There is no pre-miRNA intermediate. The excised intron simply gets loaded directly into the RISC. Two agotrons have been identified in humans and are derived from introns of the host genes Polycystic Kidney Disease-1 and Microtubule-Associated Serine/Threonine kinase-1<sup>230</sup>. Their function, however, in RNAi is unclear.

Besides miRNAs loci, there are other sources of guide RNAs derived from ubiquitous non-coding RNAs including transfer (t)RNAs and small nucleolar (sno)RNA (**Figure 1.4**). tRNAs are a fundamental class of noncoding RNAs that form a cloverleaf secondary structure<sup>231</sup> and deliver amino acids to the translation machinery for assimilation into a peptide through an aminoacyl-tRNA intermediate (reviewed in <sup>232</sup>). However, tRNAs are often endonucleolytically cleaved in

response to stressful stimuli to produce tRNA halves and small tRNA fragments that inhibit translation through different mechanisms<sup>233-238</sup>. Two endoribonucleases implicated in cleaving mature tRNAs are Dicer<sup>222,239</sup> and the RNase A superfamily member Angiogenin<sup>236,240</sup>. Cleaved tRNA fragments have been shown to associate with human Argonaute proteins<sup>237,241</sup> and have been shown to play a role in curtailing viral infections<sup>242,243</sup> and also regulating the DNA damage response<sup>244</sup>. The majority of evidence implicating tRNA fragments as functional guide RNAs, directing RISC-mediated RNAi, has come from seed match analyses of both downregulated candidate target genes and RNAs cross-linked to immunoprecipitated Argonaute and also repression of reporter constructs. However, relatively few studies have concretely demonstrated that RNAi can occur without the use of exogenous tRNA fragments. Furthermore, candidate guide RNA-target interaction inferred by seed match analysis of co-purified RNAs cross-linked to immunoprecipitated Argonaute does not always translate to an interaction that occurs and results in RNAi in living cells<sup>123,245,246</sup>. More work is needed to determine how much participation tRNA fragments play in endogenous RNAi.

snoRNAs are categorized into two groups: C/D box and H/ACA box. The former contains a 5' end C (RUGAUGA) and a 3' end D (CUGA) motif and forms an overall helix-asymmetric bulge-helix secondary structure<sup>247-255</sup>. The latter H/ACA box snoRNAs contain a 5' end H (ANANNA) and 3' end ACA motif and forms an overall hairpin-hinge-hairpin-tail secondary structure<sup>256,257</sup>. The canonical functions of the C/D box and H/ACA box snoRNAs are to direct 2'-O-ribose methylation<sup>258</sup> and pseudouridylation<sup>259</sup>, respectively, of ribosomal (r)RNAs. They recruit enzymes that catalyze these modifications—as part of snoRNA ribonucleoprotein



(snoRNP) complexes—through reverse complementarity between themselves and the target rRNA (reviewed in <sup>260</sup>)—in a manner analogous to mi/siRNA-mediated recruitment of AGO to a mRNA.

snoRNAs and miRNAs have a lot in common in terms of sequence/structure, processing, and functions. It has even been postulated both classes of molecules evolved from a common ancestral molecule; specifically, miRNAs evolved from an offshoot of ancestral snoRNAs, which are much older and common to all eukaryotes<sup>261-265</sup>. Indeed, precursor transcripts of some annotated and functional human miRNAs harbor the conserved snoRNA-associated motifs and even have the capacity to bind protein components of the snoRNPs<sup>266-268</sup>. Similarly, there are annotated snoRNAs that can be processed into fragments that get loaded in Argonaute and function as miRNAs<sup>269-272</sup>. These conclusions have been convincingly demonstrated with seed match analysis of repressed RNA targets, sequencing of Argonaute-associated RNAs, and de-repression of target/reporter expression upon inhibiting snoRNA fragments with 2'-O-methylated antisense oligonucleotides or knocking down Argonaute. Interestingly, studies have shown eliminating either Microprocessor components or Dicer can perturb generation of snoRNA guide fragments derived from H/ACA box snoRNAs<sup>269,270</sup>. In contrast, Dicer involvement in C/D box processing has only been shown in the flagellated parasite *Giardia lamblia*<sup>272</sup>.

A few scant reports in human cells have also shown ribosomal (r)RNA can be processed into miRNA hairpins, including human miRNA-712, which can induce inflammation in endothelial cells and atherosclerosis<sup>273</sup>. A recent deep sequencing and computational study conducted in 2016 by Yoshikawa and Fujii identified 17 sequences corresponding to miRNAs that were also found in rRNA sequences, with 11 of these forming a pre-miRNA-like secondary

structures<sup>274</sup>. However, whether these rRNA-hosted miRNAs contribute to normal human cell function by directing RNAi is not clear.

Thus far, release of guide RNAs has only convincingly been shown for non-coding RNA precursors in humans. Although hybridization between a sense and antisense mRNA transcript can be processed by Dicer to form endogenous siRNAs, this has only been shown in lower organisms<sup>65,275</sup>. Regardless, it is unclear whether protein-coding mRNA sequences can form *intramolecular* structures that are recognized and processed to form endogenous siRNAs in humans. The occurrence of siRNAs derived from the protein-coding portion of a single translating mRNA would be rare, considering processing enzymes would be presumably blocked by translating ribosomes traversing the ORF that disrupt recognizable secondary structure<sup>276</sup>. Furthermore, mRNAs need to encode functioning proteins using proper codon usage, which severely constrains the theoretical pool of sequences that can also function as a substrate for RNAi-processing enzymes. The UTR regions of a mRNA are also difficult substrates for guide strand production since they play an important role in post-transcriptional regulation of the mRNA through extensive interactions with regulatory RNPs that bind to evolutionarily constrained motifs<sup>277,278</sup>. It is unknown whether these evolutionary constraints on mRNA sequences and their involvement in protein production would allow these molecules to form intramolecular structures/motifs that are faithfully recognized by processing enzymes and be co-opted as a source for guide RNA generation.

Furthermore, mammals lack RNA-dependent RNA polymerase activity, which is found in certain lower organisms and can produce viable Dicer substrates, even from mRNA sources, by reverse transcribing RNA, forming a dsRNA duplex<sup>279-283</sup>. Nevertheless, RNases that cleave

indiscriminately or promiscuously may generate a large enough pool of unstructured ssRNAs that can then duplex and become incorporated into the RISC. Such indiscriminate RNA processing is common during cell death processes or times of stress<sup>284-289</sup>. It would be interesting to determine whether mRNA is processed into RISC-bound guide RNAs that contribute to cell death pathways through RNAi.

### **CD95 and CD95L**

CD95 (Fas, APO-1) and CD95L are both transmembrane proteins and members of the Tumor Necrosis Factor Receptor (TNFR)<sup>290</sup> and Ligand (TNFL)<sup>291</sup> superfamilies, respectively. The expression of CD95 is ubiquitous in nature<sup>292-294</sup>, whereas CD95L is largely restricted to activated T lymphocytes, natural killer cells, and sites of immune privilege (e.g. testis and eye)<sup>291,295-297</sup>.

Engagement of CD95 with CD95L induces apoptosis in sensitive cells<sup>291</sup>. This interaction is critical in immune cell homeostasis by eliminating peripheral autoreactive T lymphocytes through an apoptosis-related process called Activation-Induced Cell Death (AICD), which is dependent on CD95 engagement and is triggered by prolonged and intense stimulation with an antigen<sup>298-301</sup>.

Indeed, *lpr* and *gld* mice, which contain loss-of-function mutations in CD95 and CD95L genes, respectively, develop severe lymphoproliferative disorders accompanied by an autoimmune disease-like phenotype, which is due to unrestrained accumulation of autoreactive T lymphocytes<sup>300,302-309</sup>.

In addition to the failsafe role CD95-mediated apoptosis plays in immune cell homeostasis,

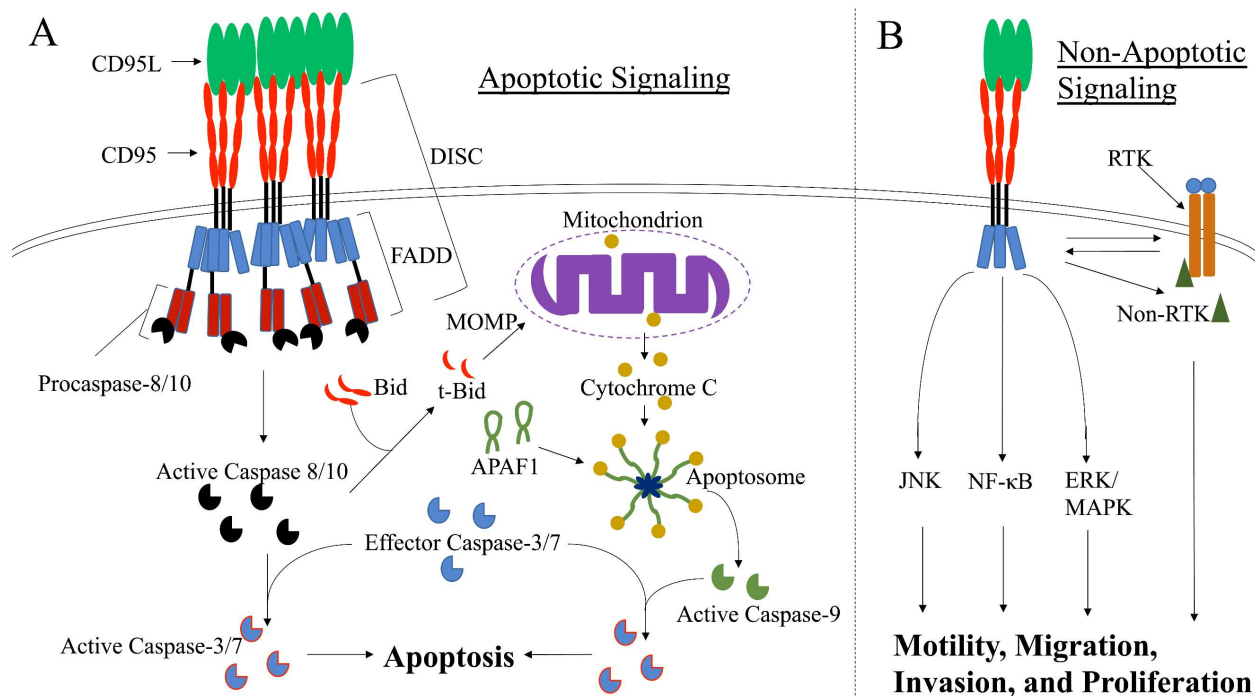


**Figure 1.5 – Signaling downstream of CD95 stimulation.** (A) Interaction between CD95 and CD95L leads to formation of the Death-Inducing Signaling Complex (DISC) and autoproteolytic activation of initiator caspase-8/10. These initiator caspases cleave and activate effector caspases, which then cleave death substrates resulting in apoptosis. If caspase-8/10 activation is below the apoptotic threshold, insufficient effector caspase activation fails to induce apoptosis. To amplify the apoptotic signal, the initiator caspases cleave the pro-apoptotic Bcl-2 protein Bid, which produces truncated Bid (t-Bid)<sup>310</sup>. This t-Bid then inserts in the outer mitochondrial membrane, forming a perforating channel<sup>311</sup>. The resulting Mitochondrial Outer Membrane Permeabilization (MOMP) causes release of mitochondrial cytochrome C, which then forms a heptameric complex with Apoptotic Protease Activating Factor 1 (APAF1). Procaspase-9 interacts with this complex and is activated by proximity<sup>312,313</sup>. Activated caspase-9 provides the necessary amplification and cleaves sufficient amounts of effector caspases to induce apoptosis<sup>312</sup>. (B) Low-level or aggregation-independent CD95 stimulation or activation in apoptosis-resistant cells can lead to different non-apoptotic signaling pathways that modify nuclear transcription and regulate a variety of cell behaviors<sup>314-316</sup>.

activated T lymphocytes and natural killer cells use CD95L to induce apoptosis in pathogen-infected cells and cancer cells as part of the adaptive immune system<sup>317-324</sup>.

CD95-induced apoptosis follows a well-orchestrated sequence of events (**Figure 1.5A**). Pre-assembled homotrimers of membrane-bound CD95L and CD95 interact<sup>315,325-328</sup>, which leads to higher-order complexes of CD95/CD95L at the cell surface<sup>329,330</sup>. This recruits the initiator procaspases-8 and 10 through the adapter protein Fas-Associated protein with Death Domain (FADD), which functions through homotypic domain interactions with the cytoplasmic death

domain of CD95 and the death effector domain of procaspase-8/10<sup>331-335</sup>. This complex is called the Death-Inducing Signaling Complex (DISC)<sup>331</sup> and leads to proximity-induced autoproteolytic activation of the initiator caspases<sup>336,337</sup>. The activated caspase-8/10 then induce activation of effector caspases-3 and 7 either directly through cleavage<sup>338,339</sup> or indirectly by inducing Mitochondrial Outer Membrane Permeabilization (MOMP), which leads to activation of caspase-9 in the apoptosome complex that then cleaves the effector caspases<sup>310-313,340-342</sup>. These effector caspases then cleave a variety of protein substrates, which ultimately results in apoptosis<sup>343-347</sup>.

Although activation of CD95 was originally discovered by its ability to induce apoptosis, it is now appreciated that CD95 signaling is multifaceted and plays various non-apoptotic roles in development and normal cell function. Indeed, CD95 activation plays critical roles in neurite outgrowth<sup>348</sup>, proliferation of activated T lymphocytes<sup>349,350</sup>, hepatocyte proliferation following partial liver resection<sup>351</sup>, motility/recruitment of peripheral myeloid cells<sup>352</sup>, and transmigration of lymphocytes across endothelial cells<sup>353</sup>. CD95 stimulation initiates these non-apoptotic responses by stimulating different signaling pathways, including c-Jun N-terminal kinases (JNK)<sup>354</sup>, Mitogen-Activated Protein Kinase (MAPK)/Extracellular signal-Regulated Kinase (ERK)<sup>355</sup>, and Nuclear Factor kappa-light-chain-enhancer of activated B cells (NF- $\kappa$ B)<sup>356</sup>. CD95 also participates in crosstalk with both receptor tyrosine kinases (RTKs) and non-RTKs<sup>352,357-359</sup> (**Figure 1.5B**).

CD95 activation was first discovered to induce significant tumor regression in a human B cell lymphoma xenograft in mice<sup>360</sup> and, at the time, was believed to have potential as a cancer therapy. Unfortunately, systemic treatment with mouse-specific CD95-activating antibodies causes massive liver toxicity in mice<sup>292</sup>, thereby precluding it as a viable treatment option.

Moreover, the multifaceted signaling events activated by CD95 complicates its role in

cancer progression. Indeed, resistance to apoptosis is a hallmark of cancer, yet CD95 is still expressed in many cancers<sup>361-365</sup>, which suggests there is selective pressure to maintain CD95 signaling. Consistently, the non-apoptotic signaling pathways triggered by CD95, particularly in apoptosis-resistant tumor cells, can actually promote the oncogenic process, as its stimulation has been shown to enhance cancer cell motility/invasiveness<sup>366</sup>, metastatic potential<sup>361</sup>, and even plays a critical role in maintaining the cancer stem cell population<sup>367,368</sup>. CD95 has been described as a dual-natured receptor, capable of either tumor suppressive or oncogenic signaling<sup>369-371</sup>. The switch in behavior can be controlled by a number of things such as whether the cell over-expresses anti-apoptotic factors<sup>372,373</sup> and the level of CD95 stimulation/aggregation<sup>316,374,375</sup> (**Figure 1.5**).

CD95 has even been shown to stimulate cancer cell proliferation *in vivo*<sup>364</sup>, presumably through CD95L expressed on tumor-infiltrating lymphocytes. In a report by Hadji *et al.*, various cancer cell types were shown to undergo a novel form of death triggered by si/shRNAs targeting CD95 or CD95L that cancer cells could not develop resistance to<sup>376</sup>. This mode of death was demonstrated with multiple non-overlapping si/shRNAs and shown to occur regardless of cancer cell type. Moreover, Cowely *et al.* conducted a massive parallel lentiviral-shRNA library screen across 216 different cancer cell types targeting ~11,000 genes with five shRNAs per gene to look for fundamental survival genes<sup>377</sup>. The results showed that shRNAs derived from these two genes are generally toxic across all tumor types—particularly those derived from the CD95L mRNA sequence (**Figure 3.1C**). However, a role for cell-autonomous CD95L as a cancer survival factor is dubious, as the ligand is not detectable using conventional Western blot or Real Time quantitative PCR (RT-qPCR) in most cancer cells.

## Central Hypothesis and Rationale

The death induced by multiple non-overlapping CD95/CD95L-derived si/shRNAs is intriguing, given the lack of CD95L expressed at the endogenous level. It is possible the kinetics of CD95L expression preclude its detection through conventional means that only assess expression at a single time point. However, many of these cancer cell lines are sensitive or can be made sensitive to apoptosis upon addition of CD95L protein or CD95-activating antibodies. Together, this suggests si/shRNAs derived from CD95/CD95L mRNA sequences may all be able to evoke a singular and recurring phenotype, in this case toxicity, independent of the protein gene products.

Therefore, the main hypothesis of this work is **multiple non-overlapping si/shRNAs derived from CD95 and CD95L kill cancer cells, even in the absence of the intended target sites in these genes, through a specific and recurring form of RNAi-based OTE, likely a unique sOTE, that is triggered by the non-identical seed sequences of the CD95/CD95L-derived si/shRNAs.**

Enrichment of toxic RNA sequences derived from CD95 and CD95L would suggest an evolutionary conserved function of the mRNA for these two genes. Given such enrichment does exist, it can be further hypothesized that **the full-length mRNAs of these genes may, themselves, be toxic, by triggering an RNAi-mediated mechanism through processing mRNA-derived guide RNAs.**

## Summary and Significance

The presented work demonstrates, for the first time, that seed-based targeting by many si/shRNAs with non-identical seed sequences can evoke the same predictable biological response, despite the exact off-target repertoire being different from amongst the RNAi reagents. Indeed, si/shRNAs derived from the sequences of CD95 and CD95L are massively toxic to cancer cells, even in the absence of their endogenous on-target site. The mRNA sequences of CD95 and CD95L are enriched in these toxic si/shRNAs, with the ORF of CD95L showing the most enrichment. These si/shRNAs evoke this toxicity by preferentially targeting survival genes through 3' UTR seed-based targeting. This form of cancer cell death is, therefore, called DISE or Death Induced by Survival gene Elimination. This form of death can be triggered by CD95/CD95L-derived si/shRNAs in multiple cancers of both human and mouse origin, suggesting functional conservation<sup>376</sup>. The role of DISE as a cell-autonomous tumor surveillance system is currently being investigated. Additionally, the Peter lab has recently published a list of genes that also exhibit this behavior besides CD95 and CD95L by screening shRNAs derived from other genes that induce morphological and biochemical changes typical of DISE<sup>378</sup>.

Enrichment of DISE-inducing si/shRNAs in the ORF of CD95L suggested the CD95L mRNA could be toxic. Expression of the mRNA can evoke toxicity in the absence of CD95 expression. Over-expression of CD95L mRNA also preferentially downregulates survival genes and produces numerous small RNAs associated with Argonaute, suggesting mRNA toxicity is evoked by the release of embedded guide RNAs triggering DISE. This is the first time a protein-coding mRNA is suggested to produce guide RNAs that evoke a response through RNAi in human.



Besides the biological relevance of these findings, DISE represents a whole new paradigm of cancer treatment. DISE is best characterized as a combination of different modes of cell death—the result of targeting multiple survival genes—and therefore, cancer cells cannot develop resistance. Moreover, cancer stem cells and transformed cells are more sensitive to DISE than normal cells<sup>367,376</sup>. Dicer and Drosha knock out cells are hypersensitive to DISE, which suggests endogenous miRNAs compete with the DISE-inducing si/shRNAs for RISC occupancy. This result could explain our previous observation that these toxic si/shRNAs preferentially affect cancer stem cells and transformed cells<sup>367,376</sup>, as tumor cells, in general, express less miRNAs than normal cells<sup>379,380</sup>. Taken together, this shows DISE is a promising alternative to targeted therapies and offers unique advantages. Indeed, the Peter lab has recently published work showing efficacy of DISE-inducing siRNAs in mouse xenograft models<sup>381</sup>.

## **Chapter 2: Materials and Methods**

### **Reagents and Antibodies**

Primary antibodies for Western blot: anti- $\beta$ -actin antibody (Santa Cruz #sc-47778, RRID:AB\_626632; 1/5000 dilution), anti-human CD95L (BD Biosciences #556387, RRID:AB\_396402; 1/500 dilution), anti-human CD95 (Santa Cruz #sc-715, RRID:AB\_2100386; 1/1000 dilution), anti-human AGO1 (Abcam #AB98056, RRID:AB\_10680548; 1/500 dilution and Cell Signaling #5053, RRID:AB\_10692649; 1/1000 dilution), anti-human AGO2 (Abcam #AB186733, RRID:AB\_2713978; 1/2000 dilution and Abcam #AB32381, RRID:AB\_867543; 1/1000 dilution), anti-human Drosha (Cell Signaling #3364, RRID:AB\_10828827; 1/1000

dilution), and anti-human Dicer (Cell Signaling #3363, RRID:AB\_2093073; 1/1000 dilution). Secondary antibodies for Western blot: Goat anti-rabbit; IgG-HRP (Southern Biotech #SB-4030-05, RRID:AB\_2687483; 1/5000 dilution and Cell Signaling #7074, RRID:AB\_2099233; 1/2000 dilution) and Goat anti-mouse; IgG1-HRP; (Southern BioTech #1070-05, RRID:AB\_2650509; 1/5000 dilution). Conjugated antibody and isotype control for CD95 surface staining were FITC-mouse anti-human CD95 (BD Biosciences #556640, RRID:AB\_396506) and FITC-mouse IgG1,  $\kappa$  isotype control (BD Biosciences #551954, RRID:AB\_394297).

Recombinant soluble S2 CD95L and leucine-zipper tagged (Lz)CD95L were described before<sup>363</sup>. Reagents used: propidium iodide (PI; Sigma-Aldrich #P4864), puromycin (Sigma-Aldrich #P9620), G418 (Affymetrix #11379), zVAD-fmk (Sigma-Aldrich #V116, used at 20  $\mu$ M), doxycycline (DOX) (Sigma-Aldrich #9891), Lipofectamine 2000 (ThermoFisher Scientific #11668027), and Lipofectamine RNAiMAX (ThermoFisher Scientific #13778150), phenylmethylsulfonyl fluoride (PMSF; ThermoFisher Scientific #36978), Protease Inhibitor Cocktail tablets (Sigma-Aldrich #11697498001), 4-(2-aminoethyl) benzenesulfonyl fluoride hydrochloride (AEBSF; Sigma-Aldrich #A8456), 1,4-dithiothreitol (DTT; Sigma-Aldrich #10197777001), L-glutathione (Sigma-Aldrich #G4251), IGEPAL CA-630 (Sigma-Aldrich #I8896), and sodium orthovanadate (NEB #P0758).

### **Acquired Cell Lines**

The ovarian cancer cell line HeyA8 (RRID:CVCL\_8878), the neuroblastoma cell line NB7 (RRID:CVCL\_8824), and the breast cancer cell line MCF-7 (RRID:CVCL\_0031) were grown in RPMI medium (Cellgro #10-040-CM), 10% heat-inactivated FBS (Sigma-Aldrich), 1% L-

glutamine (Mediatech Inc), and 1% penicillin/streptomycin (Mediatech Inc). The human embryonic kidney cell line 293T (RRID:CVCL\_0063) and Phoenix AMPHO (RRID:CVCL\_H716) cells were cultured in DMEM (Cellgro #10-013-CM), 10% heat inactivated FBS, 1% L-Glutamine, and 1% penicillin/streptomycin. HCT116 *Drosha*<sup>-/-</sup> and *Dicer*<sup>-/-</sup> cells were generated by Narry Kim's group<sup>60</sup>. HCT116 parental (KCTC #HC19023, RRID:CVCL\_0291), a *Drosha*<sup>-/-</sup> clone (clone #40, KCTC #HC19020) and two *Dicer*<sup>-/-</sup> clones (clone #43, KCTC #HC19023 and clone #45, KCTC #HC19024; the data presented used clone #43; both clones #43 and #45 was used in replicative experiments) were purchased from Korean Collection for Type Cultures (KCTC). All HCT116 cells were cultured in McCoy's medium (ATCC #30-2007), 10% heat-inactivated FBS, 1% L-Glutamine, and 1% penicillin/streptomycin. The mouse colon adenocarcinoma cell line CT26 (RRID:CVCL\_7254) and CT26L, which was engineered to over-express human CD95L<sup>382</sup>, were cultured in DMEM (Cellgro #10-013-CM), 10% heat inactivated FBS, 1% L-Glutamine, and 1% penicillin/streptomycin. All cell lines were authenticated using STR profiling and tested monthly for mycoplasma using Plasmotest (Invitrogen).

### **Generation of Lentiviral and Retroviral Plasmid Constructs**

RNAi reporters for CD95L and CD95-targeting si/shRNAs were synthesized as minigenes inserted into a pIDTblue (or pIDT) plasmid by IDT. The minigene sequences were as follows: a 5' XbaI restriction site, followed by the Venus ORF sequence (accession number DQ092360.1) and then either the CD95L ORF (accession number NM\_000639.2) or the CD95 ORF (accession number BC012479.1) sequence lacking the adenine nt at the start codon (to prevent expression of the CD95L or CD95 protein inserts), and a 3' EcoRI restriction site following the stop codon.

These inserts were sub-cloned into the modified CD510B vector<sup>368</sup> using XbaI (NEB #R0145) and EcoRI (NEB #R0101). Ligation was done with T4 DNA ligase (NEB #M0202) at 16°C over night.

The pLenti-CD95L constructs were synthesized by sub-cloning an insert containing the CD95L ORF (wild type or mutant) cDNA (synthesized by IDT as a minigene with flanking 5' NheI RE site and 3' XhoI RE sites in pIDTblue or pIDT vectors) into the pLenti-GIII-CMV-RFP-2A-Puro vector (ABM Inc). The insert and the backbone were digested with NheI (NEB #R0131) and XhoI (NEB #R0146) restriction enzymes. Subsequent ligation with T4 DNA ligase created the pLenti-CD95L cDNA lentiviral vectors. The CD95L-WT insert consisted of the NM\_000639.2 ORF sequence. The CD95L-L1MUT insert consisted of the CD95L-WT sequence with 8 silent mutations at the shL1 target site (5'-GCATCATCTTTGGAGAAGCAA-3' -> 5'-GCCTCGTCCCTAGAAAAACAG-3'). The CD95L-L3MUT insert consisted of the CD95L-WT sequence with 8 silent mutations at the shL3 target site (5'-ACTGGGCTGTACTTTGTATAT-3' -> 5'-ACCGGATTATATTTTCGTGTAC-3'). The CD95L<sup>MUT</sup> insert consisted of the CD95L-WT sequence with 2 nucleotide substitutions in codon 218 (*TAT* -> *CGT*) resulting in replacement of tyrosine for arginine (Y218R), which has been described to inhibit binding to CD95<sup>326</sup>. The CD95L<sup>MUT</sup>NP insert consisted of the CD95L-WT sequence containing both the Y218R mutation and a single nucleotide substitution at the second codon (*CAG* -> *TAG*), resulting in a premature stop codon right after the start codon to prevent generation of full-length CD95L protein.

The pLNCX2-CD95R6MUT vector was synthesized by replacing a 403bp fragment of the CD95 ORF insert from the pLNCX2-CD95-WT vector<sup>376</sup> with a corresponding 403bp fragment that had 8 silent mutation substitutions at the shR6 site (5'-GTGCAGATGTAAACCAAACCTT-3' -> 5'-ATGTCGCTGCAAGCCCAATTT-3') using BstXI (NEB #R0113) and BamHI (NEB

#R3136) restriction enzymes (mutant insert was synthesized in a pIDTblue vector with 5' end BstXI site and 3' end BamHI RE site).

The Dox-inducible vectors (pTIP and pTIG) expressed shRNAs of the form 5'-CCGGNNNNNNNNNNNNNNNNNNNNNNNNNNNNCTCGAGnnnnnnnnnnnnnnnnnnnnTTTT-3' and were used previously<sup>376</sup>. The poly-N represents the two 21 bp sequences that transcribe for the sense (N) and antisense (n) shRNA arms. Besides the shRNA cassette, the pTIP and pTIG vectors express a puromycin resistance cassette or GFP, respectively.

miR-30-based shRNAs were generated by The Gene Editing & Screening Core, at Memorial Sloan Kettering, NY, by converting the 21mers expressed in the pLKO and pTIP/pTIG vectors into 22mers followed by cloning into the Dox-inducible LT3REPIR vector as described<sup>383</sup>. A vector expressing an shRNA against Renilla luciferase was used as control<sup>383</sup>.

### **Generation of Stable Over-Expressing Cells**

6.5 million 293T cells were seeded on a 10 cm dish and transfected with 6 µg of pCMV-dR8.9 and pMD.G packaging plasmids and 12 µg of lentiviral vector using 60 µL Lipofectamine 2000 the following day to generate lentiviruses for infections. 10 mL of antibiotic-free DMEM was used for transfection. Media was changed the day after transfection with 10 mL of fresh complete DMEM, and viruses were harvested 48 hrs later. Viral supernatants were passed through a 45 µM filter and stored at -80 °C. Retroviruses were generated similarly, except Phoenix AMPHO cells were transfected with 6 µg VSVg packaging plasmid and 12 µg retroviral vector.

Unless otherwise stated, infections with lentiviral or retroviral supernatants were done in the same basic way: Cells were seeded on a 6-well plate. The next day, media was replaced with

1 mL of fresh media containing enough polybrene so the final concentration would be 8  $\mu\text{g}/\text{mL}$ . The viral supernatant was added, and the cells were centrifuged at room temperature at 2700 RPM for 1 hr. The cells were put back in the 37°C incubator. The following day, the media was replaced with 2 mL of fresh media. The cells were allowed to recover for an additional day, before selection began. Selection was complete when all uninfected cells were dead.

NB7 cells over-expressing CD95L cDNAs (**Figure 3.3C and D**) were generated by infecting cells seeded at 100,000 cells per well on a 6-well plate with empty pLenti-GIII-CMV-RFP-2A-Puro (referred to as empty pLenti), pLenti-CD95L-WT, pLenti-CD95L-L1MUT, and pLenti-CD95L-L3MUT with 8  $\mu\text{g}/\text{ml}$  polybrene and 4 mL of cleared lentiviral supernatant. Media was replaced the day after infection and selection was done with 3  $\mu\text{g}/\text{ml}$  puromycin the following day for at least 1 week before experimentation. Generating NB7 cells co-overexpressing CD95 and CD95L cDNAs (**Figure 4.9A**) was done by plating 100,000 NB7 cells and infecting them first with 1 mL of empty pLenti or pLenti-CD95L-WT with 8  $\mu\text{g}/\text{ml}$  polybrene followed by puromycin selection and then, after selection was complete, super-infecting these cells with 1 mL of either empty pLNCX2 or pLNCX2-CD95 retroviral supernatants with 8  $\mu\text{g}/\text{ml}$  polybrene. Media was replaced day after infection and selection was done with 200  $\mu\text{g}/\text{ml}$  G418 the following day.

MCF-7 cells overexpressing CD95 cDNAs (**Figure 3.3F and G**) were generated by seeding cells at 100,000 per well in a 6-well plate followed by infection with 3 mL of empty pLNCX2, pLNCX2-CD95, or pLNCX2-CD95R6MUT cleared viral supernatant in the presence of 8  $\mu\text{g}/\text{ml}$  polybrene followed by selection with 200  $\mu\text{g}/\text{ml}$  G418.

The HeyA8 cells used in **Figure 3.8D** and **Figure 3.9** carried a lentiviral Venus-siL3 sensor vector as described previously<sup>381</sup>; these cells were also infected with NucLight Red lentivirus

(Essen Bioscience #4476) with 8 µg/ml polybrene at a Multiplicity of Infection (MOI) of 3. Selection was done with 3 µg/ml puromycin and then sorted for high Venus expression 48 hours later.

HeyA8  $\Delta$ shR6 clone #2 over-expressing the conjugate Venus-CD95L reporter construct (**Figure 3.8A to C and H**) were generated by infecting 50,000 cells seeded on a 6-well plate with 0.5 mL CD510B-Venus-CD95L lentiviral supernatant with 8 µg/ml polybrene. Media was replaced the next day, and cells were sorted for high Venus expression 48 hours later. NB7 cells over-expressing either the Venus-CD95L sensor or the Venus-CD95 reporters were generated in a similar manner (**Figure 3.20A**).

### **Generation of Deletion and Knock Out Clones with CRISPR**

Clones harboring homozygous deletions of si/shRNA target sites and entire genes were generated by designing CRISPR guide RNAs (g)RNAs that will recruit Cas9 to sites upstream and downstream of the target site to be deleted. The CRISPR gRNAs were based off a conjugate design that combines both the scaffold trans-activating RNA and the CRISPR RNA, which contains the targeting sequence<sup>384</sup>. These gRNAs were synthesized as dsDNA gene blocks from IDT and consisted of the sequence 5'-TGTACAAAAAAGCAGGCTTTAAAGGAACCAATTCAGTCGACTGGATCCGGTACCAAGGTCGGGCAGGAAGAGGGCCTATTTCCCATGATTCTTCATATTTGCATATACGATACAAGGCTGTTAGAGAGATAATTAGAATTAATTTGACTGTAAACACAAAGATATTAGTACAAAATACGTGACGTAGAAAGTAATAATTTCTTGGGTAGTTTGCAGTTTTAAAATTATGTTTTAAAATGGACTATCATATGCTTACCGTAACTTGAAAGTATTTTCGATTTCTTGGCTTTATATATCTTGTGGAAAGGACGAAACACCG

NNNNNNNNNNNNNNNNNNNNNGTTTTAGAGCTAGAAATAGCAAGTTAAAATAAGGCT  
 AGTCCGTTATCAACTTGAAAAAGTGGCACCGAGTCGGTGCTTTTTTTCTAGACCCAG  
 CTTTCTTGACAAAGTTGGCATT-3'. The poly-NNNNNNNNNNNNNNNNNNNNNNNN  
 represents the 19nt target sequence.

The two 19nt target sequences for excision of the shL3 site in CD95L ( $\Delta$ 41 deletion) were 5'-CCTTGTGATCAATGAAACT-3' and 5'-GTTGTTGCAAGATTGACCC-3'. The two target sequences for the  $\Delta$ 227 deletion of the shR6 site in CD95 were 5'-GCACTTGGTATTCTGGGTC-3' and 5'-TGTTTGCTCATTTAAACAC-3'. The two target sequences for  $\Delta$ 64 deletion of the siL3 site in CD95L were 5'-TAAAACCGTTTGCTGGGGC-3' and 5'-TATCCCCAGATCTACTGGG-3'. The two target sequences for the deletion of the entire CD95 gene were 5'-GTCAGGGTTCGTTGCACAAA-3' and 5'-TGCTTCTTGGATCCCTTAGA-3'. The CRISPR gRNA algorithm found at <http://crispr.mit.edu/> was used to find candidate target sequences; only gRNAs with scores over 50 were used.

Efficiency of the gRNAs were first tested in 293T cells. Briefly, 400,000 cells were seeded per well on a 6-well plate the day prior to transfection. Each well was transfected with 940 ng of Cas9-GFP plasmid (pMJ920)<sup>385</sup> and 75 ng of each gRNA using 10  $\mu$ L Lipofectamine 2000 according to the manufacturer's protocol. Media was replaced next day, and two days later, genomic DNA was isolated. PCR using the Choice Taq Blue mastermix system (Denville Scientific #CB4065-8) was used to amplify the DNA sequence surrounding the deletion site to determine whether the expected deletion occurred. Both a primer pair flanking the region to be deleted and another pair containing one of the flanking primers and one internal primer were used. For detection of the  $\Delta$ 41 deletion of the shL3 site, the flanking external primers were 5'-



TCTGGAATGGGAAGACACCT-3' (Fr primer) and 5'- CCTCCATCATCACCAGATCC-3' (Rev primer), and the internal Rev primer was 5'-ATATACAAAGTACAGCCCAGT-3'. For detection of the  $\Delta 227$  deletion of the shR6 site, the flanking external primers were 5'-GGTGTCATGCTGTGACTGTTG-3' (Fr primer) and 5'-TTTAGCTTAAGTGGCCAGCAA-3' (Rev primer), and the internal Rev primer was 5'-AAGTTGGTTTACATCTGCAC-3'. For detection of the  $\Delta 64$  deletion of the siL3 site, the flanking external primers were 5'-CTTGAGCAGTCAGCAACAGG-3' (Fr primer) and 5'-CAGAGGTTGGACAGGGAAGA-3' (Rev primer), and the internal Rev primer was 5'-ATATGGGTAATTGAAGGGCTG-3'. For the  $\Delta 41$  shL3,  $\Delta 227$  shR6, and the  $\Delta 64$  siL3 sites, deletion was detected by the flanking primers amplifying a stretch of DNA shorter than the wild type locus. For detection of the CD95 gene deletion, a primer pair was designed to flank the CD95 gene; these primer sequences were 5'-TGTTTAATATAGCTGGGGCTATGC-3' (Fr primer) and 5'-TGGGACTCATGGGTAAATAGAAT-3' (Rev primer). An internal reverse primer (5'-GACCAGTCTTCTCATTTTCAGAGGT-3') and forward primer (5'-TTACTTGTGTTTACCACGTTGCTT-3') was also designed. In this case, the flanking primers are too far apart to amplify when the CD95 is present. However, when CD95 is deleted, the flanking primers are brought close enough together to produce a PCR product.

After verifying the gRNAs resulted in successful deletion, the gRNA gene blocks were sub-cloned into pSC-B-amp/kan plasmids using the StrataClone Blunt PCR Cloning kit (Agilent Technologies #240207) according to the manufacturer's protocol so that the gRNAs could be maxiprep'd (Qiagen) to produce enough material for multiple experiments. Also, plasmid DNA

has higher transfectability than linearized DNA<sup>386</sup>, which would presumably increase the efficiency of CRISPR-mediated deletions.

To generate clones with homozygous deletions, 400,000 293T cells, 400,000 HeyA8 cells, and 250,000 MCF-7 cells were seeded on a 6-well plate. These cells were then transfected with 940 ng of pMJ920 Cas9-GFP plasmid and 450 ng of each pSC-B-gRNA plasmids using Lipofectamine 2000 (10  $\mu$ L for 293T, 7  $\mu$ L for HeyA8, and 10  $\mu$ L for MCF-7 cells). Media was changed the next day, and the cells were then sorted (BD FACSAria SORP system) for top 50% GFP expression to isolate cells that were successfully transfected with the pMJ920 Cas9-GFP plasmid. The cells were then cultured for about a week to let them recover and then sorted by FACS (BD FACSAria SORP system) directly into 96-well plates containing a 1:1 ratio of fresh media:conditioned media for single cell cloning. Approximately two to three weeks later, genomic DNA was isolated from clones and amplified using the external flanking primer pair and the flanking/internal primer pair. Homozygous deletion of the si/shRNA target sites generated a smaller deletion band with the flanking primers and no band with the flanking/internal primers. Deletion of the entire CD95 gene was detected by successful amplification using the flanking external primers and a lack of product with the internal primer pair. After screening the clones with PCR, Sanger sequencing was performed to confirm that the proper deletion had occurred. Three clones were pooled for each si/shRNA target site deletion in 293T and HeyA8 cells (unless otherwise indicated) except for HeyA8  $\Delta$ shR6, for which only clone #11 showed homozygous deletion of the shR6 site (**Figure 3.5A to E**); clones #1 and 2 were not complete shR6 deletion mutants, but frame-shift mutations did occur in each non-deleted allele (as in clone #11) making them CD95 knock out clones as depicted in **Figure 3.7**. Successful homozygous deletion of CD95

was also achieved in MCF-7, and two clones were generated—F2 and FA4. Two shR6 deletion clones were also isolated in MCF-7 cells—clones #3 and #21 (**Figure 4.3**).

### Assessing Toxicity of Over-Expressing CD95L cDNA

To assess the toxicity of CD95L cDNA over-expression, cells were infected with empty pLenti, pLenti-CD95L-WT, pLenti-CD95L<sup>MUT</sup>, or pLenti-CD95L<sup>MUT</sup>NP lentiviral supernatant in the presence of 8 µg/ml polybrene overnight. HeyA8 ΔshR6 clone #11 (**Figure 4.1A; right panel**) and MCF-7 cells (**Figure 4.3F**) were seeded at 75,000 in a 6-well plate and infected with 0.5 and 1 mL of viral supernatant per well, respectively. NB7 expressing empty pLNCX2 or pLNCX2-CD95 (**Figure 4.9B**) were seeded at 100,000 cells per well in a 6-well plate and infected with 0.5 mL empty pLenti or pLenti-CD95L lentiviruses per well. HCT116 parental, HCT116 Droscha<sup>-/-</sup>, and HCT116 Dicer<sup>-/-</sup> cells were seeded at 500,000 cells per well in a 6-well plate and infected with 0.5 mL of viral supernatant (**Figure 4.4A and B and Figure 4.7A and B**).

The media was changed the next day after infection and selected with 3 µg/ml either that evening or the following day. The infected cells were plated on a 96-well plate 1 day after selection in the presence of 3 µg/ml puromycin (uninfected cells were all dead after 1 day in presence of puromycin). Their growth was monitored using the IncuCyte.

To assess toxicity of over-expressing CD95L cDNAs when apoptosis is blocked (**Figure 4.1A; left and center panels**), HeyA8 parental cells were seeded at 750 cells per well on a 96-well plate (50 µL of media per well) and infected with the empty pLenti and pLenti-CD95L lentiviruses using 50 µL of virus (enough virus to ensure 100% infection) in the presence of 8 µg/ml polybrene and 20 µM zVAD-fmk overnight; media was changed next day in the presence of 20 µM zVAD-

fmk or DMSO as a control. Next day, 3 µg/ml of puromycin was added. Cell growth was monitored using the IncuCyte starting at the addition of the viral supernatants.

To quantify expression of the CD95L wild type and mutant cDNA constructs, parental HeyA8 cells were plated at 75,000 in a 6-well plate followed by infection with 1 mL of the corresponding lentiviral supernatant in the presence of 8 µg/ml polybrene and 20 µM zVAD-fmk overnight. Next day, the media was replaced with fresh media supplemented with 20 µM zVAD-fmk. The following day, 3 µg/ml of puromycin was added. After two days, of selection, total RNA and protein were isolated for RT-qPCR and Western blot (**Figure 4.1B**).

#### **Knock Down of CD95 and CD95L with shRNAs**

Cells were infected with the following pLKO.1 MISSION Lentiviral Transduction Particles (Sigma): pLKO.1-puro non-targeting (scramble control) shRNA particles (Sigma-Aldrich #SHC002V), 8 non-overlapping shRNAs against human CD95L mRNA, TRCN0000058998 (shL1: GCATCATCTTTGGAGAAGCAA), TRCN0000058999 (shL2: CCCATTTAACAGGCAAGTCCA), TRCN0000059000 (shL3: ACTGGGCTGTACTTTGTATAT), TRCN0000059001 (shL4: GCAGTGTTCAATCTTACCAGT), TRCN0000059002 (shL5: CTGTGTCTCCTTGTGATGTTT), TRCN0000372231 (shL6: TGAGCTCTCTCTGGTCAATTT), TRCN0000372232 (shL2': TAGCTCCTCAACTCACCTAAT), and TRCN0000372175 (shL5': GACTAGAGGCTTGCATAATAA), and 9 non-overlapping shRNAs against human CD95 mRNA, TRCN0000218492 (shR2: CTATCATCCTCAAGGACATTA), TRCN0000038695

(shR5: GTTGCTAGATTATCGTCCAAA), TRCN0000038696 (shR6:  
 GTGCAGATGTAAACCAAACCTT), TRCN0000038697 (shR7:  
 CCTGAAACAGTGGCAATAAAT), TRCN0000038698 (shR8:  
 GCAAAGAGGAAGGATCCAGAT), TRCN0000265627 (shR27':  
 TTTTACTGGGTACATTTTATC), TRCN0000255406 (shR6':  
 CCCTTGTGTTTGGAATTATAA), TRCN0000255407 (shR7':  
 TTAAATTATAATGTTTGACTA), and TRCN0000255408 (shR8':

ATATCTTTGAAAGTTTGTATT). Infection of cells was carried out according to the manufacturer's protocol (**Figure 3.1A, Figure 3.5F and H, Figure 3.8F, Figure 3.10A and D, Figure 3.11A and D, and Figure 3.18**). In brief, 50,000 to 100,000 cells were seeded in a 6-well plate. The following day, media was replaced with 1 mL of fresh media and cells were infected with each lentivirus at a MOI of 3 in the presence of 8 µg/ml polybrene overnight. Media was changed the next day. Selection with 3 µg/ml puromycin was started the following day and was complete by 48 hours (or until puromycin killed all the non-infected control cells). At this point, the cells would be plated or harvested for downstream experimentation or processing.

For infection of NB7 cells over-expressing pLenti-CD95L cDNAs with pLKO lentiviral particles as in **Figure 3.3C and D**, cells were seeded at 50,000 per well on a 6-well plate (**Figure 3.3C**) or 5,000 per well on a 24-well plate (**Figure 3.3D**) and infected with a MOI of 20 to ensure complete infection, as both the pLKO and pLenti vectors contain a puromycin-resistance cassette. For infection of MCF-7 cells over-expressing pLNCX2-CD95 cDNAs with pLKO lentiviruses as in **Figure 3.3G**, cells were seeded at 15,000 per well on a 24-well plate and infected with the lentiviral particles at a MOI of 3. Media was changed the next day, and selection was done with 3

$\mu\text{g/ml}$  puromycin the afternoon. Infection of HCT116, *Drosha*<sup>-/-</sup>, and *Dicer*<sup>-/-</sup> cells, as done to generate the data in **Figure 3.8E**, was done by seeding 100,000 per well in a 24-well plate and infecting with the shRNA lentiviral particles at a MOI of 3. Media was changed the next day, and selection with 3  $\mu\text{g/ml}$  puromycin was started the following day and considered complete when all uninfected cells were dead. Infections done in 24-well plate used 0.5 mL of media during infection.

After selection, cells were plated either on a 96-well plate for time-course experiments in the IncuCyte or plated in a larger well for Western blot, RT-qPCR, PI staining, or other downstream processing in the presence of puromycin.

### **Dox-Induced shRNA Knock Down**

50,000 to 100,000 cells were seeded per well in a 6-well plate and infected the following day with 1 mL pTIP-shRNA (**Figure 3.2D**, **Figure 3.5G**, **Figure 3.10A**, and **Figure 3.11C**) or pTIG-shRNA (**Figure 3.4**) lentiviral supernatant in the presence of 8  $\mu\text{g/ml}$  Polybrene. Media was replaced next day, and selection with 3  $\mu\text{g/ml}$  puromycin was done the following day. For pTIG-infected cells, selection was done by sorting green cells via FACS. For infection with the LT3REPIR-shRNA lentiviruses (**Figure 3.2B and C**), cells were plated, infected and selected as described above for pTIP-shRNA viruses. Induction of shRNA expression was achieved by adding 100 ng/ml Dox to the cell suspension right before plating for an experiment.

### **Transfection with Short Oligonucleotides**

The siRNAs used in this work were purchased from Dharmacon (**Figure 3.1A**, **Figure 3.5I**, and **Figure 3.10D**) or custom-synthesized by IDT (**Figure 3.8A to D, G, and H**, **Figure 3.9**,

and **Figure 3.16B**) as sense and antisense RNA oligos and annealed. The sense RNA oligonucleotides had two 3' deoxy-T overhangs. The antisense RNA oligos were 5'-phosphorylated and had two 3' deoxy-A overhangs.

The siRNAs targeting CD95L (and controls) were as follows: siScr or Non-Targeting (NT) (sense: UGGUUUACAUGUUGUGUGA), siL1 (sense: UACCAGUGCUGAUCAUUUA), siL2 (sense: CAACGUAUCUGAGCUCUCU), siL3 (sense: GCCCUUCAAUUACCCAUAU), siL4 (sense: GGAAAGUGGCCCAUUUAAC), and siL3MUT (sense: GGACUUCAACUAGACAUCU). The siL3 DNA oligos (sense: GCCCTTCAATTACCCATAT) and siScr DNA oligos (sense: TGGTTTACATGTTGTGTGA) were used in **Figure 3.8B**. The blunt-end siL3 and siScr RNA oligos without the two 3' deoxy-T or -A overhangs and the siL2 and siL3 RNA oligos modified with Cy5-labelled 5' or 3' ends (IDT) were used in **Figure 3.8C**. The Dicer-substrate siRNA (Dsi)RNA used in **Figure 3.1A and B** were purchased from IDT and consisted of Dsi13.X (sense RNA oligo: CAGGACUGAGAAGAAGUAAAACcdGdT, antisense RNA oligo: ACGGUUUUACUUCUUCUCAGUCCUGUA), DsiL3 (sense RNA oligo: CAGCCCUUCAAUUACCCAUAUCCdCdC, antisense RNA oligo: GGGGAUAUGGGUAAUUGAAGG GCUGCU), Dsi-13.2 (sense RNA oligo: AUCUUACCAGUGCUGAUCAUUUAdTdA, antisense RNA oligo: UAUAAAUGAUCAGCACUGGUAAGAUUG), Dsi-13.3 (sense RNA oligo: AAAGUAUACUCCGGGGUCAAUcdTdT, antisense RNA oligo: AAGAUUGACC CCGGAAGUAUACUUUGG), Dsi-13.9 (sense RNA oligo: CUUCCGGGGUCAAU CUUGCAACAdAdC, antisense RNA oligo: GUUGUUGCAAGAUUGACC CCGGAAGUA), and a non-targeting DsiRNA control Dsi-NC1 (Sense: CGUAAUCGCGUAUAAUA CGCGUdAdT, antisense: AUACGCGUAUUUAUACGCGAUUAACGAC, IDT #51-01-14-03).

Pre-designed siRNA SmartPools (Dharmacon) used in **Figure 3.10C** and **Figure 3.12B and C** consisted of 4 On-Targetplus siRNAs, which contain chemical modifications in the passenger strand and in the seed sequence of the guide strand to mitigate sOTE. The following SmartPools were used: L-014208-02 (NUCKS1); L-012212-00 (CAPZA1); L-018339-00 (CCT3); L-013615-00 (FSTL1); L-011548-00 (FUBP1); L-017242-00 (GNB1); L-014597-01 (NAA50); L-020893-01 (PRELID3B); L-019719-02 (SNRPE); L-003941-00 (TFRC); L-006630-00 (HIST1H1C). On-Targetplus non-targeting control pool (D-001810-10) was used as a control.

Knock down of human AGO2, as done in **Figure 4.10**, was also achieved with a pool of 4 On-Targetplus siRNAs (Dharmacon #L-004639-00-0005).

HeyA8 cells and cells derived from HeyA8 cells were seeded at 750 to 1000 cells per well on a 96-well plate one day before transfection. Cells were transfected with 0.1  $\mu$ l of Lipofectamine RNAiMAX reagent per well according to the manufacturer's recommendation. HCT116 cells, HCT116 Dicer<sup>-/-</sup>, and HCT116 Drosha<sup>-/-</sup> cells were seeded at 3000 to 4000 cells per well on a 96-well plate. The following day, 0.2  $\mu$ l of Lipofectamine RNAiMAX was used for transfection according to the manufacturer's recommendation. Transfection efficiency was assessed by transfecting cells with 25 nM siGLO Red (Dharmacon) followed by flow cytometric analysis to ensure equal transfection, as shown in **Figure 3.8G** (*inset*). Transfection experiments done in larger vessels (i.e. 6-well plate) were scaled up according to the manufacturer's recommendation.

Media was changed the day after transfection for all experiments. For 96-well plate experiments, the cells were analyzed in the IncuCyte beginning at the time of transfection. For all experiments involving larger vessels, cells were expanded following transfection and media changed before analysis.



### **Treatment with Recombinant CD95L Protein**

NB7 cells were seeded at 500 cells per well in a 96-well plate and infected with the Sigma scrambled pLKO or pLKO-shL1 lentiviral particles at an MOI of 50 (to achieve 100% transduction efficiency under conditions omitting the puromycin selection step) with 8 µg/ml polybrene and 100 ng/ml of S2 CD95L or LzCD95L for 16 hrs. NB7 cells were used because they lack caspase-8 expression and are resistant to apoptosis<sup>387</sup>. The next day, fresh media was added containing varying amounts of the recombinant CD95L proteins and growth was monitored in the IncuCyte using confluency as a surrogate for growth, as indicated in **Figure 3.3A**.

### **Reverse Transcription Quantitative PCR**

QIAzol Lysis reagent (QIAGEN) was added to cell pellets or directly to plated cells to form a cell lysate, and the miRNeasy kit (QIAGEN) was used to extract total RNA. High-Capacity cDNA reverse Transcription kit (Applied Biosystems #4368814) was used to generate cDNA from 200 ng of total RNA using random primers and a thermocycle profile of 25°C for 10 min (step one), 37°C for 120 min (step two), and 85°C for five min (step three), according to the manufacturer's protocol. The cDNA was then diluted 1:5 with water. RT-qPCR reaction mixtures used the Taqman Gene expression master mix (ThermoFisher Scientific #4369016) and ThermoFisher Scientific gene expression probes according to the manufacturer's protocol; reactions were performed in technical triplicates. Ct values were determined using the Applied Biosystems 7500 Real Time PCR system with a thermocycle profile of 50°C for two min (step one), 95°C for 10 min (step two), and then 40 cycles of 95°C for 15 s (step three) and 60°C for 1 min (step four). The  $\Delta\Delta C_t$  values between the gene of interest and the control were calculated to

determine relative abundance of mRNAs. The primer/probes used were from ThermoFisher Scientific and were as follows: GAPDH (Hs00266705\_g1; used as a control), human CD95 for **Figure 3.18** and **Figure 4.9A** (Hs00163653\_m1) and for **Figure 4.3C** (Hs00531110\_m1 and Hs00236330\_m1), human CD95 3'UTR in **Figure 3.5F** (custom probe, Fr primer: GGCTAACCCCACTCTATGAATCAAT, Rev primer: GGCCTGCCTGTTCAGTAACT, Probe: CCTTTTGCTGAAATATC), human CD95L for **Figure 4.1B** and **Figure 4.9A** (Hs00181225\_m1), the shL3 target site in CD95L in **Figure 3.5D** (custom probe, Fr primer: GGTGGCCTTGTGATCAATGAAA, Rev primer: GCAAGATTGACCCCGGAAGTATA, Probe: CTGGGCTGTACTTTGTATATT), and downstream of the shL3 site in **Figure 3.5D** (custom probe, Fr primer: CCCCAGGATCTGGTGATGATG, Rev primer: ACTGCCCCCAGGTAGCT, Probe: CCCACATCTGCCCAGTAGT).

Custom RT-qPCR probes designed to specifically detect small RNA species were used to detect CD95L fragments in **Figure 4.7B**. These probes were designed using ThermoFisher's Custom TaqMan Small RNA Assay Design Tool (<https://www.thermofisher.com/order/custom-genomic-products/tools/small-rna/>) to target the cluster 8 sequence (5'-AAGGAGCTGGCAGAACTCCGAGA-3') and the cluster 21 sequence (5'-TCAACGTATCTGAGCTCTCTC-3'). Detection of these fragments involves a two-step amplification protocol used to detect miRNAs. In the first step, the High-Capacity cDNA reverse Transcription kit is used to selectively reverse transcribe the two clusters to be quantified using specific primers and the thermocycle profile 16°C for 30 min (step one), 42°C for 30 min (step two), and 85°C for five min (step three). The cDNA is diluted 1:5. The RT-qPCR reaction mixture is composed of the diluted cDNA, the custom probes, and the Taqman Universal PCR Master Mix

(Applied Biosystems #43240018). Reactions were performed in triplicate. Ct values were determined using the Applied Biosystems 7500 Real Time PCR system with a thermocycle profile of 50°C for two min (step one), 95°C for 10 min (step two), and then 40 cycles of 95°C for 15 s (step three) and 60°C for 1 min (step four). The  $\Delta\Delta C_t$  values between the small RNA of interest and the control were calculated to determine relative abundance of the small RNA. In this case, the control was Z30 (#4427975 ThermoFisher Scientific).

To perform the arrayed RT-qPCR (**Figure 3.11**), total RNA was extracted and used to make cDNA as described before. For Taqman Low Density Array (TLDA) profiling, custom-designed 384-well TLDA cards (Applied Biosystems #43422489) were used and processed according to the manufacturer's instructions. Briefly, 50  $\mu$ L cDNA from each sample (200 ng total input RNA) was combined with 50  $\mu$ L TaqMan Universal PCR Master Mix (Applied Biosystems) and hence a total volume of 100  $\mu$ L of each sample was loaded into each of the 8 sample loading ports on the TLDA cards that were preloaded with assays from ThermoFisher Scientific for human GAPDH control (Hs99999905\_m1) and for detection of ATP13A3 (Hs00225950\_m1), CAPZA1 (Hs00855355\_g1), CCT3 (Hs00195623\_m1), FSTL1 (Hs00907496\_m1), FUPB1 (Hs00900762\_m1), GNB1 (Hs00929799\_m1), HISTH1C (Hs00271185\_s1), NAA50 (Hs00363889\_m1), NUCKS1 (Hs01068059\_g1), PRELID3B (Hs00429845\_m1), SNRPE (Hs01635040\_s1), and TFRC (Hs00951083\_m1) after the cards reached room temperature. The RT-qPCR reactions were performed using Quantstudio 7 (ThermoFisher Scientific). Since each of the ports load each sample in duplicates on the TLDA card and because two biological replicates of each sample were loaded onto two separate ports, quadruplicate Ct values were obtained for

each sample. Again, the  $\Delta\Delta C_t$  values were calculated between the gene of interest and the GAPDH control to determine relative abundance.

### **Western Blot Analysis**

Protein extracts were collected by lysing cells with RIPA lysis buffer (50mM Tris-HCl, pH 8.0, 150mM NaCl, 1% (W/V) Sodium dodecyl sulfate (SDS), 1% (V/V) Triton X-100, 1% (W/V) deoxycholic acid) supplemented with PMSF and 1 protease inhibitor cocktail tablet (1 tablet per 10 mL). Chromatin was sheared by running lysate through a 27.5 gauge needle and then boiled at 95°C for 5 min. Protein concentration was quantified using the DC Protein Assay kit (Bio-Rad). 15 to 30  $\mu$ g of protein was mixed with 10  $\mu$ L of 5x sample buffer (250 mM Tris-HCl, pH 6.8, 10% SDS, 30% (v/v) Glycerol, 10 mM DTT, 0.05% (w/v) Bromophenol Blue) to achieve a final volume of 50  $\mu$ L and were resolved on 8 to 12% SDS-PAGE gels at 100 V and transferred to nitrocellulose membranes (Protran, Whatman) overnight at 25 mA. Membranes were incubated with blocking buffer (5% non-fat milk in 0.1% TBS/Tween-20) for 1 hour at room temperature. Membranes were then incubated with the primary antibody diluted in blocking buffer over night at 4°C. Membranes were washed 3 times with 0.1% TBS/Tween-20. Secondary antibodies were diluted in blocking buffer and applied to membranes for 1 hour at room temperature. After 3 more additional washes, detection was performed using the ECL reagent (Amersham Pharmacia Biotech) and visualized with the chemiluminescence imager G:BOX Chemi XT4 (Synoptics).

### **CD95 Surface Staining**

Cell surface CD95 expression was quantified in **Figure 3.7D** and **Figure 4.3D**. Cell pellets of about 300,00 cells were resuspended in about 100  $\mu$ L of PBS on ice. After resuspension, 5  $\mu$ L of either anti-CD95 primary antibody (BD #556640) conjugated with fluorescein isothiocyanate (FitC), or the matching Isotype control (BD #551954), Mouse IgG1  $\kappa$  conjugated with FitC, were added. Cells were incubated on ice at 4°C, in the dark, for 25 minutes, washed twice with PBS, and percent green cells were determined by flow cytometry (Becton, Dickinson).

### **Cell Death Quantification with PI Staining**

Media was collected along with trypsinized cells (~500,000 cells) and washed with PBS. The pellet was resuspended in 0.1% sodium citrate, pH 7.4, 0.05% Triton X-100, and 50  $\mu$ g/ml PI stain. After resuspension, cells were incubated 2 to 4 hours in the dark at 4°C. The percent of subG1 nuclei (fragmented DNA) was determined by flow cytometry (Becton, Dickinson). As an additional measure, reactive oxygen species were also detected using 2',7'-dichlorodihydrofluorescein diacetate (ThermoFisher Scientific #D399) according to the manufacturer's instructions.

### **Assessing Cell Growth and Fluorescence Over Time**

After treatment/infection, cells were seeded at 500 to 4,000 per well in a 96-well plate in at least in triplicate. 750 cells per well for HeyA8 cells, 2000 to 4000 cells per well for HCT116 cells, 800 to 900 cells per well for NB7 cells, 1500 cells per well for 293T cells, and 2000 to 4000 cells per well for MCF-7 cells were plated on a 96-well plate. Images were captured at indicated

time points using the IncuCyte ZOOM live cell imaging system (Essen BioScience) with a 10x objective lens. Percent confluence, red object count, and the green object integrated intensity were calculated using the IncuCyte ZOOM software (version 2015A).

### **RNA-Seq Analysis to Find Deregulated Genes Upon Toxic shRNA or CD95L Expression**

The samples for the RNA-Seq represented in **Figure 3.10A and D** were produced as follows: HeyA8  $\Delta$ shR6 clone #11 cells were infected with Sigma pLKO-shScr or pLKO-shR6 lentiviral particles at a MOI of 3 as described earlier (see section **Knock Down of CD95 and CD95L with shRNAs**). A pool of three 293T  $\Delta$ shL3 clones was infected with either pTIP-shScr or pTIP-shL3 lentiviral supernatants as described earlier (see section **Dox-Induced shRNA Knock Down**). These target site deletion clones were chosen so that the expressed shRNAs would not target CD95 or CD95L, as expression changes that happen independently of CD95/CD95L expression were the focus of this study. After selection with 3  $\mu$ g/mL puromycin was complete (after two days), the pTIP-shScr and pTIP-shL3-infected 293T  $\Delta$ shL3 cells were seeded at 500,000 cells per T175 flask in the presence of 100 ng/mL Dox in duplicate. The pLKO-shScr and pLKO-shR6-infected HeyA8  $\Delta$ shR6 clone #11 cells were plated at 750,000 cells per T175 flask in duplicate. Total RNA was harvested 50 hours and 100 hours after plating with the miRNeasy kit to capture gene expression changes before the onset of DISE and afterward.

The additional samples for the RNA-Seq analyzed in **Figure 3.10D** were produced as follows: Wild type 293T cells were infected with pTIP-shScr or pTIP-shL1 lentiviruses followed by 48 hrs of puromycin selection as described previously (see section **Knock Down of CD95 and CD95L with shRNAs**); total RNA was isolated 100 hrs after plating (in the presence of Dox) in

duplicate in a T175 following puromycin selection. Finally, parental HeyA8 cells were seeded at 250,000 and transfected with RNAiMAX in 6-wells with siScr (NT2) or siL3 oligonucleotides (Dharmacon) at 25 nM. The transfection mix was removed after 9 hours. Total RNA was isolated 48 hours after initial transfection. Total RNA was isolated using the miRNeasy kit.

Analyses shown in **Figure 4.1E to G** were generated from RNA-Seq data gathered from samples prepared in the following manner: HeyA8  $\Delta$ shR6 clone #11 cells were plated at 75,000 cells on a 6-well plate and infected the next day with either empty pLenti or pLenti-CD95L-WT using 0.5 mL lentiviral supernatants per well. Media was changed the following day, and the cells were expanded to a 15 cm dish. Selection with 3  $\mu$ g/mL puromycin began the day after. The next day, the cells were seeded at 600,000 per 15 cm dish in duplicate and RNA extracted 2 days later.

An on-column digestion step using the RNase-free DNase Set (Qiagen #79254) was included for all total RNA samples submitted for RNA-Seq analysis. RNA libraries were generated and sequenced at the Genomics Core facility at the University of Chicago. The quality and quantity of the RNA samples were checked using an Agilent bio-analyzer. All samples had RNA-Seq libraries generated using Illumina TruSEQ Total RNA kits using the Illumina provided protocol (including a RiboZero rRNA removal step). Small RNA-Seq libraries were also generated using Illumina small RNA-Seq kits using the protocol provided by Illumina. Two types of small RNA-Seq sub-libraries were generated: one containing library fragments 150-160 nts in size and one containing library fragments 160-240 nts in size (both including the sequencing adaptor of about 130bp). Both the RNA-Seq and the two small RNA-Seq libraries were generated for the 293T  $\Delta$ shL3 pTIP-shScr/shL3 and HeyA8  $\Delta$ shR6 pLKO-shScr/shR6 samples, whereas only RNA-Seq libraries were generated for the pTIP-shScr/shL1 293T cells and the siL3-transfected HeyA8 cells.

A standard RNA-Seq library was generated for HeyA8  $\Delta$ shR6 clone #11 cells infected with pLenti-CD95L-WT. All libraries were sequenced on an Illumina HiSEQ4000 using Illumina-provided reagents and protocols. The large RNA-Seq libraries were run using paired-end 100 base-pair sequencing, and the small libraries were sequenced using single-read 50 base-pair sequencing.

Adaptor sequences were removed from sequenced reads using TrimGalore ([https://www.bioinformatics.babraham.ac.uk/projects/trim\\_galore](https://www.bioinformatics.babraham.ac.uk/projects/trim_galore)), and the trimmed reads were mapped to the hg38 assembly of the human genome with Tophat and bowtie2. Raw read counts were then assigned to genes using HTSeq. Differential gene expression was analyzed with the R Bioconductor DESeq2 package<sup>388</sup> using shrinkage estimation for dispersions and fold changes to improve stability and interpretability of estimates. P values and adjusted P values were calculated using the DESeq2 package.

To identify differentially expressed RNAs using a method unbiased by genome annotation, the raw 100 nt reads for differential abundance were also analyzed. First, the second end in each paired end read was reverse complemented, so that both reads were on the same strand. Reads were then sorted and counted using the core UNIX utilities sort and uniq. Reads with fewer than 128 counts across all samples were discarded. A table with all of the remaining reads was then compiled, summing counts from each sequence file corresponding to the same sample. The R package edgeR (<http://bioinformatics.oxfordjournals.org/content/26/1/139>) was used to identify differentially abundant reads, and then these reads were mapped to the human genome using blat (<http://genome.cshlp.org/content/12/4/656.abstract>) to determine chromosomal location whenever possible. Homer (<http://homer.salk.edu/homer/>) was used to annotate chromosomal locations with



overlapping genomic elements (such as genes). Raw read counts in each sequence file were normalized by the total number of unique reads in the file.

To identify the most significant changes in expression of RNAs shared between the 293T  $\Delta$ shL3 pTIP-shScr/shL3 and HeyA8  $\Delta$ shR6 pLKO-shScr/shR6 samples between the shScr and shR6 or shL3-infected cells shown in **Figure 3.10A and B**, both methods of RNA-Seq analyses (alignment and read-based) were used to reach high stringency. All samples were prepared in duplicate and for each RNA the average of the two duplicates was used for further analysis. In the alignment-based analysis, only RNAs that had a base mean of >2000 reads and were significantly deregulated between the groups (adjusted p-value <0.05) were considered for further analysis. RNAs were scored as deregulated when they were more than 1.5 fold changed in the shL3-expressing cells at both time points and in the shR6-expressing cells at either time points (each compared to shScr expressing cells) (**Table 3.1.1 and 3.1.2**). This was done because the pLKO-driven expression of shR6 was found to be a lot lower than the pTIP-driven expression of shL3 (see the quantification of the two shRNAs in **Figure 3.16A**). In the read-based analysis, reads were only considered if they had both normalized read numbers of >10 across the samples in each treatment, as well as less than 2 fold variation between duplicates and >1.5 fold change between treatment groups at both time points and both cell lines (**Table 3.1.3 and 3.1.4**). After filtering, reads were mapped to the genome and associated with genes based on chromosomal localization. Finally, all RNAs were counted that showed deregulation in the same direction with both methods. This resulted in the identification of 11 RNAs that were down and 1 that was upregulated in cells exposed to the shRNAs shL3 and shR6 (**Figure 3.10B**).

Differential gene expression in the other RNA-Seq data sets also utilized the alignment-based and read-based methods.

To determine the number of shL3 and shR6 seed matches in the 3'UTR of downregulated genes in **Figure 3.14B**, the 3' UTRs of the 11 mRNAs were extracted from the Homo sapiens gene (GRCh38.p7) dataset of the Ensembl 86 database using the Ensembl Biomart data mining tool. For each gene, only the longest deposited 3'UTR was considered. Seed matches were counted in all 3' UTRs using in-house Perl scripts.

GSEA used in **Figure 3.10D** and **Figure 4.1E** was performed using the GSEA v2.2.4 software from the Broad Institute ([www.http://software.broadinstitute.org/gsea](http://software.broadinstitute.org/gsea)); 1000 permutations were used. The Sabatini survival and non-survival gene lists (**Table 3.2**; described below) were set as custom gene sets to determine enrichment of survival genes versus the non-survival control genes in downregulated genes from the RNA-Seq data; The nominal p-values below 0.05 were considered significantly enriched. The GSEA done in **Figure 4.1E** was generated using RNA-Seq data after genes with a basemean expression below 3 were filtered out to curtail the number of false positives.

The GO enrichment analysis shown in **Figure 3.10F** and **Figure 4.1G** was performed using all genes that after alignment and normalization were found to be at least 1.5 fold downregulated with an adjusted p-values of  $<0.05$ , using the software available on [www.Metaspape.org](http://www.Metaspape.org) and default running parameters.

### Conversion of shL3 and shR6 to siRNAs

Sequencing of the small RNA-Seq libraries allowed us to analyze the exact sequences of the mature siRNAs processed from the shRNAs expressed in the HeyA8  $\Delta$ shR6 pLKO-shR6-infected cells and the 293T  $\Delta$ shL3 pTIP-shL3-infected cells upon treatment with Dox. The most abundant mature siRNA forms were both shifted by one nucleotide, indicating the predominant location of Dicer cleavage (**Figure 3.16A**). Based on this, shL3 and shR6 sequences were converted to transfectable siRNAs, which were used in **Figure 3.16B** to demonstrate that the actual siRNA produced from these shRNAs were toxic. The mRNA target sequence for shL3 (21nt) is 5'-ACUGGGCUGUACUUUGUAUAU-3'. For the shL3 $\Rightarrow$ siL3 sense strand, one G was added before the A on the 5' end while the last U on the 3' end was deleted, and second and third to the last ribonucleotides on the 3' end (UA) were replaced with deoxyribonucleotides for stabilization. For shL3 $\Rightarrow$ siL3 antisense strand, the last three nucleotides on the 5' end (AUA) were deleted and one U and two dTs (UdTdT) were added after the last U on the 3' end. The shL3 $\Rightarrow$ siL3 sense strand is 5'-GACUGGGCUGUACUUUGUAdTdA-3' and antisense strand is 5'-/5Phos/UACAAAGUACAGCCCAGUUdTdT-3'. The shR6 $\Rightarrow$ siRNA was designed in a similar fashion except that two Gs instead of one G were added to the 5' end of the sense strand while UUdTdT instead of UdTdT was added to the 3' end of the antisense strand. The mRNA target sequence for shR6 (21nt) is 5'-GUGCAGAUGUAAACCAAACUU-3'. The shR6 $\Rightarrow$ siR6 sense strand is 5'-GGGUGCAGAUGUAAACCAAAdCdT-3' and antisense strand is 5'-/5Phos/UUUGGUUACAUCUGCACUUdTdT-3'. Annealing the sense and antisense strands produced the final shL3 $\Rightarrow$ siL3 and shR6 $\Rightarrow$ siR6 siRNAs.

### **Purification of Flag-GST-T6B Peptide**

The T6B peptide consists of amino acids 599 to 683 of the GW182 protein TNRC6B and interacts specifically with human AGOs1 to 4, allowing efficient pull-down of RISC and associated RNAs<sup>389</sup>. Two flag-GST-T6B constructs expressed from pGEX-6p1 were received from Markus Hafner's group: wild type flag-GST-T6B, which binds to AGO, and mutant flag-GST-T6B, which harbors five tryptophan to alanine substitutions that destroy its AGO-binding ability. These peptides were isolated following a protocol adapted from Hauptmann *et al*<sup>389</sup>.

The pGEX-6p1-flag-GST-T6B-wt and pGEX-6p1-flag-GST-T6B-mut expression plasmids<sup>389</sup> were transformed into BL21-Gold(DE3)pLysS (Agilent Tech #230123) using heat shock and then plated on ampicillin (100 µg/mL) plates. Colonies were harvested from each plate, and the plasmid sequences were verified. A 10 mL starter culture was inoculated at 37°C containing both 34 µg/mL Chloramphenicol and 100 µg/mL ampicillin with either of the two verified colonies, which was then used to inoculate two 1 L cultures. When the optical density reached ~0.5, 1 mM IPTG was added to induce peptide expression, and the 1 L cultures were transferred to 14°C while shaking at 225 rpm. The next day, the bacteria were pelleted and resuspended in 30 mL cold lysis buffer (PBS, 1 mM AEBSF, 1 mM DTT, and 1 mg/mL lysozyme (ThermoFisher Scientific #89833)) on ice. The suspension was split into separate 1.5 mL eppendorfs and sonicated six times for 10 s each at an amplitude of 35% (Qsonica) and then again an additional five times at 45% until the suspension was clear. The supernatants were cleared via centrifugation at maximum speed at 4°C for 40 min.

The flag-GST-T6B peptides were isolated from the cleared supernatant through gravity-flow column purification using PD-10 columns (Sigma-Aldrich #GE17-0435-01) filled with

glutathione sepharose 4B beads (Sigma-Aldrich #GE17-0756-01). After the supernatant flowed through the column, the beads were washed three times with cold lysis buffer (without lysozyme). The peptide was eluted from the column using elution buffer (Tris, pH 8.0, PBS, and 10 mM glutathione). Finally, the eluted peptide was de-salted using Zeba Spin De-salting columns (ThermoFisher Scientific #89892). Peptide was quantified using the Nanodrop 2000c with an extinction coefficient/1000 of 44.34 and MW of 36.9 kDa for the flag-GST-T6B-mut and an extinction coefficient/1000 of 71.85 and MW of 37.3 kDa for the flag-GST-T6B-wt.

#### **Pull-Down of Human AGO2 in HCT116 and Drosha<sup>-/-</sup> Cells**

The interaction between human AGO2 and T6B in the absence of Drosha was interrogated by performing an AGO2 pull-down with the flag-GST-T6B peptide in wild type HCT116 cells and in Drosha<sup>-/-</sup> HCT116 cells in **Figure 4.5**. Eight million cells were harvested and resuspended in 6 mL NP-40-alternate lysis buffer (20 mM Tris, pH 7.5, 150 mM NaCl, 2 mM EDTA, 1% (v/v) IGEPAL CA-630, 1 mM sodium orthovanadate, 0.5 mM DTT, and 1 mM AEBSF) on ice for 15 min. Cell suspension was then sonicated in 10 s bursts at an amplitude of 35% a total of six times followed by three 20 s bursts at 60% amplitude. Lysate was cleared by centrifugation at 12,000xg for 20 min at 4°C. The lysate was split in two and 200 µg of the flag-GST-T6B-wt or flag-GST-T6B-mut was added to either half along with 60 µL of anti-flag M2 magnetic beads (Sigma-Aldrich #M8823). The lysate was rotated at 4°C for 2 hrs to allow binding to occur. The bound beads were then washed three times with cold NP-40-alternate lysis buffer. 10% of the beads, along with the input samples, were analyzed via Western blot for human AGO2.

### **Pull-Down of Loaded RISC and RNA-Seq of Unbound and Bound Small RNAs**

HeyA8  $\Delta$ shR6 clone #11 were seeded at 75,000 cells per well on 6-well plates, and the HCT116 and HCT116 Drosha<sup>-/-</sup> cells were both seeded at 500,000 per well on 6-well plates. The HeyA8  $\Delta$ shR6 clone #11 cells were infected with 0.5 mL of empty pLenti or pLenti-CD95L-WT viral supernatant per well as described earlier. The HCT116 and HCT116 Drosha<sup>-/-</sup> cells were infected with 0.5 mL empty pLenti or pLenti-CD95L<sup>MUT</sup>NP viral supernatant per well as described earlier (**Figure 4.4 and Figure 4.6**). Medium was changed the next day and the cells were pooled and expanded to multiple 15 cm dishes. Selection with 3  $\mu$ g/mL puromycin began the following day. The next day, the infected HeyA8  $\Delta$ shR6 clone #11 cells were seeded at 600,000 cells in multiple 15 cm dishes; the HCT116 and HCT116 Drosha<sup>-/-</sup> cells were seeded at 5 million cells in multiple 15 cm dishes. This was all done in duplicates. Two days later, each of the samples was pelleted and split in two: one pellet was lysed and processed for small RNA sequencing as in the manner described earlier, and the other pellet was flash frozen in liquid nitrogen. The pellets were stored at -80°C until they could be used for the AGO pull-down experiment. The purpose of splitting the sample was to compare the total cellular pool of small RNAs to the fraction that was bound to the RISC. This way, the processing CD95L-derived fragments from the full-length mRNA in the cytosol to the final mature RISC-bound form could be mapped.

To begin the AGO pull-down experiment, between 10 and 25 million cells were lysed in NP40 lysis buffer (20 mM Tris, pH 7.5, 150 mM NaCl, 2 mM EDTA, and 1% (v/v) NP40) supplemented with phosphatase inhibitors on ice for 15 minutes. The lysate was sonicated three times for 30 s at 60% amplitude (Sonics, VCX130) and cleared by centrifugation at 12,000g for 20 minutes. Human AGOs1 to 4 were pulled down with 500  $\mu$ g of Flag-GST-T6B peptide and

with 60  $\mu$ L anti-Flag M2 magnetic beads (Sigma-Aldrich #M8823) for 2 hrs at 4°C. The pull-down fraction was washed 3 times in NP40 lysis buffer. During the last wash, 10% of beads were removed and incubated at 95°C for 5 minutes in 2x SDS-PAGE sample buffer. Samples were run on a 4-12% SDS-PAGE and transferred to nitrocellulose membrane. The pull-down efficiency was determined by immunoblotting against human AGO1 and AGO2. To the remaining beads, 500  $\mu$ l TRIzol reagent was added and the RNA extracted according to the manufacturer's instructions. The RNA pellet was diluted in 20  $\mu$ l of water.

The RNA samples were split, and half of each sample was dephosphorylated with 0.5 U/ $\mu$ l of CIP alkaline phosphatase (NEB #M0290) at 37°C for 15 min and subsequently radiolabeled with 0.5  $\mu$ Ci  $\gamma$ -<sup>32</sup>P-ATP and 1 U/ $\mu$ l of T4 PNK kinase (NEB #M0201) for 20 min at 37°C. The AGOs1 to 4-interacting RNAs were visualized on a 15% urea-PAGE through autoradiography. The remaining RNA was taken through a small RNA library preparation as previously described<sup>390</sup>. Briefly, RNA was ligated with 3' adenylated adapters and separated on a 15% denaturing urea-PAGE. The RNA corresponding to an insert size of 19-35 nts was eluted from the gel, ethanol precipitated followed by 5' adapter ligation. The samples were separated on a 12% Urea-PAGE and extracted from the gel. Reverse transcription was performed using Superscript III reverse transcriptase (ThermoFisher Scientific #18080093) and the cDNA amplified by PCR. The cDNA was sequenced on Illumina HiSeq 3000. The adapter sequences were as follows: Adapter

1	–	NNTGACTGTGGAATTCTCGGGTGCCAAGG;	Adapter	2	–
		NNACACTCTGGAATTCTCGGGTGCCAAGG,	Adapter	3	–
		NNACAGAGTGGAATTCTCGGGTGCCAAGG,	Adapter	4	–
		NNGCGATATGGAATTCTCGGGTGCCAAGG,	Adapter	47	–

NNTCTGTGTGGAATTCTCGGGTGCCAAGG,	Adapter	48	–
NNCAGCATTGGAATTCTCGGGTGCCAAGG,	Adapter	49	–
NNATAGTATGGAATTCTCGGGTGCCAAGG,	Adapter	50	–
NNTCATAGTGGAATTCTCGGGTGCCAAGG.	RT primer		sequence:
GCCTTGGCACCCGAGAATTCCA;	PCR primer		sequences:

CAAGCAGAAGACGGCATAACGAGATCGTGATGTGACTGGAGTTCCTTGGCACCCGAG AATTCCA. To find all small RNA sequences derived from CD95L, the adaptor sequences were removed from all the reads (all conditions in duplicate) and were BLASTED against the CD95L ORF sequence (HeyA8  $\Delta$ shR6 clone #11 cells infected with pLenti-CD95L-WT; derived from NM\_000639.1) or the CD95L<sup>MUT</sup>NP ORF (HCT116 and HCT116 Drosha<sup>-/-</sup> cells infected with CD95L<sup>MUT</sup>NP). Only reads were considered with an e-value of less than 0.05 and 100% identity across the entire length of the read. This resulted in the loss of a few reads less than 19/20 nts in length. The resulting list of matches were then graphed onto the coordinates of the CD95L mRNA sequence using the plotBed function in the R Sushi library.

### Construction and Functional Validation of pTIP-shRNA Libraries

The pTIP-shRNA libraries were constructed by sub-cloning libraries of 143nt PCR inserts of the form 5'-XXXXXXXXXXXXXXXXXXXXXXXXXXXXXXXXATAGAGATCGNNNNNNNNNN NNNNNNNNNNNNCTCGAGNNNNNNNNNNNNNNNNNNNNNNNNNTTTTTGTACCGAGCTC GGATCCACTAGTCCAGTGTGGGCATGCTGCGTTGACATTGATT-3' into the pTIP-shR6 vector<sup>376</sup> after excising the shR6 insert. The poly-N region represents the 21-mer sense and antisense shRNA hairpin. The intervening CTCGAG is the loop region of the shRNA. The 5



libraries targeting Venus, CD95L ORF, CD95L 3'UTR, CD95 ORF, or CD95 3'UTR were composed of every possible 21-mer shRNA, with each nearest neighbor shRNA shifted by 1 nucleotide (**Figure 3.19A**). These libraries were synthesized together on a chip as 143 nt single-stranded DNA oligos (CustomArray Inc, Custom 12K oligo pool). Each shRNA pool had its own unique 5' end represented by the poly-X region. This allowed selective amplification of a particular pool using 1 of 5 unique Fr primers (CD95L ORF: 5'-TGGCTTTATATATCTCCCTATCAGTG-3', CD95L 3' UTR: 5'-GGTCGTCCTATCTATTATTATTCACG-3', CD95 ORF: 5'-TCTTGTGTCCAGACCAATTTATTTTCG-3', CD95 3'UTR: 5'-CTCATTGACTATCGTTTTAGCTACTG-3', Venus: 5'-TATCATCTTTCATGATGACTTTCCGG-3') and the common reverse primer 5'-AATCAATGTCAACGCAGCAT-3'. Phusion High Fidelity Polymerase (NEB #M0530) was used to amplify each library pool; standard PCR conditions were used with an annealing temperature of 61°C and 15 cycles; a lower number of PCR cycles were used to ensure the reaction was kept in the linear phase to prevent formation of heteroduplex products. PCR reactions were purified using PCR Cleanup kit (QIAGEN). The pTIP-shR6 vector and each of the amplified libraries were digested with BsaBI (NEB #R0537) and SphI-HF (NEB #R3182). Digested PCR products were run on either a 2% Agarose gel or a 20% polyacrylamide (29:1) gel made with 0.5 x TBE buffer. PCR products were extracted using either Gel Extraction kit (QIAGEN) for extraction from Agarose gels or via electro-elution using D-Tube Dialyzer Mini columns (Novagen #71504) for extraction from the polyacrylamide gel. Purified PCR inserts were then ligated to the linearized pTIP vector with T4 DNA ligase for 24 hours at 16°C. The ligation mixtures were transformed via electroporation in MegaX DH10B T1 cells (Invitrogen #C6400)

and plated on 24 cm ampicillin dishes. At least 10 colonies per pool were picked and sequenced to verify insertion of the shRNA-expressing cassette. After verification, all colonies per library were pooled together separately and plasmid DNA extracted using the MaxiPrep kit (QIAGEN). The 5 pTIP-shRNA library DNA preps were used to produce virus in 293T cells as described previously. A schematic outlining the sub-cloning procedure is presented in **Figure 3.19B**.

The RNAi capability of each pTIP-shRNA library was tested in the NB7 Venus-CD95 and NB7 Venus-CD95L reporter cells (**Figure 3.20A**). These cells were seeded at 50,000 cells per well on a 6-well plate the day prior to infection. The NB7 Venus-CD95 cells were infected with the pTIP-shRNA libraries targeting Venus, CD95 ORF, and CD95 3' UTR. The NB7 Venus-CD95L cells were infected with the pTIP-shRNA libraries targeting Venus, CD95L ORF, and CD95L 3' UTR. Infection was done with 8 µg/mL polybrene and 250 µL lentiviral supernatant; a lower amount of supernatant was used than normal to limit the occurrence of multiple viral integrations. Knock down efficiency of the pTIP-shRNA libraries was assessed by monitoring the overall green integrated intensity over time in the IncuCyte.

### **Lethality Screen with pTIP-shRNA Libraries**

NB7 cells were seeded at 1.5 million cells per 145 cm<sup>2</sup> dish. Two dishes were infected with each of the 5 libraries with enough lentiviral supernatant (120 µL per plate) to achieve a transduction efficiency of about 10 to 20%. Media was replaced the next day, followed by selection with 1.5 µg/ml puromycin. After selection was complete, cells infected with the Venus, CD95L ORF, and CD95L 3'UTR-targeting pTIP-shRNA libraries were pooled in a 1:1:1 ratio to make the CD95L cell pool. Likewise, cells infected with the Venus, CD95 ORF, and CD95 3'UTR-targeting

pTIP-shRNA libraries were pooled to make the CD95 receptor cell pool. The CD95 and the CD95L cell pools were plated separately each in 2 sets of duplicates seeded at 600,000 cells per 145 cm<sup>2</sup> dish. One set received 100 ng/ml Dox, and the other one was left untreated (total of 4 dishes per combined pool; 2 received no treatment and 2 received Dox). NB7 cells infected with the different libraries were also plated individually in triplicate with or without Dox on a 96-well plate at 800 cells per well to assess the overall toxicity of each pool in the IncuCyte using cell confluence as a surrogate for growth (**Figure 3.20B**). HCT116 and 293T cells were also infected with the individual subpools as described for NB-7 cells except 300  $\mu$ L per plate of virus was used instead of 120. Cells were then plated on a 96-well plate to measure confluency in the IncuCyte (**Figure 3.21**).

NB7 genomic DNA was collected from each 145 cm<sup>2</sup> dish 9 days after Dox addition. The shRNA barcodes were amplified from the harvested DNA template using NEB Phusion Polymerase using 30 cycles at an annealing temperature of 52°C with 4 different pairs of primers (referred to as N, N+1, N+2, and N+3) in separate reactions per DNA sample. The N pair consisted of the primers originally used to amplify the CD95L ORF library (Fr: 5'-TGGCTTTATATATCTCCCTATCAGTG-3' and Rev: 5'-AATCAATGTCAACGCAGCAT-3'). The N+1 primers had a single nucleotide extension at each 5' end of the N primers corresponding to the pTIP vector sequence (Fr: 5'-TTGGCTTTATATATCTCCCTATCAGTG-3' and Rev: 5'-TAATCAATGTCAACGCAGCAT-3'). The N+2 primers had 2 nucleotide extensions (Fr: 5'-CTTGGCTTTATATATCTCCCTATCAGTG-3' and Rev: 5'-ATAATCAATGTCAACGCAGCAT-3'), and the N+3 primers had 3 nucleotide extensions (Fr: 5'-TCTTGGCTTTATATATCTCCCTATCAGTG-3' and Rev: 5'-

AATAATCAATGTCAACGCAGCAT-3'). The barcodes from the pTIP-shRNA library plasmid preparations were also amplified using Phusion Polymerase with the N, N+1, N+2, and N+3 primer pairs. Extending the number of cycles to 30 did not seem to lead to over-amplification when the template was genomic DNA, unlike when the template is pure synthetic DNA such as an oligo. Because of this, the pure plasmid template was amplified using only 15 cycles to prevent over-amplification.

The shRNA barcode PCR products were purified from a 2% Agarose gel and submitted for 100 bp paired-end deep sequencing (Genomics Core facility at the University of Chicago). DNA was quantitated using the Qubit. The 4 separate PCR products amplified using N, N+1, N+2, and N+3 were combined in equimolar amounts for each sample. Libraries were generated using the Illumina TruSeq PCR-free kit using the Illumina provided protocol. The libraries were sequenced using the HiSEQ4000 with Illumina-provided reagents and protocols. Raw sequence counts for DNAs were calculated by HTSeq. shRNA sequences in the PCR pieces of genomic DNA were identified by searching all reads for the sense sequence of the mature shRNA plus the loop sequence CTCGAG. To avoid a division by zero problem during the subsequent analyses all counts of zero in the raw data were replaced with 1. A few sequences with a total read number <10 across all plasmids reads were not further considered. In the CD95L pool this was only one shRNA (out of 2362 shRNAs) (L792') and in the CD95 20 shRNAs (out of 3004 shRNAs) were not represented (R88, R295, R493, R494, R496, R497, R498, R499, R213', R215', R216', R217', R220', R221', R222', R223', R225', R226', R258', R946', R1197', R423'). While most shRNAs in both pools had a unique sequence two sequences occurred 6 times (L605', L607', L609', L611', L613', L615', and L604', L606', L608', L610', L612', L614'). In these cases, read counts were divided by 6. Two

shRNAs could not be evaluated: 1) shR6 in the CD95 pool. It had a significant background due to the fact that pTIP-shR6 was used as a starting point to clone all other shRNAs. 2) shL3 was found to be a minor but significant contaminant during the infection of some of the samples. For each condition, two technical duplicates and two biological duplicates were available. To normalize reads to determine the change in relative representation of shRNAs between conditions, the counts of each shRNA in a subpool (all replicates and all conditions) was divided by the total number of shRNAs in each subpool (%). First, the mean of the technical replicates (R1 and R2) was taken. To analyze the biological replicates and to determine the changes between conditions, two analyses were performed (**Figure 3.19C and D**): 1) The change in shRNA representation between the cloned plasmid library and cells infected with the library and then cultured for 9 days without Dox (infection -Dox). Fold downregulation was calculated for each subpool as  $[(\text{plasmid \%}/-\text{Dox1 \%} + \text{plasmid \%}/-\text{Dox2 \%})/2]$ . 2) The difference in shRNA composition between the infected cells cultured with and without Dox (infection +Dox). Fold downregulation was calculated for each subpool as  $[(-\text{Dox1 \%}/+\text{Dox1 \%}) + (-\text{Dox1 \%}/+\text{Dox2 \%}) + (-\text{Dox2 \%}/+\text{Dox1 \%}) + (-\text{Dox2 \%}/+\text{Dox2 \%})/4]$ . The reason both analyses were done is because Dox-inducible vectors permit “leaky” expression even in the absence of Dox<sup>391</sup> (**Figure 3.22A**). Only shRNAs were considered that were at least 5-fold underrepresented in either of the two analyses (**Figure 3.22B and Table 3.3**).

### Arrayed siRNA Screen

An arrayed siRNA screen was conducted to determine the level of toxicity associated with each possible 6mer seed sequence permutation. The siRNA backbone has been described previously<sup>392</sup> and is based on a non-targeting control siRNA (antisense strand: 5'-

UCCACAACAUGUAAACCA-3'; two 3' deoxy-T nts for the sense strand; two 3' deoxy-A nts on the antisense strand). A total of four central nts were replaced with complementary nts to eliminate any congruency between the siL3 and the backbone. A 2'-O-methylation at positions one and two of the sense (passenger) strand were added to prevent its incorporation into the RISC<sup>393</sup>. Positions two to seven of the antisense strand (guide RNA) comprise the seed sequence and were replaced with one of the 4096 possible 6mer permutations.

HeyA8 cells were reverse-transfected. Each siRNA was diluted in 30  $\mu$ L of Optimem so the final concentration of siRNA would be 10 nM. This was done in a 384-well plate using Multidrop Combi. Then, the RNAiMAX transfection reagent was diluted (9  $\mu$ L RNAiMAX per 1 mL of Optimem). Following a 5 min incubation at room temperature, 30  $\mu$ L of the diluted RNAiMAX was dispersed to each well containing an siRNA dilution (total volume was 60  $\mu$ L). The solution was mixed by pipetting up and down three times using the PerkinElmer EP3 and left to incubate at room temperature for 20 min. Following an additional round of mixing, 15  $\mu$ L of the RNAiMAX/siRNA Optimem solution was transferred to single well on three new 384-well plates to make triplicates using the PerkinElmer EP3. Each well then received a 50  $\mu$ L suspension of 320 HeyA8 cells (total volume was 65  $\mu$ L). Following a 30 min incubation at room temperature to allow the cells to adhere, the plates were transferred to the 37°C incubator. After 96 hours, cell viability was assessed by the level of cellular ATP content using the CellTiter-Glo (Promega) assay. A total of 35  $\mu$ L of medium was replaced with 30  $\mu$ L of the CellTiter-Glo reagent (Promega #G7570). The plates were shaken for 5 min and incubated at room temperature for 15 min. The luminescence was quantified using the BioTek Synergy NEO2. The toxicity score (sTOX) for each siRNA was calculated as the % viability.

### Assigning a Toxicity Score to Every miRNA

Sequence and conservation information on all annotated human miRNAs was downloaded from TargetScan Human 7.1<sup>131</sup> ([http://www.targetscan.org/vert\\_71/](http://www.targetscan.org/vert_71/)). Targetscan 7.1 partitions the seed sequences into four conservation groups: highly conserved (group #2), conserved (group #1), low conservation but still annotated as a miRNA (group #0), and lowest conservation with the possibility of misannotation (group #-1). The 6mer seed sequences (positions two to seven) of each miRNA arm for groups -1 and 2 were gathered and assigned a sTOX based on the toxicity observed by the corresponding seed in the 4096 siRNA arrayed screen. The distributions of the sTOX scores for the -1 and 2 groups were then compared using the Kolmogorov-Smirnoff test for **Figure 5.4B**.

### Identification of Survival and Nonsurvival Gene Sets

A list of survival genes recently described in a CRISPR/Cas9 lethality screen by the Sabatini group was generated<sup>394</sup>. The “survival genes” used in this study were defined by having a CRISPR score of  $< -0.1$  and an adjusted p-value of  $< 0.05$ . The control group to these top essential genes were the bottom nonessential genes and had an inverse criteria (CRISPR score of  $> 0.1$  and adjusted p-value of  $< 0.05$ ); these are referred to as the "nonsurvival genes" (**Table 3.2**).

### The Toxicity Index (TI) and GC Content Analysis

The TI in **Figure 3.23A** is defined by the sum of the counts of a seed match in the 3' UTRs of critical survival genes divided by the seed match counts in the 3' UTRs of nonsurvival genes. Both counts were normalized for the numbers of genes in each gene set. 3' UTRs were retrieved as described above using Biomart. For the survival genes 1846 and for the nonsurvival genes 416

3' UTRs were found. For each gene, all annotated 3' UTRs were considered. The TI was calculated for each of the 65536 possible 8mers. These numbers were then assigned to the results of the shRNA screen (**Table 3.4**). Two alternate TIs were also calculated by (1) considering only the longest 3' UTR for each gene of the survival and nonsurvival genes and normalizing the number of seed matches in each gene to the length of the 3' UTR and (2) considering only the longest 3' UTR of the most highly expressed (average read count across all control RNA-Seq datasets >1000) ~850 survival genes (identified in the two genome-wide lethality screens in **Figure 3.11B**) and ~850 expression-matched nonsurvival genes (**Figure 3.24B**).

For the analyses in **Figure 3.23C and D**, the GC content % was calculated for every 6mer seed in the CD95L ORF pTIP-shRNA pool. The GC content % was plotted against the log(Fold down) for each shRNA in the CD95L ORF shRNA after infection (compared to the plasmid composition) in **Figure 3.23C** and after addition of Dox (compared to cells infected but not treated with Dox) in **Figure 3.23D**. In **Figure 3.23E**, the log(TI) (in this case, the TI was calculated using 6mer seeds and all available 3' UTRs) and GC content % was extracted for every possible 6mer and plotted. Pearson correlation coefficient and associated p-value were calculated in R3.3.1.

### Sylamer Analysis

Sylamer is a tool to find enrichment or depletion of small words (i.e. seed matches) in the sequences of genes most down or upregulated according to a gene list ranked according to the magnitude and direction of differential expression<sup>126</sup> (<http://www.ebi.ac.uk/research/enright/software/sylamer>). For short stretches of RNA (in this case length 6, 7, and 8 in length corresponding to the lengths of the determinants of seed region binding



in RNAi-type binding events), Sylamer tests, for all possible motifs of this length, whether the motif occurrences are shifted in sequences associated with the list under consideration, typically 3' UTRs when analyzing RNAi-type binding events. A shift or enrichment of such a motif towards the down-regulated end of the gene list is consistent with upregulation of a small guide RNA that has the motif as the seed sequence. Sylamer tests in small increments along the list of genes, using a hypergeometric test on the counts of a given word, comparing the leading part of the gene list to the universe of all genes in the list. Enriched motifs stand out from the background of all motifs tested, as visible in the Sylamer plot. The plot consists of many different lines, each line representing the outcomes of a series of tests for a single word, performed along regularly spaced intervals (increments of 200 genes) of the gene list. Each test yields the log-transformed p-value arising from a hypergeometric test as indicated above. If the word is enriched in the leading interval the log-transformed value has its value plotted on the positive y-axis (sign changed), if the word is depleted the log-transformed value is plotted on the negative y-axis.

3' UTRs were used from Ensembl, version 76. As required by Sylamer, they were cleaned of low-complexity sequences and repetitive fragments using, respectively, Dust<sup>395</sup> with default parameters and the RSAT interface<sup>396</sup> to the Vmatch program, also run with default parameters. Sylamer (version 12-342) was run with the Markov correction parameter set to 4.

## **Statistical Analyses**

Continuous data were summarized as means and standard deviations (except for all IncuCyte experiments where standard errors are shown) and dichotomous data as proportions.

Continuous data were compared using t-tests for two independent groups and one-way ANOVA for 3 or more groups.

For evaluation of continuous outcomes (e.g. cell confluence or integrated fluorescence from IncuCyte measurements) over time, two-way ANOVA was used with one factor for the treatment conditions of primary interest and a second factor for time treated as a categorical variable to allow for non-linearity. Comparisons of single proportions to hypothesized null values were evaluated using binomial tests. Statistical tests of two independent proportions were used to compare dichotomous observations across groups.

The effects of treatment on wild type versus either *Dicer*<sup>-/-</sup> or *Drosha*<sup>-/-</sup> cells were statistically assessed by fitting regression models that included linear and quadratic terms for value over time, main effects for treatment and cell type, and two- and three-way interactions for treatment, cell-type and time. The three-way interaction on the polynomial terms with treatment and cell type was evaluated for statistical significance since this represents the difference in treatment effects over the course of the experiment for the varying cell types.

To test if higher TI is enriched for shRNAs that were highly downregulated, p-values were calculated based on permuted datasets using Mann-Whitney U tests. The ranking of TI was randomly shuffled 10,000 times and the W statistic from our dataset was compared to the distribution of the W statistic of the permuted datasets. Test of enrichment was based on the filtered data of at least 5-fold difference, which was defined as biologically meaningful.

Fisher Exact Tests were performed to assess enrichment of downregulated genes (i.e. >1.5 downregulated with adjusted p-value <0.05) amongst genes with at least one si/shRNA seed match. All analyses were done in Stata 14 or R 3.3.1 in Rstudio.

### **Treatment of Outliers and Research Integrity**

In most cases, potential outliers were counted as part of a dataset, as parametric tests take into account standard error and non-parametric tests are more robust against outliers. Inclusion of deviating data points will, therefore, be the more conservative approach, assuming the statistical test chosen is appropriate. However, in cases, where an individual technical or biological replicate is seen to deviate significantly from the others and/or when there is reason to believe an individual replicate may be compromised (e.g. contamination, temperature fluctuations affecting cell dispersion in wells on the edge of a culture plate, mishandling of samples, etc), then closer scrutiny may be employed. Obviously, this excludes datasets that are composed of a duplicate. In this study, potential outliers were identified as any point lying outside one standard deviation from the mean. This liberal demarcation is balanced by the conservative courses of action the investigator(s) must take when dealing with these potential outliers. There are one of several responses: (1) The outlier is included in the dataset and the appropriate statistical test is used. (2) The outlier is excluded if the experiment is repeated and the same conclusion is supported by both experiments. (3) The outlier is excluded if the dataset containing the outlier is part of a titration analysis consisting of multiple datasets and the conclusion of the experiment would stand even if the entire questionable dataset is excluded.

As a matter of integrity, all critical experiments are repeated more than once, often by different investigators. The number of repeated experiments is indicated in the figure legends.

**Data Availability:** Expression datasets can be accessed with GSE87817 at Gene Omnibus.

### **Chapter 3: Many si/shRNAs can Kill Cancer Cells by Targeting Multiple Survival Genes through an Off-Target Mechanism**

#### **Introduction**

RNAi is used to selectively inhibit expression of a target gene through post-transcriptional gene regulation that relies on the RISC's enzymatic slicer activity to cleave the target mRNA<sup>13</sup> or through it recruiting factors that degrade the mRNA and/or inhibit translation<sup>89</sup>. RNAi is directed against a specific mRNA target according to base-pairing between a small RISC-bound guide RNA (19 to 23 nts) and the target<sup>12,14,15</sup>. Scientists use si/shRNAs as sources of guide RNAs with 100% reverse complementarity to the intended on-target, which results in potent cleavage-mediated RNAi<sup>85</sup>. However, guide RNAs can induce RNAi with much less reverse complementarity. Indeed, mRNA targeting is most dependent on contiguous base-pairing between the guide RNA's seed sequence (positions two to seven/eight) and a site in the target mRNA's 3' UTR<sup>118</sup>. Indeed, this is the basis for metazoan miRNA targeting and is why a single miRNA can regulate hundreds of targets simultaneously. In a similar manner, yet not fully explored, artificial si/shRNAs also direct RNAi through this seed-based targeting, resulting in wide-spread off-targeting<sup>108,169</sup>. This seed-based off-targeting could reveal unappreciated facets of seed-based RNAi in the absence of confounding selective pressures that skew the targeting profile of endogenous miRNAs.

The interaction between CD95 (Fas/APO-1) and the CD95 ligand (CD95L) induces apoptosis<sup>291</sup>, which plays important roles in immune system homeostasis<sup>300,306,307,309</sup> and surveillance<sup>317,318</sup> and organismal development<sup>397,398</sup>. In the context of cancer, the apoptosis-inducing activity of CD95 was originally classified as tumor-suppressive, but more recent studies

have shown CD95 activation actually elicits multiple tumor-promoting activities, including enhancing motility/invasiveness<sup>366</sup>, promoting cell growth<sup>364</sup>, and maintaining the cancer stem cell population<sup>367,368</sup>. The Peter lab demonstrated tumors have a severe growth deficit *in vivo* when the CD95 gene was knocked out<sup>364</sup>. It therefore, seemed consistent with a follow-up study showing that multiple si/shRNAs target CD95 or CD95L are extremely toxic to cancer cells, evoking a novel kind of death best described as multiple death pathways being activated simultaneously. This unique cell death preferentially affects transformed and cancer stem cells and cannot be blocked with standard death pathway inhibitors or via knock-down of any single gene<sup>368,376</sup>.

In this work, si/shRNAs are found to be toxic to cancer cells through an RNAi mechanism that is independent of on-target silencing. Indeed, CD95/CD95L-derived si/shRNAs are toxic to cancer cells by preferentially targeting survival genes through seed-based targeting, which triggers a unique mechanism of cell death, despite the seed sequences of these toxic si/shRNAs being different. Therefore, this unique sOTE is termed Death Induced by Survival gene Elimination (DISE).

## Results

### *si/shRNAs Kill Cells in the Absence of the Targeted Site*

Previously, over 80% of commercially available si/shRNAs designed to target CD95 or CD95L were shown to be toxic to multiple solid tumor cell types<sup>376</sup>. This result was validated

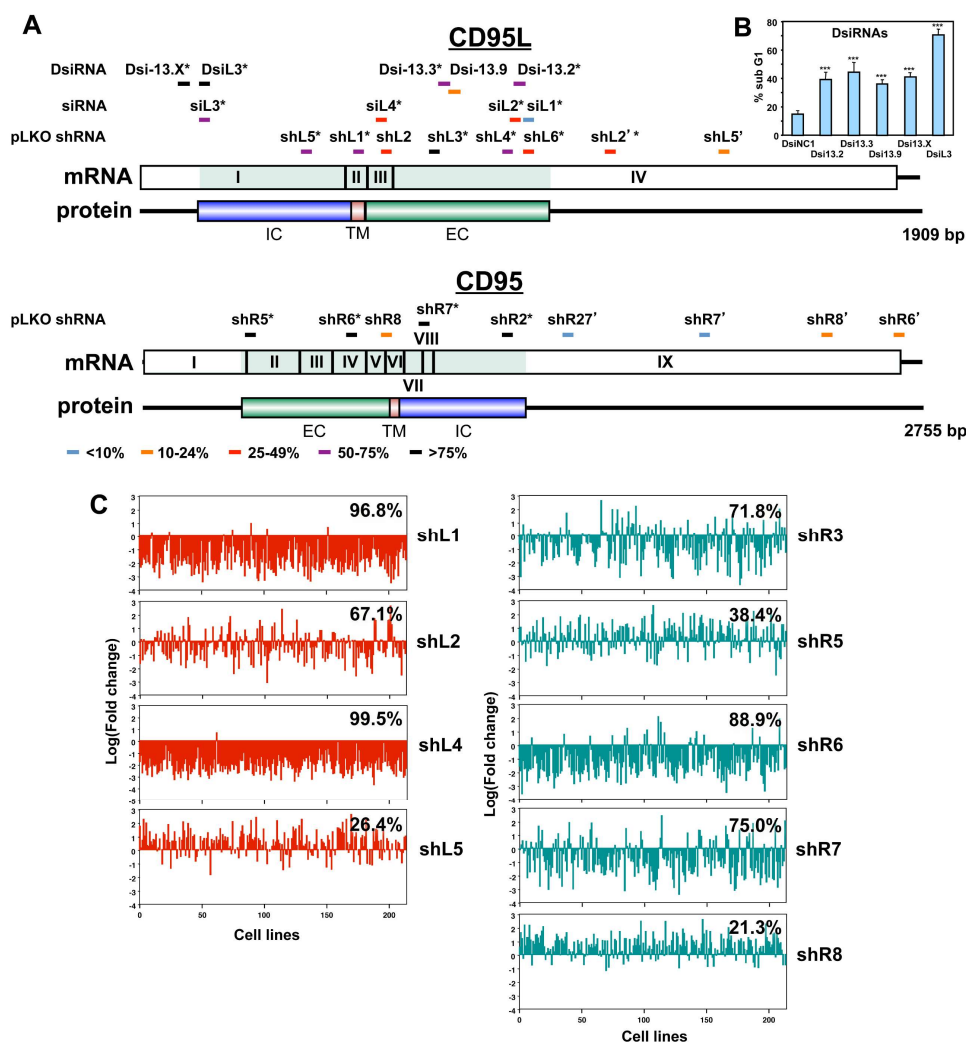


**Figure 3.1 - The majority of siRNAs and shRNAs targeting CD95L or CD95 are toxic.** (A) Location of target sites, growth inhibitory activities, and toxicity of all tested siRNAs, DsiRNAs, and pLKO-shRNAs targeting CD95L and CD95. Experiments were performed in HeyA8 cells at a MOI of 3 for pLKO-shRNA infection or transfected with 25 nM of siRNAs or 5 nM of DsiRNAs. Color code indicates the level of growth reduction caused by each reagent. The si/shRNAs labeled with an asterisk induced significant cell death as monitored by nuclear PI staining. Both exon/intron structure and protein domains are shown for both CD95L and CD95. EC, extracellular domain; TM, transmembrane domain; IC, intracellular domain. Data on growth reduction of siRNAs were performed in triplicates and in two independent experiments. Data on growth reduction of shRNAs were performed in triplicate and in two independent experiments. Data on nuclear fragmentation by siRNAs were performed in triplicate in two independent experiments. Data on nuclear fragmentation by shRNAs were performed in triplicate. (B) PI staining was used to quantify percent subG1 of HeyA8 cells 4 days after transfection with 5 nM of CD95L-derived DsiRNAs. Data are representative of three independent experiments. Each bar represents mean  $\pm$ SD of four replicates ( $p$ -value  $***p < 0.0001$ , unpaired t-test). (C) Level of underrepresentation (toxicity) of shRNAs targeting either CD95L (*left column*) or CD95 (*right column*) across 216 human cancer cell lines as described by Cowley *et al*<sup>377</sup>. The fraction of cell lines for which an shRNA was found to be toxic is given as a percentage, for shL5, data were only available on 197 cell lines. Quan Gao performed experiments for **Figures 3.1A and B** and analysis for **Figure 3.1C**; Monal Patel performed experiment for **Figure 3.1A**.

using a different platform to deliver siRNAs called Dicer substrate siRNAs (DsiRNAs). These DsiRNAs are 27mer RNA duplexes that have one blunt end with deoxynucleotides on the passenger strand and the other end with a two deoxynucleotide 3' overhang that is recognized by Dicer<sup>399</sup>. This configuration ensures proper Dicer cleavage to produce the desired mature siRNA and is advertised as more potent<sup>400</sup>. Transfection of all five DsiRNAs designed to target CD95L represses growth (**Figure 3.1A**) and are toxic to the ovarian cancer cell line HeyA8 at 5 nM (**Figure 3.1B**). The results of a published parallel genome-wide RNAi lethality screen conducted in 216 different solid and blood cancer cell lines using the RNAi Consortium (TRC) shRNA library were also analyzed, and the following shRNAs used in **Figure 3.1A** were found to inhibit growth in the indicated percentage of the 216 cell types: shL1 (96.8%), shL2 (67.1%), shL4 (99.5%), shL5 (26.4%), shR3 (71.8%), shR5 (38.4%), shR6 (88.9%), shR7 (75.0%), and shR8 (21.3%) (**Figure 3.1C**). This independent analysis, even when only considering shRNAs that kill more than half of the 216 cells, shows that 67% of shRNAs targeting CD95 or CD95L are toxic to cancer cells.

The toxicity shown in **Figure 3.1A** was triggered using shRNAs driven from polymerase III promoters and expressed within the conventional hairpin structure and loop sequence used for the TRC library shRNAs, which are prone to heterogenous Dicer processing<sup>72</sup>. On the other hand, shRNAs embedded in a human miRNA-30 backbone are processed much more precisely<sup>72</sup> and are less likely to evoke an immune response<sup>401</sup>. Interestingly, a recent RNAi lethality screen using these miRNA-30-embedded shRNAs (miR-30-based shRNAs) showed none of their modified shRNAs designed to target CD95 or CD95L were toxic<sup>402</sup>. Therefore, Dox-inducible miR-30-based shRNAs were generated based on our most toxic CD95/CD95L-derived TRC shRNAs including shL1, shL3, shL4, shR5, shR6, and shR7 (**Figure 3.2A**). Consistent with the results of

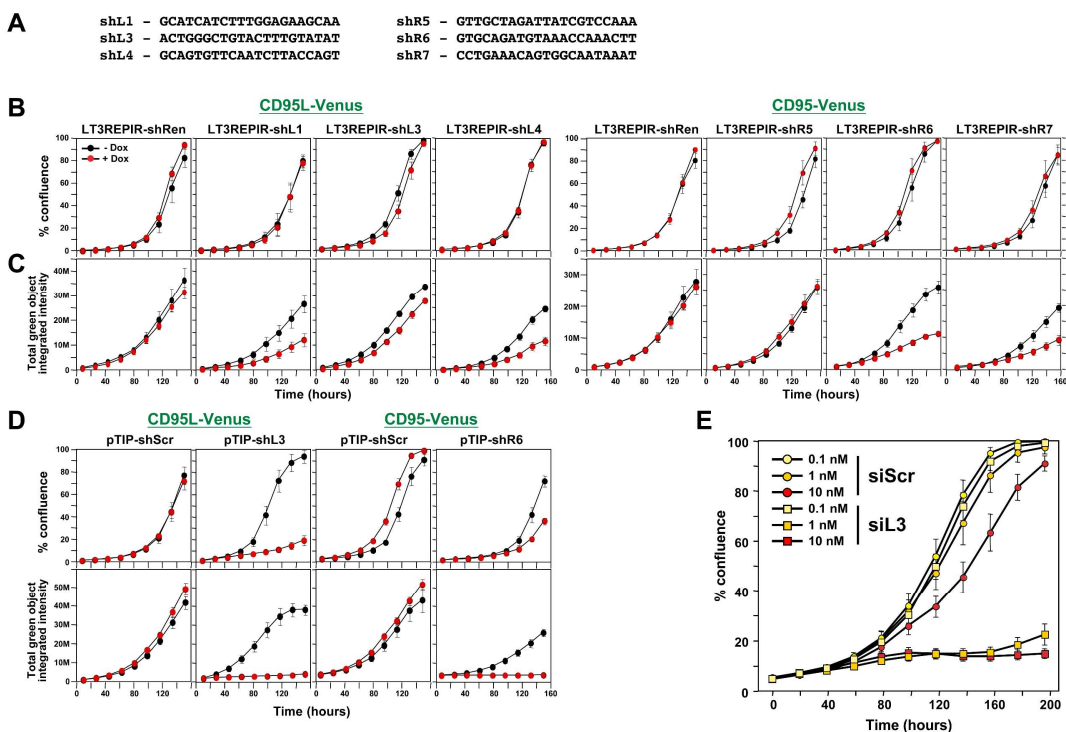


**Figure 3.2 – Toxicity of si/shRNAs is dose dependent.** (A) Sequences of the six toxic TRC shRNAs (pLKO vector) that were converted into miR-30-based shRNAs (Dox-inducible LT3REPIR vector<sup>383</sup>). (B) Confluence over time of NB7-Venus-CD95L (*left*) or NB7-Venus CD95 (*right*) cells infected with the LT3REPIR vector minus/plus Dox to induce expression of the indicated shRNAs. (C) Total green fluorescence over time of the experiment shown in B. shREN refers to the control shRNA designed to target Renilla luciferase. (D) Confluence (*top*) and total green fluorescence (*bottom*) over time of NB7-Venus-CD95L (*left*) or NB7-Venus CD95 (*right*) cells infected with the pTIP vector minus/plus Dox to induce expression of the indicated shRNAs. (E) Confluence over time of HeyA8 cells transfected with the indicated concentration of either siScr or siL3. Each data point in this figure represents mean  $\pm$ SE of six replicates. The experiment was repeated three times. Monal Patel performed experiments for **Figures 3.2A to D**; Andrea Murmann performed experiment for **Figure 3.2E**.

the miR-30-based shRNA screen, their expression was not very toxic to HeyA8 cells (**Figure 3.2B**). However, expression of these miR-30-based shRNAs also did not induce any appreciable knock down of either the Venus-CD95 or Venus-CD95L conjugate fluorescent reporters (**Figure 3.2C**). In contrast, both shL3 and shR6, when expressed from the Dox-inducible pTIP vector using the standard TRC short hairpin structure, were able to knock down reporter expression and induce severe toxicity in HeyA8 cells (**Figure 3.2D**). These results suggested that miR-30-based shRNAs are unable to deliver enough processed AGO-bound guide RNA to evoke toxicity in cancer cells. Since shRNAs delivered via lentivirus are difficult to titer, the minimum concentration of siRNA



that is toxic to cells was determined. The toxic CD95L-derived siL3 could be transfected at 1 nM and still evoke toxicity in HeyA8 cells (**Figure 3.2E**), even though the recommended concentration for standard siRNA transfection experiments is between 5 and 50 nM. Together, these data suggest shRNAs embedded in miR-30-based shRNA cassettes are not expressed highly enough to evoke toxicity, although the amount of CD95/CD95L-derived si/shRNAs required to reduce growth is still very low. These results were also consistent with toxicity being mediated by off-targeting, as OTEs are often mitigated by decreasing the amount of RNAi reagent used<sup>403</sup>. However, the high percentage of si/shRNAs designed to target CD95 and CD95L that are toxic supported a role of these two genes as cancer survival factors.

To distinguish between these two possibilities, shRNA-resistant CD95 and CD95L gene products were introduced to rescue cells from toxicity. First, cells expressing the CD95L-derived shL1 were treated with either the recombinant S2 CD95L protein, which is a truncated soluble form shown to selectively trigger CD95 non-apoptotic signaling, or Leucine-zipper (Lz)CD95L protein, which is conjugated to a leucine-zipper domain that allows multimerization and potent CD95 activation<sup>363</sup>. The LzCD95L protein was shown to be functional under cell culture conditions, as it was able to induce apoptosis in sensitive MCF-7 cells (**Figure 3.3A; right panel**). To prevent apoptosis induction, the recombinant CD95L rescue experiments were performed in the neuroblastoma cell line NB7, which lacks expression of caspase-8<sup>404</sup>. The results show shL1-mediated toxicity is not appreciably mitigated in the presence of varying concentrations of either S2 or LzCD95L protein (**Figure 3.3A; left and center panels**). Although a definitive rescue was not achieved, it did seem recombinant CD95L mildly promoted cell growth in a dose-dependent manner (**Figure 3.3A; left and center panel**), which is consistent with previous reports showing a

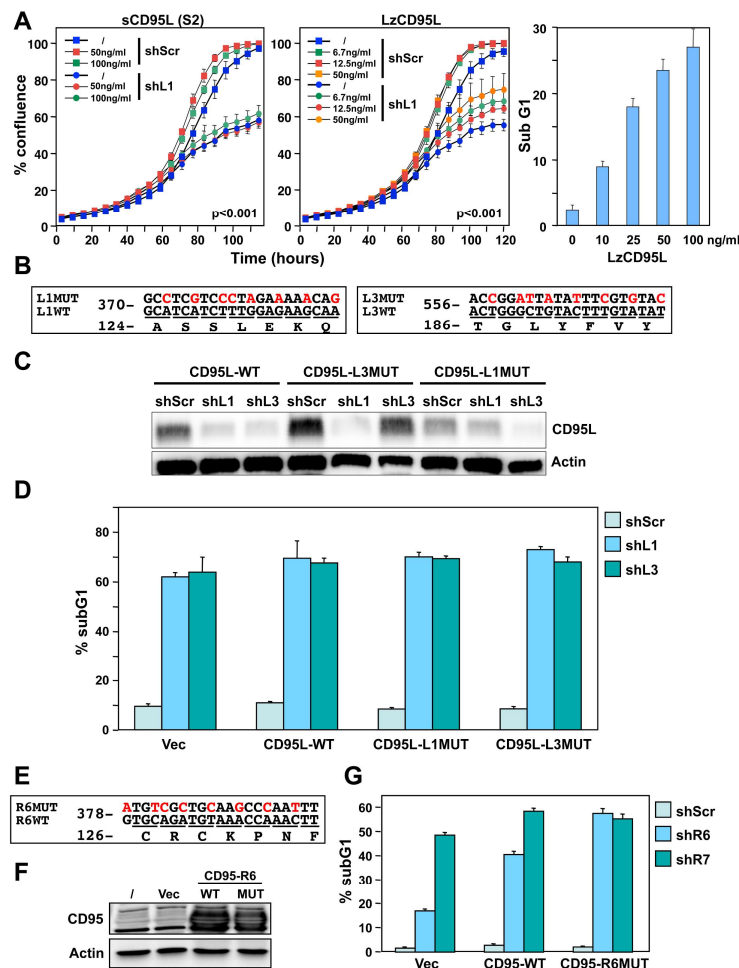


**Figure 3.3 - Exogenous CD95L or CD95 proteins do not protect cells from toxicity of CD95L/CD95-derived shRNAs.** (A) *Left:* Percent cell confluence over time of NB7 cells after infection with either pLKO-shScr or pLKO-shL1 and concurrent treatment with different concentrations of soluble CD95L protein (S2). Two-way ANOVA was performed for pairwise comparisons of % confluence over time between shScr expressing cells untreated (/) or treated with 100 ng/ml S2. Each data point represents mean  $\pm$ SE of three replicates. *Center:* Percent cell confluence over time of NB7 cells after infection with either pLKO-shScr or pLKO-shL1 and concurrent treatment with different concentrations of leucine zipper-tagged (Lz)CD95L protein. Two-way ANOVA was performed for pairwise comparisons of % confluence over time between shScr-expressing cells untreated or treated with 50 ng/ml LzCD95L. Each data point represents mean  $\pm$ SE of three replicates. *Right:* Percent nuclear PI staining of MCF-7 cells 24 hrs after adding different amounts of LzCD95L. (B) Schematic of the eight silent mutations introduced to the shL1 and the shL3 target sites of CD95L. (C) Western blot analysis of CD95L and  $\beta$ -actin in NB7 cells over-expressing CD95L-WT, CD95L-L1MUT, or CD95L-L3MUT 3 days after infection with pLKO-shScr, pLKO-shL1, or pLKO-shL3. Shown is one of two repeats of this analysis. (D) Percent nuclear PI staining of NB7 cells expressing empty pLenti vector, CD95L-WT, CD95L-L1MUT, or CD95L-L3MUT 6 days after infection with either pLKO-shScr, pLKO-shL1, or pLKO-shL3. Each bar represents mean  $\pm$ SD of three replicates. (E) Schematic of the eight silent mutations introduced at the shR6 site of CD95. (F) Western blot analysis of CD95 and  $\beta$ -actin in MCF-7 cells over-expressing CD95-WT or CD95-R6MUT. (G) Percent nuclear PI staining of MCF-7 cells expressing empty pLNCX2 vector, CD95-WT, or CD95-R6MUT 6 days after infection with pLKO-shScr, pLKO-shR6, or pLKO-shR7. Each bar represents mean  $\pm$ SD of three replicates. Will Putzbach performed experiments for **Figures 3.3A to G**; Abdul Qadir performed experiment for **Figure 3.3A**.

growth-proliferative role for CD95 non-apoptotic signaling<sup>351,364</sup>. However, an enhanced growth rate resulting from direct CD95 stimulation is not necessarily a manifestation of cell-autonomous CD95 survival signaling. As an added measure, membrane-bound human CD95L, expressed from engineered mouse colon carcinoma CT26 cells, referred to as CT26L, was also tested for rescue potential. However, co-culturing NB7 cells expressing shL3 with either wild type CT26 cells or CT26L cells offered no distinguishable differences in survival (**Figure 3.4**).

Performing a rescue experiment by culturing cells with recombinant or cell non-autonomous membrane-bound protein to replace the RNAi-depleted gene product suffers from

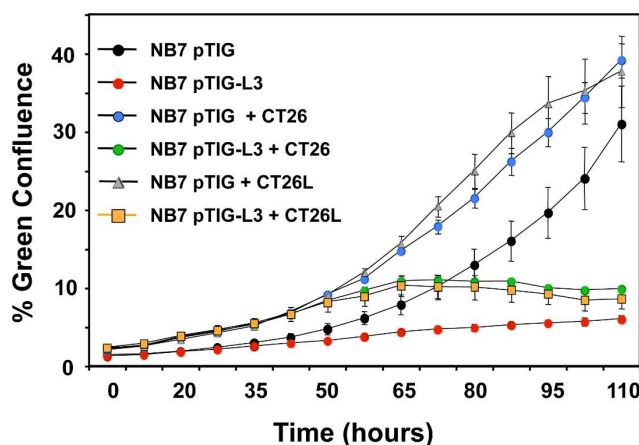


**Figure 3.4 – Membrane-bound CD95L does not protect against toxicity of CD95L-derived shRNA.** NB7 cells were infected with either pTIG-shScr or pTIG-shL3 and then co-cultured with murine CT26 or human-CD95L-expressing CT26L cells in the presence of Dox to induce shRNA expression. NB7 cell growth was tracked via confluence of green fluorescence. Each data point represents mean  $\pm$ SE of three replicates. Will Putzbach performed experiment for **Figure 3.4**.

two primary drawbacks: (1) The protein is confined to the extracellular environment and (2) it does not elucidate whether knock down of the mRNA, rather than the protein, is responsible for the phenotypic change. To circumvent these issues, either of two mutant CD95L ORF cDNAs, each containing eight synonymous mutations at the shL1 (CD95L-L1MUT) or shL3 (CD95L-L3MUT) target site, were expressed in NB7 cells using lentiviruses (**Figure 3.3B and C**). As

expected, both shL1 and shL3 were able to knock down CD95L protein expressed from wild type cDNA, but not from the mutant cDNAs harboring the eight silent mutations at the corresponding target sites (**Figure 3.3C**). Interestingly however, expression from the shRNA-resistant CD95L-L1MUT or CD95L-L3MUT cDNA constructs did nothing to prevent the toxicity evoked by shL1 or shL3, respectively (**Figure 3.3D**). The same strategy was used for CD95 in MCF-7 cells. A mutant CD95 cDNA construct with eight synonymous mutations in the shR6 site was generated (**Figure 3.3E**) and both this CD95-R6MUT mutant and WT CD95 cDNAs were over-expressed in MCF-7 cells (**Figure 3.3F**). Once again, however, no appreciable rescue was achieved expressing the CD95-R6MUT versus wild type CD95 in MCF-7 cells expressing shR6 (**Figure 3.3G**). Therefore, neither exogenous recombinant CD95L, membrane-bound CD95L protein, nor exogenously-expressed CD95L mRNA or protein can rescue from toxicity mediated by these CD95/CD95L-derived shRNAs.

However, even over-expression of the shRNA-resistant cDNAs via lentiviral delivery poses its own limitations: (1) Although the mRNA is being expressed, it still is not identical to the wild type mRNA, as it has eight synonymous mutations and lacks the majority of its 3' UTR in this case, making negative results difficult to interpret. (2) The promoter driving transcription of the cDNA is not native to the cell, and therefore, not subject to the same nuanced transcription regulation that occurs at the endogenous locus.

Therefore, cells with homozygous deletions of the endogenous si/shRNA target sites were engineered using CRISPR/Cas9 genome-editing. This was accomplished by co-transfecting a Cas9 expression plasmid with two gRNAs that target upstream and downstream of the target site. This strategy was used to generate clones that lack the endogenous target sites for the siRNA siL3 and

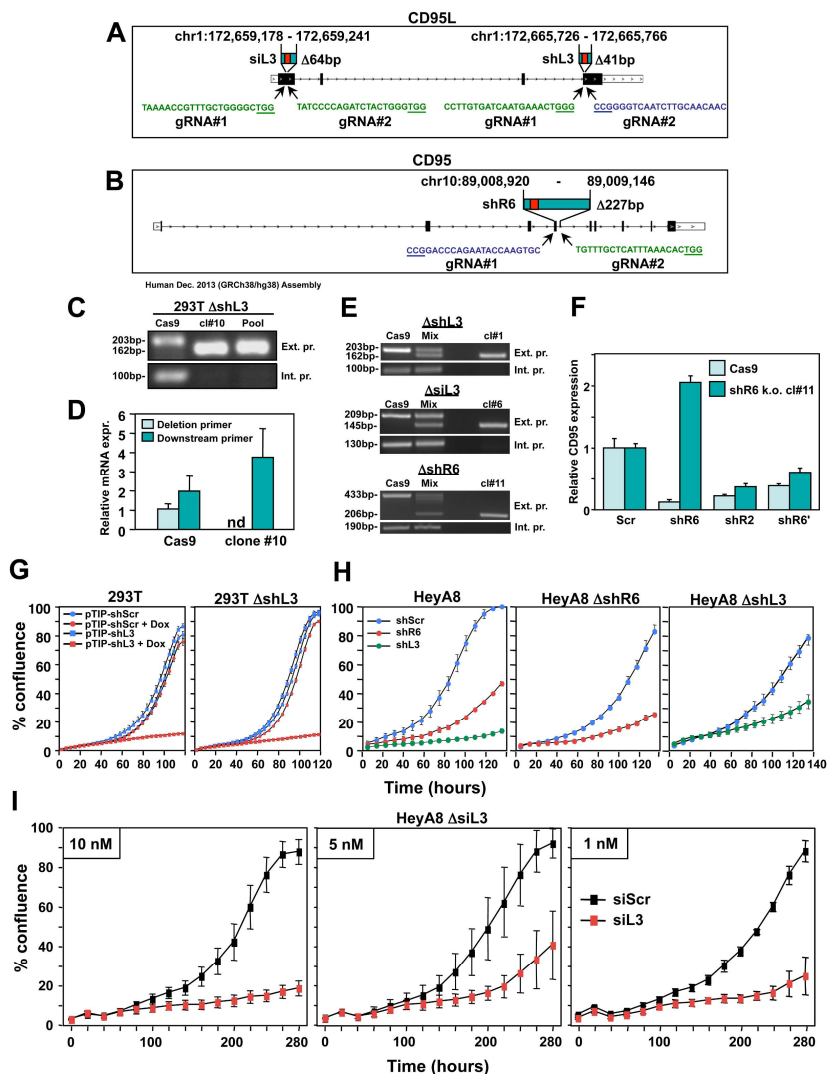


**Figure 3.5 - CD95 and CD95L derived si/shRNAs kill cells in the absence of the targeted sites in CD95 or CD95L.** (A) Schematic of the genomic locations and sequences of the gRNAs used to excise the siL3 ( $\Delta 64$ bp) and shL3 ( $\Delta 41$ bp) target sites from CD95L. PAM site is underlined. Green indicates a gRNA targeting the sense strand. Blue indicates a gRNA targeting the antisense strand. (B) Schematic showing the genomic locations and sequences of the gRNAs used to excise the shR6 ( $\Delta 227$ bp) target site. (C) PCR with flanking (*top panels*) and internal (*bottom panels*) primers used to confirm homozygous  $\Delta 41$  deletion of the shL3 site in one representative 293T shL3  $\Delta 41$  clone and the pool of three 293T shL3  $\Delta 41$  clones. Cells transfected with Cas9 only (Cas9) are wild type. (D) RT-qPCR for endogenous CD95L with a primer downstream of the  $\Delta 41$  shL3 deletion and another primer internal to the deleted region. nd, not detectable. Each bar represents mean  $\pm$ SD of three replicates. (E) PCR with flanking (*top row*) and internal (*bottom row*) primers used to confirm the presence of the shL3  $\Delta 41$  (*top panel*), siL3  $\Delta 64$  (*middle panel*), and shR6  $\Delta 227$  (*bottom panel*) deletions in HeyA8 clones. Mix, HeyA8 cells after transfection with Cas9 and gRNAs but before single cell cloning. (F) RT-qPCR for CD95 in HeyA8 cells transfected with Cas9 plasmid (Cas9) alone or the HeyA8  $\Delta$ shR6 clone #11. RNA was extracted 5 days after infection with pLKO-shScr, pLKO-shR6, pLKO-shR2, or pLKO-shR6' (targeting the 3'UTR). Each bar represents mean  $\pm$ SD of three replicates. (G) Percent cell confluence over time of 293T cells (left) and a pool of three 293T clones with a homozygous deletion of the shL3 target site (right) infected with pTIP-shScr or pTIP-shL3 and treatment with or without Dox. Data are representative of two independent experiments. Each data point represents mean  $\pm$ SE of six replicates. (H) *Left*: Percent confluence over time of HeyA8 cells infected with pLKO-shScr, pLKO-shR6, or pLKO-shL3. *Center*: Percent confluence over time

of a HeyA8 clone with a homozygous deletion of the shR6 target site infected with either pLKO-shScr or pLKO-shR6. *Right*: Percent confluence over time of a pool of three HeyA8 clones with a homozygous deletion of the shL3 site infected with either pLKO-shScr or pLKO-shL3. Data are representative of two independent experiments. Each data point represents mean  $\pm$ SE of three replicates. **(I)** Percent confluence over time of a pool of three HeyA8 clones harboring a homozygous deletion of the siRNA siL3 target site after transfection with different concentrations of siScr or siL3. Data are representative of three independent experiments. Each data point represents mean  $\pm$ SE of three replicates. Will Putzbach generated the cells used in **Figure 3.5** and performed experiments for **Figures 3.5A to F**; Monal Patel performed experiments for **Figures 3.5G and H**; Andrea Murmann performed experiment for **Figure 3.5I**.

shL3 in CD95L (**Figure 3.5A**) and shR6 in CD95 (**Figure 3.5B**). A 41 bp segment containing the shL3 site was excised in 293T cells, and three clones were isolated that contain homozygous deletion of the site and pooled together to create the 293T  $\Delta$ shL3 cells (**Figure 3.5C**). RT-qPCR using two primer/probe pairs—one within and one downstream of the deleted site—confirmed successful homozygous deletion in a representative clone (**Figure 3.5D**) as did Sanger sequencing of the DNA surrounding the excised region (**Figure 3.6A**). Using this strategy, the siL3 site (64 bp deletion), shL3 site (41 bp deletion), and shR6 (227 bp deletion) site were deleted in HeyA8 cells (**Figure 3.5E**). Again, Sanger sequencing confirmed successful deletion in each case (**Figure**

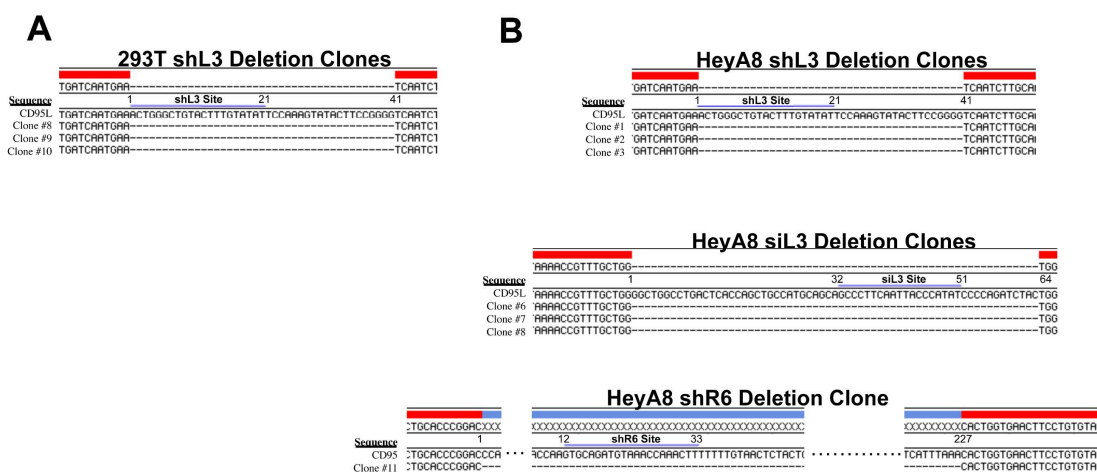


**Figure 3.6 – Sanger sequencing confirms successful deletion of si/shRNA target sites.** (A) Sequencing data showing successful  $\Delta$ 41 bp deletion encompassing the shL3 site in 293T cells for three clones. (B) Sequencing data showing successful deletion of si/shRNA target sites in HeyA8 cells. *Top panel*:  $\Delta$ 41 bp deletion encompassing the shL3 site in three clones. *Center panel*:  $\Delta$ 64 bp deletion encompassing the siL3 site in three clones. *Bottom panel*:  $\Delta$ 227 bp deletion encompassing the shR6 site in one clone—clone #11. Will Putzbach performed experiments for **Figure 3.6**.

**3.6B**). Three homozygous deletion clones were pooled together to generate both the HeyA8  $\Delta$ shL3 and HeyA8  $\Delta$ siL3 cells. Only one homozygous shR6 deletion clone was isolated for HeyA8—clone #11. For consistency, this clone is referred to as HeyA8  $\Delta$ shR6. In addition, two HeyA8 clones were generated containing the 227 bp deletion of one allele and plasmid insertions in the other, resulting in homozygous CD95 protein knock outs (**Figure 3.7**). It was then determined whether homozygous deletion of the endogenous target site would prevent on-targeting by expressing shR6 and a couple shRNAs that target outside the 227 bp deleted region (i.e. shR2 and shR6') in both the HeyA8  $\Delta$ shR6 and Cas9-transfected control cells. As expected, shR6 downregulated CD95 expression in the control cells but not the  $\Delta$ shR6 cells, whereas both shR2 and shR6' downregulated CD95 expression in both cell types (**Figure 3.5F**). This confirms homozygous deletion of the endogenous target site is incompatible with RNAi on-targeting.

It could now be tested whether expressing CD95/CD95L-derived si/shRNAs would still evoke toxicity in these engineered cells harboring a homozygous deletion of the corresponding target site. Amazingly, Dox-inducible expression of shL3 was equally toxic in 293T wild type control and  $\Delta$ shL3 cells (**Figure 3.5G**). Similarly, both HeyA8  $\Delta$ shL3 and  $\Delta$ shR6 cells were just as sensitive to expression of shL3 or shR6, respectively, as the wild type control HeyA8 cells were (**Figure 3.5H**). Finally, homozygous deletion of the siL3 site offered no protection from siL3 transfection in HeyA8, even at concentrations as low as 1 nM (**Figure 3.5I**). Together, these results conclusively show knock down of CD95 and CD95L is not the basis of the toxicity evoked by these CD95/CD95L-derived si/shRNAs.

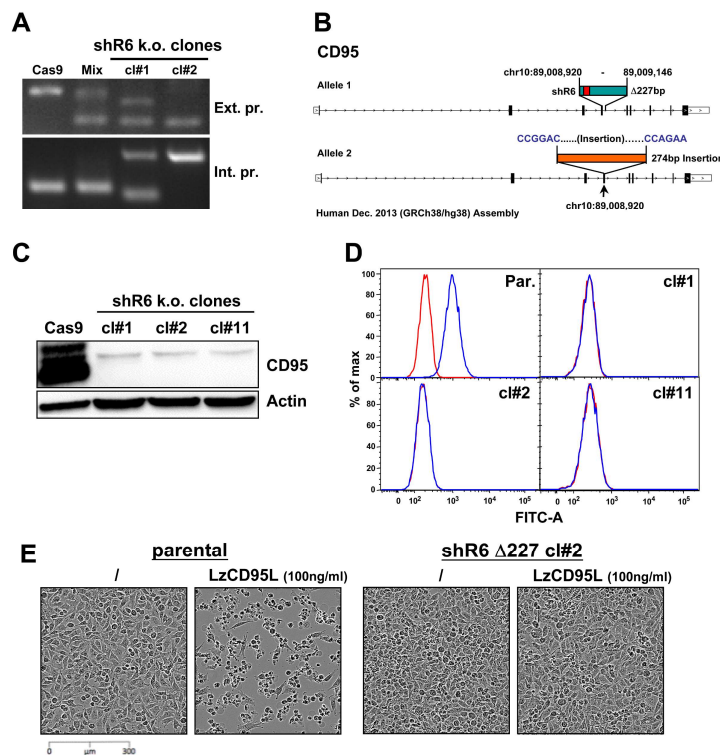


**Figure 3.7 – Knock Out of CD95 in HeyA8 cells.** (A) PCR showing a  $\Delta 227$  shR6 deletion and insertions in HeyA8 clones #1 and #2. (B) Schematic of the  $\Delta 227$  deletion in allele #1 and partial insertion of a pSC-B plasmid fragment in allele #2 in HeyA8 clone #2 based on Sanger sequencing of isolated bands from PCR shown in A. Note, cl#1 and #2 have the expected  $\Delta 227$  shR6 deletion in one allele and an insertion in the other. cl#11 has a homozygous  $\Delta 227$  shR6 deletion. The deleted region is shown in green containing the shR6 target site in red. pSC-B vector sequences are shown in blue letters, and the insertion is shown in orange. (C) Western blot for CD95 and  $\beta$ -actin in Cas9-control transfected HeyA8 cells and HeyA8 CD95 knock out clones #1, #2, and #11. Shown is one of two repeats of this analysis. (D) Surface staining for CD95 in parental HeyA8 cells and HeyA8 CD95 knock out clones #1, #2, and #11. Shown is one of two repeats of this analysis. (E) Images showing apoptosis induction with LzCD95L treatment (4.5 hr) in parental HeyA8 cells but not in clone #2. Will Putzbach performed experiments for **Figure 3.7A to C and E**; Calvin Law performed experiment for **Figure 3.7D**.

### *Involvement of Canonical RNAi*

RNAi reagents have long been known to evoke OTEs through downregulating off-targets that harbor a high degree of similarity to the on-target or through seed-based targeting, but also through RNAi-independent means such as evoking an immune response or by saturating the RNAi machinery. Therefore, a set of experiments was designed to decipher whether RNAi was at the basis of this si/shRNA-induced toxicity.



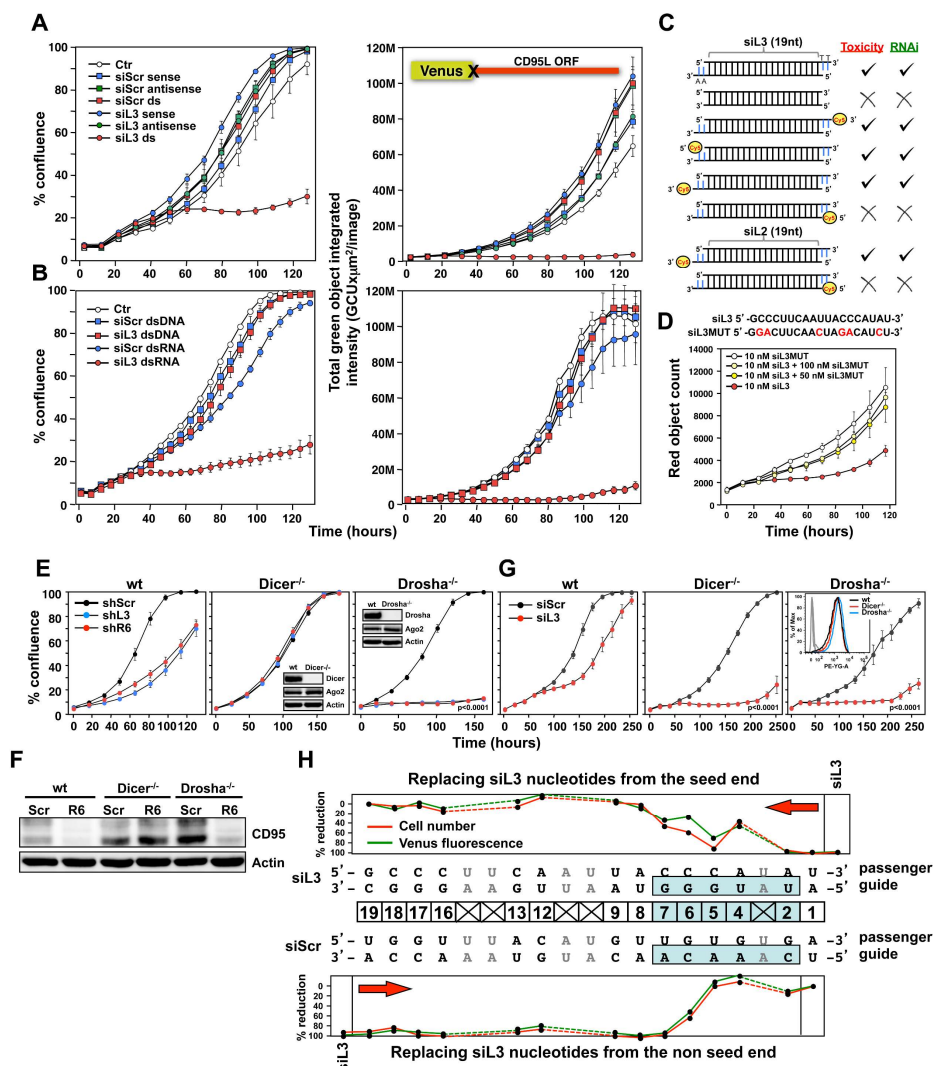


**Figure 3.8 – Toxicity of CD95L-derived siRNAs involves canonical RNAi activity.** (A) Percent cell confluence (left) and total green object integrated intensity (right) over time of a HeyA8 CD95 knock out clone ( $\Delta R6$  cl#2) expressing the Venus-CD95L sensor either untreated (Ctr) or after transfection with 25 nM of single-stranded (ss), single-stranded antisense, or double-stranded (ds) siScr or siL3 siRNAs. The CD95L sensor is schematically shown and comprises the Venus ORF fused to the CD95L ORF lacking the A of the ATG start codon (X). Data are representative of two independent experiments. Each data point represents mean  $\pm$ SE of three replicates. (B) Percent cell confluence (left) and total green object integrated intensity (right) over time of the HeyA8 CD95L sensor cell used in A after transfection with 5 nM siScr or siL3 double-stranded RNA (dsRNA) or double-stranded DNA (dsDNA). Data are representative of two independent experiments. Each data point represents mean  $\pm$ SE of three replicates. (C) Summary of experiments to test whether siL3 and siL2 siRNAs modified as indicated (left) were active (check mark) or not (X) in reducing green fluorescence or cell growth (both >70% reduction at end point) when transfected at 25 nM (except for blunt end oligonucleotides which were used at 5 nM and compared to 5 nM of siL3) into HeyA8 CD95L sensor cells used in A. Endpoints were 164 hrs for blunt end siRNA transfection, 180 hrs for modified siL3, and 144 hrs for modified siL2 siRNA transfections. Every data row is based on cell growth and green fluorescence quantification data executed as shown in A. Each analysis was done in triplicate and based on two independent repeats. (D) Red object count over time of HeyA8 cells (expressing NucRed) after transfection with different ratios of siL3 and mutant siL3 (siL3MUT). Data are representative of two independent experiments. Each data point represents mean  $\pm$ SE of three replicates. (E) Percent cell confluence over time of HCT116 parental (left

*panel*), *Dicer*<sup>-/-</sup> (*center panel*), or *Drosha*<sup>-/-</sup> (*right panel*) cells after infection with either shScr, shL3 or shR6 pLKO viruses. Inserts show the level of protein expression levels of Drosha/Dicer and AGO2 levels in the tested cells. Data are representative of three independent experiments. Each data point represents mean  $\pm$ SE of four replicates. *Drosha*<sup>-/-</sup> cells were more sensitive to toxic shRNAs than wild type cells ( $p < 0.0001$ , according to a polynomial fitting model). (F) Western blot analysis of wild type HCT116, *Dicer*<sup>-/-</sup> or *Drosha*<sup>-/-</sup> cells 4 days after infection with either pLKO-shScr or pLKO-shR6. (G) Percent cell confluence over time of wild type HCT116 (*left panel*), *Dicer*<sup>-/-</sup> (*center panel*), and *Drosha*<sup>-/-</sup> (*right panel*) cells after transfection with 25 nM siScr or siL3. Data are representative of four independent experiments. Each data point represents the mean  $\pm$ SE of three replicates, except for *Drosha*<sup>-/-</sup> cells treated with siScr where an outlier was omitted. Data in insert confirm similar uptake of transfected siRNA (25 nM of siGLO Red) into wild-type, *Dicer*<sup>-/-</sup> and *Drosha*<sup>-/-</sup> cells. *Dicer*<sup>-/-</sup> and *Drosha*<sup>-/-</sup> cells were more sensitive to siL3 than wild type cells ( $p < 0.0001$ , according to a polynomial fitting model; for the statistical analysis, the outlier was included). (H) Percent reduction in Venus expression (green) and in cell number (red object count [red]) over time of HeyA8 cells expressing the Venus-CD95L sensor and red nuclei after transfection with 5 nM of different chimeric siRNAs generated by substituting bps in the toxic siL3 with the scrambled siRNA sequence beginning at either the seed end (*top*) or the opposite end (*bottom*) of siL3 after 188 hr. The schematic in the middle shows the sequence of siL3 and the siScr siRNA (both sense and antisense strands). The 6mer seed sequence region of siL3 (positions 2 to 7) is highlighted in light blue. Nucleotides shared by siScr and siL3 are shown in grey font. Data are representative of two independent experiments. Each data point represents the mean of three replicates. Will Putzbach performed experiments for **Figures 3.8A, B, D, F, G, and inserts in E**; Quan Gao performed experiments for **Figures 3.8C, E, and H**; Andrea Murmann performed experiment for **Figure 3.8H**.

To that extent, the toxicity of siL3 constructs harboring modifications that abrogate their capacity for RNAi were assessed. The Venus-CD95L reporter was expressed in the HeyA8  $\Delta$ shR6 clone #2 cells that lack expression of CD95 protein (**Figure 3.7**) to prevent apoptosis from any CD95L conjugate protein produced by residual translation through the Venus stop codon. Then, the unaltered siL3 siRNA duplex or either the individual ssRNA sense or antisense siL3 oligonucleotides (**Figure 3.8A**) or dsDNA duplexes (**Figure 3.8B**) with the same nucleobase sequence as the siL3 siRNA were transfected into these reporter cells. In this way, the altered molecules preserve the sequence information embedded in unaltered siL3 siRNA but do not execute appreciable RNAi. The results show only dsRNA siL3 duplexes were able to knock down Venus-CD95L expression and were toxic. Both the ssRNA oligonucleotides and dsDNA siL3 duplex could not execute RNAi (**Figure 3.8A and B; right panels**) nor evoke toxicity (**Figure 3.8A and B; left panels**). Other modifications including blunt-end siL3 duplexes and different chemically modified siL2 or siL3 duplexes containing a Cy5 label at either the 5' or 3' end of the sense or antisense strand were also tested. Transfection of these dsRNA duplexes revealed that

blunt-end siL3 and siL2/siL3 with a Cy5 label at the 5' end of the antisense (guide) strand were unable to knock down Venus-CD95L nor induce toxicity (**Figure 3.8C**), which is consistent with RNAi playing a role in this toxicity since previous reports have shown dsRNA duplexes require 3' overhangs to be loaded into RISC and that chemical modifications at the 5' end of the guide RNA strand (in this case, the antisense strand) can interfere with proper RISC loading<sup>405,406</sup>.

To test whether toxicity required interaction between the siRNA and a molecular complex, which would be consistent with RISC loading, it was determined whether titering in a less toxic siRNA could mitigate toxicity evoked by siL3. Therefore, HeyA8 cells that express red nuclei and a Venus-siL3 reporter construct—composed of Venus conjugated to an artificial 3' UTR composed of a small region of the CD95L sequence surrounding the siL3 target site—were co-

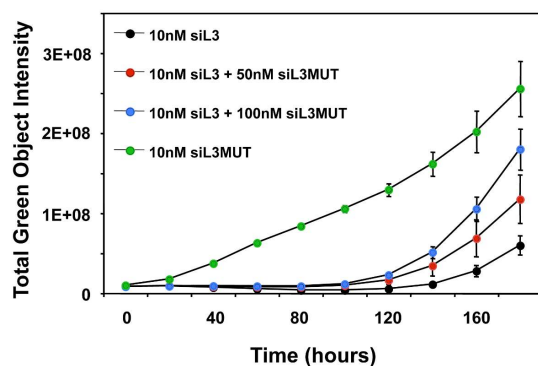


**Figure 3.9 – Knock down mediated by siL3 can be inhibited with addition of competing siRNA.** Time-course of total green intensity of the Venus-siL3 reporter expressed in HeyA8 cells used in **Figure 3.8D** after transfection with 10 nM of siL3 and varying amounts of siL3MUT. Will Putzbach performed experiment for **Figure 3.9**.

transfected with 10 nM of siL3 and increasing amounts of a mutant siL3 (siL3MUT), which contains six mutations and is less toxic (**Figure 3.8D**). As expected of two siRNAs competing for RISC association, increasing the ratio of siL3MUT to siL3 decreased the repression of the Venus-siL3 reporter (**Figure 3.9**). Interestingly, transfecting a higher ratio of siL3MUT to siL3 also

alleviated the toxicity (**Figure 3.8D**), consistent with both siRNAs competing for the same binding site on the molecular complex that mediates the toxicity.

Dicer and Drosha are critical components of the RNAi pathway (**Figure 1.2**). Therefore, HCT116 cells lacking expression of either Dicer (**Figure 3.8E; center panel inset**) or Drosha (**Figure 3.8E; right panel inset**) were tested for sensitivity to shR6 and shL3-induced toxicity. Interestingly, cell growth of wild type HCT116 (**Figure 3.8E; left panel**) and HCT116 Drosha<sup>-/-</sup> (**Figure 3.8E; right panel**) cells was impaired upon expression of shL3 and shR6, whereas HCT116 Dicer<sup>-/-</sup> cells (**Figure 3.8E; center panel**) were completely unaffected. This is consistent with shRNA toxicity being an RNAi-dependent phenomenon, as only Dicer is required to process artificial shRNAs (**Figure 1.2**). In fact, the HCT116 Drosha<sup>-/-</sup> cells were hypersensitive to shL3 and shR6-mediated toxicity compared to wild type HCT116 cells (**Figure 3.8E; left and right panels**,  $p < 0.0001$ , according to a polynomial fitting model). This is further substantiated by the Western blot analysis in **Figure 3.8F**, which shows expression of shR6 knocks down CD95 expression in wild type HCT116 and Drosha<sup>-/-</sup> cells but not in Dicer<sup>-/-</sup> cells. It should also be noted that expression of CD95 goes up in the Dicer<sup>-/-</sup> and Drosha<sup>-/-</sup> cells compared to the wild type HCT116 cells, likely due to repressive control of CD95 exerted by the miRNA let-7<sup>31</sup>. In contrast to shRNAs, siRNAs do not require processing by either Dicer or Drosha (**Figure 1.2**). Consistently, transfection of siL3 severely inhibited growth in both Dicer<sup>-/-</sup> and Drosha<sup>-/-</sup> cells (**Figure 3.8G**). In fact, both knock out cell lines were hypersensitive to siL3 compared to wild type HCT116 cells (**Figure 3.8G**;  $p < 0.0001$ , according to a polynomial fitting model).

si/shRNAs can target genes with a minimal number of six to seven contiguous bps to the guide RNA's seed sequence. To dissect the role of the seed sequence in toxicity, a library of

chimeric siRNAs was generated in which bps of the toxic siL3 were systematically replaced with bps from our non-toxic scramble control siScr starting from either the seed or non-seed end (**Figure 3.8H**). These individual chimeric siRNAs were transfected at 5 nM into HeyA8 cells expressing both red nuclei (Nuc-Red plasmid) to monitor cell number and the Venus-CD95L reporter to monitor RNAi capacity. The unaltered siL3 resulted in almost complete Venus-CD95L suppression and a high degree of growth reduction (**Figure 3.8H**). The top and bottom panels of **Figure 3.8H** summarize data gathered from libraries generated by replacing siL3 bps with those from siScr starting at either the seed or non-seed end, respectively. Interestingly, both RNAi and toxicity were alleviated when only three bps, starting from the seed end, were replaced with siScr (**Figure 3.8H; top panel**). Moreover, nearly the entire siL3 sequence could be replaced with siScr starting from the non-seed end without affecting RNAi or toxicity until bps in the seed (highlighted in blue) started to be replaced; at that point, both RNAi and toxicity lessened considerably (**Figure 3.8H; bottom panel**). These results suggest that it is the seed sequence that is responsible for both RNAi and toxicity.

#### *Toxic si/shRNAs Cause Downregulation of Survival Genes*

Seed-dependent off-target effects (sOTEs) have been described before for si/shRNAs, but it is difficult to predict which seed sequences will evoke a noticeable sOTE and what the nature of the sOTE will be. Even small seed sequence alterations can completely change the targeting profile, which makes sOTE prediction very difficult. The toxicity of our si/shRNAs is due to an RNAi-dependent sOTE. This is interesting since >80% of the tested CD95/CD95L-derived si/shRNAs (22 non-overlapping target sites) recurrently evoke this morphologically/biochemically

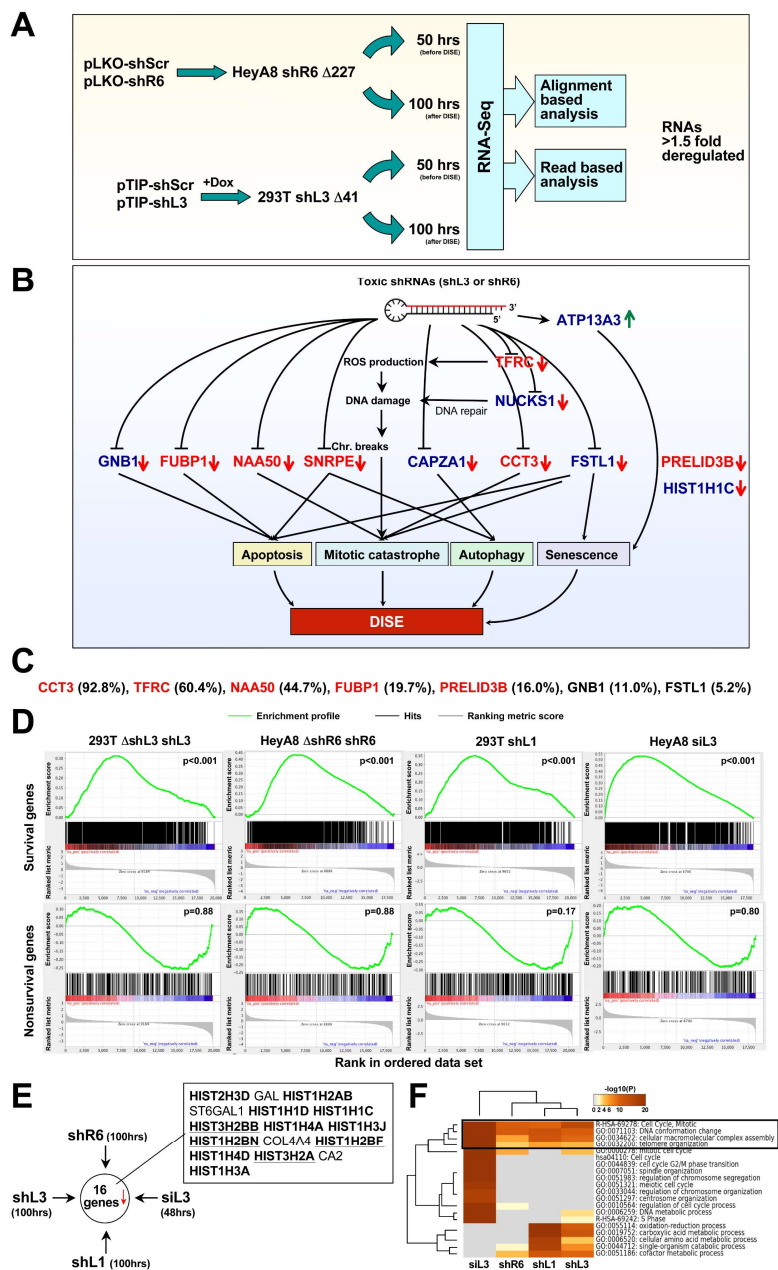


**Figure 3.10 – Toxic shRNAs derived from CD95 and CD95L cause downregulation of critical survival genes.**

(A) Schematic of RNA-Seq work flow for total RNA sample prepared both before (50 hr) and during (100 hr) DISE after expressing either shR6 or shL3 from different vector systems (i.e. pLKO-shR6 and pTIP-shL3) in different cells (HeyA8 shR6  $\Delta$ 227 cells and 293T shL3  $\Delta$ 41 cells). (B) One mRNA was up- and 11 mRNAs were downregulated in the cells treated with toxic shL3 and shR6 as shown in A. mRNAs shown in red were found to be essential cancer survival genes in two genome-wide lethality screens<sup>407,408</sup>. The number of essential genes was enriched from 6.6% of the tested genes to 54.5% in our study ( $p=3 \times 10^{-6}$  according to binomial distribution). (C) The level of growth inhibition observed in HeyA8 cells transfected with siRNA SmartPools (25 nM) designed to individually target the listed survival genes. Targeting the seven genes significantly reduced cell growth compared to cells transfected with a siScr pool at 140 hrs (samples done in quadruplicate in two independent experiments) with an ANOVA  $p < 0.05$ . (D) Gene set enrichment analysis for the group of 1846 survival genes (*top four panels*) and 416 nonsurvival genes (*bottom*

*four panels*) identified in a genome-wide CRISPR lethality screen<sup>408</sup> after introducing Dox-inducible shL3 in 293T  $\Delta$ shL3 cells after 100 hrs (*left-most panels*), shR6 in HeyA8  $\Delta$ shR6 cells after 100 hrs (*center-left panels*), Dox-inducible shL1 in parental 293T cells after 100 hrs (*center-right panels*), and siL3 in HeyA8 cells after 48 hrs (*right-most panels*). Scrambled sequences served as controls. p-values indicate the significance of enrichment. (E) Schematics showing RNAs at least 1.5-fold downregulated (adj p-value<0.05) in all cells treated as in D. Histones that are underlined contain a 3'UTR. (F) Metascape analysis of the four RNA-Seq data sets analyzed in D. The boxed GO term clusters were highly enriched in all data sets. Will Putzbach performed experiment for **Figure 3.10A**; Elizabeth Bartom performed analysis in **Figure 3.10B**; Quan Gao performed experiment in **Figure 3.10C**; Denise Scholtens performed analyses in **Figure 3.10D**; Marcus Peter performed analyses in **Figures 3.10E and F**.

distinct form of cell death, despite heterogeneity of their seed sequences. How can different seed sequences, each with a presumably distinct target profile, all trigger a specific cellular response?

To answer this question, two different shRNAs—the CD95L-derived shL3 and the CD95-derived shR6—were expressed in 293T  $\Delta$ shL3 cells and HeyA8  $\Delta$ shR6 cells, respectively. The Dox-inducible pTIP vector was used to deliver shL3, and pLKO was used to deliver shR6 (expression of shScr was also included). Total RNA was harvested 50 (before death) and 100 hrs (during death) after shRNA expression and subjected to an RNA-Seq analysis (**Figure 3.10A**). This strategy ensured any expression changes would be independent of the shRNA used, cell type, on-target effects, and delivery system. Comparison between the two cell types would reveal gene expression changes common to both, allowing us to identify how two different seed sequences can both evoke the same kind of toxicity.

To achieve high stringency, the RNA-Seq data was analyzed using both read-based and alignment-based methods. The former finds all reads that were differentially expressed >1.5 fold between the shScr and shR6/shL3 and then maps these reads to the genes they are derived from using BLAST. The latter is a conventional alignment-based method to identify genes that are >1.5 fold deregulated between the shScr and shR6/shL3 and have an adjusted p-value below 0.05. Only genes that were identified by both methods were considered (**Tables 3.1.1 to 3.1.4**).

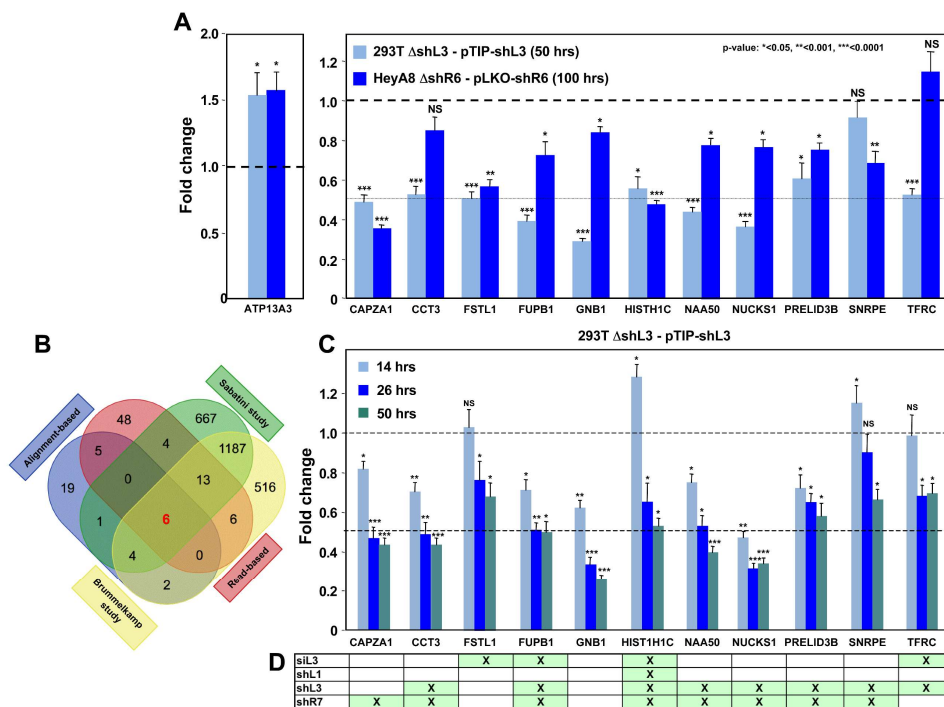


**Figure 3.11 – Down-regulation of critical survival genes after treatment with CD95 and CD95L-derived shRNAs and siRNAs.** (A) Arrayed RT-qPCR of genes found to be down-regulated (or upregulated as with ATP13A3) in **Figure 3.10B** both in 293T  $\Delta$ shL3-pTIP-shL3 cells 50 hrs post-Dox treatment and HeyA8  $\Delta$ shR6-pLKO-shR6 100 hrs post infection and puromycin selection. Data are representative of two independent experiments. Each bar represents mean  $\pm$ SD of two biological replicates and two technical replicates (p-value  $<0.05$ ,  $**<0.005$ , unpaired t-test). (B) Venn diagram showing overlap of genes determined to be down-regulated with both read-based and alignment-based analyses of the RNA-Seq data depicted in **Figure 3.10A** with the critical survival genes found in the Sabatini<sup>408</sup> and Brummelkamp<sup>407</sup> studies, all listed in **Table 3.2**. The Venn diagram was generated using <http://bioinformatics.psb.ugent.be/webtools/Venn>. (C) Kinetic RT-qPCR of the down-regulated genes in the 293T  $\Delta$ shL3 pTIP-shL3 cells. RNA was collected at 14 hrs, 26 hrs, and 50 hrs after treatment with Dox. NS, not significant. Each bar represents mean  $\pm$ SD of quadruplicates (p-value  $<0.05$ ,  $**<0.005$ , unpaired t-test). (D) Table showing which genes were significantly (p $<0.05$ ) down-regulated  $>1.5$  fold (indicated by an ‘X’) in parental HeyA8 cells 80 hrs after transfection with siL3 or 100 hrs after infection and puromycin selection with pLKO-shL1, pLKO-shL3, or pLKO-shR7. The following describes the 11 genes that were significantly down-regulated after introducing the toxic shRNAs shL3 or shR6 into cancer cells (**Figure 3.10B**) and some of their cancer relevant activities. (1) CAPZA1 (capping actin protein of muscle Z-line alpha subunit 1) is an actin-capping protein. CAPZA1 knock down has been reported to cause disassembly of autophagosomes<sup>409</sup>. It is overexpressed in malignant melanoma<sup>410</sup>. (2) CCT3 (chaperonin containing TCP1 subunit 3) is part of a chaperone complex that folds various proteins including actin and tubulin. CCT3 is required for proper mitotic progression<sup>411</sup>. (3) FSTL1 (follistatin-like 1) is a putative activin-binding protein. Knock down of FSTL1 in lung cancer cells results in mitotic arrest followed by apoptosis promoted by the activation of caspase-3 and -9<sup>412</sup>. FSTL1 is down-regulated during cellular senescence of human mesenchymal stem cells<sup>413</sup>. (4) FUBP1 (far upstream element binding protein 1); A lack of FUBP1 causes a cell-autonomous defect in the maintenance of fetal and adult hematopoietic stem cells (HSCs). FUBP1-deficient adult HSCs exhibit significant transcriptional changes, including upregulation of the cell-cycle inhibitor p21 and the pro-apoptotic Noxa molecule, suggesting they undergo apoptosis<sup>414</sup>. In addition, FUBP1 binds to an upstream element of the c-myc promoter and regulates c-myc mRNA level, thus regulating proliferation<sup>415</sup>. Finally, FUBP1 is upregulated in many tumors and acts as an oncoprotein by stimulating proliferation and inhibiting apoptosis<sup>416</sup>. (5) GNB1 (G-protein beta submit 1) is tumor-promoting in breast cancer. Data suggest that GNB1 plays an important role in the mTOR-related anti-apoptosis pathway<sup>417</sup>. (6) HIST1H1C; A specific role of this particular histone in cancer cell survival has not yet been described. (Knock down causes cell cycle arrest in MCF-7 cells<sup>418</sup>). (7) NAA50 (N(alpha)-acetyltransferase 50, NatE catalytic



subunit) is required for sister chromatid separation *in vivo*<sup>419</sup>. (8) NUCKS1 (nuclear casein kinase and cyclin-dependent kinase substrate 1) is a chromatin-associated protein with a role in the DNA damage response. Knocking down NUCKS1 causes chromosomal breaks<sup>420</sup>. (9) PRELID3B (PRELI domain containing 3B) is an inner mitochondrial protein. Knocking down PRELID3B decreases cell viability (<http://www.genecards.org/cgi-bin/carddisp.pl?gene=PRELID3B>). (10) SNRPE (small nuclear ribonucleoprotein polypeptide E); siRNA-mediated depletion of SNRPE stimulated autophagy and led to a marked reduction of cell viability in breast, lung, and melanoma cancer cell lines, whereas it had little effect on the survival of the nonmalignant MCF-10A breast epithelial cells<sup>421</sup>. (11) TFRC (transferrin receptor); Blocking TFRC function with a neutralizing antibody inhibits cell proliferation and survival<sup>422</sup>. Suppression of TFRC led to cell cycle arrest in esophageal squamous cell carcinoma cells<sup>423</sup>. Monal Patel performed experiments for **Figures 3.11A, C, and D**; Ashley Haluck-Kangas performed analysis in **Figure 3.11B**.

This combinatorial analysis identified one gene upregulated and eleven genes downregulated in common between the 293T  $\Delta$ shL3 cells and HeyA8  $\Delta$ shR6 cells upon expression of shL3 and shR6, respectively, compared to shScr (**Figure 3.10B**). These results were confirmed using an arrayed RT-qPCR platform (**Figure 3.11A**). Nine of these downregulated genes have been characterized as either upregulated and/or important for survival in cancer cells (see legend of **Figure 3.11** for details). Consistently, six of these genes were recently identified as cancer survival factors from two independent genome-wide screens<sup>407,408</sup> (**Figure 3.10 and Figure 3.11B**). These six genes are found to be highly amplified and/or mutated in cancers (**Figure 3.12A**), indicative of their role as pro-survival factors. Only ~6.6% of genes were identified as survival genes in these two screens. By comparison, there was significant enrichment (54.5%,  $p$ -value =  $3.6 \times 10^{-6}$  according to binomial distribution) of these survival genes amongst the genes downregulated by either shL3 or shR6.

Interestingly, downregulation of these genes occurred as early as 14 hrs following shRNA expression (**Figure 3.11C**). This precedes the onset of death by nearly two days, which precludes the possibility that the observed expression changes are the result of non-specific degradation that may occur in dying cells. Instead, this result is consistent with RNAi-based targeting, which is known to start within hours of shRNA expression<sup>424</sup>.

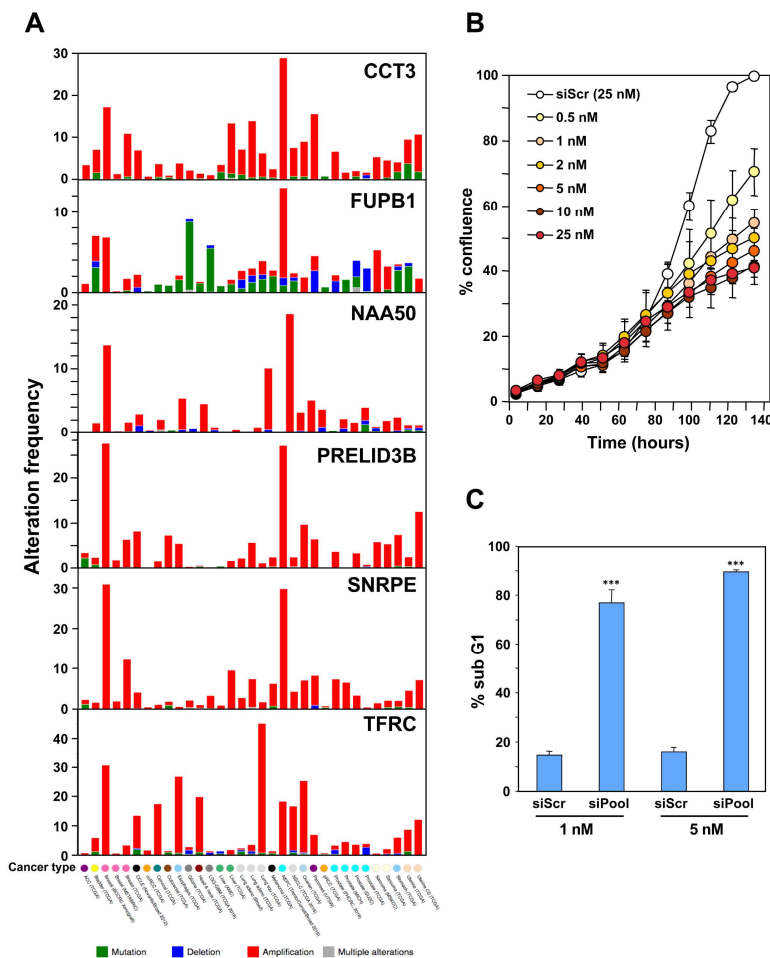


**Figure 3.12 – Characterization of the six genes downregulated in shL3 and shR6 treated cells and found to be critical survival genes in lethality screens.** (A) The six downregulated survival genes were queried individually using default settings with all studies selected in the cBioPortal for Cancer Genomics hosted by the Memorial Sloan Kettering Cancer Center (<http://www.cbioportal.org/>)<sup>425,426</sup>. Datasets with alterations in 5 out of the 6 essential genes reporting both copy number alterations and mutational data were included. To avoid reporting duplicate datasets, the Cancer Genome Atlas publications were excluded. After filtering, 33 datasets representing cancers from 23 different sites reported alterations in the downregulated survival genes. (B) Percent confluence over time of HeyA8 cells transfected with increasing concentrations of a pool of siRNAs (28 different siRNAs) targeting 7 different genes: CCT3, TFRC, NAA50, FUPB1, PRELID3B, GNB1 and FSTL1. Each siRNA SmartPool was comprised of 4 individual siRNAs. Data are representative of two independent experiments. Values were calculated from samples done in quadruplicates shown as mean  $\pm$  SE. (C) PI staining used to quantify percent subG1 for cells 4 days after transfection with 1 nM and 5 nM of combined siRNA pools targeting the 7 different survival genes as in B. Data are representative of two independent experiments. Values were calculated from samples done in quadruplicates shown as mean  $\pm$  SD. \*\*\*  $p < 0.0001$ , unpaired t-test. Ashley Haluck-Kangas performed analysis in **Figure 3.12A**; Quan Gao performed experiments for **Figures 3.12B and C**.

Together, these results show cell toxicity is caused by multiple survival genes being targeted, which is consistent with our previous observation that this unique toxicity is actually a

compilation of multiple death pathways being activated simultaneously<sup>376</sup>. Therefore, this mode of cell death is coined DISE or Death Induced by Survival gene Elimination.

The 11 genes identified as downregulated were knocked down using siRNA SmartPools to individually verify their essentiality to HeyA8 cell survival. Knock down of seven of these genes reduced cell growth (**Figure 3.10C**). However, seed-based off-targeting cannot be meaningfully mimicked using on-target siRNAs, as the former is diluted across multiple targets. In other words, each guide RNA is partitioned amongst its many off-targets. To more accurately mimic a single siRNA targeting these multiple survival genes, HeyA8 cells were treated with all seven siRNA pools simultaneously. Interestingly, transfection of this super-pool even at 1 nM (35.7 pM for each siRNA) still reduced growth of HeyA8 cells compared to siScr-transfected cells (**Figure 3.12B**) as well as induce cell death (**Figure 3.12C**). These results suggest that, although individual repression of a single survival gene through seed-based off-targeting may be small and inconsequential, the collective repression of a network of survival genes is highly toxic.

Extending these observations to additional si/shRNAs would test the generality of this toxic phenomenon. Therefore, wild type 293T cells were infected with pTIP-shScr or pTIP-shL1 and treated with Dox after selection with puromycin to induce shRNA expression. Additionally, HeyA8 cells were transfected with 25 nM of siScr or siL3. Total RNA was harvested after 100 and 48 hrs from the 293T pTIP-shL1 and siL3-transfected HeyA8 cells (and Scr-treated cells), respectively, and subjected to RNA-Seq analysis. To determine whether survival genes were preferentially downregulated, a list of ~1880 survival and ~420 nonsurvival genes identified in a recent CRISPR lethality screen was generated<sup>408</sup> (**Table 3.2**; Sabatini group). The genes included in these four RNA-Seq datasets (i.e. 293T  $\Delta$ shL3 pTIP-shL3, HeyA8  $\Delta$ shR6 pLKO-shR6, 293T

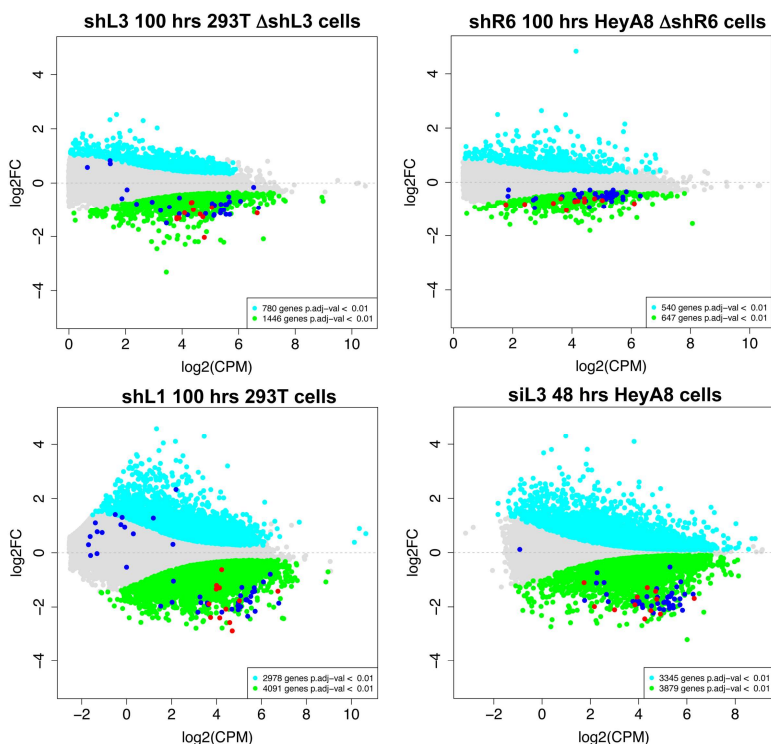


**Figure 3.13 – Histones are downregulated in all forms of DISE but are not the most highly expressed genes in cells.** MA plots comparing the expression level (counts per million, CPM) and fold change in the four RNA Seq data sets in this study. Shown are all RNAs that were >1.5 fold deregulated with an adjusted p-value of <0.01. Significantly down-regulated RNAs are shown in green, upregulated RNAs in cyan. All 73 histones are shown as dark blue dots and the 12 histones downregulated in all four data sets are shown as red dots. Elizabeth Bartom performed analyses for **Figure 3.13**.

pTIP-shL1, and HeyA8 siL3) were ranked according to fold downregulation upon expression of the targeting shRNA (compared to shScr). GSEA analyses were then performed using both the survival and nonsurvival gene sets (**Figure 3.10D**). In all four cases, the most downregulated genes were significantly enriched in survival genes, whereas no enrichment was seen with the nonsurvival gene set.

Interestingly, 12 of the 16 genes downregulated in cells treated with the four si/shRNAs were histones (**Figure 3.10E**). Although dying cells might be expected to downregulate highly expressed genes like histones, the most downregulated genes, including histones, are not the most

highly expressed (**Figure 3.13**). This suggests global histone downregulation is a specific facet of DISE.

In addition to the GSEA performed in **Figure 3.10D**, a Metascape analysis on the four ranked RNA-Seq datasets was also performed. The analysis revealed survival/housekeeping genes involved in the GO clusters mitotic cell cycle, DNA conformation change, and macromolecular complex assembly are preferentially downregulated in cells undergoing DISE induced by any of the four si/shRNAs (**Figure 3.10F**). This is consistent with our previous characterization of DISE as a form of mitotic catastrophe<sup>376</sup> and further suggests degradation of macromolecular complexes. Of note, no enrichment of any immune-related GO terms amongst the upregulated genes was detected, which might be indicative of a non-specific interferon response to the si/shRNAs.

#### *Toxic si/shRNAs Target Survival Genes in their 3' UTR*

Our results show DISE is dependent on the seed sequence and results from targeting multiple survival genes through RNAi. If DISE is, indeed, the result of seed-based targeting, there should be an enrichment of seed match sequences in the 3' UTRs of the downregulated genes. To test this, the ranked RNA-Seq datasets gathered from the 293T  $\Delta$ shL3 pTIP-shL3 and HeyA8  $\Delta$ shR6 pLKO-shR6 (50 hrs) were subjected to a Sylamer analysis, which is designed to find enriched short words corresponding to si/shRNA or miRNA seed matches in the 3' UTRs of the most down/upregulated genes using a hypergeometric statistic. The analysis identified significant enrichment of the seed matches corresponding to shL3 or shR6 in the 3' UTRs of the most downregulated genes gathered from the 293T  $\Delta$ shL3 pTIP-shL3 and HeyA8  $\Delta$ shR6 pLKO-shR6 datasets, respectively (**Figure 3.14A**). Furthermore, there was no enrichment of seed matches

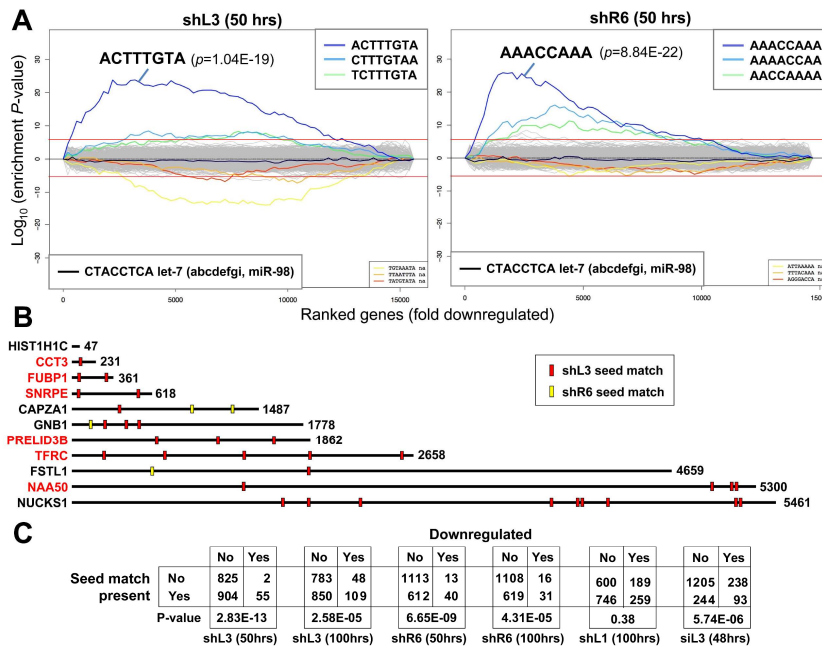


**Figure 3.14 – DISE inducing si/shRNAs target critical survival genes through RNAi.** (A) Sylamer plots for the list of genes in the shL3 experiment (*left panel*) and the shR6 experiment (*right panel*) ordered from down-regulated to up-regulated. The most highly enriched sequence is shown, which in each case is the 8mer seed match of the introduced shRNA. The red line corresponds to a p-value threshold of 0.05 after Bonferroni correction for the number of words tested (65536). Bonferroni-adjusted p-values are shown. The unadjusted p-values are  $1.58E-24$  and  $1.35E-26$ , respectively. The black line represents the sequences carrying the let-7 8mer seed match. (B) Location of the 6mer seed matches of either shL3 or shR6 in the 3'UTRs of the 11 genes (shown at scale) identified in the RNA-Seq results described in **Figure 3.10B**. Red font indicates a survival gene found in both lethality screens in **Figure 3.11B**. (C) A series of six  $2 \times 2$  contingency tables comparing whether or not a critical survival gene is downregulated after treatment with the indicated si/shRNA to whether or not its 3'UTR contains at least one seed match for the introduced sh/siRNA. p-values were calculated using Fisher's Exact Test to determine whether a significant relationship between gene downregulation and presence of seed matches in 3'UTR exists. Stijn van Dongen performed analysis for **Figure 3.14A**; Elizabeth Bartom performed analysis for **Figure 3.14B**; Will Putzbach performed analysis for **Figure 3.14C**.

found in the ORF sequences (**Figure 3.15**), which is consistent with seed-based targeting being largely restricted to the 3' UTR region.

Interestingly, the seed match found by the Sylamer analysis was shifted by 1 nt compared to the predicted seed match based on the lentiviral small hairpin-loop structure. Consistently, small RNA-Seq analysis of the 293T  $\Delta$ shL3 pTIP-shL3 and HeyA8  $\Delta$ shR6 pLKO-shR6 datasets revealed that Dicer cleavage does, in fact, produce a mature siRNA shifted 1 bp away from the shRNA loop region (**Figure 3.16A**). Using this information, two shRNA-to-siRNA converters were designed based on the predicted mature siRNA processed from shL3 and shR6. Transfection of

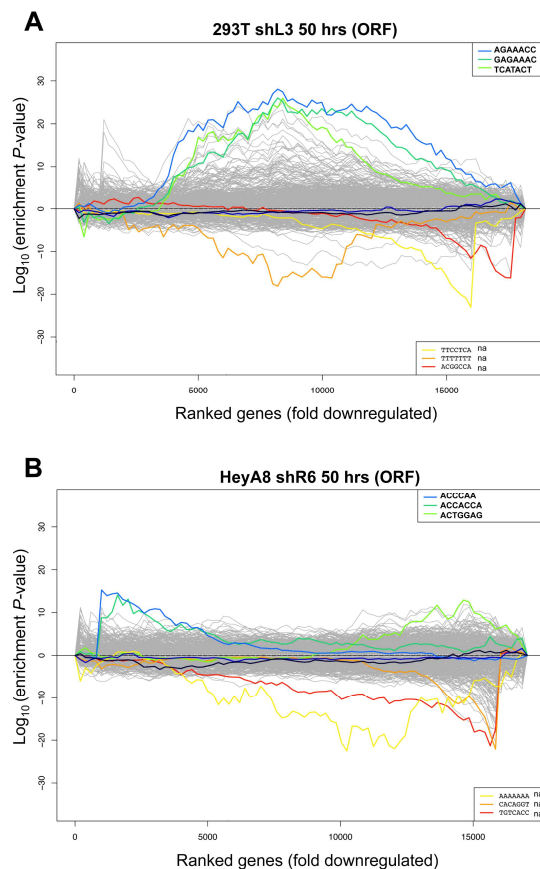


**Figure 3.15 – Sylamer analysis using ORF sequences.** Sylamer analysis of the RNA-Seq datasets gathered from the 293T  $\Delta$ shL3 (A) or HeyA8  $\Delta$ shR6 (B) cells 50 hrs after expression of shL3 and shR6 is induced using ORF sequences. Stijn van Dongen performed the analysis in **Figure 3.15**.

these shRNA-to-siRNA converts was toxic to HeyA8 cells (**Figure 3.16B**), which confirmed DISE is independent of the TRC shRNA delivery platform and only depends on the final mature siRNA sequence.

The Sylamer analysis was extended to the 293T pTIP-shL1 and siL3-transfected HeyA8 datasets. Again, in both cases, significant enrichment of corresponding seed matches in the 3' UTRs of the most downregulated genes was observed (**Figure 3.17**). Importantly, there is only enrichment of seed matches corresponding to the antisense guide strand and not to the passenger strand.

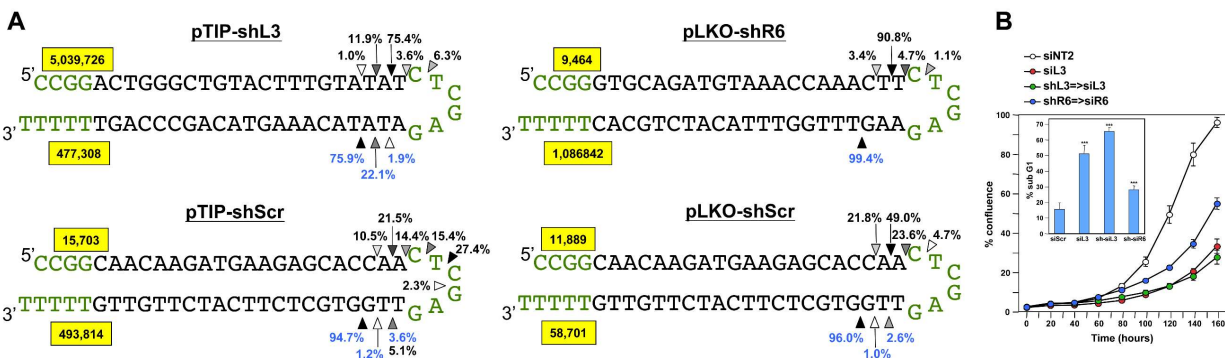


**Figure 3.16 – Quantification of the mature shRNA forms.** (A) Graphical representation of the percentage of the different Dicer cut sites to produce the mature passenger (top) and guide (bottom) strands of 3 shRNAs expressed from two vectors. All analyses were performed with cells 50 hrs after either Dox addition (in pTIP expressing cells) or 50 hrs post puromycin selection after infection with the pLKO virus. Letters in green: vector sequences; black: passenger and guide strands of shRNAs; Arrow heads label the most highly cleaved residues; the darker the arrow head the more highly cleaved. Numbers in yellow box represent total number of reads detected for passenger and guide strands. (B) Percent cell confluence in HeyA8 cells after transfection with shL3 => siL3 (shL3 converted to an siRNA) or shR6 => siR6 (shR6 converted to an siRNA). Conversion was based on the most common mature double-stranded RNA form produced as indicated by the results in A. Data are representative of two independent experiments. Each bar represents mean  $\pm$ SE of four replicates. Insert: percent DNA fragmentation in the same samples. Data are representative of two independent experiments. Each bar represents mean  $\pm$ SD of four replicates, \*\*\* $p < 0.0001$ , unpaired t-test. Elizabeth Bartom and Marcus Peter performed analysis in **Figure 3.16A**; Quan Gao performed experiment in **Figure 3.16B**.

Although certain si/shRNAs induce DISE through a seed and RNAi-dependent manner and also participate in seed-dependent targeting of mRNAs through their 3' UTRs, it was still not clear whether the most downregulated survival genes were, in fact, directly targeted through corresponding seed matches in their 3' UTRs. However, 10 of the 11 downregulated survival genes described in **Figure 3.10B** contain multiple 6mer seed matches to shL3 and/or shR6 (**Figure 3.14B**), which is consistent with these CD95/CD95L-derived si/shRNAs directly targeting a network of survival genes through seed-based RNAi. Interestingly, only four of the histones downregulated after treatment with the four different si/shRNAs contain a 3' UTR (underlined in **Figure 3.10E**), suggesting the global histone downregulation is a specific effect downstream of primary seed match-containing targets.



Whether any of the other toxic shRNAs derived from CD95 or CD95L cause downregulation of these 11 genes silenced by shL3 or shR6 was also tested. HeyA8 cells were

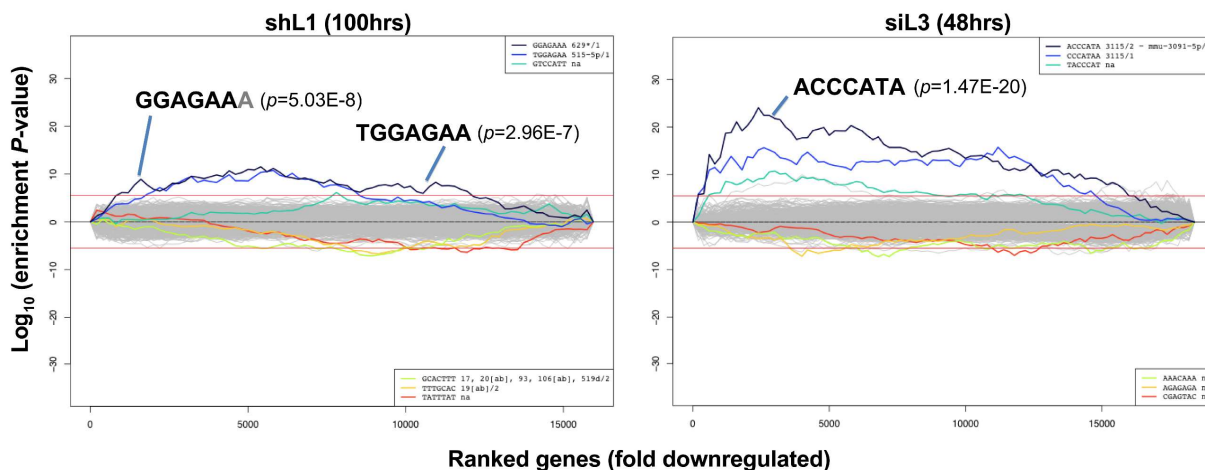


**Figure 3.17 – Identification of seed matches targeted by shL1 and siL3.** Sylamer plots for the list of genes in the shL1 experiment (293T cells 100 hrs post puromycin selection after infection with shL1; *left panel*) and the siL3 experiment (48 hrs after transfection of HeyA8 cells with siL3; *right panel*) ordered from down-regulated to up-regulated. The most highly enriched sequences are shown, which in each case is the 7mer seed match of the introduced shRNA. The red line corresponds to a p-value threshold of 0.05 after Bonferroni correction for the number of words tested. Bonferroni-adjusted p-values are shown. Stijn van Dongen performed analysis for **Figure 3.17**.

either transfected with siL3 (RNA harvested at 80 hrs) or infected with pLKO-shL1, shL3, or shL7 (RNA harvested at 100 hrs). Although shL1 did not cause significant downregulation of these particular genes, shR7 repressed seven of the 11 genes also repressed by shL3 (**Figure 3.11D**), even though their 6mer seed matches were very different (CTTTGT for shL3 and GGAGGA for shR7).

To test whether survival genes are preferentially targeted through seed-based RNAi, a Fisher's Exact Test was performed to determine whether there is any significant enrichment amongst the survival genes downregulated >1.5 fold (and p-value<0.05) and the survival genes containing at least one seed match (**Figure 3.14C**). Analysis of nearly all the RNA-Seq datasets revealed significant enrichment of downregulated survival genes amongst those that harbored at least one seed match in their 3' UTR versus none. The only exception was the 293T pTIP-shL1

cells collected at 100 hrs following Dox-induced shRNA expression. However, this is likely caused by numerous secondary effects that accumulate in dying cells at later timepoints, which masks direct targeting observed at earlier time points. This is supported by the finding that the Sylamer analysis yielded a less significant result for this dataset (**Figure 3.17**).

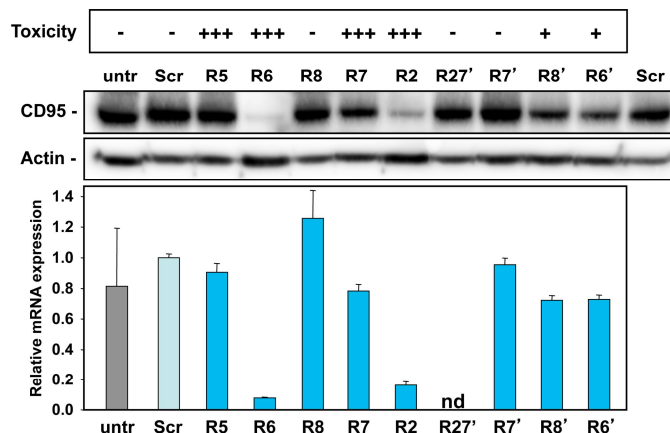


**Figure 3.18 – Activity to knock down CD95 does not determine shRNA toxicity.** HeyA8 cells infected with the indicated shRNAs from the pLKO vector were analyzed for toxicity (*top*; % percent reduction at half maximal confluency), CD95 expression by Western blot analysis (*center*, 2 days after puromycin addition) and RT-qPCR analysis (*bottom*, 3 days after puromycin addition). Shown data are representative of two independent experiments. +++, >75%; ++, >50%; +, >10%; -, <10% growth reduction. Monal Patel performed experiments for **Figure 3.18**.

Our experiments have concretely demonstrated DISE is independent of on-target knock down of CD95 or CD95L. Therefore, a perfect correlation between knock down capacity of TRC shRNAs targeting CD95 and toxicity is unlikely. Indeed, expression of different CD95-targeting TRC shRNAs in HeyA8 cells revealed that while some toxic shRNAs efficiently repressed CD95 protein expression (i.e. shR2 and shR6), there were other toxic shRNAs that did not (i.e. shR5 and shR7) (**Figure 3.18**).

Thus, our experiments show cancer cells die through DISE, which is triggered by early and preferential repression of survival genes through RNAi via seed-based targeting of seed matches in their 3' UTRs.

*Identification of Toxic shRNAs in the CD95L and CD95 mRNAs*

Our results show the majority of commercially available si/shRNAs and DsiRNAs designed to target CD95 and CD95L are toxic to cancer cells. However, these reagents are designed by algorithms that seek to mitigate off-targeting and therefore, may not be the most toxic sequences derived from CD95/CD95L. To comprehensively test all shRNAs that can be derived from CD95 and CD95L, all possible 21mer shRNAs were synthesized—starting at the A in the start codon and then shifting each nearest neighbor by one nt along the ORF and 3' UTR sequences of CD95 and CD95L to achieve 100% coverage (**Figure 3.19A**). Every possible shRNA derived from the ORF of an unrelated control gene Venus, which is not predicted to have any enrichment of toxic sequences, were also included. A total of 4,666 shRNA cassettes (700 for Venus, 825 for CD95L ORF, 837 for CD95L 3' UTR, 987 for CD95 ORF, and 1317 for CD95 3' UTR) were subcloned into our Dox-inducible pTIP vector as five individual pools (**Figure 3.19B**). The RNAi efficacy of each pool was tested by infecting NB7 Venus-CD95L and NB7 Venus-CD95 reporter cells with each corresponding pool individually (**Figure 3.20A**). Dox-induced expression of the Venus pool showed some reduction in Venus-CD95L expression, whereas expression of the CD95L ORF shRNAs seemed much more effective at repressing the reporter. The CD95L 3' UTR-targeting shRNA pool did not cause any reduction in reporter expression since the 3' UTR sequence of CD95L is not part of the Venus-CD95L reporter. Similar results were observed when the NB7 Venus-CD95 cells were infected with either the Venus, CD95 ORF, or CD95 3' UTR-targeting shRNA pools following Dox induction. To test the overall toxicity of each of the pools, the 5 individual pools were infected separately into wild type NB7 cells (the reporter cells were not used to avoid any possible sponge effect by expressing CD95 or CD95L mRNA as part of the

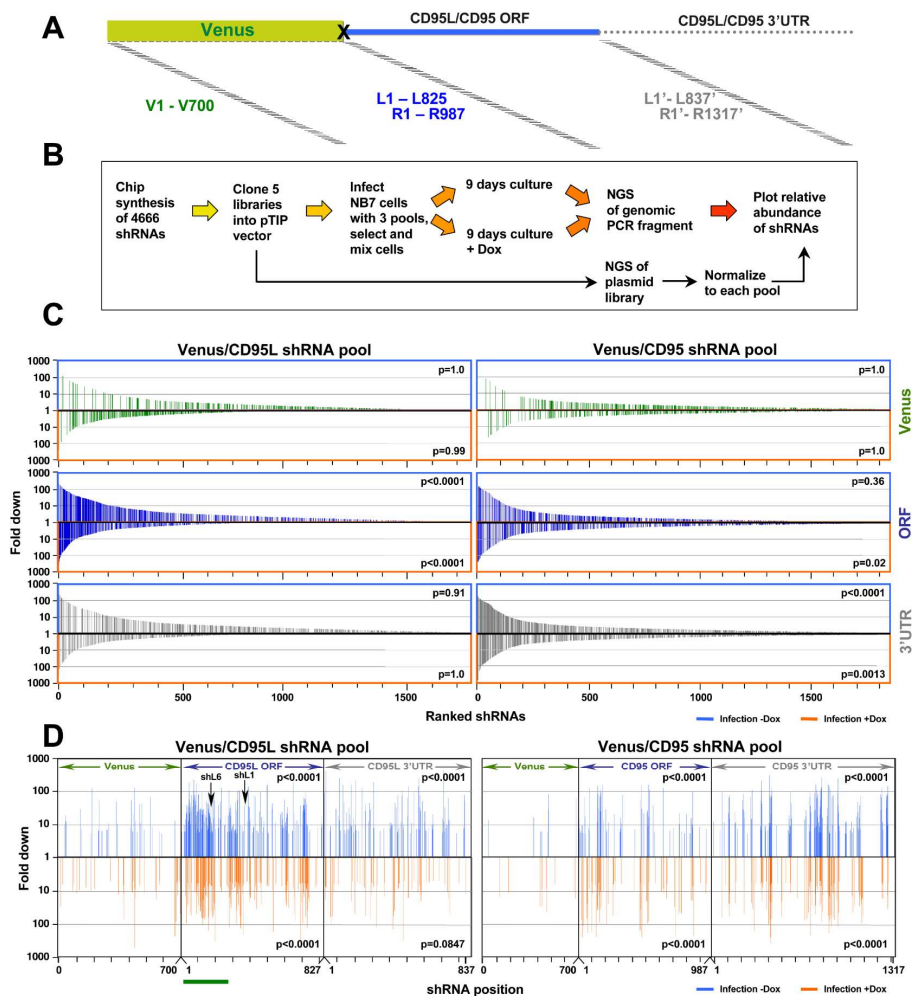


**Figure 3.19 - Identifying all toxic shRNAs derived from CD95L and CD95.** (A) Schematic showing the cloned shRNAs covering the ORF of Venus and the ORFs and 3'UTRs of CD95L and CD95. The 3'UTR is displayed as a dashed line because it was not included in the full-length Venus-CD95L/CD95 sensors. (B) Work-flow of pTIP-shRNA library synthesis, shRNA screen, and data analysis. (C) Ranked fold reduction of shRNAs spanning Venus and the CD95L ORF and 3'UTR (left three panels) and Venus and the CD95 ORF and 3'UTR (right three panels). The ranked lists were separated into the shRNAs derived from Venus (top panels), the ORFs (center panels) and the 3'UTRs (bottom panels). The p-value of enrichment for each ranked set of shRNAs is given. Only the parts of the ranked lists are shown with the downregulated shRNAs. For all six panels, the top section of each panel (boxed in blue) contains the data on shRNAs downregulated after infection of cells and cultured for 9 days without Dox when compared to the composition of the shRNA plasmid library, and the bottom half (boxed in orange) contains the data on shRNAs downregulated after culture with Dox for 9 days when compared to the culture without Dox. P-values were calculated using Mann Whitney U tests with a one-sided alternative that the rank was lower. (D) The location of all shRNAs significantly downregulated at least five-fold along the sequences of Venus, CD95L ORF, CD95L 3'UTR (left panels) and Venus, CD95 ORF, and CD95 3'UTR (right panels). The top half of each sub-panel (blue ticks) shows the shRNAs downregulated after infection and the bottom half (orange ticks) contains the data on shRNAs downregulated after culture with Dox for 9 days. Significance of enrichment in the different sub-panels is shown. p-values were calculated according to statistical tests of two proportions. Each sub-pool was compared to the corresponding Venus sub-pool to assess relative enrichment. Green line: sequence that corresponds to the intracellular domain of CD95L. Will Putzbach performed experiments for Figure 3.19A and B; Marcus Peter, Elizabeth Bartom, and Denise Scholtens performed analyses for Figures 3.19C and D.

Venus reporter construct), and the expression of the shRNAs was induced with Dox (**Figure 3.20B**). Interestingly, expression of the Venus shRNA pool caused no observable toxicity upon treatment with Dox, whereas both the CD95L ORF and CD95 3' UTR shRNA pools caused significant toxicity. The CD95L 3' UTR shRNA pool did not cause any noticeable toxicity. The CD95 ORF shRNA pool caused intermediate toxicity. A lack of toxicity seen with the Venus shRNA pool and observable toxicity with the CD95/CD95L-targeting pools were also observed in HCT116 (**Figure 3.21A**) and 293T (**Figure 3.21B**) cells, although the toxicity of each individual pool was cell type-dependent. These data suggest that the CD95L ORF and CD95 3' UTR contain the highest abundance of toxic shRNA sequences.

Now, to determine the toxicity of each individual shRNA in the pools, wild type NB7 cells were infected with the pTIP-shRNA libraries at a MOI < 1 to limit the number of multiple integrations. After puromycin selection, the infected cells were combined into two main groups by mixing cells from each of the pools in a 1:1:1 ratio. The CD95L group consisted of NB7 cells infected with the Venus, CD95L ORF, and CD95L 3' UTR shRNA libraries. The CD95 group consisted of NB7 cells infected with the Venus, CD95 ORF, and CD95 3' UTR shRNA libraries. This was done to allow for competition between shRNAs when Dox was added (**Figure 3.19B**). The cells were cultured in duplicate for nine days with or without Dox. To identify which shRNA sequences are depleted with time (surrogate for toxicity), PCR was used to amplify the shRNA barcodes from three sources: (1) The cloned pTIP-shRNA plasmid libraries, (2) the integrated pTIP-shRNA vector isolated from the genomic DNA of cells cultured in the absence of Dox, and (3) the integrated pTIP-shRNA vector isolated from the genomic DNA of cells cultured with Dox. The amplified products were then submitted for deep sequencing. Nearly all shRNAs were found

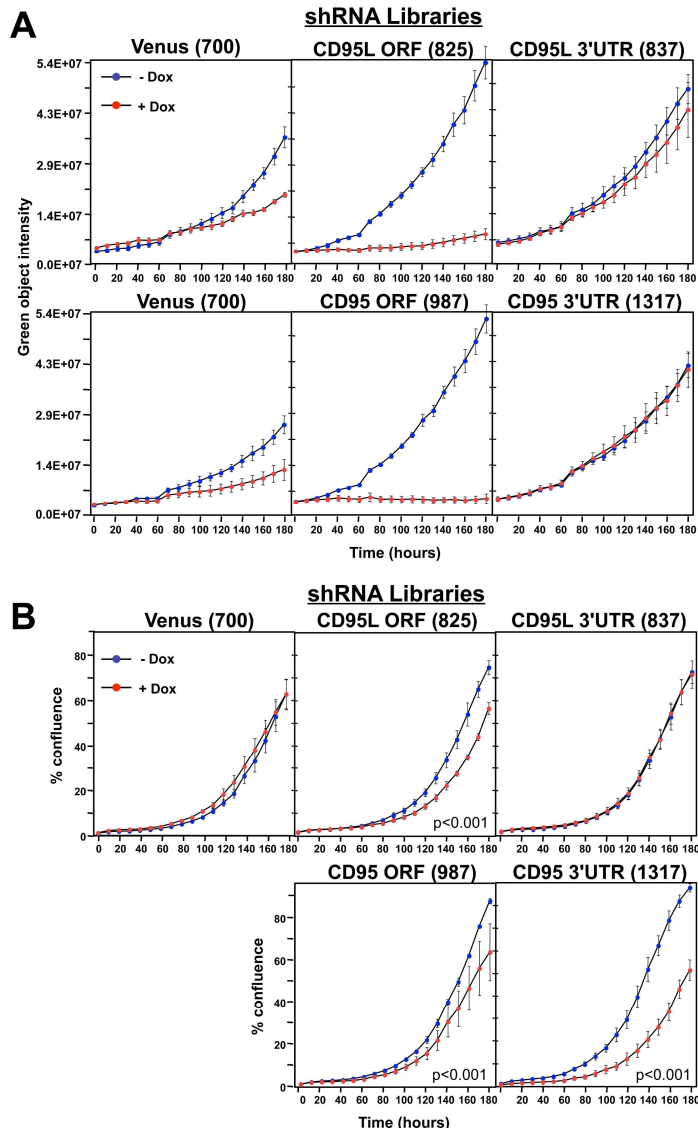


**Figure 3.20 – Toxicity and RNAi of individual shRNA pools.** (A) *Top panels:* Green object intensity over time of NB7 Venus-CD95L sensor cells infected with the pTIP-Venus shRNA pool (*left panel*), pTIP-CD95L ORF shRNA pool (*center panel*), or the pTIP-CD95L 3'UTR shRNA pool (*right panel*) with or without Dox treatment. *Bottom panels:* Green object intensity over time of NB7 Venus-CD95 sensor cells infected with the pTIP-Venus shRNA pool (*left panel*), pTIP-CD95 ORF shRNA pool (*center panel*), or pTIP-CD95 3'UTR shRNA pool (*right panel*) with or without Dox treatment. Values were calculated from samples done in quadruplicates shown as mean  $\pm$  SE. (B) Percent confluence over time of parental NB7 cells infected with the pTIP-Venus shRNA pool (*top left panel*), pTIP-CD95L ORF shRNA pool (*top center panel*), pTIP-CD95L 3'UTR shRNA pool (*top right panel*), pTIP-CD95 ORF-shRNA pool (*bottom center panel*), and pTIP-CD95 3'UTR shRNA pool (*bottom right panel*) with or without Dox treatment. Values were calculated from samples done in triplicate shown as mean  $\pm$  SE. P-values were calculated using two-way ANOVA with a factor for Dox treatment and a factor for time. Will Putzbach performed experiments for **Figure 3.20**.

in the cloned pTIP-shRNA library plasmid preps. The CD95L pool and CD95 pool shRNAs were ranked from most toxic (most underrepresented) to least toxic (**Figure 3.19C**). Interestingly, in

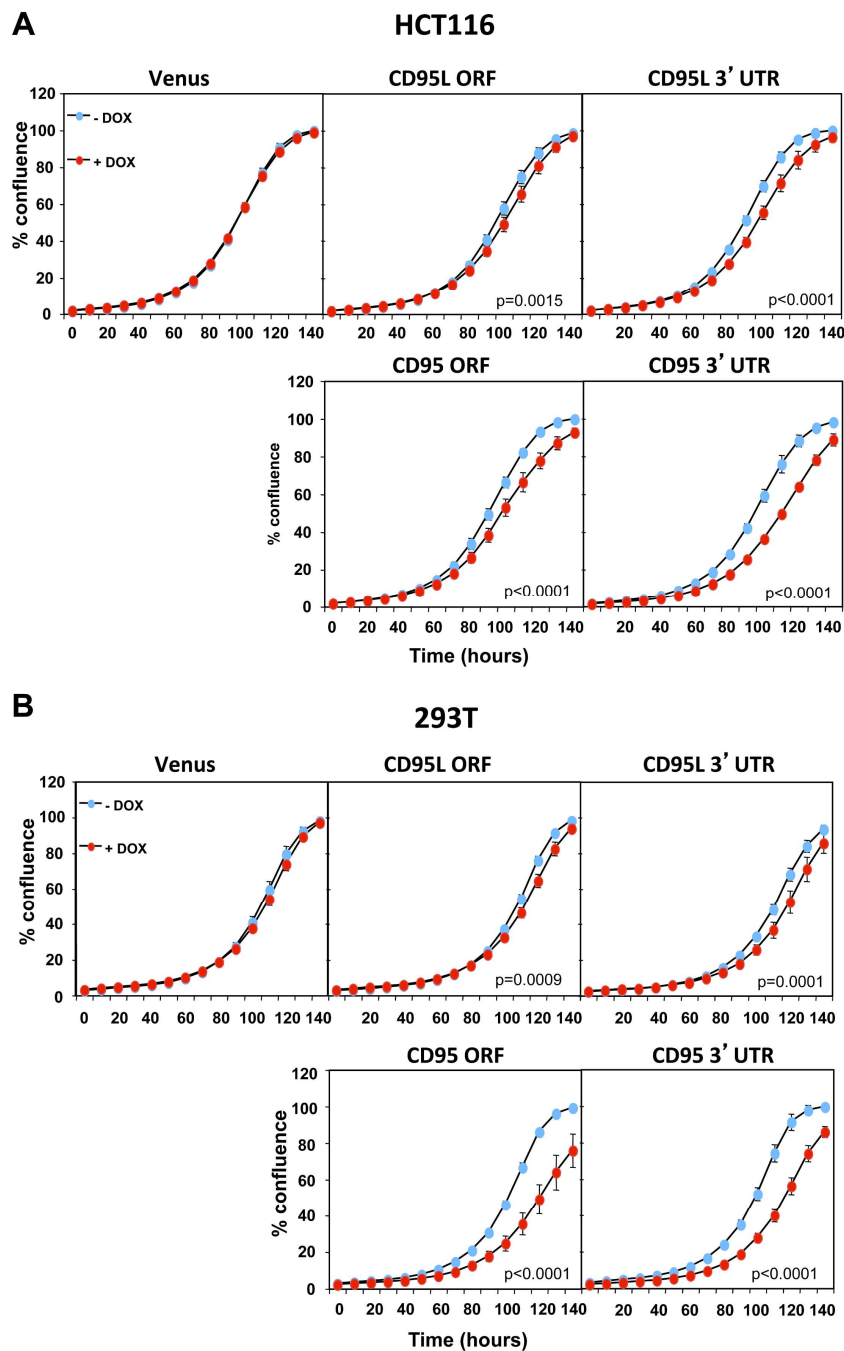


**Figure 3.21 – Toxicity of individual pTIP-shRNA in 293T and HCT116 cells. (A)** Wild type HCT116 cells were infected with the individual pTIP-shRNA pools separately. The shRNA expression was induced with treatment with 100 ng/mL Dox. Cell confluence was used to measure cell growth. Values were calculated from samples done in triplicate shown as mean  $\pm$  SE. **(B)** Wild type 293T cells were infected with the individual pTIP-shRNA pools separately. The shRNA expression was induced with treatment with 100 ng/mL Dox. Cell confluence was used to measure cell growth. Values were calculated from samples done in triplicate shown as mean  $\pm$  SE. P-values were calculated using two-way ANOVA with a factor for Dox treatment and a factor for time. Will Putzbach performed experiments for **Figure 3.21**.

addition to Dox-induced depletion of shRNA barcodes (inferred by comparing the shRNA representation in the Dox-treated to non-treated cells after infection), there was also many instances where shRNAs barcodes became depleted simply after infecting cells (inferred by

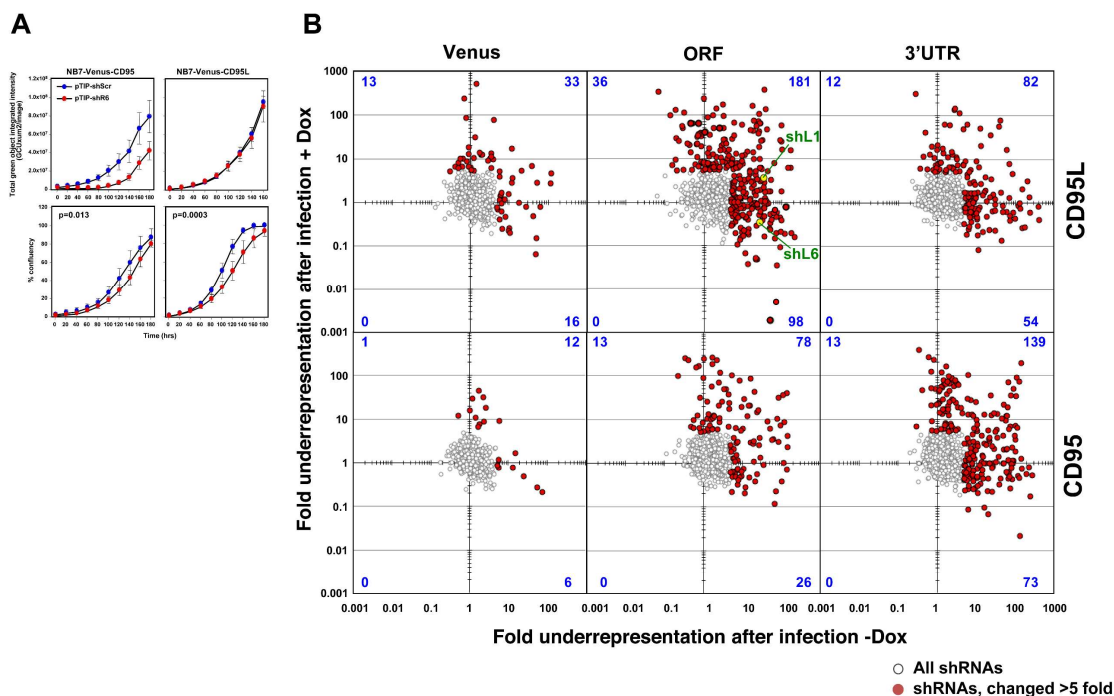


**Figure 3.22 — Fold change in shRNA representation after infection of NB7 cells and after treatment with Dox.** (A) Change in green fluorescence (top panels) and percent cell confluency (bottom panels) over time of NB7 cells expressing either Venus-CD95 (left panels) or Venus-CD95L (right panels). Cells were infected with the DOX-inducible pTIP-shR6 virus, selected for two days with puromycin and then subjected to an analysis in the IncuCyte Zoom. Values were calculated from samples done in triplicate shown as mean  $\pm$  SE. (B) Scatterplot showing the fold down of shRNAs after infection of cells and culture for 9 days without Dox when compared to the composition of the shRNA plasmid library (X axis) and the fold down of shRNAs after culture with Dox for 9 days when compared to the culture without Dox (Y axis). The red dots are the shRNAs that were significantly downregulated at least five-fold. The number of shRNAs labeled in red in each quartile is given in blue. Two of the shRNAs tested before are labeled in green. Monal Patel performed experiment for **Figure 3.22A**; Elizabeth Bartom, Marcus Peter, and Denise Scholtens performed analysis for **Figure 3.22B**.

comparing the shRNA representation in the pTIP-shRNA plasmid prep to non-treated cells after infection). This is likely due to the previously-described “leaky” expression from Dox-inducible systems in the absence of Dox<sup>427</sup>. This was confirmed by infecting NB7 Venus-CD95 reporter cells with pTIP-shR6 (**Figure 3.22A**). Therefore, the screen analysis was split in two halves: (1) The changes in shRNA abundance after infection compared to the pTIP-shRNA plasmid pool were



analyzed (infection -Dox). (2) The changes in shRNA abundance after addition of Dox to infected cells compared to infected cells cultured without Dox were analyzed (infection +Dox). The shRNAs that are underrepresented following infection are either boxed (**Figure 3.19C**) or shown (**Figures 3.19D and 3.23B and Figure 3.24B**) in blue, and those underrepresented following treatment with Dox are either boxed or shown in orange. **Figure 3.22B** shows the results for all the shRNAs, with grey dots representing all shRNAs and red dots representing those more than 5-fold downregulated (see fold down values for each shRNA in **Table 3.3**). The results show that CD95L ORF and CD95 3' UTR libraries have the highest concentration of toxic shRNAs, which is consistent with the individual pool data in **Figure 3.20B**. The toxicity is also apparent when the shRNAs of the CD95L pool (2362 shRNAs) and the CD95 pool (3004 shRNAs) are ranked according to the highest degree of down regulation within each sub-pool (**Figure 3.19C**). Again, both the CD95L ORF and CD95 3' UTR pools contain a statistically significant enrichment of underrepresented shRNAs compared to the Venus sub-pool. **Figure 3.19D** shows the location of the underrepresented (>5 fold down-regulated) shRNAs along the mRNA sequences of CD95L (*left panel*) and CD95 (*right panel*) ORFs and 3' UTRs and the Venus ORF. The toxic shRNAs seem to associate into distinct clusters in CD95 and CD95L, with the highest concentration being in the proline-rich region of the CD95L ORF (underlined in green).

#### *Predicting shRNA Toxicity—The Toxicity Index and GC Content*

Our results show certain si/shRNAs derived from the mRNA sequences of CD95 and CD95L are toxic to cancer cells by preferentially targeting survival genes. Since targeting multiple survival genes versus a single survival gene, with same number of guide RNA molecules per target,

kills cells more effectively (**Figure 3.12B and C**), we reasoned highly toxic si/shRNAs would likely have more seed matches in the survival gene set. Based on this, a toxicity index (TI) was calculated to predict an si/shRNA's toxicity; this TI is equal to the ratio of the number of seed matches in the 3' UTRs of the Sabatini survival gene set versus the nonsurvival gene set after normalization to the number of genes in each set (**Figure 3.23A**). This was done for every

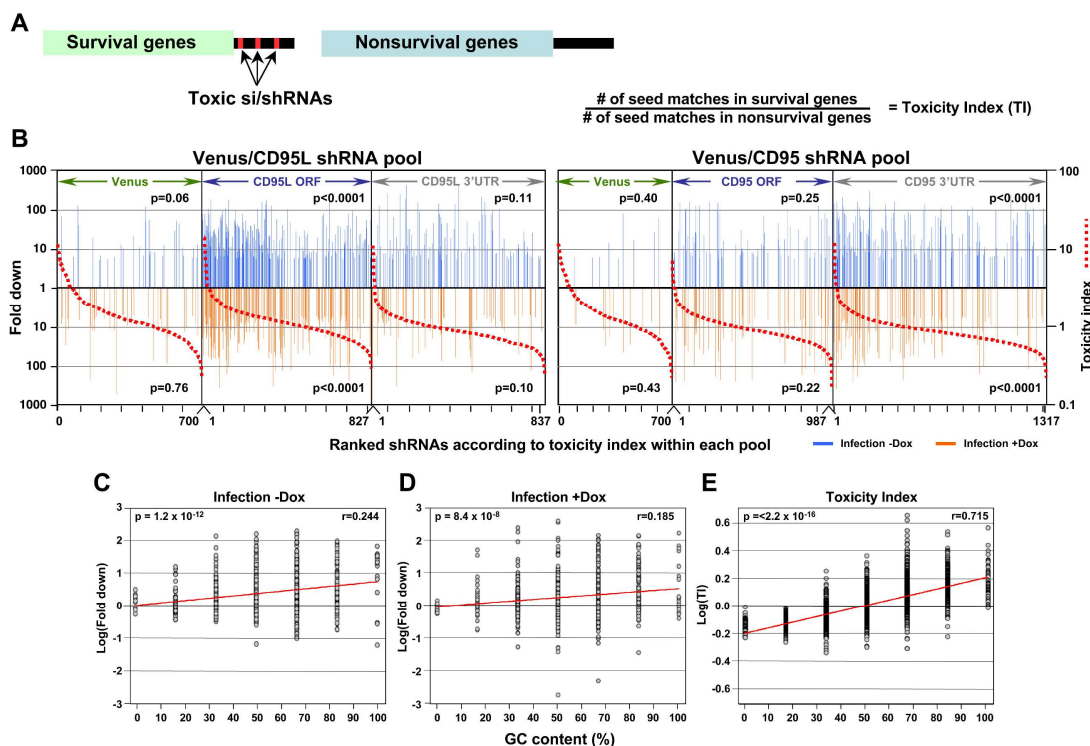


**Figure 3.23 – *In silico* prediction of DISE activity tracks with experimentally determined toxicity of shRNAs.** (A) *Left*: Schematic showing the preferential targeting of seed matches present in the 3'UTRs (red marks) of survival genes by toxic si/shRNAs. *Right*: The toxicity index (TI) is the normalized ratio of the number of 8mer (or 6mer) seed matches present in a list of survival genes versus a list of nonsurvival genes. (B) Fold downregulation versus ranked Toxicity Index (8mer seed match) for shRNAs of the Venus/CD95L pool (*left three panels*) and the Venus/CD95 pool (*right three panels*). Orange and blue tick marks indicate the same as in **Figure 3.19D**. To test if higher TI is enriched in shRNAs that were highly downregulated, p-values were calculated based on permuted datasets using Mann-Whitney U tests. The ranking of TI was randomly shuffled 10,000 times and the W statistic from our dataset was compared to the distribution of the W statistic of the permuted datasets. (C, D) Plot of  $\log_{10}$ (fold down-regulation) of toxic shRNAs derived from CD95L ORF of the toxicity screens -Dox (C) or +Dox (D) versus GC content the 6mer seed in each shRNA. (E) Plot of the  $\log_{10}$ (TI) of all 4096 possible 6mers versus GC content of the seeds. Pearson correlation coefficient and significance (p values) are given. Will Putzbach performed analyses for **Figures 3.23A and C to E**; Elizabeth Bartom, Marcus Peter, and Denise Scholtens performed analysis for **Figure 3.23B**.

8mer seed sequence found in the shRNAs of the screen (**Table 3.4**). Each shRNA was ranked according to its corresponding TI within each pool, and the Infection -Dox (blue ticks) and Infection +Dox (orange ticks) toxicities for the shRNA that were >5 fold downregulated in the screen were indicated. Visual inspection of the graph shows that the shRNAs found to be >5 fold underrepresented are enriched amongst the shRNAs with a higher TI for the CD95L ORF and CD95 3' UTR pools, which was then confirmed using a permutation test based on the Mann-Whitney U statistic (**Figure 3.23B**). Thus, the *in silico* TI is a fair predictor of actual toxicity that is based on publicly-available sequence data.

A list of the most highly expressed survival genes (~850 genes with an average read count above 1000 across all 16 control RNA-Seq datasets) identified in the two lethality screens presented in **Figure 3.11B** and a second list of expression-matched nonsurvival genes were generated (**Figure 3.24A and Table 3.2**). Two additional TIs were calculated to account for differences in the lengths of the 3' UTRs and gene expression between survival and nonsurvival genes. The first modified TI was calculated based on only the longest 3' UTR of the genes in the original Sabatini survival and nonsurvival gene sets (the original TI shown in **Figure 3.23B**; *left panel* used all available 3' UTRs); an additional normalization step was done by dividing the number of seed matches by the length of the 3' UTR for every gene. This version tracked well with observed shRNA toxicity in the screen (**Figure 3.24B**; *center panel*). Another alternate TI was calculated using only the longest 3' UTR sequence for each gene found in the two highly expressed expression-matched gene sets (**Table 3.2**). According to the analysis in **Figure 3.24B**; *right panel*, enrichment of toxic shRNAs was still enriched amongst those with a higher modified TI, although to a lesser extent than the original TI. This is consistent with our previous observation

that the most downregulated mRNAs targeted by the si/shRNAs are not necessarily the most highly expressed ones (**Figure 3.13**).

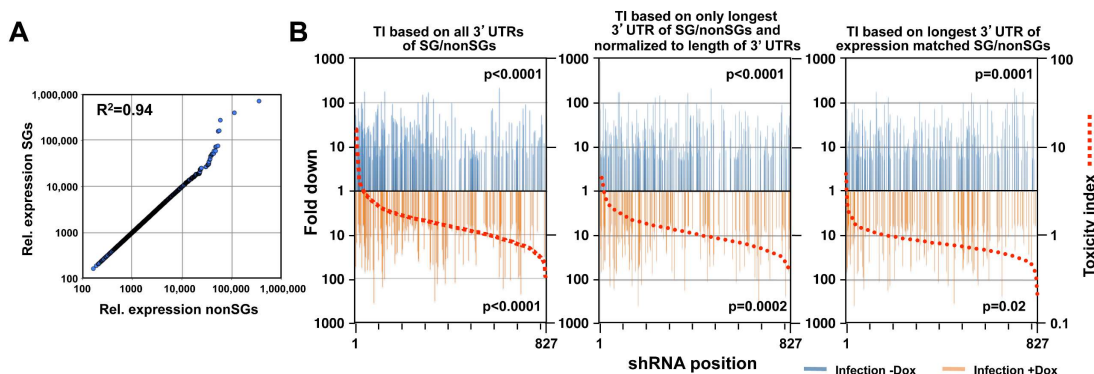


**Figure 3.24 – DISE does not just target all highly expressed genes.** (A) Correlation between all survival genes (identified as critical survival genes in the two lethality screens presented in **Figure 3.11B** and expressed at least at 100 reads in all 16 control RNA Seq samples in this study) and expression-matched nonsurvival genes (genes not identified as critical survival genes in two genome-wide lethality screens and expressed at least at 100 reads in all of the 16 control RNA Seq samples in this study). (B) Reanalysis of the CD95L ORF data in **Figure 3.23B** using two alternative TIs. *Left*: the analysis shown in **Figure 3.23B** with the shRNAs ranked using the original TI (using all known 3'UTRs for each gene group). *Center*: analysis with the shRNAs ranked using the TI calculated with only the longest 3'UTR per gene and normalizing for 3' UTR length. *Right*: analysis with the shRNAs ranked according to their TI based on the ~850 most highly expressed (>1000 average reads; **Table 3.2**) expression-matched survival and nonsurvival identified in A and using the longest 3'UTR for each gene. Whether higher TIs are enriched amongst shRNAs underrepresented in the screen was assessed with permuted datasets using the Mann-Whitney U tests. Will Putzbach performed analyses for **Figure 3.24**; Elizabeth Bartom, Marcus Peter, and Denise Scholtens performed analyses for **Figure 3.24**.

Base pairing between G-C creates a more stable interaction than between A-U. Therefore, si/shRNAs with higher GC content in their seed sequences would be expected to be more toxic, as they would be more effective in interacting with their seed match targets. Indeed, a statistically significant positive correlation was found between the seed GC content (6mers) and both Infection -Dox (**Figure 3.23C**; Pearson rho = 0.244 with p-value =  $1.2 \times 10^{-12}$ ) and Infection +Dox (**Figure 3.23D**; Pearson rho = 0.185 with p-value =  $8.4 \times 10^{-8}$ ) toxicities for the CD95L ORF pool. Interestingly, the TI (calculated using 6mer seed matches) correlated the strongest with the seed GC content (**Figure 3.23E**; Pearson rho = 0.715 with p-value <  $2.2 \times 10^{-16}$ ), which supports previous analyses showing survival/housekeeping genes are found in higher frequency in GC-rich

regions of the genome<sup>214,216</sup> and is consistent with G-C base pairing mediating more potent seed-based RNAi than A-U base pairing<sup>138</sup>.

In summary, these results show si/shRNAs, such as those derived from CD95 and CD95L, are toxic to cancer cells through targeting a network of survival genes through seed-based targeting in their 3' UTRs via RNAi.

## Discussion

OTEs are generally thought as an impediment of RNAi-based experiments and therapies—particularly RNAi screening applications. Seed-based OTEs (sOTEs) are particularly detrimental, as all si/shRNAs are theoretically capable of seed-based targeting and prediction of the genes deregulated as a result of or downstream of this seed-based targeting is difficult. Here, our results describe a unique facet of seed-based targeting discovered through a unique sOTE coined DISE, which results in simultaneous activation of multiple death pathways. This explains our previous observation that cancer cells cannot easily develop resistance to this mode of cell death<sup>376</sup>.

### *DISE Represents a Specific Form of RNAi sOTE*

There are several facets of RNAi reagents that produce undesired OTEs, including promiscuous off-targeting through RNAi<sup>108,168,428</sup>, saturation of the RNAi machinery<sup>162</sup>, general toxicity evoked by specific sequence motifs<sup>429</sup>, and/or triggering an interferon response<sup>149,150,152</sup>. The following pieces of evidence support the notion that DISE is a predictable, conserved biological response that is not evoked by any of these mechanisms.

1. Enrichment of toxic si/shRNA sequences derived from CD95 and CD95L. Multiple RNAi-based screens indicate that only between two to five percent of si/shRNAs are toxic to cells. Our own analysis of 12 independent arrayed shRNA lethality screens identified 651 candidate survival genes out of ~18,000 targeted genes<sup>376</sup>. This indicates that only a very small percentage of commercially designed shRNAs should be toxic to cells. In contrast, >80% of si/shRNAs designed to target CD95 and CD95L are toxic to cancer, which is consistent with a recently published parallel TRC-based shRNA lethality screen conducted in 216 solid and blood cancer cell lines<sup>377</sup>. Interestingly, CD95 and CD95L were not identified as candidate survival genes in this study because of low consistency scores, which indicates toxicity likely does not result from on-targeting. Indeed, this work shows si/shRNA toxicity is dependent on seed-based targeting and suggests every shRNA's seed sequence should be analyzed individually for its DISE-inducing potential.
2. DISE is not caused by saturating the RNAi machinery. Consistently, concentrations down to 5 nM, and even down to 1 nM, were toxic to cancer cells, which is well below the recommended concentration for on-target knock down. If these shRNAs were toxic by saturating the RISC, we would have detected depletion of targeting by highly expressed endogenous miRNAs like the let-7 family. However, upregulation of genes whose 3' UTRs contain seed matches for this miRNA family was not observed (black lines in **Figure 3.14A**). Finally, DISE cannot be caused by saturating the RNAi machinery since DISE can occur in the absence of Drosha or Dicer, which are depleted in ~96% of endogenous miRNAs<sup>60</sup>.

3. DISE is not the result of triggering an interferon response. Gene expression changes from multiple RNA-Seq datasets generated after introducing DISE-inducing si/shRNAs have been analyzed. There was no observable enrichment of immune-related genes (**Figure 3.10F**) amongst upregulated targets in any of these datasets. Furthermore, DsiRNAs do not evoke an interferon response<sup>399</sup>, and expression of shRNAs from an integrated lentivirus evoke less of an interferon response compared to siRNAs<sup>430</sup>. Both DsiRNAs and shRNAs were shown to evoke comparable toxicity to transfected siRNAs (**Figure 3.1A and B**).
4. Introduction of just one mutation in the seed sequence destroys toxic activity (**Figure 3.8H**). This argues against DISE being a manifestation of saturating the RNAi machinery, evoking an interferon response, or through a specific toxic motif because none of these facets depend on the seed sequence.

#### *What are the Requirements for an si/shRNA to Induce DISE?*

Our data suggest DISE manifests from seed-dependent RNAi targeting and not the result of a toxic non-seed motif such as UGGC described by Fedorov *et al*<sup>382</sup>. Consistently, the seed sequence and RNAi capacity are critical to the toxicity of DISE-inducing si/shRNAs (**Figure 3.8**). Furthermore, toxic si/shRNAs can be predicted by our *in silico* TI and tend to have a higher GC content; the latter point is not absolute, as many of the commercial si/shRNAs used in this study are designed to have a lower GC content in their seed sequences (shL3, 25%; shR6, 25%; siL3, 37.5% based on 8mers). Nevertheless, the data suggest survival and nonsurvival genes have different levels of targetability—perhaps the result of differences in base composition, sequence, or even in how survival/housekeeping genes are regulated. Specifically, base

composition/sequences of survival genes are likely more GC-rich as they are often located within isochore regions<sup>216</sup>. This could mean the 3' UTRs of these survival/housekeeping genes are biased in having a higher abundance of GC rich seed matches, which would be consistent with the analyses in **Figure 3.23C, D, and E**. Moreover, GC-rich seed matches would presumably be more targetable because of the lower binding energy. Besides a biased distribution of seed matches in survival/housekeeping genes, this fundamental class of genes, and also other genes associated with distinct GO terms, are characterized as miRNA anti-targets, which are depleted in miRNA target sites through natural selection<sup>201,203</sup>. Interestingly, mRNA targets that lack endogenous miRNA target sites in their 3' UTRs are more susceptible to seed-based off-target effects<sup>127</sup>. In addition, it is also possible DISE-inducing si/shRNAs have seed sequences that target seed match target sites enriched in these anti-targets.

#### *DISE is Caused by Loading of the Guide Strand of Toxic si/shRNAs into the RISC*

Many of the DISE-inducing shRNAs used in this study are based on the TRC hairpin design, which has been shown to participate in extensive off-targeting because of imprecise Dicer cleavage that generates multiple different species of guide RNAs with shifted seed sequences<sup>72</sup>. Moreover, the TRC shRNA has been shown to produce guide RNAs shifted by 4 nts 3' of the expected 5' start site. However, the small RNA-Seq data do not support such an elevated level of imprecision. Instead, the vast majority (99.4% for shR6) of our pTIP and pLKO-expressed shRNAs produce a single predominant guide RNA that is shifted by only 1 nt (**Figure 3.16A**). Also, Sylamer analysis shows that only one seed match is predominantly enriched in downregulated genes (**Figure 3.14A and Figure 3.17**), which is consistent with one species of



guide RNA being produced. Indeed, all four analyses showed enrichment of seed matches in the 3' UTR and not the ORF corresponding to the antisense guide strand and never the sense passenger strand (**Figure 3.14A and Figure 3.15 and Figure 3.17**).

#### *DISE has Features of the RNAi OTE Previously Reported*

Our data on DISE are consistent with numerous previous reports on sOTEs, including the requirement for reverse complementarity between the six/seven bps between the seed sequence of the introduced si/shRNA and target mRNAs' 3' UTRs<sup>108,428</sup>. Furthermore, DISE is triggered independently of the platform used to deliver the RNAi reagent.

#### *The Role of Dicer in DISE*

The Peter lab had shown that shL3 killed Dicer<sup>Exo5<sup>-/-</sup></sup> HCT116 cells (with deleted Exon 5) as effectively as in wild type HCT116, which initially suggested Dicer is not required for death to occur<sup>376</sup>. However, these Dicer<sup>Exo5<sup>-/-</sup></sup> HCT116 cells have residual Dicer expression and activity, as shown by our previous Western blot analysis<sup>376</sup>. For this study, Dicer<sup>-/-</sup> cells generated by Narry Kim's group<sup>60</sup> were used and verified to be 100% protein knock out, with no residual expression (**Figure 3.8E; center panel inset**). These cells were completely resistant to DISE induced by shRNAs. Interestingly, both Dicer<sup>-/-</sup> and Drosha<sup>-/-</sup> were hypersensitive to DISE induced by siRNAs compared to wild type HCT116 cells (**Figure 3.8G**). This hypersensitivity was interesting, as it suggested global depletion of endogenous miRNAs made DISE-inducing guide RNAs more active. This is likely due to a much higher abundance of available RISCs.

*Open questions regarding the relevance of DISE*

We propose an entirely new method of killing cancer cells through CD95/CD95L-derived si/shRNAs evoking the unique sOTE DISE through seed-based targeting. However, there are questions that remain to be answered.

1. Is DISE part of an *in vivo* anti-cancer mechanism? DISE induction is something cancer cells cannot easily develop resistance to<sup>376</sup>. This work demonstrates this is likely due to the silencing of an entire network of multiple survival genes through seed-based targeting. It may never be possible to directly show targeting these multiple survival genes is responsible for toxicity, as expressing si/shRNA-resistant mutant cDNAs of all these genes is not technically feasible. However, this limitation highlights the power of using a sOTE in cancer therapy because the cancer cells will not be able to acquire numerous mutations simultaneously either.
2. Does CD95L mRNA kill cancer cells *in vivo*? Interestingly, CD95L over-expression kills cancer cells in a manner similar to DISE, even in the absence of apoptosis (see **Chapter 4**), and the majority of toxic shRNAs identified in our screen (**Figure 3.19C and D**) are located in the CD95L ORF mRNA sequence. Others have shown stressful stimuli, like chemotherapies, upregulate CD95L mRNA expression and trigger death that occurs even in the presence of antagonistic CD95 antibodies<sup>431,432</sup>. While the amount of CD95L mRNA needed to evoke toxicity is not known, it is certainly possible CD95L (and CD95) are not the only genes with this behavior.
3. Are there other genes in the human genome containing toxic seed sequences? The Peter lab has recently published a list of genes that contain DISE-inducing shRNAs<sup>378</sup>. It is

possible when cancer cells encounter a genotoxic or stressful stimulus, this triggers the release of numerous DISE-inducing guide RNAs formerly “locked” in the transcriptome of protein-coding mRNAs.

#### *A Model for why DISE Preferentially Kills Cancer Cells*

Around 98.4% of AGO-bound small RNAs in HCT116 cells are miRNAs (99.3% in HeyA8 cells, see **Chapter 4**), as determined using AGO pull-down experiments. It has also been shown that Drosha knock out decreases the total miRNA abundance from 70 to 80% to five to six %, and Dicer knock out has a reduction down to 14 to 21%<sup>60</sup>. Additionally, this work shows, despite what others have shown in mouse embryonic stem cells<sup>433</sup>, that AGO expression remains constant even in the absence of Dicer or Drosha (**Figure 3.8E; insets**). Taken together, these data suggest, in the absence of endogenous miRNAs, the abundance of available RISC complexes increases, which allows more DISE-inducing guide RNAs to complex with RISC and kill the cell.

The Peter lab has previously shown transformed ovarian fibroblasts are more sensitive to DISE induced by shL3 and shR6 than normal fibroblasts<sup>376</sup>. Our data now suggest an interesting possibility that explains why cancer cells might be more sensitive than normal cells to DISE. Others have shown cancer cells globally downregulate miRNAs compared to normal cells<sup>379</sup>. This difference in miRNA expression would presumably translate into more available RISCs in cancer cells. Consistently, delivery of CD95L-derived siRNAs triggers significant tumor regression *in vivo*, without evoking toxicity in other normal tissues<sup>381</sup>. This unique DISE sOTE could be used as a viable cancer treatment option. Instead of selectively targeting a single oncogenic target, as does current targeted therapy does, DISE targets multiple survival genes simultaneously.

## Tables for Chapter 3

**Table 3.1.1 - Alignment-based analysis: all genes with a padj <0.05, >1.5 downregulated, and base mean expression >2000**

Gene	shL3 (50hrs) in 293T ΔshL3		shL3 (100hrs) in 293T ΔshL3		shR6 (50hrs) in HeyA8 ΔshR6		shR6 (100hrs) in HeyA8 ΔshR6	
	log <sub>2</sub> (FC)	padj	log <sub>2</sub> (FC)	padj	log <sub>2</sub> (FC)	padj	log <sub>2</sub> (FC)	padj
BZW1	-2.27	0	-2.21	3.23E-83	0.23	0.086202763	0.13	0.463555192
NUCKS1	-2.23	0	-2.09	8.62E-83	-0.07	0.716553303	-0.28	0.071622388
CHCHD2	-1.84	3.39E-261	-2.13	3.12E-64	0.08	0.732811942	-0.11	0.692726258
PFN2	-2.13	2.90E-213	-2.19	3.12E-64	-0.28	0.035011127	-0.20	0.280746126
HIST1H1D	-1.57	3.83E-125	-2.03	8.29E-52	0.08	0.744633818	-0.67	0.000228158
SNRPE	-1.73	2.53E-185	-1.82	6.77E-48	-0.17	0.392285524	-0.33	0.096482893
LIN7C	-1.83	1.41E-170	-1.62	1.02E-36	-0.16	0.369266908	-0.01	0.982456218
PTTG1IP	-1.77	1.40E-170	-1.47	2.49E-31	-0.21	0.189732231	-0.37	0.007102135
KCTD20	-1.63	6.61E-143	-1.41	3.74E-30	0.20	0.172823941	0.06	0.801014692
GALNT1	-1.57	7.18E-152	-1.39	3.23E-29	0.14	0.518786659	0.11	0.643652546
CDK4	-1.22	7.49E-115	-1.35	2.70E-27	0.03	0.903684132	-0.10	0.669884296
PCNP	-1.66	1.78E-148	-1.31	1.03E-25	-0.01	0.963639563	-0.09	0.707086093
GNB1	-1.29	1.21E-114	-1.25	4.64E-24	-0.27	0.047219636	-0.16	0.364692178
RDX	-1.57	3.55E-127	-1.25	1.18E-23	-0.74	1.05E-10	-0.63	1.84E-06
HIST1H4B	-0.60	1.35E-29	-1.22	4.66E-22	-0.17	0.437287262	-0.58	0.001194437
EID1	-0.90	5.70E-51	-1.21	7.13E-21	-0.06	0.808265497	-0.31	0.058418704
MTDH	-1.04	9.48E-91	-1.08	9.59E-21	-0.19	0.171710686	-0.22	0.166182786
KIAA1147	-1.21	1.16E-85	-1.16	1.06E-20	0.54	0.000371819	0.45	0.00871053
RBM12	-1.42	7.61E-138	-1.14	2.19E-20	-0.13	0.449888373	-0.34	0.040799925
FGD5-AS1	-1.50	1.09E-130	-1.13	7.33E-20	0.23	0.125137207	0.12	0.560340681
CALU	-1.37	8.02E-163	-1.07	1.45E-19	-0.07	0.731279805	0.19	0.27694283
ADIPOR1	-1.39	1.94E-103	-1.15	4.50E-19	0.24	0.133485081	0.31	0.078178593
RQCD1	-1.18	1.29E-72	-1.11	7.61E-18	0.05	0.814552044	-0.07	0.776272412
CCT3	-0.84	6.50E-133	-1.09	9.13E-18	-0.14	0.426362494	-0.25	0.125642388
HIST1H1C	-0.63	6.31E-86	-1.13	3.08E-17	-0.10	0.658141579	-0.80	2.63E-06
AAMP	-0.88	1.95E-55	-1.07	5.40E-17	0.17	0.329788434	-0.08	0.731418466
PRDX3	-0.78	3.06E-85	-1.16	1.29E-16	0.02	0.934943404	-0.15	0.45741588
SEP15	-0.90	5.07E-51	-1.07	3.35E-16	-0.22	0.154338029	-0.19	0.252089273
BUB3	-1.04	5.31E-107	-0.97	7.57E-16	-0.05	0.822691545	-0.06	0.819480706
SPCS3	-0.97	7.17E-77	-1.04	1.78E-15	-0.30	0.022491165	-0.18	0.314264617
NAA50	-0.95	2.56E-122	-0.92	2.02E-15	-0.29	0.032722267	-0.21	0.231174536
VAMP7	-1.45	1.94E-104	-1.18	2.88E-15	0.13	0.4868436	0.16	0.444476799
EI24	-0.90	4.59E-69	-1.02	7.95E-15	-0.03	0.912721715	-0.12	0.580757249
CDK2	-0.79	5.57E-36	-1.04	1.11E-14	-0.31	0.042368806	-0.46	0.003090914
SMS	-0.75	7.06E-30	-1.08	1.37E-14	-0.34	0.014726958	-0.38	0.009786489
THRAP3	-1.05	1.42E-111	-0.90	5.01E-14	-0.09	0.597628615	-0.16	0.392039705
SUB1	-0.88	3.07E-66	-0.91	8.06E-14	0.06	0.776358652	-0.09	0.687767798
AASDHPPT	-0.80	3.31E-36	-0.99	2.95E-13	0.04	0.874853681	0.03	0.901655112
TCEA1	-1.13	2.17E-82	-0.97	4.09E-13	0.03	0.878952621	-0.01	0.966789571
DESI2	-0.94	6.09E-73	-0.90	1.39E-12	0.20	0.178751181	0.27	0.085061996
KDEL2	-0.83	3.13E-54	-0.87	3.59E-12	0.01	0.973018333	0.16	0.391877857
VHL	-0.89	4.45E-44	-0.87	6.10E-12	0.15	0.404933524	0.17	0.399168449
CAPZA1	-0.84	1.31E-73	-0.85	6.39E-12	-1.40	3.39E-41	-1.18	1.11E-22
FUBP1	-0.87	9.99E-88	-0.82	7.02E-12	-0.28	0.06852633	-0.38	0.009915218
PRKAR1A	-1.03	4.07E-92	-0.84	8.26E-12	0.15	0.352234294	0.15	0.419865667
FNDC3A	-1.10	2.22E-72	-0.89	9.06E-12	0.25	0.072792333	0.40	0.009353827
HK1	-0.78	7.93E-38	-0.88	2.45E-11	-0.02	0.914505801	0.15	0.398009217
DOCK1	-0.72	1.17E-28	-0.89	2.90E-11	-0.03	0.903272611	-0.07	0.785796032
ZNF271P	-0.92	1.30E-47	-0.89	2.92E-11	-0.32	0.069556079	-0.03	0.938554191
CSDE1	-0.70	5.14E-114	-0.79	3.03E-11	-0.12	0.466432305	-0.07	0.746178799
API5	-0.87	6.80E-66	-0.80	4.44E-11	-0.20	0.184473378	-0.16	0.395827841
ARF3	-0.62	1.31E-25	-0.85	4.85E-11	0.25	0.064118963	0.14	0.528486694
SEP11	-0.61	1.80E-30	-0.78	3.59E-10	-0.53	3.33E-06	-0.40	0.00433386
FSTL1	-0.70	2.23E-43	-0.80	4.74E-10	-1.15	3.65E-26	-0.75	2.44E-09

DNAJC10	-0.71	3.07E-40	-0.79	4.74E-10	0.30	0.023875252	0.29	0.075339697
TMED4	-0.60	4.10E-20	-0.84	5.29E-10	0.37	0.026466072	0.22	0.273441753
EIF4E	-0.66	2.77E-29	-0.83	1.12E-09	-0.04	0.881949412	-0.14	0.525067142
TXLNG	-0.74	8.98E-34	-0.78	1.31E-09	-0.05	0.858579098	-0.13	0.610427674
TMPO	-0.67	7.26E-60	-0.74	1.83E-09	-0.21	0.182775246	-0.34	0.01571158
IMPAD1	-0.79	1.47E-48	-0.76	1.94E-09	-0.04	0.845653229	0.01	0.979734438
NUP43	-0.82	1.37E-43	-0.79	4.50E-09	-0.12	0.495946982	-0.13	0.564159968
GSPT1	-0.72	1.35E-52	-0.76	4.70E-09	-0.23	0.126690544	-0.10	0.635224066
EPT1	-1.07	9.94E-71	-0.82	5.38E-09	-0.12	0.527975438	0.03	0.911645047
SLMO2	-0.72	3.68E-26	-0.82	5.55E-09	-0.25	0.168252816	-0.32	0.088322591
ZYG11B	-1.04	1.98E-53	-0.77	1.07E-08	-0.08	0.721379557	-0.02	0.953675564
TPM3	-0.63	1.97E-44	-0.74	1.14E-08	0.03	0.905801355	0.04	0.886120259
POMP	-0.75	1.82E-30	-0.85	1.25E-08	-0.05	0.841100624	-0.02	0.937513628
RPRD1A	-0.65	3.80E-40	-0.72	1.79E-08	0.00	0.998978339	-0.10	0.679921535
PSMD10	-0.68	1.19E-27	-0.86	3.69E-08	0.30	0.100898937	0.02	0.945266657
LETM1	-0.66	4.83E-27	-0.70	9.69E-08	-0.30	0.054537985	-0.29	0.105687107
FAR1	-1.05	6.59E-84	-0.70	1.02E-07	-0.38	0.003358127	-0.33	0.027691024
SNRPD1	-0.62	1.45E-28	-0.88	1.40E-07	-0.14	0.458073392	-0.30	0.132308131
NF2	-1.01	8.37E-51	-0.75	1.72E-07	0.62	1.60E-05	0.72	3.14E-06
DNAJC5	-0.66	2.38E-31	-0.68	1.88E-07	0.26	0.058875832	0.09	0.660985553
KIF1A	-0.90	9.38E-58	-0.75	3.11E-07	0.27	NA	0.08	NA
RFC1	-0.64	1.17E-26	-0.66	4.61E-07	-0.17	0.284673307	-0.21	0.22490784
ARPP19	-0.72	2.54E-36	-0.65	4.84E-07	-0.05	0.825438756	0.02	0.953964655
ACTR2	-0.59	5.06E-34	-0.63	9.42E-07	-0.20	0.227342894	0.04	0.854075703
SAR1A	-0.72	1.55E-46	-0.62	1.27E-06	0.04	0.85577452	0.04	0.861165152
DCP2	-0.79	1.92E-72	-0.58	2.07E-06	-0.25	0.134766402	-0.44	0.00442332
SLC39A9	-0.68	2.02E-26	-0.63	5.22E-06	0.11	0.582727273	-0.05	0.834118178
SS18	-0.90	1.79E-55	-0.60	6.81E-06	-0.73	1.48E-09	-0.67	1.69E-06
GNAI3	-0.64	4.84E-28	-0.61	7.59E-06	0.06	0.767436127	0.02	0.939054318
CSNK1A1	-0.59	2.32E-35	-0.60	7.66E-06	0.05	0.812472749	0.02	0.95311483
KLHL11	-0.79	3.22E-40	-0.59	1.21E-05	0.00	0.992688707	0.14	0.546281064
RAP1B	-0.82	3.64E-39	-0.60	1.44E-05	-0.19	0.200510739	-0.04	0.867037502
ZNF322	-0.82	2.79E-40	-0.60	2.23E-05	0.08	0.761908405	-0.04	0.906657342
GTF3C3	-0.76	3.17E-32	-0.56	7.31E-05	0.00	0.989884207	-0.14	0.492905768
GPR180	-0.69	2.59E-33	-0.54	8.74E-05	0.45	0.000691397	0.57	7.04E-05
BAZ1B	-0.73	2.04E-56	-0.51	0.000102348	-0.22	0.187325303	-0.23	0.197234901
BROX	-0.96	3.72E-53	-0.51	0.000310206	-0.38	0.005614498	-0.15	0.446605568
FBXL3	-0.69	1.91E-37	-0.50	0.000394642	-0.06	0.80716735	-0.02	0.957727213
SDE2	-0.68	2.45E-36	-0.47	0.000422051	0.08	0.748517498	0.07	0.81156316
HOOK1	-0.86	2.25E-40	-0.52	0.000441455	-0.02	NA	-0.08	NA
TMEM167A	-0.68	2.97E-31	-0.48	0.000858744	-0.11	0.545144839	0.06	0.81221202
ZC3HAV1	-0.82	3.76E-38	-0.52	0.001228402	-0.45	0.004012035	-0.21	0.254483235
SEC23IP	-0.75	2.39E-34	-0.47	0.001984556	-0.49	0.000568731	-0.41	0.008234794
PTBP3	-0.99	8.82E-50	-0.49	0.003005624	-0.75	3.36E-10	-0.58	1.47E-05
SORT1	-0.85	1.82E-46	-0.41	0.003218675	0.08	0.787797856	-0.34	0.112623361
GNS	-0.60	9.76E-26	-0.39	0.008235796	-0.03	0.891770595	0.15	0.42196325
NOTCH2	-0.61	3.06E-31	-0.35	0.045930752	-0.66	9.88E-08	-0.36	0.024377557
USP37	-0.69	8.26E-27	-0.30	0.055857228	-0.03	0.896008999	0.04	0.881016211
KPNA4	-0.87	1.12E-39	-0.29	0.075212583	-0.41	0.001060578	-0.18	0.359065755
UHMK1	-0.64	5.51E-29	-0.23	0.123393906	0.04	0.862008345	0.23	0.180612396
TFRC	-0.72	4.36E-91	-0.16	0.304254121	-0.44	0.00023599	0.13	0.613189554
NEAT1	-0.74	2.24E-33	-0.03	0.919376477	0.01	0.983819791	0.50	0.011518557

**Table 3.1.2 - Alignment-based analysis: all genes with a padj <0.05, >1.5 upregulated, and base mean expression >2000**

Gene	shL3 (50hrs) in 293T $\Delta$ shL3		shL3 (100hrs) in 293T $\Delta$ shL3		shR6 (50hrs) in HeyA8 $\Delta$ shR6		shR6 (100hrs) in HeyA8 $\Delta$ shR6	
	log <sub>2</sub> (FC)	padj	log <sub>2</sub> (FC)	padj	log <sub>2</sub> (FC)	padj	log <sub>2</sub> (FC)	padj
ATP13A3	1.00	3.70E-79	0.92	1.11E-13	0.56	5.13E-07	1.00	5.70E-13
PABPC1	0.70	6.74E-51	0.77	0.032862953	-0.30	0.474309023	0.05	0.902873754
DICER1	0.58	1.17E-48	0.51	5.35E-05	0.34	0.008054785	0.48	0.000651097
CACUL1	0.78	1.60E-47	0.64	7.05E-07	0.14	0.408620578	0.31	0.073424313
VWA9	0.96	2.03E-46	0.59	3.87E-05	-0.07	0.785648839	0.07	0.795342753
RPS16	0.75	8.75E-43	0.51	0.008666728	-0.35	0.433025121	0.11	0.625008419
RABL6	0.73	3.61E-41	0.42	0.003075198	0.50	4.57E-05	0.47	0.001090288
ATP2A2	0.61	1.52E-39	0.69	0.000192246	-0.30	0.131500035	0.10	0.752591282
COLGALT1	0.72	9.08E-39	0.50	0.000137222	-0.16	0.308977639	-0.15	0.419518019
SRPR	0.84	6.96E-38	0.61	2.06E-05	-0.35	0.017892216	-0.28	0.095286298
OCRL	0.65	1.63E-29	0.57	1.65E-05	0.16	0.410606777	0.31	0.075902049
NPEPPS	0.73	4.92E-29	0.60	0.000223573	0.24	0.241307209	0.56	0.000951319
DIAPH1	0.80	7.43E-27	0.86	0.016801524	-0.42	0.283191572	-0.14	0.783868917
NELFCD	0.58	1.10E-26	0.38	0.009232882	0.00	0.990674011	0.01	0.974416185
KHSRP	0.61	3.91E-26	0.46	0.012803963	-0.30	0.173270036	-0.13	0.614365827
CD2AP	0.60	1.36E-25	0.42	0.002625357	-0.91	8.23E-14	-0.82	1.70E-10
VCAN	0.68	1.48E-24	0.94	5.35E-11	-1.41	1.94E-28	-1.33	7.53E-27
NOL8	0.59	1.20E-22	0.45	0.002893609	-0.46	0.000838776	-0.22	0.262439146
DNAJC2	0.66	1.29E-22	0.36	0.044043955	-0.28	0.169221024	-0.26	0.230520443
SZRD1	0.56	2.21E-22	0.43	0.003530528	-0.80	9.24E-11	-0.68	8.85E-07
GPBP1L1	0.55	3.42E-22	0.35	0.013722058	-0.33	0.013267967	-0.21	0.22798674
SPTLC1	0.61	1.10E-21	0.56	0.000879822	0.05	0.828634294	0.12	0.568265735
AGO1	0.62	9.38E-21	0.54	0.000467802	0.25	0.186465773	0.39	0.028175444
FOXRED2	0.58	1.22E-18	0.60	0.002481159	0.02	NA	0.29	NA
DCPIA	0.54	3.43E-16	0.55	8.68E-05	-0.63	2.38E-05	-0.61	0.000144156
ATP6V0E1	0.56	9.71E-16	0.43	0.008942237	-0.16	0.348766657	0.09	0.702824606

**Table 3.1.3 - Read-based analysis: all genes with a variation <2 per duplicate and >1.5 downregulated**

Gene	shL3 (50hrs) in 293T AshL3			shL3 (100hrs) in 293T ΔshL3			shR6 (50hrs) in HeyA8 ΔshR6			shR6 (100hrs) in HeyA8 ΔshR6		
	Var Scr	Var shL3	FC	Var Scr	Var shL3	FC	Var Scr	Var shR6	FC	Var Scr	Var shR6	FC
CAPZA1	1.22	1.12	0.12	0.78	1.02	0.55	0.89	1.88	0.14	1.70	1.26	0.21
SCOC	1.08	1.00	0.23	1.64	1.33	0.30	0.67	0.53	0.36	1.18	0.89	0.31
NUCKS1	0.97	1.86	0.16	0.85	1.05	0.10	0.65	0.66	0.40	0.88	0.86	0.58
CAPZA1	1.25	0.93	0.50	1.05	1.45	0.36	1.60	1.02	0.27	1.40	0.95	0.13
CAPZA1	1.30	0.88	0.51	1.73	0.53	0.20	0.70	0.73	0.36	1.17	1.21	0.33
CAPZA1	0.91	0.81	0.40	0.74	0.75	0.31	1.68	1.05	0.31	0.75	0.60	0.39
CAPZA1	1.51	0.79	0.61	1.86	1.61	0.43	1.29	0.51	0.22	0.76	1.08	0.17
NUCKS1	0.53	1.37	0.11	1.02	1.17	0.13	1.21	1.37	0.64	1.49	1.03	0.56
RP11-146B14.1	1.00	1.08	0.27	0.96	0.70	0.13	0.79	1.12	0.62	0.78	0.98	0.47
SNRPE	1.15	1.61	0.25	0.89	1.53	0.12	0.51	0.53	0.59	0.81	1.79	0.54
SNRPE	1.24	1.02	0.41	1.65	0.82	0.17	1.01	0.99	0.38	0.66	1.26	0.57
RP11-434H2.1	0.60	0.64	0.35	0.79	0.78	0.21	0.58	1.00	0.34	0.94	0.86	0.64
CAPZA1	1.05	1.63	0.58	1.17	1.03	0.49	1.49	1.01	0.23	0.87	0.62	0.25
CAPZA1	1.10	1.68	0.41	1.42	0.69	0.43	1.33	1.71	0.30	0.78	1.03	0.43
MCL1	0.84	1.00	0.15	0.68	0.54	0.14	0.80	1.73	0.63	1.19	1.04	0.65
SNW1	1.72	0.76	0.61	1.30	1.43	0.53	0.71	0.62	0.26	1.02	0.68	0.18
CAPZA1	1.01	1.07	0.31	1.17	1.95	0.31	0.66	0.65	0.43	1.44	1.13	0.53
CAPZA1	1.87	1.42	0.53	0.55	1.75	0.38	0.90	1.58	0.41	0.85	0.55	0.29
CAPZA1	1.19	1.31	0.23	1.50	0.76	0.66	1.69	1.02	0.37	0.80	1.08	0.36
HIST3H2A	1.47	1.45	0.61	1.71	1.86	0.50	0.89	0.86	0.28	0.53	1.04	0.28
SNRPEP4	1.55	0.87	0.28	0.89	0.94	0.32	0.84	0.94	0.42	0.71	0.62	0.64
CDV3	1.82	0.76	0.51	0.78	1.01	0.23	0.88	0.56	0.59	1.34	0.62	0.38
YWHAZ	1.84	0.52	0.58	1.03	0.95	0.20	0.93	0.53	0.35	1.58	0.50	0.59
TMEM43	0.93	0.64	0.24	0.62	1.41	0.32	1.35	1.59	0.60	1.36	0.51	0.56
CAPZA1	1.56	1.01	0.54	0.97	1.10	0.42	1.25	1.17	0.36	1.56	0.79	0.43
CAPZA1	1.61	0.55	0.50	1.06	1.03	0.53	1.35	0.61	0.36	0.84	0.66	0.38
CDK4	1.47	1.82	0.49	0.68	0.53	0.35	1.74	1.45	0.47	1.29	0.83	0.46
SNW1	1.39	1.44	0.56	1.50	1.76	0.39	1.59	1.88	0.40	0.82	1.43	0.42
FSTL1	0.56	0.66	0.39	0.87	1.03	0.34	1.54	1.26	0.54	1.65	0.90	0.52
BAZ2B	1.33	0.81	0.46	0.92	1.04	0.53	1.16	1.93	0.29	1.21	1.06	0.50
SNW1	1.01	0.59	0.59	0.74	0.86	0.39	1.45	1.41	0.54	0.70	0.75	0.27
GNB1	1.22	0.64	0.35	1.41	0.50	0.34	1.11	1.23	0.52	1.48	1.01	0.59
CAPZA1	0.88	0.61	0.53	0.90	1.63	0.51	0.95	1.36	0.42	0.89	0.55	0.35
CAPZA1	1.84	0.98	0.43	0.95	0.62	0.41	1.00	0.84	0.36	0.95	1.33	0.62
SNW1	0.96	1.25	0.53	1.72	1.07	0.62	0.94	0.73	0.34	1.29	1.20	0.35
AHCY	1.34	1.49	0.65	0.74	0.69	0.22	1.45	1.82	0.37	1.48	1.26	0.60
CAPZA1	2.00	0.80	0.61	0.76	0.77	0.46	1.37	0.62	0.35	1.12	1.67	0.41
SNORD49B	0.76	1.17	0.45	1.12	1.47	0.25	1.13	1.14	0.59	1.43	1.24	0.55
TFRC	1.30	0.50	0.13	1.35	1.00	0.55	1.09	0.68	0.59	1.79	0.97	0.57
MCM4	1.57	1.34	0.44	1.59	1.59	0.51	1.28	1.11	0.63	1.11	1.33	0.30
TOP2A	1.22	0.77	0.62	0.90	0.50	0.12	1.53	1.53	0.65	0.87	1.56	0.50
CAPZA1	0.86	1.02	0.64	1.41	0.84	0.29	0.99	0.56	0.37	0.75	1.69	0.58
CAPZA1	0.61	1.21	0.47	1.87	1.13	0.34	1.02	0.97	0.62	1.02	0.80	0.46
NEDD4	0.99	0.50	0.53	1.30	1.01	0.50	1.22	0.90	0.48	0.82	0.75	0.40
METAP2	0.77	1.68	0.61	1.29	1.81	0.29	0.58	1.24	0.47	0.99	0.51	0.54
CAPZA1	1.67	0.62	0.63	1.39	1.49	0.49	1.45	1.07	0.37	1.00	1.37	0.42
MCM4	0.88	0.74	0.44	0.76	0.64	0.65	0.76	1.79	0.39	1.24	0.73	0.44
ACSL4	0.67	1.31	0.34	1.38	1.58	0.54	0.91	0.68	0.62	1.53	0.56	0.42
HIST1H4D	0.97	0.68	0.62	0.60	1.13	0.34	1.47	0.89	0.57	1.14	0.89	0.39
CAPZA1	1.44	0.62	0.54	0.54	1.12	0.49	1.08	1.85	0.42	1.19	1.50	0.48
CAPZA1	1.59	0.91	0.54	1.08	0.86	0.36	1.13	1.41	0.39	1.21	1.12	0.65
CAPZA1	1.32	0.99	0.66	1.08	1.61	0.49	1.40	0.80	0.37	1.15	1.65	0.42
CDCA4	0.95	1.51	0.41	0.68	1.95	0.27	0.56	1.00	0.66	0.85	1.35	0.61
SRPK1	1.51	0.58	0.45	0.72	0.97	0.32	1.36	1.27	0.60	1.16	0.55	0.58
CCT3	1.52	1.41	0.44	0.95	1.80	0.30	1.36	0.88	0.66	1.39	0.57	0.55
YWHAZ	0.76	1.00	0.45	0.59	0.69	0.38	0.85	0.59	0.61	1.13	0.82	0.52
SERBP1	0.94	0.76	0.60	1.46	0.89	0.40	1.51	0.54	0.57	0.79	0.62	0.42
CCT3	0.52	1.28	0.50	1.36	1.47	0.36	0.92	1.42	0.56	0.66	0.57	0.57
AHCY	1.94	0.72	0.61	0.90	1.04	0.17	1.60	0.88	0.57	0.74	1.05	0.64
CSDE1	1.36	1.19	0.53	0.76	0.52	0.48	0.78	0.56	0.66	1.06	1.23	0.33
SRP9	0.77	0.90	0.36	0.54	1.73	0.60	0.57	0.54	0.47	1.08	0.51	0.57
CAPZA1	0.52	0.69	0.66	1.34	0.63	0.53	1.00	1.10	0.39	1.30	1.98	0.42
WLS	0.57	1.15	0.62	1.46	0.82	0.59	1.28	0.61	0.39	0.91	0.95	0.41
MRPS21	1.35	0.73	0.66	1.06	1.55	0.51	1.05	0.90	0.34	1.63	0.52	0.51
CCT3	1.16	1.34	0.41	1.29	1.12	0.41	0.77	1.43	0.60	0.80	0.65	0.60

CAPZA1	0.70	1.18	0.49	0.76	0.81	0.51	1.09	0.99	0.47	1.10	1.46	0.57
PCDH11X	0.69	0.91	0.56	1.94	1.09	0.37	1.07	0.51	0.49	0.85	1.01	0.61
HIST4H4	1.54	1.16	0.44	0.62	1.59	0.48	1.42	0.86	0.66	0.80	1.13	0.47
YWHAZ	0.58	0.72	0.45	0.64	1.55	0.61	0.77	0.54	0.46	1.01	0.53	0.53
HIST1H3A	0.78	0.71	0.62	1.73	0.95	0.46	0.85	1.60	0.59	1.44	0.90	0.39
NUCKS1	0.82	1.01	0.44	1.89	1.40	0.41	1.53	0.76	0.58	0.85	0.70	0.63
CDV3	1.26	0.63	0.50	0.97	0.59	0.54	0.92	1.39	0.47	0.99	0.72	0.55
HMGB1	1.77	0.84	0.64	1.90	1.42	0.48	0.75	0.86	0.50	0.68	1.13	0.44
FUBP1	1.74	0.91	0.50	1.48	1.49	0.27	1.19	1.99	0.64	0.75	1.60	0.67
YWHAZ	0.93	1.04	0.51	1.88	1.04	0.62	1.24	1.03	0.45	0.73	1.18	0.49
NAA50	1.04	1.78	0.41	1.15	0.97	0.49	0.97	0.66	0.67	1.10	0.67	0.51
NUCKS1	1.08	0.86	0.53	0.81	0.80	0.28	1.84	0.57	0.63	0.62	1.29	0.65
AHCY	1.86	0.97	0.65	0.52	1.13	0.57	1.26	0.62	0.42	0.91	0.67	0.44
LRPPRC	0.81	0.68	0.58	0.71	1.20	0.41	1.05	1.23	0.58	1.24	0.65	0.53
PYGL	0.64	0.93	0.48	0.78	1.37	0.33	1.08	1.57	0.65	1.46	0.98	0.64
GLUD1	1.47	0.52	0.63	1.50	1.93	0.44	1.12	0.56	0.60	0.65	0.76	0.44
DESI2	0.96	1.01	0.57	1.23	1.27	0.39	1.62	1.22	0.59	0.65	0.81	0.56
CNN3	1.17	0.89	0.54	1.12	0.83	0.49	1.13	1.43	0.56	1.55	1.63	0.53
VCP	1.13	1.98	0.65	1.01	0.95	0.53	1.08	0.99	0.55	1.70	1.03	0.40
CCT3	1.15	0.97	0.57	0.95	1.27	0.41	1.22	1.68	0.57	0.93	0.53	0.57
VCP	1.31	0.82	0.60	1.69	0.83	0.37	0.80	0.68	0.53	1.10	0.51	0.64
DEPDC1	1.86	0.85	0.56	0.70	0.80	0.61	1.29	1.38	0.56	0.73	0.97	0.41
HSPA9	1.43	1.68	0.43	1.30	1.38	0.47	0.82	0.81	0.62	1.36	1.58	0.62
ARPC5	0.87	1.75	0.61	0.60	1.08	0.48	1.28	1.66	0.41	0.65	0.91	0.66
TRAM1	0.99	1.18	0.44	0.72	0.99	0.53	1.31	0.65	0.62	1.49	1.05	0.57
RN7SL1	1.20	0.70	0.38	1.31	0.82	0.63	1.91	0.51	0.63	0.64	1.50	0.53
HIST1H2BC	0.81	0.99	0.65	1.08	0.85	0.47	1.16	1.27	0.64	1.11	1.13	0.41
DAZAP1	0.62	0.69	0.52	0.62	1.18	0.37	1.63	0.62	0.64	1.13	1.56	0.66
HIST1H4H	1.24	1.19	0.52	0.60	1.77	0.39	1.37	1.41	0.63	0.88	0.92	0.65
AHSA1	1.11	1.21	0.64	0.60	1.69	0.53	1.55	0.55	0.49	0.57	0.72	0.53
GLUL	1.72	0.61	0.66	0.97	1.73	0.37	0.52	1.55	0.59	0.82	0.95	0.58
HIST1H2BC	1.03	0.82	0.59	1.33	1.03	0.30	1.19	0.88	0.65	0.79	1.68	0.66
PAICS	1.05	0.55	0.46	1.25	1.01	0.47	0.94	1.30	0.63	1.49	1.43	0.63
CAPZA1	0.85	1.09	0.44	0.54	1.83	0.60	0.69	1.36	0.53	1.03	1.31	0.63
AHCY	0.90	0.56	0.58	1.10	0.66	0.42	0.68	1.52	0.62	1.25	1.04	0.59
CCT3	1.47	1.31	0.57	0.88	1.63	0.49	1.30	0.66	0.58	1.77	0.87	0.57
HIST1H1C	1.02	1.01	0.54	1.05	0.99	0.46	0.82	0.97	0.64	0.80	0.86	0.56
VDAC1	1.71	1.07	0.64	0.82	0.86	0.60	0.78	1.03	0.63	0.82	1.43	0.35
RN7SL2	1.08	1.36	0.59	1.51	0.86	0.65	1.48	1.07	0.51	0.96	1.00	0.47
CDV3	1.03	0.59	0.62	0.93	0.82	0.51	0.85	1.02	0.50	1.21	0.86	0.59
VCP	1.94	1.27	0.66	0.77	1.79	0.47	0.64	1.26	0.53	0.85	0.53	0.57
G3MP1	0.97	1.36	0.54	0.58	0.58	0.56	1.32	0.91	0.61	0.76	1.57	0.52
HNRNPU	0.93	1.26	0.62	1.08	1.36	0.36	1.68	0.68	0.62	0.51	0.94	0.64
Intergenic	0.60	0.86	0.63	0.88	1.41	0.47	1.34	1.57	0.57	0.80	0.55	0.58
AHCY	1.45	0.69	0.61	1.00	1.79	0.40	1.06	1.12	0.63	0.99	0.61	0.61
CCT3	1.37	1.30	0.55	1.19	1.15	0.39	1.74	0.87	0.67	0.60	0.84	0.66
GSR	0.99	0.63	0.45	1.18	0.74	0.54	0.80	1.57	0.62	1.46	1.27	0.65
SRP72P2	1.21	0.95	0.56	1.52	1.46	0.48	0.88	1.45	0.59	0.50	0.75	0.65
NPS6	0.93	0.73	0.66	1.20	1.71	0.57	1.18	1.33	0.62	1.71	0.55	0.42
ACTG1	1.69	1.35	0.59	1.11	0.86	0.45	1.04	1.30	0.57	1.19	0.58	0.67
UQCRRFS1	1.37	0.92	0.65	1.65	1.46	0.49	1.52	1.34	0.54	1.88	0.84	0.60
SERF2	1.00	1.10	0.61	0.67	0.53	0.53	1.62	0.63	0.61	1.38	0.78	0.52
LDHB	1.10	0.87	0.61	0.96	1.07	0.55	0.98	1.15	0.62	1.35	0.79	0.51
CAND1	0.84	0.94	0.66	1.64	0.67	0.50	0.96	1.35	0.63	1.55	0.57	0.49
CLNS1A	0.79	1.37	0.66	0.76	1.00	0.35	1.43	0.98	0.63	1.02	1.44	0.65
HIST1H2BO	0.92	1.11	0.59	1.17	1.40	0.57	1.65	0.65	0.66	0.90	0.80	0.47
ATG10	0.94	1.17	0.59	1.56	1.49	0.53	1.64	1.70	0.66	0.89	0.82	0.52
VCP	1.84	1.02	0.62	1.39	0.63	0.60	1.44	0.96	0.46	1.58	0.83	0.62
ACTG1	1.21	1.22	0.59	0.63	0.63	0.53	1.39	0.78	0.56	0.98	0.72	0.64
YWHAZ	0.77	1.90	0.66	0.57	1.05	0.58	0.86	1.39	0.61	1.53	1.96	0.48
SERBP1	1.30	1.34	0.63	0.96	0.80	0.62	0.52	0.96	0.66	1.19	1.38	0.44
AIMP1	0.65	1.68	0.40	0.55	1.51	0.63	1.84	0.90	0.65	1.34	1.04	0.67
CSDE1	1.14	0.73	0.62	1.35	1.82	0.63	1.29	0.78	0.55	1.15	0.54	0.55
SRSF6	0.74	0.80	0.54	0.69	0.66	0.66	1.72	0.81	0.60	1.20	0.67	0.56
RPL3	0.84	1.32	0.50	1.04	1.61	0.58	0.88	1.18	0.65	0.84	0.96	0.66
NPS6	1.24	0.98	0.62	1.37	1.19	0.64	0.62	0.92	0.65	1.31	0.65	0.47
YWHAZ	1.27	0.90	0.59	0.92	0.73	0.60	0.65	1.01	0.61	0.92	0.61	0.61
PNN	0.57	0.76	0.61	0.94	0.57	0.65	0.83	1.55	0.61	1.24	0.76	0.56
YWHAZ	0.95	1.39	0.63	0.97	1.26	0.64	1.06	0.71	0.59	1.09	0.51	0.57
SLMO2	1.36	2.00	0.63	0.94	0.89	0.62	1.00	1.81	0.65	1.04	1.78	0.54
COPB1	0.64	0.83	0.52	1.29	0.78	0.65	1.16	1.43	0.60	1.30	0.61	0.66
CSE1L	1.27	1.48	0.60	1.50	0.91	0.65	0.53	1.01	0.53	1.14	0.68	0.66
YWHAZ	1.52	0.73	0.59	0.95	1.18	0.65	0.67	1.41	0.60	1.50	0.80	0.60
NAP1L1	1.41	1.53	0.59	0.90	0.50	0.66	1.21	0.77	0.66	1.36	1.05	0.55
CCNY	0.96	0.74	0.66	0.84	1.07	0.59	1.92	1.11	0.57	1.09	0.98	0.64



**Table 3.1.4 - Read-based analysis: all genes with a variation  $<2$  per duplicate and  $>1.5$  upregulated**

Gene	shL3 (50hrs) in 293T $\Delta$ shL3			shL3 (100hrs) in 293T $\Delta$ shL3			shR6 (50hrs) in HeyA8 $\Delta$ shR6			shR6 (100hrs) in HeyA8 $\Delta$ shR6		
	Var Scr	Var shL3	FC	Var Scr	Var shL3	FC	Var Scr	Var shR6	FC	Var Scr	Var shR6	FC
ATP13A3	1.16666667	0.923387097	9.1730769	0.65714286	0.841359773	3.7356322	0.71714922	0.935013263	1.892348	1.97804878	0.933030647	2.789517
ATP13A3	0.76119403	0.5	1.5762712	0.59322034	1.06626506	3.6489362	0.557739558	1.199256506	2.332808	1.6492891	1.810760668	5.420394
DCBLD2	1.0625	0.656346749	5.4040404	0.56345178	1.526548673	1.8538961	1.318975553	0.904092853	1.564759	0.633064516	0.846747519	2.757202
ATP13A3	0.528619529	0.864741641	2.7026432	0.65714286	1.874551971	4.6091954	0.845498135	0.837367883	1.555716	1.770663562	0.917151163	2.216807
ATP6V0D1	1.475524476	1.792569659	2.5480226	1.71130952	0.968152866	1.6959385	1.137566138	0.882352941	3.643564	1.902597403	0.810699588	1.96868
ATP13A3	0.706293706	0.898305085	1.8360656	1.5	0.604095563	4.0869565	0.558974359	0.91382668	1.847274	1.505194805	0.597145993	1.508554
FERMT2	1.506276151	1.670087977	3.0400668	1.0826087	1.058715596	2.34238	1.975717439	0.893351801	2.02819	0.656697009	0.830999066	1.539246
ATP13A3	0.587912088	1.426573427	2.4013841	0.52791878	1.886792453	1.5249169	1.46728972	0.654855643	1.592172	0.846969697	0.967692308	3.147662
CASP3	0.50952381	0.879194631	1.7665615	0.69259259	1.709677419	1.654267	0.736342043	0.870099923	3.328317	0.929219601	1.970903522	1.825024
RABEP1	1.833333333	0.876616915	2.5800274	1.69536424	1.903225806	1.990172	0.955810147	1.072497123	1.507113	1.127725857	1.613564669	2.426061
SLC3A2	1.435435435	1.140145985	1.8076449	1.01329787	1.889303483	3.0686922	0.644793153	0.871119473	1.725065	0.782110092	1.112592593	1.835264
NUP188	1.012847966	0.539761431	1.6478723	1.35326087	0.951219512	2.2170901	0.541322314	0.648964896	2.455764	1.486381323	1.292307692	1.865415
MORF4L1	0.67003367	0.782356729	1.8602151	1.55555556	0.875621891	1.8626482	0.740899358	1.13900135	1.949569	1.100864553	1.115294118	2.466392
KIAA0100	0.934497817	0.721635884	2.9458239	0.57615894	1.698924731	1.5819328	1.084236864	1.071282051	1.616246	1.266570605	0.542623788	1.92117
SLC3A2	1.612403101	0.863523573	2.2284866	0.83031674	1.187590188	1.8739184	0.513484358	1.553341149	1.552388	1.035928144	1.024338624	1.87549
TMED5	1.655246253	0.844660194	1.5322581	0.63424125	1.394495413	1.5535714	1.715953307	0.942696629	2.477077	0.762237762	1.681481481	1.915344
ACBD3	1.897637795	1.868286445	1.5237772	0.56998557	0.820657277	1.7821691	1.055248619	1.397660819	2.204301	0.927083333	1.052795031	1.786486
SEC11A	1.50174216	1.861829026	2.0048747	0.92459827	0.946070878	1.6223507	1.378205128	0.652173913	1.638814	0.822695035	1.050829876	1.923152
S100A10	1.453453453	1.458074534	1.9375765	0.82450331	1.481586402	1.5898367	1.048	0.795545403	1.754464	1.342565598	0.6875	1.881767
DUSP1	1.686567164	0.764150943	2.0777778	0.56521739	0.583617747	1.6111111	1.560114504	1.123921925	1.743943	1.601364522	1.14720314	1.639565
SLC25A3	0.967741935	0.961988304	1.8333333	1.68695652	1.943877551	1.8673139	1.01192053	1.486716259	1.540487	1.050092764	0.673740053	1.713122

Table 3.2 - Survival and non-survival gene sets used

Brummelkamp survival genes											
AAMP	CCDC86	DCTN1	FARS2	KAT7	MRPS15	PA2G4	PSMD14	RPS16	SPDL1	TUBE1	ZNHIT1
AARS	CCDC94	DCTN2	FARSA	KAT8	MRPS16	PABPC1	PSMD2	RPS18	SPRTN	TUBG1	ZNHIT3
AASDHPTT	CCNA2	DCTN3	FARSB	KCMF1	MRPS17	PABPN1	PSMD3	RPS19	SRBD1	TUBGCP3	ZNHIT6
AATF	CCNF	DCTN4	FAU	KDM8	MRPS18A	PAF1	PSMD4	RPS19BP1	SRCAP	TUBGCP4	ZRANB2
ABCB7	CCNH	DCTN5	FBL	KIAA0391	MRPS18B	PAFAH1B1	PSMD6	RPS2	SRD5A3	TUBGCP5	ZRSR2
ABCE1	CCNK	DDB1	FBX05	KIAA0947	MRPS18C	PAICS	PSMD7	RPS21	SREK1	TUBGCP6	ZW10
ABCF1	CCP110	DDOST	FCF1	KIAA1731	MRPS23	PAK1IP1	PSMD8	RPS23	SRF	TUFM	ZZZ3
ABT1	CCT2	DDX10	FDPS	KIF11	MRPS24	PALB2	PSMF1	RPS24	SRFBP1	TUT1	
ACACA	CCT3	DDX18	FDX1L	KIF14	MRPS25	PAM16	PSMG1	RPS25	SRP14	TWISTNB	
ACIN1	CCT4	DDX19A	FDXR	KIF18A	MRPS27	PAPOLG	PSMG2	RPS26	SRP19	TXN	
ACO2	CCT5	DDX20	FEN1	KIF4A	MRPS30	PARN	PSMG4	RPS27	SRP68	TXNL4A	
ACTL6A	CCT6A	DDX21	FGFR1OP	KIN	MRPS31	PARS2	PSTK	RPS27A	SRP72	TYMS	
ACTR10	CCT7	DDX23	FGFR1OP2	KPNA4	MRPS33	PAXBP1	PTAR1	RPS29	SRP9	U2AF1	
ACTR2	CCT8	DDX24	FH	KPNB1	MRPS35	PCBP2	PTCD3	RPS3	SRPR	U2AF2	
ACTR3	CD3EAP	DDX27	FIP1L1	KRI1	MRPS36	PCF11	PTMA	RPS3A	SRPRB	UZSURP	
ACTR6	CDC123	DDX39B	FIS1	KRR1	MRPS5	PCID2	PTP4A1	RPS4X	SRRD	UBA1	
ACTR8	CDC16	DDX3X	FLII	LAGE3	MRPS6	PCNA	PTPMT1	RP6	SRRM1	UBA2	
ADAR	CDC20	DDX46	FNBP4	LAMTOR1	MRPS7	PCNP	PTTG1	RPS6KB1	SRRM2	UBA3	
ADA2T	CDC23	DDX47	FNTB	LAMTOR2	MRPS9	PCNT	PUM1	RPS7	SRRT	UBA52	
ADSL	CDC26	DDX49	FTSJ1	LAMTOR5	MRTO4	PCYT1A	PWP1	RPS8	SRSF1	UBAP1	
ADSS	CDC27	DDX51	FTSJ3	LARS	MSL1	PDAP1	PWP2	RPS9	SRSF10	UBE2H	
AFG3L2	CDC37	DDX52	FUBP1	LARS2	MSL2	PDCD11	PYROXD1	RPSA	SRSF11	UBE2I	
AHCTF1	CDC40	DDX54	FUS	LAS1L	MTERFD2	PDCD2	QRS	RPTOR	SRSF2	UBE2L3	
AHCY	CDC42	DDX55	FXN	LDLR	MTG1	PDCL	QRS1	RPUSD4	SRSF3	UBE2M	
AIFM1	CDC45	DDX56	G3BP2	LENG1	MTHFD1	PDPK1	RABGGTB	RREB1	SRSF7	UBE2S	
AK2	CDC5L	DDX59	GAB2	LENG8	MTOR	PDRG1	RAC1	RRM1	SSB	UBE2T	
AKIRIN2	CDC6	DDX6	GABPA	LENG9	MTPAP	PDS5A	RACGAP1	RRM2	SSBP1	UBE3D	
ALDOA	CDC7	DENR	GABPB1	LEO1	MVD	PDSS1	RAD1	RRN3	SSRP1	UBE4B	
			GADD45GIP1								
ALG1	CDC73	DGCR14	I	LETM1	MYBBP1A	PDSS2	RAD17	RRP1	SSU72	UBL5	
ALG11	CDCA5	DGCR8	GAPDH	LIAS	MYBL2	PES1	RAD23B	RRP12	STIL	UBR4	
ALG13	CDIPT	DHDDS	GARI	LIG1	MZT1	PET112	RAD50	RRP15	STRAP	UBTF	
ALG14	CDK1	DHFR	GARS	LINS2	N6AMT1	PET117	RAD51	RRP36	STRIP1	UCHL5	
ALG2	CDK12	DHX15	GART	LINS4	NAA10	PFAS	RAD51AP1	RRP7A	STX18	UFD1L	
ALG8	CDK7	DHX33	GATC	LIN9	NAA15	PFDN1	RAD51B	RRP9	STX5	UMPS	
ALYREF	CDK9	DHX35	GBF1	LONP1	NAA20	PFDN2	RAD51C	RSL1D1	SUDS3	UPF1	
AMD1	CDT1	DHX36	GEMIN2	LRPPRC	NAA25	PFDN5	RAE1	RSL24D1	SUGP1	UPF2	
ANAPC1	CEBPD	DHX38	GEMIN4	LRR1	NAA30	PFDN6	RAN	RSRC2	SUGT1	UQCC	
ANAPC10	CEBPZ	DHX8	GEMIN5	LRRFIP1	NAA38	PGAM1	RANBP2	RTEL1	SUMO2	UQCR1	
ANAPC11	CENPA	DHX9	GEMIN8	LSG1	NAA50	PGD	RANBP3	RTF1	SUPT16H	UQCR2	
ANAPC13	CENPC1	DDO1	GET4	LSM10	NACA	PGGT1B	RANGAP1	RTFDC1	SUPT4H1	UQCRF51	
ANAPC15	CENPH	DIEXF	GFER	LSM11	NAE1	PGK1	RAPGEF6	RTTN	SUPT5H	UQCRQ	
ANAPC4	CENPJ	DIMT1	GFM1	LSM2	NAF1	PGM3	RARS	RUVBL1	SUPT6H	URB1	
ANAPC5	CENPL	DIS3	GGPS1	LSM3	NAPA	PGS1	RARS2	RUVBL2	SURV3L1	URB2	
ANKLE2	CENPM	DKC1	GINS1	LSM4	NAPG	PHB	RBBP4	SACMIL	SURF6	URI1	
ANKRD17	CENPN	DLG	GINS2	LSM5	NARFL	PHF23	RBBP5	SAE1	SUZ12	URM1	
ANLN	CENPW	DLST	GINS3	LSM6	NARS	PHF5A	RBBP6	SAMD4B	SYF2	UROD	
AP2S1	CEP135	DMAP1	GLE1	LTV1	NARS2	PIK3C3	RBBP8	SAMM50	SYMPK	USE1	
APC	CEP152	DNAJA3	GLTSCR2	LUC7L3	NAT10	RBM10	PIK3R4	RBM10	SAP130	USP1	
APEX1	CEP192	DNAJC11	GMNN	LYRM4	NBAS	PLK1	RBM12	SAP18	TACC3	USP36	
API5	CEP350	DNAJC19	GMPS	MAGOH	NCAPD2	PLK4	RBM14	SAP30BP	TADA1	USP37	
AQR	CEP44	DNAJC2	GNB1L	MALSU1	NCAPG	PLRG1	RBM17	SARNP	TADA2A	USP39	
ARCNI	CEP55	DNAJC8	GNB2L1	MAPK14	NCAPH	PMF1	RBM19	SARS	TAF1	USP5	
ARGLU1	CEP57	DNAJC9	GNL2	MARCH5	NCBP1	PMM2	RBM22	SARS2	TAF12	USP9X	
ARL2	CEP63	DNM1L	GNL3	MARS	NCBP2	PMPCA	RBM25	SART1	TAF13	USPL1	
ARMC7	CEP85	DNM2	GNL3L	MASTL	NCL	PMPCB	RBM28	SART3	TAF1B	UTP11L	
ARMC8	CEP97	DNMT1	GOLT1B	MAT2A	NCOA1	PMVK	RBM33	SASS6	TAF1C	UTP14A	
ARPC2	CFDP1	DNTTIP2	GON4L	MATR3	NCOA2	PNISR	RBM39	SBDS	TAF1D	UTP15	
ARPC3	CHAF1A	DOHH	GOSR2	MAU2	NDC80	PNN	RBM42	SCAF11	TAF5	UTP18	
ARPC4	CHAF1B	DONSON	GPATCH1	MAX	NDUFA9	PNO1	RBM48	SCAMP4	TAF6	UTP20	
ASCC3	CHCHD4	DPH5	GPKOW	MBNL1	NDUFAB1	PNPT1	RBM8A	SCD	TAF6L	UTP6	
ASUN	CHEK1	DPY30	GPN1	MCL1	NDUFB4	POLA1	RBMX	SCFD1	TAF8	UVRAG	
ATAD5	CHEP	DR1	GNP2	MCM10	NDUFV2	POLA2	RBMX2	SCO1	TAF9	UXT	
ATIC	CHMP2A	DSN1	GNP3	MCM2	NEDD1	POLD1	RBPJ	SDAD1	TAMM41	VARS	
ATL2	CHMP3	DTL	GRB2	MCM3	NEDD8	POLD2	RBX1	SDE2	TANGO6	VBPI	
ATP13A1	CHMP4B	DTYMK	GRPEL1	MCM5	NELFA	POLD3	RCC1	SDHA	TARDBP	VCP	
ATP1A1	CHMP6	DUT	GRWD1	MCM6	NELFB	POLE	RCL1	SDHB	TARS	VEZT	
ATP2A2	CHORDC1	DYNC1H1	GSPT1	MCM7	NELFE	POLE2	REV3L	SDHC	TARS2	VMP1	
ATP5A1	CHTF8	DYNC1I2	GTF2A1	MCM8	NFAT5	POLG2	RFC1	SDHD	TBCA	VPS13D	
ATP5B	CHTOP	DYNLRB1	GTF2A2	MCRS1	NFS1	POLR1A	RFC2	SEC13	TBCB	VPS25	
ATP5C1	CIAO1	DYRK1A	GTF2B	MCTS1	NFYA	POLR1B	RFC3	SEC16A	TBCD	VPS29	
ATP5E	CIAPIN1	E4F1	GTF2E1	MDC1	NFYB	POLR1C	RFC4	SEC61A1	TBCE	VPS33A	
ATP5F1	CINP	EAPP	GTF2F1	MDN1	NFYC	POLR1E	RFC5	SEC61B	TCEB2	VPS35	
		EBNA1BP2									
ATP5H	CIRH1A	2	GTF2F2	MED1	NGDN	POLR2A	RFT1	SEC62	TCEG1	VPS36	
ATP5J2	CIT	ECTD	GTF2H1	MED10	NGRN	POLR2B	RFWD3	SEC63	TCOF1	VPS51	
ATP5L	CKAP5	ECT2	GTF2H3	MED12	NHLRC2	POLR2C	RHOA	SEH1L	TCPI	VPS52	
ATP5O	CLASP2	EDC4	GTF3A	MED13	NHP2	POLR2D	RIF1	SEL1L	TECR	VPS53	
ATP6A1	CLASRP	EED	GTF3C1	MED13L	NHP2L1	POLR2E	RINT1	SENP6	TEFM	VPS72	

ATP6A2	CLNS1A	EEF1A1	GTF3C3	MED14	NIP7	POLR2F	RIOK1	SEPSECS	TEX10	WAC
ATP6V0B	CLP1	EEF1G	GTF3C4	MED15	NIPBL	POLR2I	RIOK2	SERBP1	TFAM	WAPAL
ATP6V0C	CLPB	EEF2	GTF3C5	MED17	NKAP	POLR2L	RM1	SF1	TFB1M	WARS
ATP6V0D1	CLSPN	EEFSEC	GTF3C6	MED18	NLE1	POLR3A	RNASEH2A	SF3A1	TFB2M	WARS2
ATP6V1A	CLTC	EFTUD2	GTPBP10	MED19	NMD3	POLR3B	RNASEH2B	SF3A2	TFIP11	WBP11
ATP6V1D	CMPK1	EHMT1	GTPBP4	MED20	NMNAT1	POLR3C	RNF168	SF3B1	TFRC	WBPA
ATP6V1E1	CNOT1	EIF1	GTPBP5	MED21	NOB1	POLR3E	RNF20	SF3B14	THOC1	WBSRCR22
ATP6V1F	CNOT10	EIF1AD	GUK1	MED22	NOC3L	POLR3F	RNF4	SF3B2	THOC5	WDHD1
ATP6V1G1	CNOT11	EIF1AX	HARS	MED23	NOC4L	POLR3H	RNF40	SF3B3	THOC7	WDR12
ATR	CNOT2	EIF2B1	HARS2	MED26	NOL10	POLR3K	RNF8	SFPQ	THRAP3	WDR18
ATRIP	CNOT3	EIF2B2	HAUS1	MED27	NOL11	POMP	RNGTT	SFSWAP	TICRR	WDR20
ATRX	COA5	EIF2B3	HAUS2	MED28	NOL12	POP4	RNMT	SGOL1	TIMELESS	WDR25
ATXN10	COASY	EIF2B4	HAUS3	MED29	NOL6	POP7	RNPC3	SHFM1	TIMM10	WDR3
AURKA	COG1	EIF2B5	HAUS4	MED31	NOL7	PPA1	RNPS1	SHMT2	TIMM22	WDR33
							RP11-93B14.6	SHOC2	TIMM23	WDR36
B4GALT5	COG2	EIF2S1	HAUS5	MED4	NOL8	PPA2	93B14.6	SHOC2	TIMM23	WDR36
BANF1	COG3	EIF2S2	HAUS6	MED6	NOL9	PPAN	RP1A	SHQ1	TIMM44	WDR4
BANP	COG4	EIF2S3	HAUS7	MED7	NOLC1	PPAT	RP2	SKA1	TIMM50	WDR43
BARD1	COG5	EIF3A	HAUS8	MED8	NOM1	PPIE	RPAIN	SKA2	TIMM9	WDR44
BCAS2	COG7	EIF3B	HBS1L	MED9	NONO	PPIL1	RPAP1	SKA3	TINF2	WDR46
BCCP	COG8	EIF3D	HCFC1	METAP1	NOP10	PPIL2	RPAP3	SKIV2L2	TIPRL	WDR5
BCL2	COPA	EIF3I	HEATR1	METAP2	NOP14	PPIL4	RPE	SKP1	TKT	WDR55
BCL2L1	COPB1	EIF3J	HEATR3	METTL1	NOP16	PPME1	RPF1	SLBP	TMA16	WDR59
BCLAF1	COPB2	EIF3M	HELQ	METTL14	NOP2	PPP1CB	RPF2	SLC25A19	TMED10	WDR70
BCS1L	COPE	EIF4A1	HINFP	METTL16	NOP56	PPP1R10	RP1A	SLC25A26	TMED2	WDR74
								SLC25A3	A	WDR75
BDP1	COPG1	EIF4A2	HJURP	METTL3	NOP58	PPP1R11	RPL10A	SLC25A3	TMEM167	WDR75
BECN1	COPS2	EIF4A3	HMGCR	MFAP1	NOP99	PPP1R15B	RPL11	SLC35B1	TMEM199	WDR77
BET1	COPS3	EIF4B	HMGCS1	MFN2	NPAT	PPP1R2	RPL12	SLC39A10	TMEM238	WDR82
BIRC5	COPS4	EIF4E	HNRNPA1	MGEA5	NPL0C4	PPP1R7	RPL13	SLC7A6OS	TMEM258	WDR92
			HNRNPA2B1							
			I	MINOS1	NPM1	PPP1R8	RPL13A	SLIRP	TMEM41B	WEE1
BLM	COPS6	EIF4G1	HNRNPC	MIPPE	NRDE2	PPP2CA	RPL14	SLMAP	TMEM48	WIBG
BMS1	COPS8	EIF4G2	HNRNPF	MIS12	NRF1	PPP2R1A	RPL15	SLMO2	TMX2	WNK1
BNIP1	COPZ1	EIF5	HNRNPH1	MIS18A	NSA2	PPP2R2A	RPL17	SLU7	TNPO3	WRB
BOD1L1	COQ3	EIF5A	HNRNPK	MIS18BP1	NSF	PPP2R3C	RPL18	SLX4	TOMM20	XAB2
BORA	COQ4	EIF5B	HNRNPL	MKI67IP	NSL1	PPP2R4	RPL18A	SMARCA5	TOMM22	XPO1
BPTF	COQ5	EIF6	HNRNPM	MMS19	NSMCE1	PPP4C	RPL19	SMARCB1	TOMM40	XPO5
BRCA1	COX10	ELAC2	HNRNPU	MMS22L	NSMCE4A	PPP6C	RPL21	SMARCE1	TOMM70A	XRCC1
BRCA2	COX11	ELL	HSCB	MNAT1	NSRP1	PPRC1	RPL22	SMC1A	TOP1	XRCC2
BRD4	COX15	ELP2	HSD17B10	MNF1	NSUN4	PPWD1	RPL22L1	SMC2	TOP2A	XRCC3
BRD8	COX17	ELP4	HSD17B12	MOB4	NUBP1	PRC1	RPL23	SMC3	TOP3A	XRCC6
BRF1	COX5B	ELP5	HSPA14	MPDU1	NUBP2	PRCC	RPL23A	SMC4	TOPBP1	XRNI
BRIP1	COX6B1	ELP6	HSPA5	MPHOSPH10	NUDC	PRDM10	RPL24	SMC5	TP53RK	XRN2
BRIX1	COX7B	EMC3	HSPA8	MPHOSPH6	NUDCD3	PREB	RPL26	SMC6	TP1	YAE1D1
BTA1F	COX7C	EMC4	HSPA9	MRPL10	NUDT21	PRELID1	RPL27	SMG1	TPR	YARS1
BTF3	CPSF2	EMC7	HSPD1	MRPL11	NUF2	PRIM1	RPL27A	SMG5	TPT1	YARS2
BUB1	CPSF3	ENO1	HSPF1	MRPL12	NUFIP1	PRKRIR	RPL28	SMG6	TPX2	YBX1
BUB1B	CPSF6	EPRS	HSPF1	MRPL12	NUFIP1	PRKRIR	RPL28	SMG6	TPX2	YBX1
BUB3	CRCP	ERAL1	HTATSF1	MRPL16	NUP107	PRMT1	RPL29	SMG7	TRA2B	YEATS2
BUD13	CREBBP	ERCC2	HUS1	MRPL17	NUP133	PRMT5	RPL3	SMNDC1	TRAP1	YEATS4
BUD31	CRLS1	ERCC3	IARS	MRPL18	NUP153	PRPF18	RPL31	SMU1	TRAPPC1	YKT6
BYSL	CRNKL1	ERCC4	IDI1	MRPL19	NUP155	PRPF19	RPL32	SNAPC1	TRAPPC11	YLPM1
C12orf45	CSD1E1	ERH	IGBP1	MRPL2	NUP160	PRPF3	RPL34	SNAPC3	TRAPPC3	YMEI1L
C14orf166	CSE1L	ESF1	IK	MRPL20	NUP188	PRPF31	RPL35	SNF8	TRAPPC4	YMEI1L
C15orf41	CSNK1A1	ETF1	IKBKAP	MRPL21	NUP205	PRPF38A	RPL37	SNIP1	TRAPPC8	YRDC
C16orf80	CSNK2B	EWSR1	ILF2	MRPL22	NUP214	PRPF38B	RPL37A	SNRNP200	TRIAP1	YTHDC1
C18orf21	CSTF1	EXOC1	ILF3	MRPL23	NUP43	PRPF39	RPL38	SNRNP27	TRIT1	YY1
C19orf43	CSTF2	EXOC2	IMMT	MRPL24	NUP50	PRPF4	RPL39	SNRNP35	TRMT10C	ZBTB11
C1orf131	CSTF3	EXOC4	IMP4	MRPL27	NUP54	PRPF40A	RPL4	SNRNP40	TRMT5	ZBTB17
C21orf59	CTC1	EXOC5	IMPDH2	MRPL3	NUP85	PRPF4B	RPL41	SNRNP48	TRMT6	ZBTB2
C22orf28	CTCF	EXOSC1	INCENP	MRPL32	NUP88	PRPF6	RPL5	SNRNP70	TRMT61A	ZBTB80S
									TRNAU1A	
C3orf17	CTDP1	EXOSC10	INO80	MRPL33	NUP93	PRPF8	RPL6	SNRPA	P	ZC3H11A
C6orf48	CTDSP2	EXOSC2	INO80C	MRPL34	NUP98	RPL7A	RPL7A	SNRPA1	TRNT1	ZC3H13
C6orf57	CTNNB1	EXOSC3	INSIG1	MRPL35	NUPL1	PSMA2	RPL7L1	SNRPB	TRPM7	ZC3H18
C7orf73	CTPS1	EXOSC5	INTS12	MRPL37	NUPL2	PSMA3	RPL9	SNRPC	TRRAP	ZC3H4
C9orf114	CTR9	EXOSC7	INTS2	MRPL38	NUS1	PSMA5	RPLP0	SNRPD1	TRUB2	ZC3H8
C9orf78	CTU1	EXOSC8	INTS3	MRPL39	NUSAP1	PSMA7	RPLP1	SNRPD2	TSC22D2	ZCHC9
CAB39	CTU2	EXOSC9	INTS4	MRPL4	NUTF2	PSMB1	RPLP2	SNRPD3	TSEN15	ZCRB1
CAD	CUL1	EZH2	INTS5	MRPL40	NVL	PSMB2	RPN1	SNRPE	TSEN2	ZFC3H1
CALM2	CUL2	FAF2	INTS7	MRPL42	OGDH	PSMB3	RPN2	SNRPF	TSEN54	ZFR
CAMLG	CWC22	FAM178A	IPO11	MRPL44	OGT	PSMB4	RPP14	SNRPG	TSNG101	ZMAT2
CAPNS1	CWC25	FAM204A	IPO7	MRPL45	OIP5	PSMB5	RPP30	SNW1	TSR1	ZMAT5
CAPZB	CWF19L2	FAM210A	IPO9	MRPL47	OPA1	PSMB6	RPP38	SOD1	TSR2	ZMYND8
CARS	Cxor156	FAM32A	IPPK	MRPL48	ORAOV1	PSMB7	RPP40	SOD2	TTC1	ZNF131
CASC3	CYCS	FAM50A	ISCA1	MRPL49	ORC1	PSMC1	RPRD1B	SON	TTC27	ZNF143
CASC5	DAD1	FAM60A	ISCU	MRPL50	ORC2	PSMC3	RPRD2	SP1	TTC4	ZNF148
CCAR1	DAP3	FAM96B	ISG20L2	MRPL51	ORC3	PSMC4	RPS10	SPAG5	TFPI	ZNF207
CCDC115	DARS	FAM98B	ISY1	MRPL52	ORC4	PSMC5	RPS11	SPATA5	TF2	ZNF236
CCDC130	DARS2	FANCB	IWS1	MRPL54	ORC5	PSMC6	RPS12	SPATA5L1	TTI1	ZNF259
CCDC174	DBR1	FANCC	KANSL1	MRPL9	ORC6	PSMD1	RPS13	SPC24	TTK	ZNF335
CCDC47	DCAF7	FANCD2	KANSL2	MRPS10	OSBP	PSMD11	RPS14	SPC25	TUBA1B	ZNF407
CCDC59	DCP2	FANCL	KANSL3	MRPS12	OSGEP	PSMD12	RPS15	SPCS2	TUBB	ZNF574
CCDC84	DCPS	FANCM	KARS	MRPS14	OXA1L	PSMD13	RPS15A	SPCS3	TUBD1	ZNF622

## Sabatini survival genes

AAMP	CBWD5	DAXX	EXOSC4	HMG81	MCM6	NDUF66	PNN	RBBP8	SAMSN1	STRIP1	TYMS
AARS	CBWD6	DBR1	EXOSC5	HMGCR	MCM7	NDUF68	PNPT1	RBM10	SAP18	STRN	TYRO3
AASDHPPPT	CCAR1	DCAF15	EXOSC6	HMGCS1	MCM9	NDUF82	POLA1	RBM14	SAP30BP	SUDS3	UZAF1
AATF	CCAR2	DCP2	EXOSC7	HMGXB3	MCMBP	NDUFV1	POLA2	RBM14-RBM4	SARNP	SUGP1	UZAF2
ABCE1	CCDC101	DCPS	EXOSC8	HNRNPC	MCRS1	NEDD8	POLD2	RBM17	SARS	SUGT1	UBA1
ABHD11	CCDC115	DCTN1	EXOSC9	HNRNP3	MDC1	NELFB	POLD3	RBM18	SARS2	SULT1A3	UBA2
ABL1	CCDC130	DCTN2	EXTL1	HNRNPK	MDN1	NELFCD	POLE	RBM19	SART1	SULT1A4	UBA3
ABT1	CCDC33	DCTN3	EXTL3	HNRNPL	MECR	NFATC2IP	POLE2	RBM25	SART3	SUPT20H	UBA52
ACAD9	CCDC47	DCTN4	EZH2	HNRNPU	MED1	NFS1	POLG	RBM28	SBNO1	SUPT5H	UBAP1
ACBD4	CCDC58	DCTN5	F8A1	HSCB	MED11	NGDN	POLG2	RBM39	SCAF1	SUPT6H	UBE2I
ACIN1	CCDC59	DDB1	F8A2	HSD17B10	MED12	NHP2	POLR1A	RBM5	SCAF11	SUPT7L	UBE2K
ACLY	CCDC84	DDI2	F8A3	HSD17B12	MED15	NHP2L1	POLR1B	RBM8A	SCAP	SUPV3L1	UBE2L3
ACO2	CCDC86	DDOST	FAF2	HSF1	MED17	NIP7	POLR1C	RBMX	SCD	SURF1	UBE2M
ACTB	CCDC94	DDX1	FAM103A1	HSPA14	MED19	NIPBL	POLR1E	RBPJ	SCO1	SUV39H1	UBE2S
ACTG2	CCNA2	DDX10	FAM122A	HSPA5	MED20	NKAP	POLR2A	RBX1	SCO2	SUZ12	UBE4B
ACTL6A	CCNH	DDX18	FAM210A	HSPA9	MED21	NLE1	POLR2B	RCC1	SCYL1	SYF2	UBL5
ACTR1A	CCNT1	DDX19A	FAM50A	HSPD1	MED22	NMD3	POLR2C	RCL1	SDAD1	SYMPK	UBL7
ACTR2	CCT2	DDX20	FAM72D	HSPE1	MED24	NMNAT1	POLR2D	RCOR1	SEDE2	SYK1	UBR4
ACTR3	CCT3	DDX21	FAM96A	HTATSF1	MED27	NOB1	POLR2E	REV3L	SDHA	SVVN1	UBTF
ACTR5	CCT4	DDX23	FAM96B	HUS1	MED30	NOC2L	POLR2F	REXO2	SDHA1	TACC3	UFD1L
ACTR8	CCT5	DDX24	FANCA	HUWE1	MED8	NOC4L	POLR2G	RFC1	SDHB	TADA1	UMPS
ADAT3	CCT6A	DDX27	FANCC	HYOU1	MEPCE	NOL10	POLR2H	RFC2	SDHD	TADA2B	UNC45A
ADRM1	CCT7	DDX28	FANCF	HYPK	METAP1	NOL11	POLR2I	RFC3	SEC13	TADA3	UPF1
ADSL	CCT8	DDX39A	FANCI	IARS	METTL1	NOL12	POLR2J	RFC4	SEC16A	TAF10	UPF2
ADSS	CD3EAP	DDX39B	FANCM	IARS2	METTL4	NOL6	POLR2J2	RFC5	SEC61A1	TAF15	UQC2C
AFG3L2	CDAN1	DDX41	FARS2	IBA57	METTL16	NOL7	POLR2J3	RFK	SEC63	TAF1C	UQCRB
AGO2	CDC123	DDX42	FARSA	IDH3A	METTL17	NOL8	POLR2L	RFT1	SEHIL	TAF5L	UQCRC1
AGPS	CDC16	DDX46	FARSB	IKBKAP	METTL3	NOL9	POLR3A	RPWD3	SEPHS2	TAF6	UQCRC2
AHCTF1	CDC20	DDX47	FASN	IKZF2	MFAP1	NOM1	POLR3C	RGPD5	SEPECS	TAF6L	UQCRCFS1
AHCY	CDC23	DDX49	FASTKD5	IL16	MFN2	NOP14	POLR3D	RGPD6	SERF1A	TAF8	UQCRH
AIFM1	CDC40	DDX51	FAU	IL9R	MGAT1	NOP16	POLR3E	RHEB	SERF1B	TAMM41	URB2
AK2	CDC45	DDX52	FBX05	ILF2	MGEA5	NOP2	POLR3H	RHOA	SETD1A	TANGO6	UROD
AK6	CDC5L	DDX54	FBXW11	IMMT	MINOS1	NOP56	POLR3K	RINT1	SETD8	TARS	USP10
AKIRIN2	CDC6	DDX56	FBXW7	IMP3	MIOS	NOP58	POP1	RIOK1	SF1	TARS2	USP14
ALAD	CDC73	DDX6	FCGR1A	IMP4	MIPEP	NOP9	POP4	RIOK2	SF3A1	TAZ	USP36
ALAS1	CDIPT	DEX1	FCGR1B	IMPDH2	MIS18BP1	NOSIP	POP7	RNA5EH2A	SF3A2	TBC1D3	USP37
ALDH18A1	CDK1	DGCR14	FDPS	INCENP	MMGT1	NOTCH2NL	POT1	RNA5EH2B	SF3A3	TBC1D3B	USP39
ALDOA	CDK12	DGCR8	FDX1L	ING5	MMS19	NPAT	POTEH	RNA5EH2C	SF3B2	TBC1D3C	USP5
ALG11	CDK13	DHDDS	FDXR	INO80	MMS22L	NPIB5	POU2F1	RNF113A	SF3B3	TBC1D3F	USP8
ALG14	CDK2	DHFR	FEN1	INO80E	MNAT1	NPLC4	PPA1	RNF168	SF3B4	TBC1D3G	USP11
ALG2	CDK9	DHODH	FH	INTS1	MOCS3	NR2C2AP	PPA2	RNF214	SF3B5	TBCA	UTP11L
ALYREF	CDT1	DHX15	FIP1L1	INTS3	MOC5	NRBP2	PPAN	RNF31	SFPQ	TBCB	UTP14A
AMD1	CDX2	DHX16	FIS1	INTS4	MORF4L1	NRDE2	PPAN-P2RY11	RNF4	SHARPIN	TBCC	UTP15
AMHR2	CEBPA	DHX30	FKBP1	INTS5	MPHOSP10	NRF1	PPAT	RNF40	SHMT2	TBCD	UTP20
ANAPC11	CEBPD	DHX33	FLCN	INTS7	MP1	NSA2	PPCDC	RNF8	SHO1	TBCE	UTP23
ANAPC15	CEBPZ	DHX36	FLII	INTS8	MRTG3	NSF	PPCS	RNGTT	SHAH1	TBL3	UTP3
ANAPC2	CENPA	DHX38	FNBP4	INTS9	MRPL10	NSL1	PIIB	RNMT	SIK2	TCEA1	UTP6
ANAPC4	CENPC	DHX8	FNTB	IPO11	MRPL11	NSMCE1	PIIE	RNPC3	SIN3A	TCP1	VARS
ANAPC5	CENPE	DHX9	FOXRED1	IPO13	MRPL12	NSMCE2	PII2	ROMO1	SKA1	TEFM	VARS2
ANKDD1A	CENPI	DIAPH1	FPGS	IPO7	MRPL14	NSMCE4A	PPP5K2	RPA1	SKA3	TELO2	VCP
ANKRD11	CENPM	DID01	FTSJ2	IPO9	MRPL15	NSUN4	PPP1CA	RPA3	SKIIV2L2	TERF2	VCPIP1
ANKRD52	CENPW	DIEXF	FTSJ3	IPPK	MRPL16	NUBP1	PPP1CB	RPAIN	SLC20A1	TEX10	VEZT
AP2S1	CEP192	DIMT1	FUBP1	IREB2	MRPL17	NUBP2	PPP1CC	RPAPI	SLC25A1	TFB2M	VMA21
APEX2	CEP55	DIS3	GAB2	IRF2BP1	MRPL19	NUDC	PPP1R10	RPAPI2	SLC25A3	TFIP11	VMP1
APRT	CEP57	DKC1	GABPB1	IRF2BP2	MRPL20	NUDCD3	PPP1R15B	RPGRIP1	SLC25A32	TFPT	VPS13D
AQR	CEP85	DL1	GADD45GIP1	ISCA1	MRPL21	NUDT21	PPP1R2	RPL10	SLC28A1	TFRC	VPS16
ARCN1	CFL1	DLST	GAK	ISCA2	MRPL23	NUDT4	PPP1R35	RPL10A	SLC31A1	TGS1	VPS18
ARHGAP1	CHAF1A	DNAA3	GALE	ISCU	MRPL24	NUF2	PPP2CA	RPL11	SLC35B1	THAP1	VPS25
ARID1A	CHAF1B	DNAAJ4	GAPDH	ISG20L2	MRPL28	NUFIP2	PPP2R1A	RPL12	SLC38A5	THAP11	VPS28
ARH1	CHAMP1	DNAAJ17	GAR1	ITPK1	MRPL3	NUP107	PPP2R2A	RPL13	SLC3A2	THAP4	VPS29
ARL2	CHCHD1	DNAAJ9	GART	IWS1	MRPL33	NUP133	PPP2R3C	RPL13A	SLC5A3	THG1L	VPS33A
ARMC7	CHD1	DNLZ	GATA2	KANSL1	MRPL34	NUP155	PPP2R4	RPL14	SLC6A17	THOC1	VPS45
ARPC4	CHD4	DNM1L	GBF1	KANSL2	MRPL35	NUP160	PPP4C	RPL15	SLC7A11	THOC2	VPS4A
ASH2L	CHD5	DNM2	GCLC	KANSL3	MRPL37	NUP188	PPP6C	RPL17	SLC7A60S	THOC3	VPS51
ASNA1	CHD7	DNMT1	GCSH	KARS	MRPL38	NUP214	PPP6R3	RPL18	SLMO2	THOC5	VPS52
ASUN	CHD8	DNTTIP2	GEMIN2	KAT2A	MRPL39	NUP43	PPRC1	RPL18A	SLTM	THOC7	VPS72
ATAD5	CHEK1	DOHH	GEMIN4	KAT5	MRPL4	NUP54	PRC1	RPL19	SMARCA4	TICRR	WARS
ATF4	CHKA	DOLK	GEMIN5	KAT7	MRPL41	NUP62	PRCC	RPL23	SMARCA5	TIGD3	WARS2
ATG9A	CHMP1B	DOLPP1	GET4	KCMF1	MRPL42	NUP85	PREB	RPL23A	SMARCAL1	TIMELESS	WBP4
ATIC	CHMP2A	DONSON	GFER	KDM4A	MRPL43	NUP88	PRELID1	RPL24	SMARCB1	TIMM10	WBSR16
ATL2	CHMP4B	DPAGT1	GF11	KDM8	MRPL44	NUP93	PRIM1	RPL26	SMARCC1	TIMM13	WBSR22
ATP1A1	CHMP6	DPH1	GMF1	KDSR	MRPL45	NUP98	PRKAA1	RPL27A	SMARCD2	TIMM23	WDHD1
ATP2A2	CHORDC1	DPH3	GFME2	KIAA0100	MRPL46	NUS1	PRKRIP1	RPL27A	SMARCE1	TIMM44	WDR1
ATP5A1	CHTF8	DPH5	GFPT1	KIAA0196	MRPL48	NVL	PRKRIR	RPL29	SMCIA	TIMMDC1	WDR12
ATP5B	CIAO1	DPH6	GGPS1	KIAA0391	MRPL51	NXF1	PRMT1	RPL3	SMC2	TIPRL	WDR18
ATP5D	CINP	DPY30	GID8	KIAA0947	MRPL52	OAZ1	PRMT5	RPL30	SMC3	TKT	WDR24
ATP5J2-PTCD1	CIRH1A	DROSHA	GIGYF2	KIAA1033	MRPL53	OBFC1	PRPF19	RPL31	SMC4	TLE3	WDR25
ATP5O	CITED2	DSCC1	GINS1	KIAA1199	MRPL9	OGDH	PRPF3	RPL32	SMC5	TMED2	WDR3
ATP6AP1	CKAP5	DTL	GINS2	KIAA1429	MRPS11	OGT	PRPF31	RPL34	SMC6	TMEM147	WDR33
ATP6V0B	CLASRP	DTYMK	GINS3	KIAA1524	MRPS12	OPA1	PRPF38A	RPL35	SMG1	TMEM199	WDR36



ABL1	CCDC84	DCTN5	EXTL3	HNRNPL	MED11	NGDN	POLG	RBM25	SART1	SULT1A3	U2AF2
ABT1	CCDC86	DDBI	EZH2	HNRNPU	MED12	NHP2	POLG2	RBM28	SART3	SULT1A4	UBA1
ACAD9	CCDC94	DDI2	F8A1	HSCB	MED15	NIP7	POLR1A	RBM39	SBNO1	SUPT20H	UBA2
ACBD4	CCNA2	DDOST	F8A2	HSD17B10	MED17	NIPBL	POLR1B	RBM5	SCAF1	SUPT5H	UBA3
ACIN1	CCNH	DDX1	F8A3	HSD17B12	MED19	NKAP	POLR1C	RBM8A	SCAF11	SUPT6H	UBA52
ACLY	CCNT1	DDX10	FAF2	HSF1	MED20	NLE1	POLR1E	RBMX	SCAP	SUPT7L	UBAP1
ACO2	CCT2	DDX18	FAM103A1	HSPA14	MED21	NMD3	POLR2A	RBPJ	SCD	SUPV3L1	UBE21
ACTB	CCT3	DDX19A	FAM122A	HSPA5	MED22	NMNAT1	POLR2B	RBX1	SCO1	SURF1	UBE2K
ACTG2	CCT4	DDX20	FAM210A	HSPA9	MED24	NOB1	POLR2C	RCC1	SCO2	SUV39H1	UBE2L3
ACTL6A	CCT5	DDX21	FAM50A	HSPD1	MED27	NOC2L	POLR2D	RCL1	SCYL1	SUZ12	UBE2M
ACTR1A	CCT6A	DDX23	FAM72D	HSPE1	MED30	NOC4L	POLR2E	RCOR1	SDAD1	SYF2	UBE2S
ACTR2	CCT7	DDX24	FAM96A	HTATSF1	MED8	NOL10	POLR2F	REV3L	SDE2	SYMPK	UBE4B
ACTR3	CCT8	DDX27	FAM96B	HUS1	MEPCE	NOL11	POLR2G	REXO2	SDHA	SYS1	UBL5
ACTR5	CD3EAP	DDX28	FANCA	HUWE1	METAP1	NOL12	POLR2H	RFC1	SDHAF1	SYVN1	UBL7
ACTR8	CDAN1	DDX39A	FANCC	HYOU1	METTL1	NOL6	POLR2I	RFC2	SDHB	TACC3	UBR4
ADAT3	CDC123	DDX39B	FANCF	HYPK	METTL14	NOL7	POLR2J	RFC3	SDHD	TADA1	UBTF
ADRM1	CDC16	DDX41	FANCI	IARS	METTL16	NOL8	POLR2J2	RFC4	SEC13	TADA2B	UFD1L
ADSL	CDC20	DDX42	FANCM	IARS2	METTL17	NOL9	POLR2J3	RFC5	SEC16A	TADA3	UMPS
ADSS	CDC23	DDX46	FARS2	IBA57	METTL3	NOM1	POLR2L	RFK	SEC61A1	TAF10	UNC45A
AFGL2	CDC40	DDX47	FARSA	IDH3A	MFAP1	NOP14	POLR3A	RFT1	SEC63	TAF15	UPF1
AGO2	CDC45	DDX49	FARSB	IKBKAP	MFN2	NOP16	POLR3C	RFWD3	SEH1L	TAF1C	UPF2
AGPS	CDC5L	DDX51	FASN	IKZF2	MGAT1	NOP2	POLR3D	RGPD5	SEPHS2	TAF5L	UQC2
AHCTF1	CDC6	DDX52	FASTKD5	IL16	MGEA5	NOP56	POLR3E	RGPD6	SEPSECS	TAF6	UQCRB
AHCY	CDC73	DDX54	FAU	IL9R	MINOS1	NOP58	POLR3H	RHEB	SERF1A	TAF6L	UQCRC1
AIFM1	CDIPT	DDX56	FBXO5	ILF2	MIOS	NOP9	POLR3K	RHOA	SERF1B	TAF8	UQCRC2
AK2	CDK1	DDX6	FBXW11	IMMT	MPEP	NOSIP	POP1	RINT1	SETD1A	TAMM41	UQCRCF51
AK6	CDK12	DEXI	FBXW7	IMP3	MIS18BP1	NOTCH2NL	POP4	RIOK1	SF1	TANGO6	UQCRH
AKIRIN2	CDK13	DGCR14	FCGRIA	IMP4	MMGT1	NPAT	POP7	RIOK2	SF3A1	TARS	URB2
ALAD	CDK2	DGCR8	FCGRI1B	IMPDH2	MMS19	NP1B5	POT1	RNASEH2A	SF3A2	TARS2	UROD
ALAS1	CDK9	DHDDS	FDP5	INCENP	MMS22L	NLOC4	POTEH	RNASEH2B	SF3A3	TAZ	USP10
ALDH18A1	CDT1	DHFR	FDXR	ING5	MNAT1	NR2C2AP	POU2F1	RNASEH2C	SF3B2	TBC1D3	USP14
ALDOA	CDX2	DHODH	FEN1	INO80	MOCS3	NRBP2	PPA1	RNF113A	SF3B3	TBC1D3B	USP36
ALG11	CEBPA	DHX15	FH	INO80E	MOGS	NRDE2	PPA2	RNF168	SF3B4	TBC1D3C	USP37
ALG14	CEBPD	DHX16	FIP1L1	INTS1	MORF4L1	NRF1	PPAN	RNF214	SF3B5	TBC1D3F	USP39
ALG2	CEBPZ	DHX30	FIS1	INTS3	MPHOSPH10	NSA2	PPAN-P2RY11	RNF31	SFPQ	TBC1D3G	USP5
ALYREF	CENPA	DHX33	FKBP1	INTS4	MPI	NSF	PPAT	RNF4	SHARPIN	TBCA	USP8
AMD1	CENPC	DHX36	FLCN	INTS5	MRPL10	NSL1	PPCDC	RNF40	SHMT2	TBCB	USP11
AMHR2	CENPE	DHX38	FLII	INTS7	MRPL11	NSMCE1	PPCS	RNF8	SHQ1	TBCC	UTP14A
ANAPC11	CENPI	DHX8	FNBP4	INTS8	MRPL12	NSMCE2	PP1B	RNGTT	SHAH1	TBCD	UTP15
ANAPC15	CENPM	DHX9	FNTB	INTS9	MRPL14	NSMCE4A	PP1E	RNMT	SIK2	TBCE	UTP20
ANAPC2	CENPW	DIAPH1	FOXRED1	IPO11	MRPL15	NSUN4	PP1L2	RNPC3	SIN3A	TBL3	UTP23
ANAPC4	CEP192	DIDO1	FFGS	IPO13	MRPL16	NUBP1	PPP5K2	ROMO1	SKA1	TCEA1	UTP3
ANAPC5	CEP55	DIEXF	FTSJ3	IPO7	MRPL17	NUBP2	PPP1CA	RPA1	SKA3	TCP1	UTP6
ANKDD1A	CEP57	DIMT1	FUBP1	IPO9	MRPL19	NUDC	PPP1CB	RPA3	SKIV2L2	TEFM	VARS
ANKRD11	CEP85	DIS3	GAB2	IPPK	MRPL20	NUDCD3	PPP1CC	RPAIN	SLC20A1	TELO2	VARS2
ANKRD52	CFL1	DKC1	GABPB1	IREB2	MRPL21	NUDT21	PPP1R10	RPAP1	SLC25A1	TERF2	VCP
AP2S1	CHAF1A	DL1	GADD45GIP1	IRF2BP1	MRPL23	NUDT4	PPP1R15B	RPAP2	SLC25A3	TEX10	VCP1P1
APEX2	CHAF1B	DLST	GAK	IRF2BP2	MRPL24	NUF2	PPP1R2	RPGRIP1	SLC25A32	TFB2M	VEZT
APRT	CHAMP1	DNAJA3	GALE	ISCA1	MRPL28	NUFIP2	PPP1R35	RPL10	SLC28A1	TFP11	VMA21
AQR	CHCHD1	DNAJA4	GAPDH	ISCA2	MRPL3	NUP107	PPP2CA	RPL10A	SLC31A1	TFPT	VMP1
ARCN1	CHD1	DNAJC17	GAR1	ISCU	MRPL33	DNAJC17	PPP2R1A	RPL11	SLC35B1	TFRC	VPS13D
ARHGAP1	CHD4	DNAJC9	GART	ISG20L2	MRPL34	NUP155	PPP2R2A	RPL12	SLC38A5	TGS1	VPS16
ARID1A	CHD5	DNLZ	GATA2	ITPK1	MRPL35	NUP160	PPP2R3C	RPL13	SLC3A2	THAP1	VPS18
ARH1	CHD7	DNM1L	GBF1	IWS1	MRPL37	NUP188	PPP4C	RPL13A	SLC5A3	THAP11	VPS25
ARL2	CHD8	DNM2	GCLC	KANSL1	MRPL38	NUP214	PPP6C	RPL14	SLC6A17	THAP4	VPS28
ARMC7	CHEK1	DNMT1	GCSH	KANSL2	MRPL39	NUP43	PPP6R3	RPL15	SLC7A11	THG1L	VPS29
ARPC4	CHKA	DNTTIP2	GEMIN2	KANSL3	MRPL4	NUP54	PPRC1	RPL17	SLC7A60S	THOC1	VPS33A
ASH2L	CHMP1B	DOHH	GEMIN4	KARS	MRPL41	NUP62	PRC1	RPL18	SLTM	THOC2	VPS45
ASNA1	CHMP2A	DOLK	GEMIN5	KAT2A	MRPL42	NUP85	PRCC	RPL18A	SMARCA4	THOC3	VPS4A
ASUN	CHMP4B	DOLPP1	GET4	KAT5	MRPL43	NUP88	PREB	RPL19	SMARCA5	THOC5	VPS51
ATAD5	CHMP6	DONSON	GER	KAT7	MRPL44	NUP93	PRELID1	RPL23	SMARCAL1	THOC7	VPS52
ATF4	CHORDC1	DPAGT1	GF11	KCMF1	MRPL45	NUP98	PRIM1	RPL23A	SMARCB1	TICRR	VPS72
ATG9A	CHTF8	DPH1	GFM1	KDM4A	MRPL46	NUS1	PRKAA1	RPL24	SMARCC1	TIGD3	WARS
ATIC	CIAO1	DPH3	GFM2	KDM8	MRPL48	NVL	PRKRIP1	RPL26	SMARCC2	TIMELSS	WARS2
ATL2	CINP	DPH5	GFPT1	KDSR	MRPL51	NXF1	PRMT1	RPL27	SMARCE1	TIMM10	WB4
ATP1A1	CITED2	DPH6	GGPS1	KIAA0100	MRPL52	OAZ1	PRMT5	RPL27A	SMC1A	TIMM13	WBSR22
ATP2A2	CKAP5	DPY30	GID8	KIAA0196	MRPL53	OBFC1	PRPF19	RPL29	SMC2	TIMM23	WDHD1
ATP5A1	CLASRP	DROSHA	GIGYE2	KIAA0391	MRPL9	ORFH	PRPF3	RPL3	SMC3	TIMM44	WDR1
ATP5B	CLEC18C	DSCC1	GINS1	KIAA1033	MRPS11	OGT	PRPF31	RPL30	SMC4	TIMMDC1	WDR12
ATP5D	CLK3	DTL	GINS2	KIAA1429	MRPS12	OPA1	PRPF38A	RPL31	SMC5	TIPRL	WDR18
ATP5J2-PTCD1	CLP1	DTYMK	GINS3	KIAA1524	MRPS14	OAOV1	PRPF38B	RPL32	SMC6	TKT	WDR24
ATP5O	CLPB	DUT	GLE1	KIF11	MRPS15	ORC1	PRPF39	RPL34	SMG1	TLE3	WDR25
ATP6A1	CLPX	DYNC1H1	GLMN	KIF15	MRPS16	ORC2	PRPF4	RPL35	SMG5	TMED2	WDR3

ATP6V0B	CLSPN	DYNCL1	GLRX5	KIF18A	MRPS18A	ORC3	PRPF6	RPL35A	SMG6	TMEM147	WDR33
ATP6V0C	CLTC	EZF3	GLTSCR2	KIF20A	MRPS18B	ORC6	PRPF8	RPL36	SMG7	TMEM199	WDR36
ATP6V1A	CMIP	E4F1	GMPPB	KIF23	MRPS18C	OSBP	PRR13	RPL36AL	SMG8	TMEM209	WDR4
ATP6V1B2	CMTR1	EARS2	GMPS	KIN	MRPS2	OSGEP	PSMA1	RPL37	SMG9	TMEM30A	WDR43
ATP6V1C1	CNOT1	EBNA1BP2	GNB1L	KLF16	MRPS21	OTUD5	PSMA2	RPL37A	SMN1	TMX2	WDR46
ATP6V1D	CNTROB	ECD	GNL2	KMT2A	MRPS22	OXSM	PSMA3	RPL38	SMN2	TNIP1	WDR5
ATP6V1F	COA5	ECT2	GNL3	KMT2D	MRPS24	PABPN1	PSMA5	RPL4	SMNDC1	TNPO3	WDR55
ATP6V1G1	COASY	EED	GNL3L	KNTC1	MRPS25	PAF1	PSMA6	RPL5	SMU1	TOMM20	WDR61
ATPAF2	COG3	EEF1A1	GOLGA6L1	KPNA2	MRPS26	PAFAH1B1	PSMA7	RPL6	SNAPC1	TOMM22	WDR62
ATR	COG4	EEF1G	GOLGA6L9	KPNA4	MRPS27	PAICS	PSMB1	RPL7	SNAPC2	TOMM40	WDR7
ATRP	COG8	EEF2	GOLGA8O	KPNB1	MRPS34	PAK1IP1	PSMB2	RPL7A	SNAPC3	TONSL	WDR70
AURKA	COMMD4	EEFSEC	GON4L	KRAS	MRPS35	KRAS	PSMB3	RPL7L1	SNAPC4	TOP1	WDR74
AURKAIP1	COMMD5	EFTUD2	GOSR2	KRI1	MRPS5	PAM16	PSMB4	RPL8	SNAPC5	TOP1MT	WDR75
AURKB	COPA	EGLN2	GPI	KRR1	MRPS6	PANK3	PSMB5	RPL9	SNF8	TOP2A	WDR77
B3GNT2	COBP1	EIF1	GPKOW	KRTAP10-9	MRPS7	PAPD5	PSMB6	RPLP0	SNIP1	TOP3A	WDR83
BAG6	COPB2	EIF1AD	GPN1	KRTAP4-8	MRPS9	PAPOLG	PSMB7	RPLP1	SNRNP200	TP53H13	WDR92
BANF1	COPE	EIF2B1	GPN2	KTI12	MSTO1	PARS2	PSMC2	RPLP2	SNRNP25	TP53RK	WEE1
BCL2	COPG1	EIF2B2	GPN3	LAMTOR2	MTCH2	PAXBP1	PSMC3	RPN1	SNRNP27	TP53TG3	WHAMM
BCR	COPS3	EIF2B3	GPS1	LAMTOR4	MTFMT	PCBP1	PSMC4	RPN2	SNRNP35	TP53TG3B	WIPI2
BCS1L	COPS4	EIF2B4	GRB2	LARS	MTG1	PCBP2	PSMC5	RPP14	SNRNP48	TP53TG3C	WNK1
BECN1	COPS5	EIF2B5	GRPEL1	LARS2	MTG2	PCBP1	PSMD1	RPP21	SNRPA	TP53TG3D	WRB
BICD2	COPS6	EIF2S1	GRWD1	LAS1L	MTHFD1	PCID2	PSMD11	RPP30	SNRPD1	TP1	WTAP
BIRC2	COPZ1	EIF2S2	GSPT1	LCMT1	MTHFD1L	PCM1	PSMD12	RPP40	SNRPD2	TPR	XAB2
BIRC5	COQ2	EIF3A	GSS	LDB1	MTHFD2	PCNA	PSMD13	RPRD1B	SNRPD3	TPT1	XAGE1A
BMS1	COQ3	EIF3B	GTF2B	LENG8	MTIF2	PCYT1A	PSMD14	RPS10	SNRPE	TPX2	XAGE1B
BORA	COQ4	EIF3C	GTF2E1	LETM1	MTO1	PDCD11	PSMD2	RPS11	SNRPF	TRA2B	XPO1
BPTF	COQ5	EIF3CL	GTF2F2	LIAS	MTOR	PDCD2	PSMD3	RPS12	SNUPN	TRAF2	XPO5
BRCA1	COQ6	EIF3D	GTF2H1	LIG1	MTAP	PDCD7	PSMD4	RPS13	SOD1	TRAIIP	XRCC3
BRCA2	COX10	EIF3F	GTF2H2	LIG3	MTRF1L	PDCL	PSMD6	RPS14	SOD2	TRAPPC1	XRCC5
BRD1	COX11	EIF3G	GTF2H2C	LIMS3	MVD	PDE1B	PSMD7	RPS15	SON	TRAPPC11	XRCC6
BRD8	COX15	EIF3I	GTF2H3	LIN54	MVK	PDE4DIP	PSME3	RPS15A	SOS1	TRAPPC4	XRN2
BRD9	COX17	EIF3J	GTF2H4	LIN9	MYB	PDSSA	PSMG1	RPS16	SPAG5	TRAPPC5	XYLT2
BRF1	COX20	EIF3L	GTF3A	LIFT1	MYBBP1A	PDSS1	PSMG3	RPS17	SPAG7	TRAPPC8	YAE1D1
BRF2	COX41I	EIF4A1	GTF3C1	LIFT2	MYBL2	PDSS2	PSMG4	RPS18	SPANXA1	TRAPPC9	YARS
BRIX1	COX5B	EIF4A3	GTF3C2	LMAN1L	MYC	PDXK	PSTK	RPS19	SPANXA2	TRIAPI	YARS2
BRPF1	COX6B1	EIF4G1	GTF3C3	LMO2	MYH9	PELO	PTAR1	RPS2	SPATA31A5	TRIM28	YBEY
BTA1F	COX7C	EIF4G2	GTF3C4	LOXL1	N6AMT1	PELP1	PTCD1	RPS21	SPATA5	TRIM73	YKT6
BUB1B	CPSF1	EIF5A	GTPBP4	LRPPRC	NAA10	PE51	PTCD3	RPS23	SPATA5L1	TRIM74	YLPM1
BUB3	CPSF2	EIF5AL1	GTPBP8	LRR1	NAA15	PET117	PTPMT1	RPS25	SPC24	TRIP13	YME1L1
BUD13	CPSF3	EIF5B	GUK1	LRWD1	NAA25	PEX10	PTPN23	RPS27A	SPC25	TRIP4	YRDC
BUD31	CPSF3L	EIF6	H2AFB2	LSG1	NAA30	PEX12	PUF60	RPS28	SPEN	TRMT1	YTHDC1
BYSL	CPSF4	ELAC2	H2AFB3	LSM11	NAA35	PEX14	PWP1	RPS29	SP11	TRMT10C	YY1
C10orf2	CPSF6	ELL	H2AFX	LSM12	NAA50	PEX3	PWP2	RPS3	SPIDR	TRMT112	ZARIL
C14orf80	CPSF7	ELP2	HAP1	LSM2	NADK	PEX5	PYROXD1	RPS3A	SPOP	TRMT5	ZBED2
C15orf39	CREB3	ELP3	HARS	LSM3	NAE1	PEX7	QARS	RPS4X	SPRTN	TRMT6	ZBTB11
C15orf41	CREBBP	ELP5	HARS2	LSM7	NAF1	PFAS	QRICH1	RPS5	SPTLC1	TRMT61A	ZBTB45
C16orf59	CRLS1	ELP6	HAUS1	LTV1	NAMPT	PFDN2	QRS1L	RPS6	SPTLC2	TRNAU1A P	ZBTB80S
C16orf72	CRNLK1	EMC1	HAUS2	LUC7L2	NAPA	PFDN6	RAB34	RPS7	SPTSSA	TRPM7	ZC3H13
C17orf53	CSE1L	EMC3	HAUS3	LUC7L3	NARFL	PFN1	RAB6C	RPS8	SRBD1	TRRAP	ZC3H18
C17orf89	CSNK1A1	EMC6	HAUS4	MAD2L1BP	NARS	PGAM1	RABGGTA	RPS9	SRCAP	TRUB2	ZC3H3
C19orf43	CSNK1G1	EMC7	HAUS5	MAD2L2	NARS2	PGD	RABGGTB	RPSA	SRD5A3	TSEN2	ZC3H4
C19orf52	CSNK2B	ENO1	HAUS8	MAF1	NAT10	PGGT1B	RABIF	RPTOR	SREBF1	TSEN34	ZCCHC14
C19orf53	CSTF1	ENY2	HDAC3	MAGED4	NBAS	PGK1	RACGAP1	RPUSD4	SRF	TSEN54	ZEB2
C19orf70	CSTF3	EP300	HEATR1	MAGED4B	NCAPD2	PGM3	RAD1	RRAGA	SREBP1	TSFM	ZFC3H1
C1orf109	CT45A2	EPG5	HECTD1	MAGOH	NCAPG	PGS1	RAD17	RRM1	SRM	TSPAN31	ZFP36
C1QBP	CTC1	EPT1	HELQ	MAK16	NCAPH	PHB	RAD21	RRM2	SRP54	TSR1	ZFP36L1
C21orf59	CTCF	ERAL1	HEXIM1	MALSU1	NCBP1	PHB2	RAD23B	RRN3	SRPRB	TSR2	ZFP36L2
C7orf26	CTDSPL2	ERCC2	HGS	MAN2C1	NCBP2	PHF5A	RAD51	RRP1	SRRM1	TTC1	ZFP91
C8orf33	CTNBNL1	ERCC3	HINFP	MARS	NCL	PI4KA	RAD51B	RRP12	SRRM2	TTC27	ZMAT2
C9orf114	CTPS1	ERCC4	HIST1H2AI	MARS2	NCLN	PI4KB	RAD51C	RRP15	SRRT	TTC37	ZMIZ1
CAB39	CTU2	ERG	HIST1H2AJ	MASTL	NCOA2	PIK3C3	RAD51D	RRP7A	SRSF1	TTI1	ZMYND8
CAD	CUL3	ERH	HIST2H2AA3	MAT2A	NCOR2	PISD	RAD54B	RRP9	SRSF10	TTI2	ZNF131
CALR	CWC25	ERLIN2	HIST2H2AA4	MATR3	NDC80	PITRM1	RAD9A	RRS1	SRSF2	TTK	ZNF335
CAND1	CWF19L2	ESPL1	HIST2H2AB	MAU2	NDOR1	PKM	RAE1	RSL24D1	SRSF3	TUBA1B	ZNF407
CAPZB	CYB5B	ETAA1	HIST2H2BE	MBNL1	NDUFA11	PKMYT1	RAF1	RTCB	SRSF7	TUBB	ZNF574
CARS	CYCI	ETF1	HIST2H2BF	MBTPS1	NDUFA13	PLK1	RAN	RTEL1	SSI1L2	TUBB8	ZNF622
CARS2	CYCS	ETV6	HIST2H3A	MCL1	NDUFA2	PLK4	RANBP1	RTFDC1	SSBP4	TUBD1	ZNF830
CASC3	CYP11A1	EXOC1	HIST2H3C	MCM2	NDUFA1B	PMF1	RANBP3	RTTN	SSRP1	TUBE1	ZNHIT2
CASC5	DAD1	EXOC2	HIST2H3D	MCM3	NDUFA1F	PMPCA	RANGAP1	RUNX1	SSU72	TUBE1	ZNHIT6
CBFB	DAP3	EXOC4	HIST2H4A	MCM3AP	NDUFAF3	PMPCB	RARA	RUVBL1	STAC2	TUBGCP2	ZNRD1
CBLL1	DARS	EXOSC1	HIST2H4B	MCM4	NDUFAF7	PMVK	RARS	RUVBL2	STAG3	TUBGCP5	ZSWIM8
CBWD3	DARS2	EXOSC10	HJURP	MCM5	NDUFB10	PNISR	RARS2	SACM1L	STAT5B	TUBGCP6	ZWINT

CBWD5	DAXX	EXOSC2	HK2	MCM6	NDUF6	PNKP	RBBP5	SAE1	STIL	TUFM	ZZZ3
CCAR1	DBR1	EXOSC3	HMBS	MCM7	NDUF8	PNN	RBBP6	SAMD4B	STK11	TUT1	
CCAR2	DCAF15	EXOSC4	HMGBl	MCM9	NDUF2	PNPT1	RBBP8	SAMM50	STOML2	TWISTNB	
<b>Sabatini non-survival genes with annotated 3' UTRs</b>											
ABC85	BPY2C	CCDC90B	CYP2C9	FATE1	HMSD	LDOC1	OPCML	RAB3D	SP100	TMEM178 B	ZMYND12
ACRV1	BSPH1	CCL20	CYP4F3	FFAR4	HP	LRAT	ORMDL1	RAB9A	SP140	TMEM207	ZNF154
ACSL3	BTN2A2	CCL8	CYP51A1	FGD6	HRASLS	LRRRC26	PACRG	RBBP9	SPACA1	TMEM237	ZNF177
ADCYAP1	C11orf21	CCNJL	DCX	FGF13	HRASLS	LRRN1	PAFAH1B2	RBM24	SPANXN5	TMEM45B	ZNF19
AGAP1	C11orf71	CCNY	DDIT4	FN3K	HSD17B11	LSMEM1	PANK4	RBM1Y1D	SPATA4	TMEM47	ZNF26
AKR7A2	C12orf42	CD300C	DDIT4L	FOSL1	IDUA	MAGEB18	PAR6B	RBM1Y1E	SPEG	TMSB4Y	ZNF267
AKT3	C12orf66	CD70	DEFB113	FOXO3	IFI27	MARK2	PATE1	RBP7	SPHKAP	TMX1	ZNF280C
ALDH3A2	C12orf71	CD93	DEFB114	FXYD4	IFT5	MC2R	PAX1	RD3L	SPINK13	TMX3	ZNF280D
ALDH5A1	C14orf79	CDK17	DEFB126	GABRA6	IL12RB2	MCTP2	PCDH11X	RGS21	SPINK14	TNFRSF18	ZNF354B
ALPPL2	C18orf63	CDK5	DEPDC1	GALNT11	IL13RA2	MEGF10	PCDH11Y	RGS5	SPINK9	TNFSF10	ZNF385D
AMELY	C18orf8	CDK8	DEPDC5	GALR1	IL15	MEST	PCDH18	RIMKLA	SPRR1B	TNMD	ZNF420
ANKAR	C1QL1	CDY1	DHX32	GAS2L3	IL33	MFAP5	PCDHB13	RPS4Y2	SPRR3	TRIB2	ZNF468
ANKEF1	C1QL4	CDY1B	DISP1	GATM	IRAK1BP1	MFAP5	PCDHGA3	RTP4	SPTY2D1	TRIM62	ZNF540
ANKRD28	C2CD5	CDY2A	DNAJC15	GIMAP6	ITMC2	MID1P1	PCSKIN	S100G	SRD5A1	TRMT2B	ZNF547
ANKRD45	C4orf51	CDY2B	DNASE1L2	GLT8D2	JAGN1	MLANA	PEX5L	SCGB1D4	SRY	TSC1	ZNF559- ZNF177
APBP2	C5orf52	CFH	DTNBP1	GLYR1	JKAMP	MLLT11	PFN3	SCML1	SSR1	TSC2	ZNF562
ARHGAP28	C6orf10	CHAT	DTWD1	GNAS	KBTBD3	MOGAT1	PHEX	SCML2	SSR3	TSPY2	ZNF600
ARHGAP36	C7orf57	CHEK2	DYNAP	GPC1	KCNA7	MORC2	PHI1D2	SCN4B	STAR3NL	UBE2F	ZNF611
ARNTL	C9orf135	CLEC2D	EHHADH	GPC3	KCNK10	MPHOSPH8	PIKFYVE	SDK1	STEAP1	UGT2B17	ZNF626
ARTN	C9orf153	CLEC4M	EIF1AY	GPM6B	KCNMB1	MURC	PLA2G2E	SEMA6D	STK33	UGT2B7	ZNF649
ASB3	CACNA2D3	CMBL	ELAVL1	GPR174	KCNMB4	NAP1L3	PLD5	SERGEF	STRC	UPK3A	ZNF662
ASB5	CACNB2	CMC4	ENTPD1	GRM6	KHDRBS1	NDST4	PLEKHA8	SERPINB8	SULT1A2	URAD	ZNF669
ASB7	CACYBP	CNDP2	ENTPD3	GRTPI	PLD5	NECAP2	PLS3	SEN2	SUM04	USP28	ZNF670
ASZ1	CALCA	CNGA2	EPB41	GSTM1	KLK8	NETO1	POU2AF1	SETDB1	SUSD2	UTY	ZNF679
ATAD3B	CARD18	CNIH1	ERVV-2	GSTT1	KLRD1	NFATC1	POU4F3	SH3BGL	SYNJ2BP	VAX2	ZNF695
ATF7IP	CASP3	CNIH3	ESX1	GUCA2B	KLRF1	NLGN4Y	PPM1A	SIGLEC14	SZT2	VGLL4	ZNF709
ATOX1	CASP4	CNOT8	ETV3L	GULP1	KLRF2	NME8	PPP1R17	SLC26A1	T	VRK2	ZNF765
ATP11C	CASP7	CNPY1	EVA1C	GYG2	KRT38	NOS1AP	PREP	SLC39A2	TAPBPL	VVA5A	ZNF793
ATP4B	CASP8	COBL	F8	HFE	KRTAP1-1	NPRL2	PRF1	SLC7A1	TAS2R40	VVC2L	ZNF808
B9D1	CCBE1	CRYGS	F9	HIF1A	KRTAP11-1	NPS	PSG2	SLCO1B7	TBC1D7	WBP2NL	ZNF836
BCL11A	CCDC126	CNS3	FADD	HIST1H1C	KRTAP19-4	NPC21	PTPN2	SMCO3	TCF20	WDFC9	ZNF845
BDNF	CCDC15	CSTL1	FAM19A3	HIST1H1E	KRTAP22-1	NRGN	PXDC1	SMIM17	TEAD4	WNT7B	ZNF846
BIK	CCDC150	CXCL10	FAM19A5	HIST1H2BA	KRTAP22-2	NRN1	QPC1	SMKR1	TECTB	WT1	ZNF853
BPY2	CCDC152	CXCL13	FAM200B	HIST1H3J	KRTAP25-1	NT5C2	R3HCC1L	SNX3	TIAM1	ZBP1	
BPY2B	CCDC172	CYB5R2	FAM208A	HMGN4	LCORL	NXPH1	RAB38	SOX1	TLR2	ZFP42	
<b>Highly expressed and expression-matched survival genes with 3' UTRs</b>											
MRPL42	RBM8A	HAUS2	RFWD3	SUZ12	NUP85	NMD3	GLE1	WDR74	RPL11	SSRP1	RPS27A
SOD2	SMARCA5	PRPF39	MARS	RRM2	SRCAP	RUVBL2	DDX20	DARS2	MRPS18B	PES1	EIF4A3
RBM28	LAS1L	MRPL35	ACTR2	POLR3E	SPRTN	RPL4	RAE1	CHAF1A	RIOK1	RBBP6	TBCB
SUGT1	PSMA2	FAF2	EZH2	UBA2	NCL	BTAF1	CDK1	RPL38	MRPS5	NUP188	PSMB3
REV3L	DDX10	CLTC	DNM1L	SEC61A1	SEC16A	IPO11	RACGAP1	PRIM1	GEMIN4	TIMM23	COX5B
CPF2	PRPF38A	KPNB1	RPRD1B	RPL15	ZFC3H1	WEE1	CNOT1	SDHD	BUB1B	ERH	PSMB6
DCTN5	RBPJ	PPP6C	PNISR	GINS2	DDX18	MCRS1	RPS14	NAT10	C19orf43	COPS6	SUPT5H
KRR1	ATP6AP1	SNRNP48	PPP1R2	YKT6	EIF3J	ECT2	PRC1	RBX1	EIF6	AAMP	EBNA1BP2
PTAR1	YLPM1	AK2	UTP6	PMPCB	ACTR8	PSMD13	ADSS	SARNP	KIF18A	POLR2A	SARS
SCO1	RBM25	EIF2S1	RNGTT	MRPS16	NUP160	PAXBP1	GADD45GIP1	NBAS	MCM3	MYBL2	RPS3A
IPO9	INTS7	EXOSC9	DDX46	MGEA5	THOC1	SMG5	WARS	CAPZB	EIF2B3	EIF3I	CDC123
DIS3	MED1	PNPT1	GON4L	YME1L1	NUP133	HSD17B12	ECD	AURKA	RPS6	MRPL9	GNL3
KAT7	RPL27A	RNF168	CHTF8	GFM1	NSF	PNN	TUBGCP6	ATP6V0B	DNAJC9	THOC7	CCT7
DCP2	KIAA0391	VPS13D	RBM39	PPAT	DONSON	EIF2B1	HARS	RFC2	NDC80	PRPF31	NSMCE4A
CEP192	ATPSA1	LSM3	UBA52	IN080	CDC47	GTF2F2	MED8	SART1	EIF3D	MCM7	PSMD6
RPL37	TPT1	SKIV2L2	SRSF1	ATIC	TUBA1B	RSL24D1	LARS	SNRNP3	TP11	IWS1	NOP58
POLR1A	GRWD1	PSMA5	GTF2H3	WDR5	CCT5	TMX2	IARS	FAU	USP39	FTSJ3	ALDOA
RPP14	WDR75	MAU2	CAB39	AIFM1	ZNF131	TIMELESS	OGDH	GEMIN5	SF3B2	NOL7	CCT8
KPNA4	FLII	LETM1	EIF3A	NCBP2	RPL32	WDR77	RHOA	TFIP11	GBF1	PGD	XRCC6
WDR3	NCAPD2	RRP7A	UBE2L3	MATR3	ABCE1	MRPL17	SUPT6H	NOP2	PSMB5	RRP12	DYNC1H1
POLE	SEC63	IP07	MCM2	GRPELL1	DHX38	FARSB	VCP	DAP3	EXOSC8	MASTL	PAF1
RRP15	MRPS25	PSMD12	CARS	MFN2	MNAT1	EFTUD2	TUBG1	EIF4G2	EIF3B	MRPL51	FH
NUDC3	SCD	SCAF11	TOMM40	DLD	KIF11	CDC23	POLA1	AHCY	USP5	RPL35	EXOSC10
RPS29	METTLL16	RPA1	POLR3A	NOL11	POLR2F	COPZ1	TUBB	UFD1L	GTF3A	UBE2M	SNRPA
BUB3	NCOA2	DDX24	ORC2	POLA2	RARS	RPUSD4	UQCRC1	RPS21	TTC27	BANF1	RPS7
NAA30	POLR1B	SRSF10	TPR	EIF5B	DKC1	HNRNPK	PPP4C	PSMD2	SRRM2	ACO2	FAM50A



RPL14	BMS1	DHFR	SACM1L	SAE1	NUP54	NAE1	ISCU	NAA10	EXOC1	AATF	UROD
GMPS	CRNKL1	TWISTNB	GART	RBM17	PRMT5	CTCF	PSMC5	PCDC11	VPS25	ATPSO	PRPF3
DIEXF	CDK12	ADSL	GRB2	COG3	TOMM22	GNP1	UBA3	YARS	PSMD4	ENO1	RBM10
WDR12	SMARCE1	NAA25	POLD3	HEATR1	COX15	RFC1	INCENP	RPS2	ANAPC5	FDPS	COX6B1
KCMF1	ATR	MCL1	SRSF7	LARS2	CCNH	NOL10	TOP2A	FEN1	CSE1L	SOD1	MRPL16
GTF3C4	PAFAH1B1	USP10	SEHIL	TBCA	DDX49	DUT	FARSA	GTF3C1	NOP16	ORC1	IMP4
SMC1A	MTPAP	SDAD1	ZBTB11	SAP30BP	GOSR2	DDX56	STIL	PSMC3	MYBBP1A	PSMA7	MRPL38
ELP2	RPL13	ERS23	PPP2R2A	TMED2	LIG1	RCC1	RANGAP1	TPX2	MRPL3	TXN	HSPE1
SF3B3	NUP155	RRM1	RPL23	EIF1	CEP57	COX7C	DDX23	RUVBL1	MRPL20	RPS25	GAPDH
XPO1	PSMB2	TOMM20	PCDC2	RPS15A	RPS19	MED21	SNRPF	MRPL52	RPL18	VPS27	UBA1
NUP93	DIDO1	STRIP1	NCAPG	CHEK1	ZMYND8	UBE4B	CKAP5	RPL1	COPG1	SMARCB1	SNRPD2
LUC7L3	CDC5L	BRD8	DDX21	COX11	XPO5	LSG1	NOP56	DBB1	BRIX1	SMC3	POLR2B
SMU1	PFAS	GTPBP4	UBR4	DHX8	EXOC2	POLR1E	RFC5	PHF5A	EEF2	HTATSF1	RPS15
SPATA5	YTHDC1	DCTN4	UQCRCF51	CCT3	EMC3	UPF2	MTOR	NUDC	SRRT	SEC13	RPSA
BRCA1	NOL8	PPP1R15B	UBE2I	TRA2B	GTF3C3	PRPF4	RPL13A	SNRNP200	NCAPH	PCNA	PRPF8
WDR33	SSU72	ERCC3	ARCN1	AASDHPPPT	SFPQ	CHORDC1	PWP1	DTYMK	UTP20	PAK1IP1	RNASEH2A
NAA50	PPP1CB	RPL37A	ETF1	IKBKAP	COPS3	DCTN2	PHB	CLSPN	PRMT1	ORC3	WDR46
YY1	NUS1	VEZT	UBTF	PRPF38B	NIPBL	DNAA3	CLPB	RPL29	XRN2	DAD1	COPE
UMPS	DHX36	ZC3H13	PCBP2	CASC3	RRP1	TNPO3	CEP55	YARS2	UQCRC2	ATP1A1	SDHB
ACTR3	WDR36	WNK1	HNRNPC	TRAPP1C11	RPP30	STRAP	MRP57	MDC1	PSMA3	RPL2	DLTB
ATP2A2	SRSF3	TFRC	PSMD1	SHMT2	ARPC4	EXOC4	MRPL11	PLK4	TTC1	TTK	UTP14A
PAICS	CYCS	CDC6	RIOK2	DGCR8	MAT2A	HNRNPL	PPA2	EIF5A	RPL23A	RFC4	CEBPZ
AQR	SUDS3	NUP43	RNF40	HMGR	MDN1	SRRM1	ZMAT2	POLR2L	RBBP8	PPA1	SAMM50
GSP71	NUDT21	BRBP5	TARS	DIMT1	SON	NOL6	PBSM1	U2AF2	GNL3L	SDHA	ATP5B
KANSL3	DNTTIP2	CCAR1	SYMPK	RAN	PMPCA	CCDC86	MIS18BP1	MPHOSPH10	NUP88	PLK1	RPL3
DNMT1	NPLOC4	CSTF1	OSBP	CEP85	MRPS27	MCM6	PGAM1	EIF2B5	FUBP1	COPB1	POLR3C
CTDSPL2	PPP2R1A	AMD1	EEF1A1	SAP18	ISCA1	PSMD3	CTPS1	DARS	HSPD1	PSMD14	PSMC4
SLC25A3	MTHFD1	MRPL7	POLR2E	ATL2	METAP1	RFC3	IMMT	FBX05	COPB2	DHX9	MRPL37
CP5F6	NOM1	ATP6V1A	CASC5	PDCL	BRCA2	CCNA2	ATP6V1D	SRBD1	TRMT10C	PSMA1	PSMB7
SMG1	PGK1	PDS5A	RNF4	HSPA5	RPS3	TOP1	VPS29	NOB1	CCT2	ASUN	UBL5
EIF4G1	TBCD	SHQ1	OGT	HMGS1	DCTN1	RTFDC1	FNBP4	ATP6V1G1	RPL5	NHP2	PFDN2
USP37	NSA2	SF3A1	SMC2	NPAT	KARS	NUP214	CCT6A	RPS4X	TTI1	AP2S1	CTNNBL1
CSNK1A1	PPP2CA	SDE2	ABT1	SRPRB	RBM19	VMP1	URB2	RPL26	DHX15	RPN2	PSMB4
MMS22L	MBNL1	COG4	RPS9	TICRR	SAMD4B	MCM5	NOPI4	SPAG5	NVL	HSD17B10	TEX10
ZNHIT6	RPL7L1	THOC5	LRPPRC	RRN3	NIP7	GTF2H1	POLR2C	BECN1	RPN1	PPRC1	RPL9
PTCD3	ACIN1	MRPL19	CDC40	UPF1	NLS1	PSMD7	RPL18A	PCID2	NEDD8	RPS11	PRPF6
RNMT	RFT1	DDX19A	SF1	SMC4	METTL3	TACC3	TRRAP	AFG3L2	PRPF19	DDX27	POLD2
POLR2D	NUP107	PSMD11	BPTF	RANBP3	SNAPC1	SNF8	COPA	NELFB	COPS4	NUF2	PSMB1
TRPM7	NAA15	GINS1	TRAPPC8	AHCTF1	WDR43	HSPA14	FANCM	SNRPE	RPL34	CIAO1	MRPL39
DDX52	DHX33	INTS3	BIRC5	DDX54	KANS12	HSPA9	HJURP	CSTF3	ACTL6A	RPS16	MRPL24
NOL9	HNRNPU	SMC5	RPL31	TSR1	EIF2S2	PPP1R10	KRI1	DDOST	RABGGTB	GUK1	RPS8
RBMX	UTP15	PCF11	QARS	UBE2S	C21orf59	NUP98	WDR70	ILF2	ELAC2	CDC45	CPSF3
PGM3	MMS19	NCBP1	MCMBP	SMC6	TIMM44	ZZZ3	VPS51	NDUFAB1	DDX47	ALYREF	RPL19
TRUB2	OPA1	WDHD1	TIPRL	PREB	DLST	NARS	RBM14	TCP1	AARS	MRPL12	EEF1G
SNRPD1	MED22	RAD23B	DTL	TARS2	FIP1L1	MRPS35	RPLP0	CCT4	CAD	LTV1	VAR5
DDX6	CDC73	SART3	SRSF2	CSNK2B	TKT	EXOSC2	DNM2	TUFM	PRELID1	CDC16	RRP9
MRPS15	SUPV3L1	RPL7A	IMPDH2	GLTSCR2	RPL12	RPS18	RPS13	RPLP2	GNL2	RPL10A	CDC20
RPL6	RPS12										

### Highly expressed and expression-matched non-survival genes with 3' UTRs

ABI2	ETNK1	UBE2H	SCAMP1	STK10	LONP1	DCAF8	HIST2H2BF	EPB41L2	SLC25A13	GLA	GSS
NCKAP1	SMURF2	KLHL15	RPF2	LAMC1	AGK	ZHX1	ABCD3	NUP37	PSMC6	PSPC1	ZNF638
LPP	ERC1	CAPZA2	PIGK	NAMPT	FAM120B	DDX5	RAC1	LAMP1	DNAAJC8	DUSP1	BTF3
TMED3	VPS13A	CCDC6	NMT1	UBE2G2	TRUB1	RIOK3	RDH11	TM9SF2	RTN4	MORF4L2	PHB2
TTL	KDM3B	RAB11A	MINA	RASA1	CORO1C	GNPTAB	HEATR5A	SRP9	DEGS1	CFL1	PEPD
FAM204A	TMEM59	LARP4	GLYR1	DEPDC1	OCLR	SPDL1	TUBA1C	MSMO1	CEP290	USP32	C19orf48
RAP1B	NUCKS1	EYA3	NUP50	PAM	STT3A	MCCC2	GOLPH3	SF3A3	SPG21	NDUFA12	HMGB2
HOOK3	CYLD	PTPN11	SMARCAD1	PCMTD1	SURF4	PKM	DNAAJC11	ETF4	GPBP1L1	GCN1	RPL21
AGO2	SEL1L	USP7	TMF1	HERC2	TNKS2	TBC1D1	PNPO	SUPT16H	NO3CL	NABP2	PIK3R4
NAP1L1	EEA1	UCHL5	ZFP91	GAS2L3	RAB6A	CANT1	NCOA4	TMEM165	NRDX6	MANF	RPL30
APIM1	ANKRD52	LEPROT	TRAK2	FAM53C	PLCB4	ADAMTS1	WSB2	LRRFIP2	EIF3L	TCEAL8	NDUFB8
NABP1	USP38	ZDHHC20	KLHL9	SUV39H2	FLOT2	DAP	PTBP1	ARF4	POLDIP2	SLC1A5	RPL8
CDK6	KDM5A	TMEM237	FRMD4A	EFR3A	VOPPI	TRIM65	TCF19	LRBA	NOSIP	ANXA2	P14KA
GOLGB1	MLEC	USP9X	WDFY1	RGBM	SNX9	RPS24	CYDL	ANLN	CYR61	FTH1	EDC4
PANK3	EXT1	HELLS	SH2B3	CERK	PTRF	CDC25A	TRAM1	BCOR	STMN1	PTPN13	PPP1CA
DR1	COPS2	TMEM19	BAG5	PPP2R5C	SHFM1	PICALM	FLNB	FSCN1	STRN4	EIF3K	OGFR
SKP1	MCC	GGA2	MME	PBRM1	MSL2	ABCC1	CAPZA1	NGLY1	FUCA2	FBL	TRMT1
G3BP1	CTBP2	DZIP1	RAB14	GOLTB1B	KDM6A	RND3	RPL10	EZR	PPP1R18	NDUFB9	SQLE
ABL2	YOD1	CD47	BRD7	GLUL	CLNS1A	FOXC1	MKRN1	PLXNB2	POLQ	YBX3	TONSL

SLC44A1	RCN2	SCP2	ATP13A3	RNF185	UBR7	CAPRIN1	RPS17	DNAJB1	PABPC4	UBXN6	TMA7
SNTB2	BZW1	BOD1L1	LYSMD3	RRP1B	RABGEF1	STK26	AMFR	ARHGDI1A	DVL1	FKBP3	KDM1A
EXOC5	NEDD4	WASF2	HAUS6	ACSL4	UBXN4	GNB1	VAT1	VASP	NUSAP1	EIF3E	HSP90B1
TNPO1	NDUFA5	UBXN2B	RBMXL1	CSPPI	FKBP4	SNX12	PSIP1	LDHA	SMARCD2	ARAP1	MYL12A
BCAT1	MXRA7	FAM91A1	SRSF6	USP24	KAT2A	SASS6	SH3BP5L	MAN1B1	IDH1	HPRT1	MRPL18
ANKRD11	KIF1B	TLK1	PDCD6P	ERCC6L2	ACTN4	LRRC59	ZNF410	PTGES3	PLIN3	HMOX2	MT2A
NF1	SLC35D1	UBE2V2	CTBP1	SENP6	MKNK2	ANKLE2	BCCIP	CSNK1G2	RNPS1	BABAM1	SSB
TSC22D2	KCTD12	TIAL1	RBM26	PRKD3	SBF1	SET	CD59	CTSD	PCMT1	KIF2C	UQCRRH
MPRIP	PLXNA2	EIF3M	CFAP97	TENM3	MTMR4	PAPSS2	ADH5	NIPSNAP1	PTMA	MRPL47	MDH1
MON2	FOXO3	STX6	SPIRE1	SOX4	RNF11	ELOVL5	CDC42	EP300	AHNAK	FAM83D	GMNN
CEP250	SYAP1	NF2	PLCG1	ELK3	SIPAL13	C5orf42	TIMM50	CAP1	RPL35A	PAPSS1	PRDX1
ZNF451	HEG1	ZBTB38	PHF20L1	CSNK1G3	ZC3H11A	HIST1H4H	CTTN	FN1	TJP2	CALR	HSP90AB1
ZBTB44	DYRK1A	NIPAL3	DIS3L	G3BP2	STOM	FUT8	EIF4A2	CTNNB1	CENPB	DEAF1	NACA
ZNF740	XRN1	GATC	HN1L	CMTM6	STX12	MAP2K1	PIGT	H2AFX	DYNCL1L1	BCAS2	MAP2K2
CLOCK	TMX4	RPS6KB1	CPNE3	TSN	RBM5	PIIA	NUP62	GBAS	HMGN2	KIAA1551	PPP1R14B
N4BP2L2	HBS1L	SLC38A2	WDR82	PLS3	ANKRD36C	SARAF	HNRNPH1	FERMT2	AHNAK2	AGTPBP1	HIG25A
GPR180	NDST1	TARDBP	NOLC1	ZDHHC3	ZBTB18	FAM120A	FHL1	EI24	TXNDC12	XPO6	SNRPG
UHMK1	THADA	BDP1	SSR3	ENC1	THUMPD3	PIP5K1A	PPP1CC	XRCC5	SLC20A1	CKS1B	HIST1H2BC
CAND1	ATF7IP	SSX2IP	SLC39A14	CTSB	SS18	PRRC2C	NISCH	SLC04A1	FANCI	SNDI	TARBP1
RIF1	ARHGFE12	SMCHD1	ATPAF1	NRP1	CHD7	TPM4	IMPA1	COX4I1	MSH2	STOML2	SLC25A5
RBMS2	OPHN1	TRIP11	MYNN	FBXW11	CMPK1	NT5C2	MYH9	NONO	IFRD2	PIBF1	CLIC1
ZNF24	PHIP	LHFPL2	ANKRD28	HNRNPA1	SPG7	IVNS1ABP	CBX1	HDCC2	GD1I	CPVL	RPL36
SBN01	AVL9	SLC30A6	UBE2D3	HNRNPA2B1	NUDCD1	EIF2AK4	ACTB	RPS28	CENPF	ARPC2	CWC22
EPT1	PSME4	OSBP13	DGKZ	TMEM123	MLLT4	M6PR	MCM4	HIST1H4E	APEH	VPS45	TMSB10
BTBD7	CARD8	CNIH4	XPOT	CTNNA1	ACAD9	SLU7	IP6K2	CEP152	FAM35A	SNX2	ATP5H
ZBTB10	GTF2A1	VPS13C	ACSL3	MK167	AP15	ATPIF1	ZNFX1	ATP6V0D1	PEBP1	NOCL2	HSPA8
ZNF678	ARNTL2	FBN1	DNAJB12	PTPN1	FRYL	HIVEP2	VWA8	FKBP8	BSG	BIRC2	IK
CREB3L2	NSD1	NDUFB5	DDAH1	TMPO	TXNRD1	RAB1A	SRI	MORF4L1	BAZ1A	SMS	KIFC1
ATG2B	ATAD2	ITCH	PDS5B	SF3B1	PDPN	MSANTD4	GNPDA1	PRKDC	HMGN4	GSTP1	MCTS1
RICTOR	RAP2A	PRPF4B	IDE	NDC1	SLC16A1	UBE2D2	IRAK1	RHNO1	PARP1	DRG1	TUBA1A
APC	AKAP13	WSB1	INPP5B	MRS2	ARFGEF1	ARID4B	PPT1	NUP153	MARCKSL1	PABPC1	UCHL3
IGF2R	FSTL1	CALM1	IDH3A	LDLR	TMBIM6	UBE3C	CD55	TRIP6	MTCH1	UAP1	LDHB
WHSC1	HMGB1	CUL4A	CC2D1B	DDX17	RHOQ	NBR1	VIM	ERP29	RPL7	SMARCA4	PYGL
UGGT1	GPSM2	LARP1	KBTBD6	SERP1	MSN	TPD52L2	CCNG1	TUBB6	DECR1	TMEM14C	PARP4
XPO4	KIAA1143	MED14	NFATC3	DLC1	ERLIN1	USP25	DYNC2H1	GOT2	CDC37	STIP1	RPL39
UBE3A	LRRC8C	TPM1	OGFOD1	ALCAM	CD46	ECHDC1	ZNF460	SDF4	ADIPOR1	VDAC2	HAX1
UBA6	MYO6	TAP2	GTPBP1	SERF2	PSMD9	PNRC2	TIMMDC1	SPEN	CALM2	NDUFA13	TRIM28
MTR	MAD2L1	GPD2	ITPR2	PRSS23	EIF4B	ARL6IP1	SUMO3	EIF4G3	C1orf43	COX6C	ROMO1
CELF1	MP1	SLC25A36	WIP2	RAB10	CDK17	TBC1D23	ILK	KIAA1429	NPM1	BCAP31	UBB
C14orf166	FAM73A	PTPRJ	SPTBN1	RDX	HACD3	KIF21A	RB1CC1	DST	CAPN1	CD63	FTL
SEC22B	FNTA	PSMA4	EIF3H	ADD1	RMDN1	SUCO	TIMM13	SLC25A46	ACTG1	PSMD8	NDUF55
OSBPL10	DOCK5	MESDC2	KLHL18	RBL1	MACF1	UBA5	CBX3	PRPS1	FOXDI	CABIN1	SERPINB6
ZC3H12C	CDC42BPA	GATAD2A	SERINC3	PHAX	LMO7	PAK1	MFAP3	CKB	CUTA	GNPAT	USMG5
CCNT1	ARHGAP35	MAP4K4	LIMCH1	AP3B1	UBE2Z	FBXO7	NT5DC2	ANXA7	FAM208B	SPG11	DHX16
AK4	DCUN1D4	SYNE2	ANGEL2	UGCG	MRPL30	STT3B	FAM136A	USO1	FASTKD2	EEF1D	PRDX5
KIAA1549L	FBXO28	USP22	MAGT1	USP28	DMXL1	HSP90AA1	SACS	SPTBN2	GOLGA4	EIF3G	UBC
KATNAL1	RAD18	DCBLD2	FAM134A	TLE4	PGAM5	TCEA1	LTA4H	LMNA	UQCRI0	RPL41	CPSF1
BBX	UBR3	PTDSS1	SLC25A24	HNRNPD1	C9orf69	RFX5	B2M	CLTA	RBBP7	TMSB4X	ATP5G1
FGF2	BCLAF1	TNKS1BP1	BRD2	CPSF3L	CAV1	FBN2	YTHDF1	ACP1	TAOK2	SRP54	GTF3C6
HNRNPR	PAK2	SPIN1	SEC24C	SRPK1	KIF14	GNAS	USP34	VBP1	ZW10	SMYD2	AURKAIP1
PIK3CA	TMTC3	HM13	EXOC8	HDLBP	GORASP2	CDKN1A	DMXL2	ANXA5	PRIM2	VRK1	HIST1H1E
TRAF3	NEMP1	WDR48	RNF216	TPM3	AIDA	TTC3	RNF145	ZFAND1	FBXO38	YBX1	MTIF2









Table with multiple columns of numerical data, organized in rows and columns, possibly representing a sequence or mapping between values. The table is dense and spans the majority of the page.









L147	2.17	0.52	L217'	4.77	7.40	V275	0.55	1.02	R469	1.35	1.46	R376'	8.42	4.42	R1270'	1.37	1.04
L148	1.37	2.63	L218'	1.04	0.77	V276	1.17	1.60	R470	0.68	1.22	R377'	1.18	1.05	R1271'	135.38	0.02
L149	15.48	5.23	L219'	3.24	0.80	V277	1.58	1.18	R471	1.13	1.43	R378'	8.35	0.51	R1272'	10.08	1.90
L150	15.72	4.36	L220'	2.29	1.97	V278	1.30	1.04	R472	1.47	1.62	R379'	0.87	0.76	R1273'	3.03	0.83
L151	3.23	15.43	L221'	0.82	2.11	V279	1.08	1.20	R473	1.29	0.59	R380'	6.13	3.58	R1274'	0.74	2.43
L152	46.67	1.74	L222'	0.82	0.79	V280	0.80	1.15	R474	0.73	1.27	R381'	1.81	3.67	R1275'	3.35	1.46
L153	2.27	1.55	L223'	2.46	0.47	V281	1.10	3.14	R475	0.74	1.76	R382'	0.97	5.30	R1276'	1.31	2.37
L154	2.11	1.07	L224'	1.02	0.86	V282	1.66	0.96	R476	2.57	1.72	R383'	1.82	37.20	R1277'	1.85	1.78
L155	6.07	3.92	L225'	0.34	1.34	V283	1.17	1.39	R477	0.93	1.31	R384'	1.28	2.54	R1278'	1.02	3.14
L156	6.39	0.65	L226'	1.22	8.21	V284	2.06	1.58	R478	0.64	1.33	R385'	1.09	0.44	R1279'	0.69	1.16
L157	8.79	7.66	L227'	0.69	1.28	V285	1.62	0.42	R479	4.46	6.73	R386'	1.34	2.11	R1280'	0.91	0.60
L158	41.40	1.07	L228'	1.24	1.42	V286	0.94	0.86	R480	1.55	1.62	R387'	2.19	1.55	R1281'	2.06	0.67
L159	0.06	1.33	L229'	1.08	0.56	V287	0.76	3.86	R481	20.52	3.15	R388'	2.76	0.71	R1282'	0.78	2.18
L160	73.27	0.58	L230'	0.55	2.04	V288	1.74	1.43	R482	1.21	3.17	R389'	1.58	1.23	R1283'	0.98	2.02
L161	18.47	156.82	L231'	2.34	2.10	V289	1.85	1.23	R483	1.93	0.83	R390'	0.94	3.61	R1284'	1.26	1.72
L162	28.02	63.63	L232'	3.79	0.91	V290	2.37	1.00	R484	1.08	1.51	R391'	2.48	0.75	R1285'	0.82	1.29
L163	7.04	6.17	L233'	39.05	56.50	V291	2.23	0.53	R485	0.73	0.80	R392'	1.20	1.65	R1286'	0.60	1.21
L164	0.31	1.65	L234'	24.20	34.66	V292	1.38	1.80	R486	0.83	1.00	R393'	1.00	1.89	R1287'	1.26	0.85
L165	22.59	54.24	L235'	4.35	0.83	V293	2.67	0.89	R487	2.07	1.46	R394'	1.19	0.77	R1288'	0.54	1.35
L166	35.65	0.71	L236'	0.66	1.92	V294	0.93	1.08	R488	1.83	1.35	R395'	0.67	1.01	R1289'	0.82	1.29
L167	17.59	0.71	L237'	1.26	1.16	V295	1.53	1.12	R489	2.27	0.63	R396'	1.43	1.02	R1290'	0.66	0.85
L168	3.10	3.39	L238'	0.87	1.10	V296	1.35	0.75	R490	1.93	1.89	R397'	6.46	102.16	R1291'	1.03	0.89
L169	20.62	1.63	L239'	3.14	0.45	V297	2.06	1.96	R491	2.38	4.41	R398'	1.24	0.75	R1292'	0.73	1.14
L170	0.26	0.99	L240'	0.89	0.63	V298	1.22	1.97	R492	0.72	1.38	R399'	1.14	0.87	R1293'	1.01	0.74
L171	13.55	0.80	L241'	1.02	0.52	V299	1.01	2.74	R493	0.32	0.89	R400'	1.03	1.01	R1294'	0.81	1.34
L172	0.16	7.04	L242'	0.61	1.25	V300	0.97	2.65	R494	0.32	0.89	R401'	0.78	3.78	R1295'	1.00	1.78
L173	0.14	0.52	L243'	2.37	0.48	V301	1.67	1.86	R495	4.95	0.89	R402'	2.06	1.04	R1296'	1.99	0.48
L174	5.61	2.26	L244'	0.48	1.61	V302	1.21	1.55	R496	0.32	0.89	R403'	1.82	1.99	R1297'	2.06	0.82
L175	16.35	43.19	L245'	2.36	0.55	V303	1.43	0.53	R497	0.32	0.89	R404'	1.48	0.55	R1298'	1.51	0.78
L176	30.38	1.07	L246'	1.11	0.79	V304	1.41	1.50	R498	0.32	0.89	R405'	10.81	0.45	R1299'	0.93	1.56
L177	4.91	6.87	L247'	2.17	4.69	V305	1.21	1.70	R499	0.32	0.89	R406'	2.46	1.65	R1300'	0.96	1.00
L178	10.57	0.72	L248'	3.81	0.73	V306	0.63	0.79	R500	2.55	20.68	R407'	0.72	20.61	R1301'	0.92	2.36
L179	5.23	7.07	L249'	1.18	0.92	V307	0.86	0.66	R501	21.59	0.38	R408'	287.87	0.53	R1302'	1.06	0.88
L180	6.03	2.00	L250'	0.39	0.90	V308	0.70	0.59	R502	15.87	20.54	R409'	1.48	76.11	R1303'	0.92	1.32
L181	2.66	2.28	L251'	0.67	1.70	V309	1.16	0.67	R503	0.19	1.78	R410'	8.09	12.50	R1304'	0.81	0.68
L182	1.45	2.26	L252'	11.55	0.08	V310	0.89	0.69	R504	0.23	97.34	R411'	0.63	256.91	R1305'	1.48	0.56
L183	8.29	3.91	L253'	1.53	0.84	V311	1.38	0.64	R505	25.88	16.21	R412'	76.38	6.75	R1306'	1.07	0.90
L184	5.46	0.31	L254'	1.26	1.07	V312	0.80	1.20	R506	1.66	1.25	R413'	61.16	2.02	R1307'	1.65	0.66
L185	0.43	19.93	L255'	1.54	4.91	V313	1.04	0.98	R507	0.63	1.05	R414'	0.34	378.29	R1308'	0.92	1.05
L186	6.12	65.41	L256'	0.73	0.33	V314	0.88	1.04	R508	0.80	1.10	R415'	0.42	45.33	R1309'	0.80	1.00
L187	0.29	54.23	L257'	3.12	0.46	V315	1.38	1.15	R509	2.47	2.22	R416'	1.11	21.75	R1310'	0.93	0.83
L188	75.33	0.57	L258'	3.16	1.69	V316	1.88	1.28	R510	8.78	0.47	R417'	10.39	5.90	R1311'	0.95	0.73
L189	73.82	0.46	L259'	42.29	75.63	V317	1.14	1.11	R511	3.20	1.13	R418'	1.95	0.57	R1312'	0.87	0.64
L190	1.28	1.20	L260'	1.90	0.85	V318	0.62	0.56	R512	1.29	0.26	R419'	3.04	23.20	R1313'	0.85	0.63
L191	14.61	0.24	L261'	26.51	0.63	V319	1.70	0.73	R513	148.57	4.18	R420'	20.44	0.22	R1314'	0.87	0.49
L192	7.50	1.13	L262'	2.31	0.89	V320	0.59	0.80	R514	44.42	8.95	R421'	10.61	9.67	R1315'	0.51	0.94
L193	101.42	23.94	L263'	1.87	1.13	V321	0.91	1.06	R515	16.48	84.09	R422'	67.88	68.56	R1316'	0.98	0.59
L194	0.84	38.20	L264'	2.49	12.77	V322	1.30	0.62	R516	9.53	5.48	R423'	1.06	0.96	R1317'	1.80	0.32
L195	2.63	1.02	L265'	3.23	0.94												

- \* The number of the ID corresponds to the position along the mRNA the first nt of the shRNA sense strand starts at.
- \*Dark green and light green-highlighted IDs indicate the Venus-derived shRNAs used in the CD95L and CD95 screens, respectively.
- \*Red-highlighted IDs indicate ORF-derived shRNAs used in the CD95L (indicated by “L” in the ID) and CD95 (indicated by “R” in the ID) screens.
- \*Light purple-highlighted IDs indicate 3’ UTR-derived shRNAs used in the CD95L (indicated by “L” in the ID) and CD95 (indicated by “R” in the ID) screens.













V511	0.45	L330	2.89	L24'	0.70	L543'	0.82	R225	0.88	R743	0.85	R274'	0.72	R792'	1.21	R1310'	1.14
V512	1.23	L331	2.26	L25'	1.35	L544'	0.71	R226	1.52	R744	1.84	R275'	1.74	R793'	0.92	R1311'	0.86
V513	0.83	L332	1.66	L26'	0.76	L545'	1.16	R227	1.34	R745	1.10	R276'	1.42	R794'	1.10	R1312'	0.93
V514	1.36	L333	0.79	L27'	1.14	L546'	0.76	R228	1.14	R746	1.84	R277'	0.76	R795'	0.64	R1313'	0.61
V515	1.13	L334	0.70	L28'	0.76	L547'	0.99	R229	1.64	R747	0.69	R278'	0.88	R796'	1.04	R1314'	0.65
V516	0.92	L335	0.50	L29'	0.81	L548'	0.62	R230	3.74	R748	0.43	R279'	0.86	R797'	0.54	R1315'	0.73
V517	4.00	L336	2.23	L30'	0.77	L549'	0.66	R231	2.81	R749	0.54	R280'	0.38	R798'	0.70	R1316'	0.80
V518	0.42	L337	3.36	L31'	1.56	L550'	0.52	R232	3.17	R750	0.68	R281'	0.35	R799'	0.81	R1317'	0.78
V519	1.35	L338	1.41	L32'	1.13	L551'	0.58										

\* The number of the ID corresponds to the position along the mRNA the first nt of the shRNA sense strand starts at.

\*Dark green indicates the Venus-derived shRNAs.

\*Red-highlighted IDs indicate ORF-derived shRNAs used in the CD95L (indicated by “L” in the ID) and CD95 (indicated by “R” in the ID) screens.

\*Orange-highlighted IDs indicate 3' UTR-derived shRNAs used in the CD95L (indicated by “L” in the ID) and CD95 (indicated by “R” in the ID) screens.

## Chapter 4: CD95L mRNA is Toxic to Cells

### Introduction

CD95 and CD95L are members of the TNFR<sup>290</sup> and TNFL<sup>291</sup> superfamilies, respectively. Activation of CD95 through interaction with its cognate CD95L or receptor-activating antibodies induces apoptosis in sensitive cells. Immune cells expressing CD95L conduct surveillance by killing harmful target cells, such as virus-infected cells or tumor cells, which express CD95<sup>317,318,322-324</sup>. Canonical CD95-induced apoptosis involves formation of the DISC and activation of cysteine-aspartic proteases called caspases, which cleave various protein substrates and ultimately kills the cell (**Figure 1.5A**). CD95 signaling is, however, multifaceted and can prompt non-apoptotic outcomes like enhancing tumor invasiveness/motility<sup>366</sup>, promoting neurite outgrowth<sup>348</sup>, and elevate cellular proliferation<sup>351,364</sup> and cancer stemness<sup>367,368</sup> (**Figure 1.5B**).

A gene's protein product often overshadows the obligatory mRNA, as the latter is often seen as merely the template for the translation. All research on CD95 and CD95L has focused on interaction between these proteins triggers protein-based signaling cascades downstream.

However, the mRNA of CD95 and CD95L harbors sequences that can elicit distinct biology. The mRNA of these two genes, when converted into siRNAs, cause massive and robust toxicity (see **Chapter 3**). These CD95/CD95L-derived siRNAs target a network of survival genes, resulting in the simultaneous activation of multiple death pathways through RNAi in a process coined DISE.

In the following, the expression of the CD95L mRNA, itself, is shown to be toxic to cells even without artificial conversion to siRNA species. Furthermore, this toxicity is independent of CD95L protein and expression of the CD95 receptor and is not canonical apoptosis. This toxicity is likely an RNAi-based phenomenon. Multiple small RNAs are generated within cells from the mRNA of CD95L and loaded into the RISC, which is the key mediator of RNAi.

## Results

### *Expression of CD95L cDNA is Toxic in the Absence of Apoptosis*

The results in the previous chapter demonstrated an enrichment of sequences in the CD95L mRNA, that when converted to si/shRNAs, are toxic to cancer cells. We were now curious whether expression of the entire CD95L mRNA—without artificial pre-processing into siRNAs—would be toxic to cancer cells. Only the mRNA of the CD95L ORF was considered, as this was shown to contain the highest enrichment of toxic siRNA sequences (**Figure 3.19C and D**).

Therefore, three different CD95L cDNAs (**Figure 4.1A**; *schematic*) were sub-cloned into the pLenti vector: wild type CD95L, a CD95L mutant containing a Y218R mutation that disables CD95 binding (referred to as CD95L<sup>MUT</sup>), and a CD95L mutant cDNA containing both the Y218R mutation<sup>326</sup> and an inserted premature stop codon directly following the start codon (referred to as

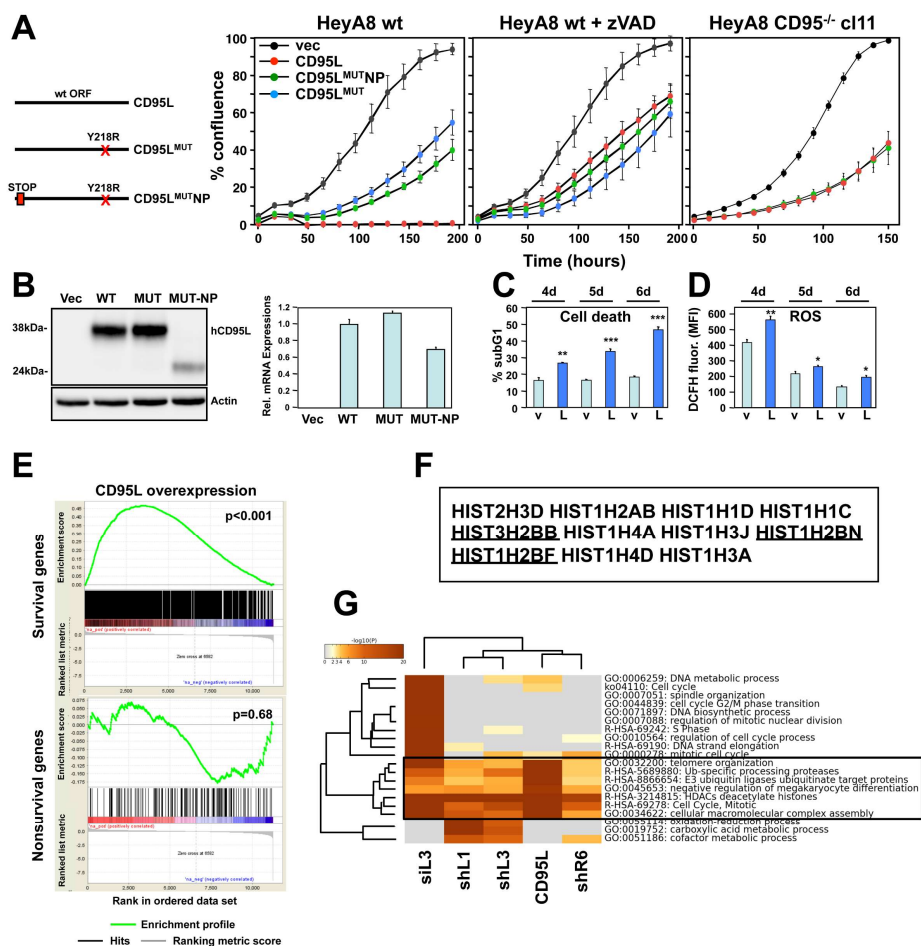


**Figure 4.1 – Over-expression of CD95L is toxic independently of apoptosis.** (A) *Left*: Schematic of the different CD95L mutants used. *Right*: Percent cell confluence over time of HeyA8 parental cells in the absence (*left panel*) or in the presence of 20  $\mu$ M zVAD-fmk (*center panel*) or HeyA8 CD95<sup>-/-</sup> cells (*right panel*) over-expressing CD95L cDNAs. Data are representative of one of three independent experiments. Values were calculated from samples done in triplicate or quadruplicate shown as mean  $\pm$  SE. (B) *Left*: Western blot analysis of HeyA8 cells overexpressing different CD95L mutant cDNAs. Cells expressing CD95L<sup>MUT</sup> or CD95L were pretreated with zVAD-fmk. Note, the small amount of truncated CD95L in cells infected with CD95L<sup>MUT</sup>NP does not have CD95 binding activity. *Right*: RT-qPCR analysis for CD95L of the same samples. Data are representative of two independent experiments. Each bar represents mean  $\pm$  S.D. of three replicates. (C, D) Quantification of cell death (C) and ROS production (D) in cells expressing either pLenti (v) or pLenti-CD95L (L) at different time points (days after infection). Data are representative of two independent experiments. Each bar represents mean  $\pm$  SE of three replicates. \* p < 0.05, \*\* p < 0.001, \*\*\* p < 0.0001, unpaired t-test. (E) Gene set enrichment analysis for the 1846 survival genes (*top panel*) and the 416 nonsurvival genes (*bottom panel*) of mRNAs downregulated in CD95L-expressing HeyA8 CD95<sup>-/-</sup> cells compared to HeyA8 CD95<sup>-/-</sup> cells infected with pLenti virus. p-values indicate the significance of enrichment. (F) The histone genes downregulated in cells treated with DISE-inducing si/shRNAs (Figure 3.10E) or in the HeyA8 CD95<sup>-/-</sup> cells over-expressing CD95L. Histones underlined contain a 3'UTR. (G) Metascape analysis of 5 RNA-Seq data sets indicated. The boxed GO term clusters were highly enriched in all 5 data sets. Will Putzbach performed experiments for Figures 4.1A and B and analysis for Figure 4.1E; Quan Gao performed experiments for Figures 4.1A and C to D; Monal Patel performed experiments for Figures 4.1C and D; Marcus Peter performed analyses for Figures 4.1F and G.

CD95L<sup>MUTNP</sup>). Over-expressing CD95L in HeyA8 cells, which are highly sensitive to CD95-mediated apoptosis, killed cells within a few hours after pLenti-CD95L infection (**Figure 4.1A; left panel and Figure 4.2A**). Interestingly, severe growth reduction occurred when CD95L<sup>MUT</sup> or CD95L<sup>MUTNP</sup> was expressed without any signs of apoptosis, although the cells were obviously stressed compared to empty pLenti-infected cells (**Figure 4.1A; left panel and Figure 4.2A and**

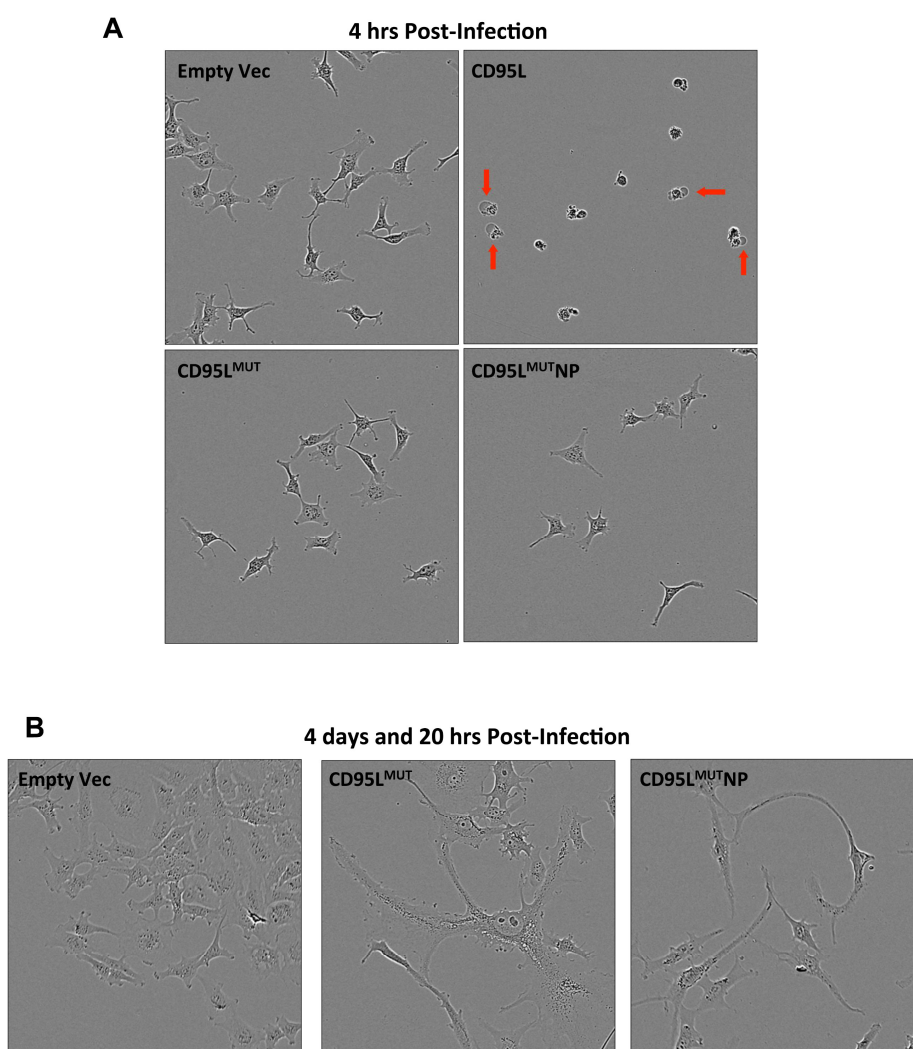


**Figure 4.2 – Expression of CD95L<sup>MUT</sup> and CD95L<sup>MUTNP</sup> does not induce cell death with morphology of apoptosis.** These pictures were taken 4 hrs (**A**) or ~5 days (**B**) after infection with empty pLenti, pLenti-CD95L, pLenti-CD95L<sup>MUT</sup> and pLenti-CD95L<sup>MUTNP</sup> in HeyA8 cells. Note the characteristic blebbing that occurs during apoptosis in the cells infected with pLenti-CD95L. Will Putzbach performed experiments for **Figure 4.2**.

**B).** Western blot analysis of CD95L protein produced from the three cDNA constructs demonstrated that both CD95L and CD95L<sup>MUT</sup> produce comparable amounts of full length protein, whereas CD95L<sup>MUT</sup>NP produces a truncated protein expressed at a significantly reduced level (**Figure 4.1B; left panel**). The RT-qPCR analysis showed all three constructs expressed comparable amounts of mRNA, although CD95L<sup>MUT</sup>NP produced slightly less (**Figure 4.1B; right panel**). These results suggested that the CD95L mRNA could be toxic to HeyA8 cells in a manner independent of CD95L protein inducing apoptosis. This was re-affirmed by expressing the three CD95L cDNA constructs in the presence of the pan-caspase inhibitor zVAD-fmk (**Figure 4.1A; center panel**). Even with suppressed apoptosis, all three constructs were equally toxic to HeyA8 cells. Finally, HeyA8  $\Delta$ shR6 clone #11 (now referred to as HeyA8 CD95<sup>-/-</sup>, confirmed to express no CD95 protein (**Figure 3.7**)) were tested. In these cells, wild type CD95L and CD95L<sup>MUT</sup>NP were equally active in severely reducing the growth of the cells (**Figure 4.1A; right panel**). Cell death was confirmed by quantifying nuclear fragmentation (**Figure 4.1C**), and a significant increase of ROS in cells expressing CD95L<sup>MUT</sup>NP was also detected (**Figure 4.1D**), in a similar manner to cells undergoing DISE<sup>376</sup>. To exclude the possibility that truncated CD95 protein (not detected with the C-terminal-specific antibody used in **Figure 4.1B; left panel**) or any part of the CD95 mRNA would play a role in this toxicity, the entire CD95 gene was deleted in MCF-7 cells using CRISPR/Cas9, which resulted in the generation of the homozygous deletion clone FA4 (The F2 clone was not further tested, as it displayed a severe growth defect). In addition, two clones with homozygous  $\Delta$ shR6 (clones #3 and #21) were also isolated and are homozygous CD95 protein knock outs (**Figure 4.3A to E**). Wild-type CD95L over-expression significantly reduced the growth of these cells (**Figure 4.3F**).

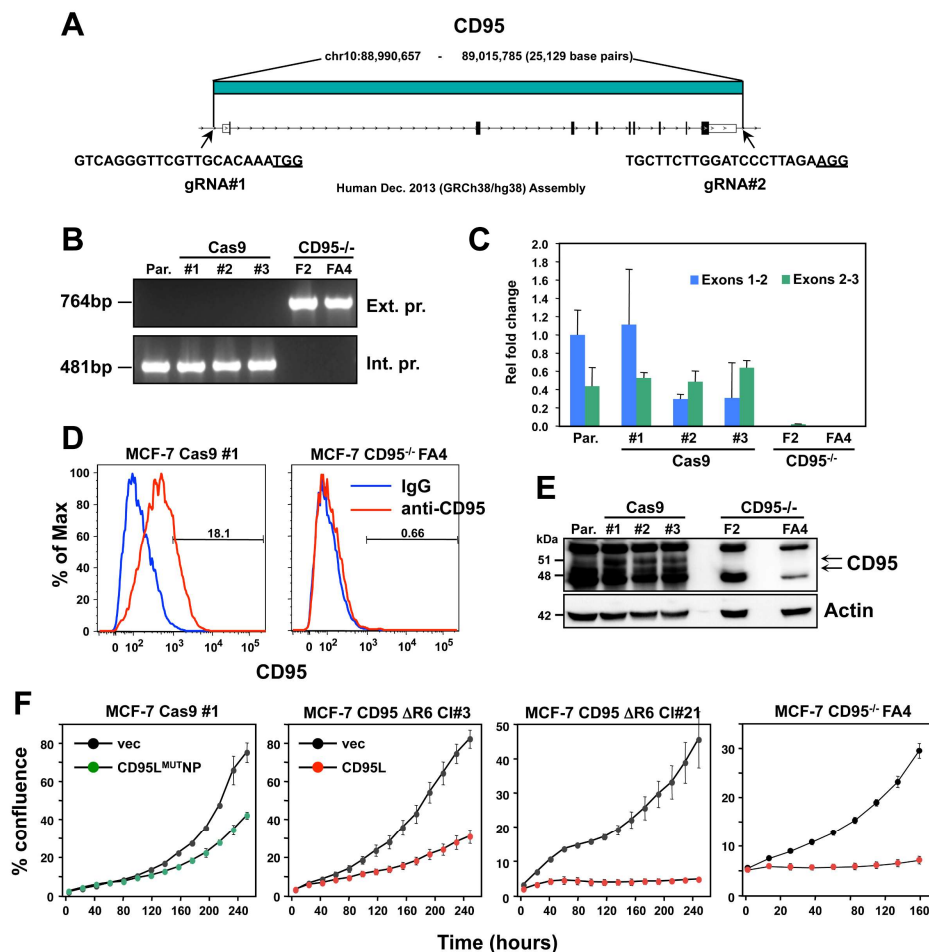


**Figure 4.3 – CD95L is toxic to MCF-7 cells lacking the entire CD95 gene.** (A) Schematic of the genomic locations and sequences of the gRNAs used to excise the entire CD95 gene in MCF-7 cells. PAM site is underlined. (B) PCR with flanking (*top panels*) and internal (*bottom panels*) primers used to confirm the absence of the CD95 gene in MCF-7 clones. Parental cells and three clones transfected with Cas9 only (Cas9) and two complete CD95 deletion clones (F2 and FA4) are shown. (C) RT-qPCR analysis of the indicated clones using primers spanning either exon 1/2 or exon 2/3 of the CD95 gene. (D) Surface staining for CD95 of one wild type and one deletion clone FA4. (E) Western blot analysis of both CD95 deletion clones. (F) *Far left panel*: Confluency over time of MCF-7 Cas9 clone #1 infected with empty pLenti vector or with pLenti-CD95L<sup>MUTNP</sup>. *The three right panels*: MCF-7 CD95 deletion clone FA4 and the two MCF-7 clones (#3 and #21) in which the shR6 site was deleted (resulting in an out-of-frame shift) after infection with either empty pLenti vector or pLenti-CD95L. The F2 clone was omitted because of a severe growth deficit. Data are representative of two independent experiments. Each data point represents mean  $\pm$  SE of three replicates. Austin Stults generated the CD95 deletion cells and performed experiments in **Figures 4.3A to C and E**; Calvin Law performed experiment in **Figure 4.3D**; Will Putzbach performed experiment in **Figure 4.3F**

To determine the cause of cell death induced by CD95L over-expression in HeyA8 CD95<sup>-/-</sup> cells, an RNA-Seq analysis was performed. Interestingly, expression of CD95L caused preferential downregulation amongst the ~1800 critical survival genes used in **Figure 3.10D** and

not the nonsurvival gene control set (**Figure 4.1E**). In addition, cell death induced by CD95L overexpression resulted in a substantial loss of 11 of the 12 histones shown to be downregulated in cells treated with DISE-inducing si/shRNAs (**Figure 4.1F**). A Metascape analysis confirmed that nucleosome assembly, regulation of mitosis, and genes consistent with the involvement of histones were among the most significantly downregulated mRNAs across all cells in which DISE was induced by any of the four DISE-inducing si/shRNAs (i.e. siL3, shL3, shR6, and shL1) or by the expression of CD95L (**Figure 4.1G**). These data suggest CD95L mRNA expression causes downregulation of GO terms involved in basic cellular processes needed for survival, in a manner similar to DISE-inducing si/shRNAs.

#### *Over-Expression of CD95L cDNA may Kill Cells through RNAi*

Given our previous work on CD95L-derived si/shRNA toxicity, we hypothesized CD95L mRNA kills cells through an RNAi-based mechanism—perhaps by being processed into small guide RNAs that incorporate into the RISC. Cells lacking the majority of endogenous miRNAs would presumably be hypersensitive to RNAi-based toxicity because of the elevated pool of unoccupied RISCs. Consistently, *Drosha*<sup>-/-</sup> cells were hypersensitive to the expression of CD95L<sup>MUTNP</sup> compared to wild type HCT116 cells (**Figure 4.4A**;  $p=0.014$ , according to a polynomial fitting model) and now virtually all cells died (**Figure 4.4B**). To test the hypothesis that *Drosha*<sup>-/-</sup> cells were more sensitive because their RISCs were not occupied by copious amounts of endogenous miRNAs and to determine whether CD95L mRNA could give rise to small RNAs that incorporate into the RISC, small RNAs associated with AGOs1 to 4 were pulled down and analyzed in wild type and *Drosha*<sup>-/-</sup> HCT116 cells after expressing the CD95L<sup>MUTNP</sup> cDNA. For

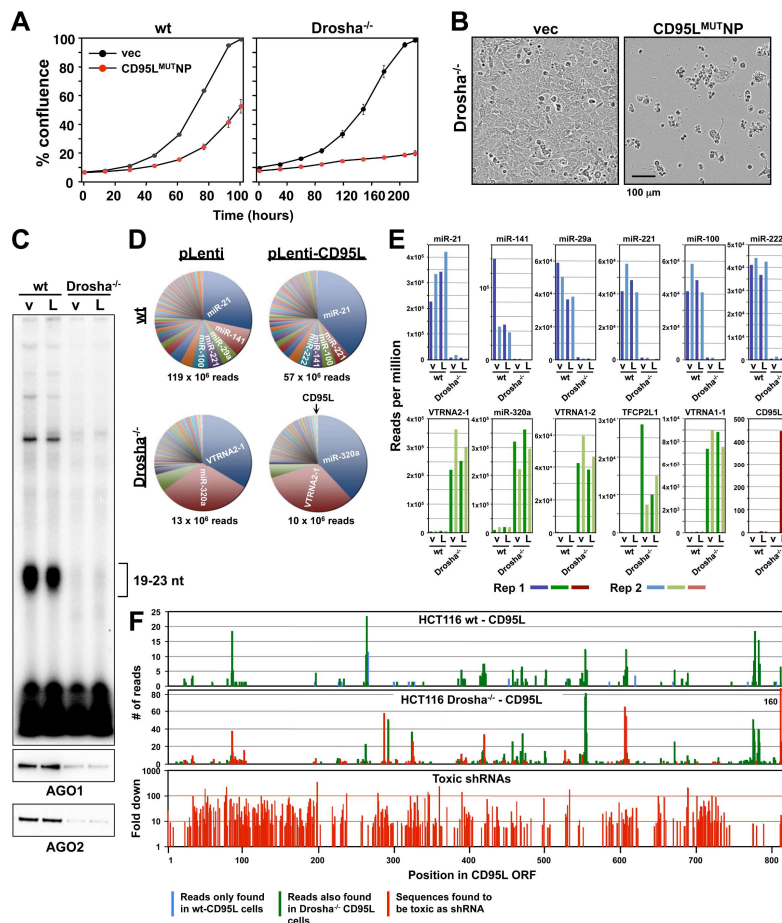


**Figure 4.4 - Toxic small RNAs are generated in cells expressing CD95L mRNA and loaded into the RISC.** (A) Percent cell confluence over time of HCT116 parental (*left*) or Drosha<sup>-/-</sup> (*right*) cells after infection with pLenti-CD95L<sup>MUTNP</sup>. Data are representative of three independent experiments. Each data point represents the mean ± SE of three replicates. (B) Phase contrast images of Drosha<sup>-/-</sup> cells 9 days after infection with either empty pLenti or pLenti-CD95L<sup>MUTNP</sup>. (C) *Top*: autoradiograph of small RNAs pulled down with the AGO binding peptide. *Bottom*: Western blot analysis of pulled down AGO proteins. v, pLenti; L, pLenti-CD95L<sup>MUTNP</sup> expressing cells. (D) Pie charts showing the relative ratio of small RNAs pulled down with the AGO proteins in HCT116 wild type and Drosha<sup>-/-</sup> cells. Depicted are all the amounts of all small RNAs that contributed at least 0.01% to the total RNA content. Only in the Drosha<sup>-/-</sup> cells was a significant amount of CD95L derived AGO bound reads found. They represented the 75<sup>th</sup> most abundant small RNA species (arrow). The average number of total sequenced reads (of two duplicates) are shown for each condition. (E) *Top*: Number of reads (normalized per million) of the top five most abundant small RNAs in the RISC of either wild type HCT116 or Drosha<sup>-/-</sup> cells infected with either pLenti or pLenti-CD95L<sup>MUTNP</sup>. *Bottom*: Number of reads (per million) of the top five genes with small RNAs most abundant in the RISC of either wild type HCT116 or Drosha<sup>-/-</sup> cell infected with either pLenti or pLenti-CD95L<sup>MUTNP</sup>. Note: miR-21 is not included as it is already shown in the top row. *Bottom right panel*: Abundance of AGO-bound CD95L-derived small RNAs. Shown in all panels is the abundance of RNAs in the four samples (two sets of duplicates). (F) Alignment of the detected AGO-associated CD95L-derived reads within the ORF of CD95L in wild type (*Top*) and Drosha<sup>-/-</sup> (*Center*) HCT116 cells after infection with pLenti-CD95L<sup>MUTNP</sup>. *Bottom panel*: The location of all downregulated shRNAs (>5 fold reduction after averaging the fold downregulation for the Infection -DOX and Infection +DOX in the toxicity screen in **Figure 3.19D**) along the ORF of the CD95L mRNA. Quan Gao performed experiments for **Figures 4.4A and B**; Aishe Sarshad performed experiment for **Figures 4.4C to D**; Elizabeth Bartom and Marcus Peter performed analyses for **Figure 4.4D to F**.



the pull-down, a peptide derived from GW182 recently described to bind to all four human AGO proteins<sup>389</sup> was used. As expected, in wild type HCT116 cells, copious amounts of small RNAs (19-23nt in length) were detected that were bound to the AGO proteins; both AGO1 and AGO2 were efficiently pulled down (**Figure 4.4C and D**). In contrast, in the *Drosha*<sup>-/-</sup> cells, which cannot process canonical miRNAs, less small RNAs were detected confirming the absence of miRNAs in the RISC (**Figure 4.4C and D**). Surprisingly, the amount of pulled down AGO proteins was

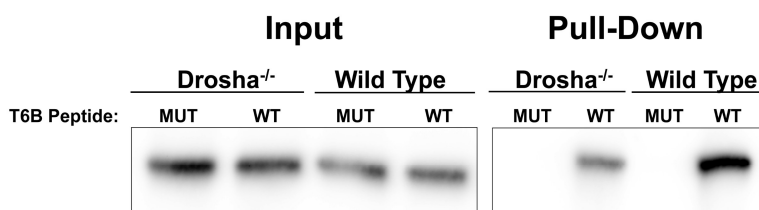


**Figure 4.5 – Pull-down efficiency of human AGO2 in HCT116 versus *Drosha*<sup>-/-</sup> cells.** Western blot detection of human AGO2 in pull-down fractions from wild type HCT116 and *Drosha*<sup>-/-</sup> cells. The WT T6B indicates pull-down with the wild type peptide, whereas MUT T6B indicates the pull-down with the mutant peptide that cannot bind to AGO<sup>389</sup>. Input was harvested from lysate before pull-down. Will Putzbach performed the experiment for **Figure 4.5**.

severely reduced despite the fact these *Drosha*<sup>-/-</sup> cells express comparable levels of AGO2 (**Figure 4.4C and Figure 3.8E; insets**). This suggests the peptide does not bind AGO proteins as efficiently in the absence of *Drosha*. This was independently confirmed by pulling down human AGO2 in wild type HCT116 and *Drosha*<sup>-/-</sup> cells after normalizing the input for AGO2 expression; there is significantly less human AGO2 pulled down in the *Drosha*<sup>-/-</sup> cells compared to the wild type HCT116 cells (**Figure 4.5**). It is currently unknown why this is, although it has been shown GW182 binds AGO2 with higher affinity when in bound to a guide RNA<sup>130</sup>.

The analysis of all AGO-bound small RNAs showed that in the wild type HCT116 cells, >98.4% of bound RNAs were miRNAs. In contrast, only 34% of bound small RNAs were miRNAs in *Drosha*<sup>-/-</sup> cells (**Figure 4.4D**). These included miRNAs that are processed independently of *Drosha* such as miRNA-320a<sup>60,224</sup>. Consistently, this miRNA became a major RNA species bound

to AGO proteins in *Droscha*<sup>-/-</sup> cells (**Figure 4.4D**). In both wild type and *Droscha*<sup>-/-</sup> cells, a significant increase in CD95L-derived small RNAs bound to the AGO proteins was detected in cells infected with the pLenti-CD95L<sup>MUT</sup>NP versus the empty pLenti vector. They corresponded to 0.0006% and 0.043% of all the AGO-bound RNAs in the wild type cells and *Droscha*<sup>-/-</sup> cells, respectively (**Figure 4.4D and E**). Toxicity of CD95L mRNA was, therefore, not due to overloading the RISC. The reduction of AGO-bound miRNAs in *Droscha*<sup>-/-</sup> cells was paralleled by a substantial increase in binding of other small RNAs to the AGO proteins (**Figure 4.4E**). Interestingly, the amount of AGO-bound CD95L derived small RNAs was >100 times higher in the *Droscha*<sup>-/-</sup> cells compared to the wild type cells (red columns in **Figure 4.4E**). These data support the hypothesis that *Droscha*<sup>-/-</sup> cells are more sensitive to CD95L mRNA-mediated toxicity due to their ability to take up more toxic small RNAs, perhaps those derived from CD95L mRNA, into the RISC in the absence of most endogenous miRNAs.

Many regions in CD95L mRNA gave rise to small RNAs. As expected many of the same small RNAs detected in wild type cells were also detected in *Droscha*<sup>-/-</sup> cells but at much higher counts in the latter (green peaks in **Figure 4.4F**; *top and center panels*). Comparing the AGO-bound CD95L-derived RNAs that overlapped the sequences of the shRNAs in our toxicity screen revealed that a large number of the AGO-bound RNAs derived from regions in the CD95L ORF overlapped the sequences of shRNAs identified as toxic in the pTIP-shRNA screen (red peaks in **Figure 4.4F**; *center panel and Figure 3.19D*). There were also multiple reads that were located at positions in CD95L that did not overlap with toxic shRNAs (green peaks in **Figure 4.4F**; *center panel*). This could be due to cell type differences; the pTIP-shRNA toxicity screen was performed in NB7 cells, whereas the AGO pull-down experiments were performed in HCT116 cells.

Consistently, the collective toxicity of CD95L ORF-derived shRNAs was different between NB7 and HCT116 cells (**Figure 3.20B** and **Figure 3.21A**). Alternatively, it could point at activities of CD95L-derived small RNAs other than cell death induction.

*CD95L ORF is Degraded into Small RNA Fragments that are then Loaded into the RISC*

Interestingly, not only did AGO proteins in *Drosha*<sup>-/-</sup> cells bind more CD95L-derived small RNAs than in the wild type cells upon CD95L<sup>MUT</sup>NP over-expression, but also the length of the most abundant AGO-bound RNA species increased from 20 to 23 nts (**Figure 4.6A**; *top panel* and **Figure 4.6B**). To determine the sites within the CD95L mRNA that gave rise to small AGO-bound RNAs, all small AGO-bound RNAs detected in all conditions were Blasted against the CD95L ORF sequence. This allowed us to align all CD95L-derived reads to the CD95L mRNA (**Figure 4.6B to C** and **E to F**). This analysis identified 22 clusters in the CD95L ORF that gave rise to small RNAs that could be bound by AGO proteins (**Figure 4.6B**). To determine whether these small RNAs were formed in the cytosol and then loaded into the RISC, all small RNAs in the total RNA fraction isolated from CD95L<sup>MUT</sup>NP-expressing HCT116 *Drosha*<sup>-/-</sup> cells were aligned with the CD95L ORF (technically the CD95L<sup>MUT</sup>NP sequence; **Figure 4.6C**). Very similar regions of small RNAs were found. The average read length and broadness of the distribution of the read lengths of small RNAs derived from CD95L bound to AGO proteins was smaller than in the total small RNA fraction (**Figure 4.6A**; *center and bottom panels* and **Figure 4.6B** and **C**), suggesting fragments get trimmed to the appropriate length either before loading into the RISC or by RISC itself. This was obvious for cluster 3, which seemed to undergo 3' trimming upon entering the RISC (**Figure 4.6B**; *bottom panel* and **C**). Moreover, small RNA fragments that were derived

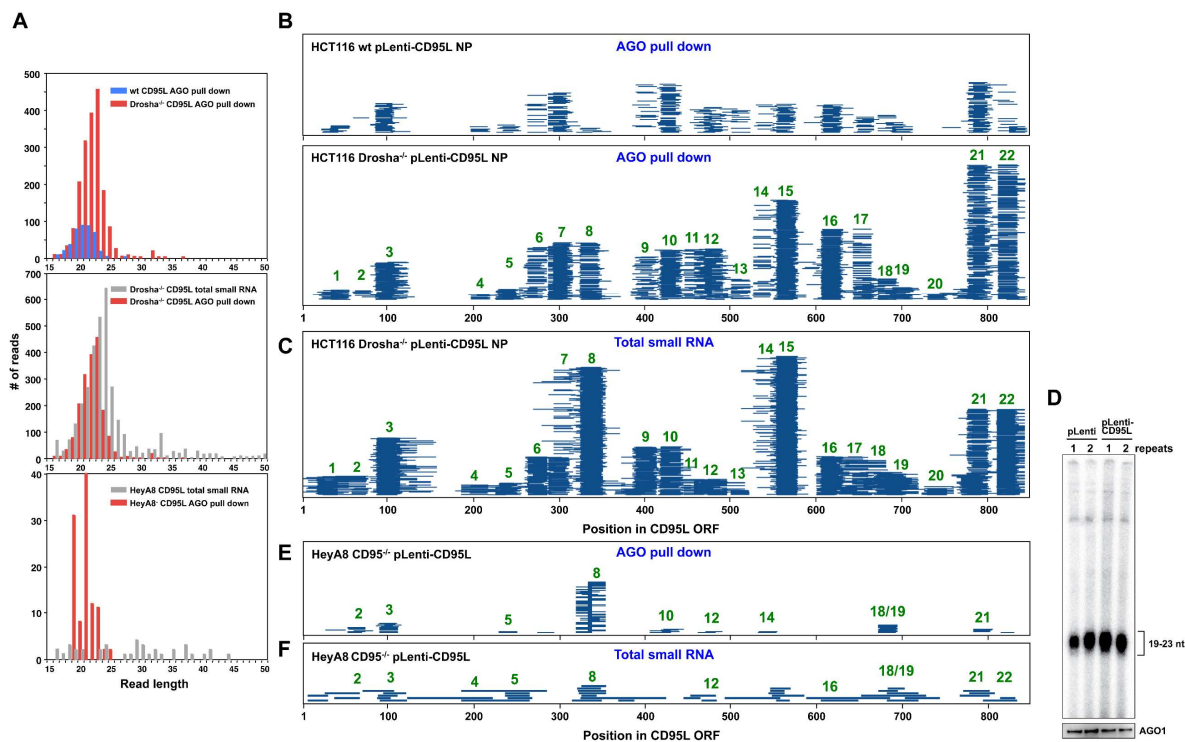


**Figure 4.6 – The entire CD95L mRNA gives rise to small RNAs that bind to the RISC.** (A) Length distribution of CD95L-derived reads in various analyses in wild type HCT116 and Drosha<sup>-/-</sup> cells over-expressing CD95L<sup>MUTNP</sup> (*top and center panels*) and HeyA8 CD95<sup>-/-</sup> cells over-expressing CD95L (*bottom panel*). (B, C) Location of read alignments along the CD95L<sup>MUTNP</sup> ORF sequence for the derived small RNAs pulled down with AGO proteins from wild type HCT116 (B, *top*) and Drosha<sup>-/-</sup> (B, *bottom*) cells and from total small RNAs from HCT116 Drosha<sup>-/-</sup> cells (C) after infection with pLenti-CD95L<sup>MUTNP</sup>. (D) *Top*: autoradiograph on RNAs pulled down with the AGO binding peptide of HeyA8 CD95<sup>-/-</sup> cells. *Bottom*: Western blot analysis of pulled down AGO1. (E, F) Location of read alignments along the CD95L ORF sequence for the derived small RNAs pulled down with AGO proteins (E) or from total small RNAs (F) from HeyA8 CD95<sup>-/-</sup> cells after infection with pLenti-CD95L. Each horizontal blue bar corresponds to a normalized read. Elizabeth Bartom and Marcus Peter performed analyses for **Figures 4.6A to C and E and F**; Aishe Sarshad performed experiment in **Figure 4.6D**.

from certain clusters were more abundant in the AGO-bound fraction compared to the total cellular small RNA fraction. These included RNAs in clusters 11, 12, 16, 21 and 22 (compare **Figure 4.6C** with **Figure 4.6B**; *bottom panel*).

To determine whether this type of processing was specific for HCT116 Drosha<sup>-/-</sup> cells, the AGO-bound small CD95L-derived RNAs in HeyA8 CD95<sup>-/-</sup> cells after expression of wild type CD95L (**Figure 4.6D** and **E**) was quantified and compared with the total cellular RNA fraction (**Figure 4.6F**). While fewer CD95L-derived reads were found in these cells, which made it difficult

to determine the relative abundance of small RNAs between the AGO-bound fraction and total small RNAs, the general location of some of the read clusters overlapped with the ones found in the *Drosha*<sup>-/-</sup> cells (**Figure 4.6B; bottom panel and C**) and wild type HCT116 cells (**Figure 4.6B; top panel**) infected with pLenti-CD95L<sup>MUT</sup>NP. Again, both the average and distribution of RNA lengths was smaller in the AGO-bound fraction versus the total RNA fraction (**Figure 4.6A; bottom panel**). Together, these data suggest that CD95L mRNA can be processed into smaller RNA fragments, which are then trimmed (perhaps at the 3' end) to a length appropriate for incorporation into the RISC. Additionally, this processing occurs in different cell types.

*The Degradation of CD95L mRNA is Independent of Dicer and May be Determined by its Secondary Structure*

Our data suggest that the CD95L mRNA, when overexpressed, is toxic to cells due to the formation of AGO-bound small RNAs that are incorporated into the RISC and kill cells through RNAi. This process is independent of *Drosha*. To determine whether *Dicer* is required for either processing of CD95L mRNA or loading the small RNAs into the RISC, CD95L<sup>MUT</sup>NP was expressed in wild type and *Dicer*<sup>-/-</sup> HCT116 cells (**Figure 4.7A**). *Dicer*<sup>-/-</sup> cells were still sensitive to toxicity induced by CD95L<sup>MUT</sup>NP expression, suggesting the toxicity of the CD95L mRNA does not require processing by either *Drosha* or *Dicer*. Custom RT-qPCR primers that specifically detect the small RNAs from clusters 8 and 21 were also generated. Both *Drosha*<sup>-/-</sup> and *Dicer*<sup>-/-</sup> cells over-expressing CD95L<sup>MUT</sup>NP generated more fragments from these clusters than in wild type cells (**Figure 4.7B**), demonstrating these enzymes are not involved in processing CD95L mRNA. All the reported small RNAs derived from CD95L corresponded to the sense strand of the

expressed mRNA, raising the question of how they could be processed into double-stranded siRNAs in the absence of an antisense strand. To get a preliminary answer to this question, the

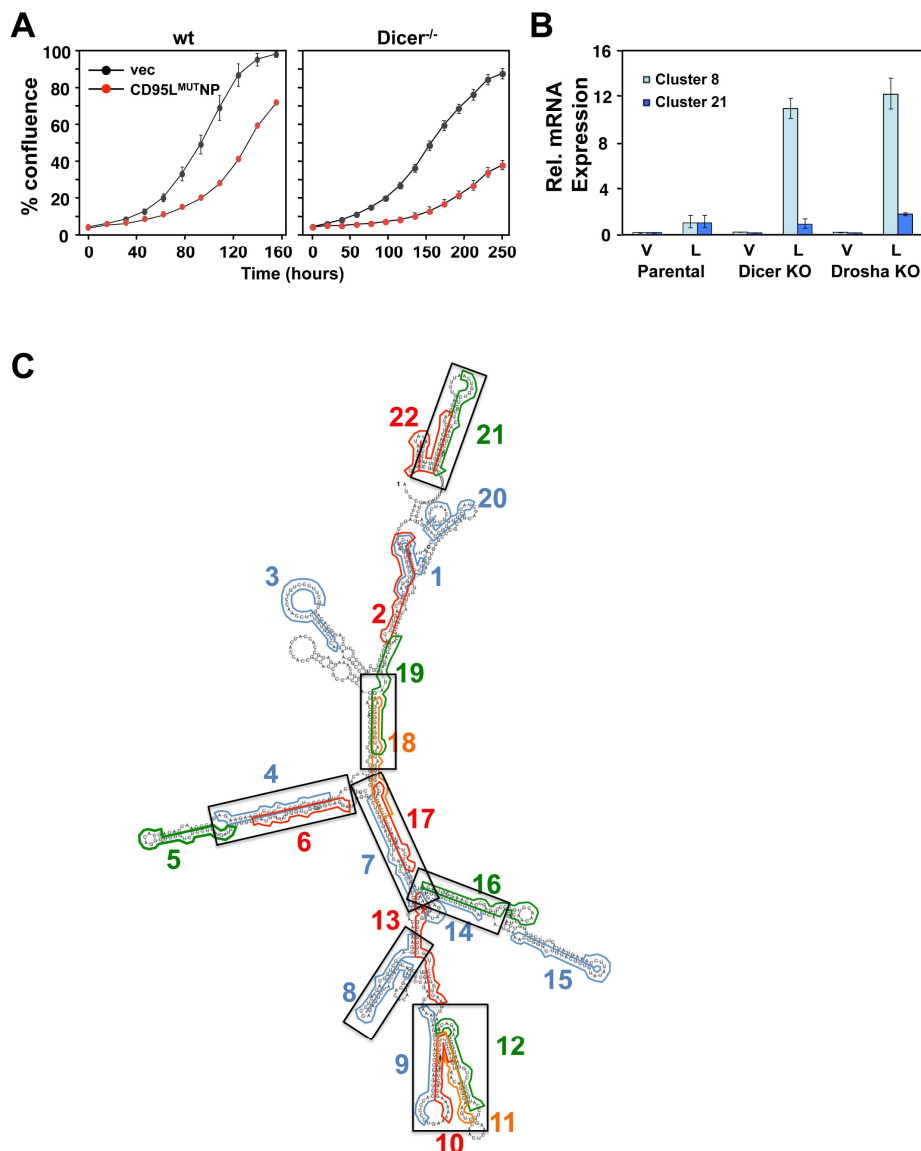


**Figure 4.7 - Maximal CD95L mRNA toxicity requires full-length wt sequence and is independent of Dicer.** (A) Percent cell confluence over time of wild type HCT116 (*left*) or Dicer<sup>-/-</sup> (*right*) cells after infection with CD95<sup>MUTNP</sup>. Data are representative of two independent experiments. Each data point represents the mean  $\pm$  SE of three replicates. (B) RT-qPCR analysis of clusters 8 and 21 fragments in parental (wild type) HCT116, Dicer<sup>-/-</sup>, or Drosha<sup>-/-</sup> cells after infection with pLenti-CD95<sup>MUTNP</sup>. Each bar represents mean  $\pm$  S.D. of three replicates. (C) The CD95L<sup>MUTNP</sup> RNA was subjected to a secondary RNA structure analysis (<http://rna.tbi.univie.ac.at>) using default settings. The locations of 22 reads representative of the 22 read locations (Figure 4.6B and C) are shown. Regions with potential duplex formation are boxed. Quan Gao performed experiment for Figure 4.7A; Ashley Haluck-Kangas performed experiment in Figure 4.7B; Marcus Peter performed analysis for Figure 4.7C.

CD95L ORF (technically the CD95L<sup>MUTNP</sup>) mRNA sequence was subjected to a secondary structure prediction (**Figure 4.7C**). According to this analysis, the CD95L ORF mRNA forms a tightly folded structure with many of the small RNAs of the 22 clusters juxtaposing each other in stem-like structures creating regions of significant complementarity. These may provide the duplexes needed to be processed by endoribonucleases and loaded into the RISC.

#### *Puromycin Does Not Kill Cells Because of Differences in Viral Titer*

To confirm toxicity is not due to puromycin killing cells because of differences in viral titer between our empty vector and CD95L-expressing vectors, the HeyA8 CD95<sup>-/-</sup> clone was infected with CD95L and CD95L<sup>MUTNP</sup> vectors and varying lower concentrations of the empty

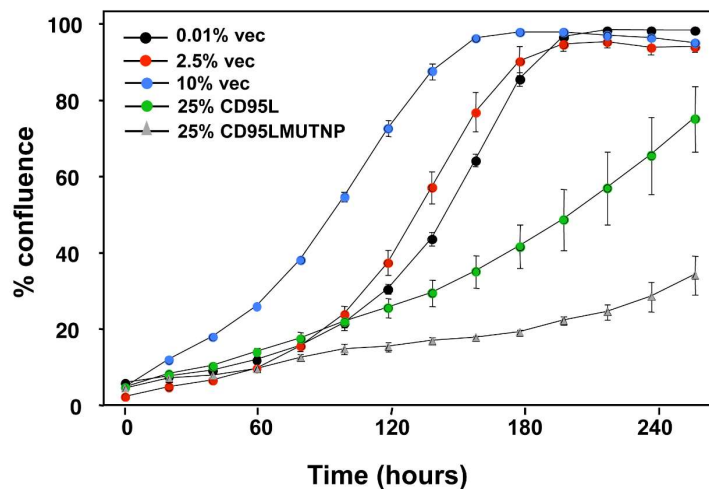


**Figure 4.8 - CD95L mRNA toxicity is not the result of puromycin on cells with different levels of lentiviral infection.** Percent cell confluence over time of HeyA8 CD95<sup>-/-</sup> cells after infection with CD95L or CD95L<sup>MUTNP</sup> cDNAs and lessening amounts of empty vector pLenti (vec). Data are representative of two independent experiments. Each data point represents the mean  $\pm$  SE of three replicates. Ashley Haluck-Kangas performed experiments for **Figure 4.8**.

vector. Even cells infected with CD95L and CD95L<sup>MUTNP</sup> at 2500 times the volume of the empty vector viral supernatant still exhibited toxicity (**Figure 4.8**), which demonstrates the cells infected

with the CD95L expression vectors are not dying because of puromycin killing uninfected cells due to a lower viral titer.

### *Stabilization of CD95L Expression Enhances Toxicity*

We took advantage of an interesting facet of CD95/CD95L regulation to demonstrate that expression from the CD95L cDNA construct causes the toxicity. Specifically, over-expression of

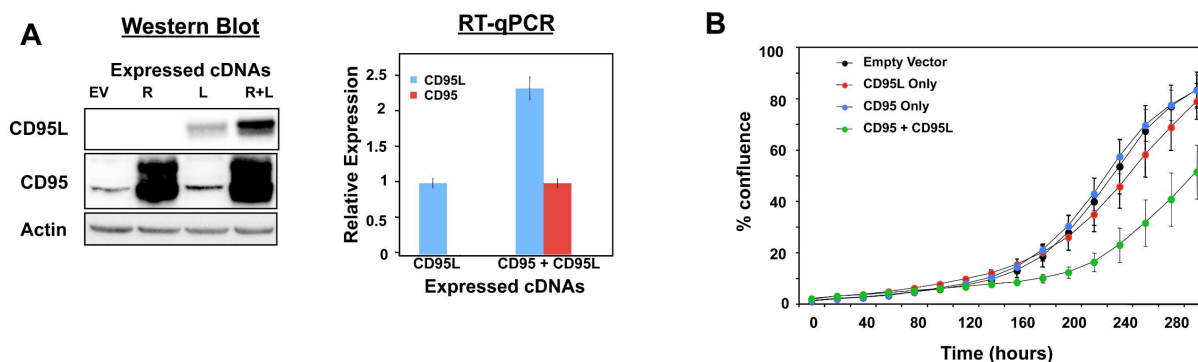


**Figure 4.9 - Co-expression of CD95 cDNA stabilizes expression of transgenic CD95L and enhances toxicity.** (A) Western blot (*left panel*) and RT-qPCR (*right panel*) analysis of CD95L and CD95 protein in NB7 cells co-over-expressing pLNCX2 or pLNCX2-CD95 and pLenti or pLenti-CD95L. EV is empty vectors; R is CD95 receptor; L is CD95 ligand. (B) Percent confluence over time of NB7 cells expressing either empty pLNCX2 or pLNCX2-CD95 and then super-infected with either empty pLenti or pLenti-CD95L. Each data point represents the mean  $\pm$  SE of three replicates. Will Putzbach performed experiments for **Figures 4.9**.

CD95 stabilizes both the protein (**Figure 4.9A; left panel**) and mRNA (**Figure 4.9A; right panel**) of co-over-expressed CD95L in NB7 cells. Although the mechanism by which this stabilization occurs is unknown, it could still be used to test whether stabilized expression of CD95L would enhance toxicity. Indeed, over-expression of CD95L in apoptosis-resistant NB7 cells also co-over-expressing CD95 had a reduced growth rate compared to NB7 cells over-expressing only CD95L (and the empty pLNCX2 vector), which is consistent with more toxicity being evoked from by more CD95L mRNA because of the stabilization afforded by CD95 co-over-expression (**Figure 4.9B**).



*Apoptosis-Independent Toxicity of CD95L Over-Expression Depends on AGO2*

Our data suggests CD95L mRNA can be processed into small RISC-associated guide RNAs that evoke toxicity through an RNAi-dependent mechanism. If this hypothesis is correct, then elimination of AGO should attenuate the toxicity evoked by CD95L over-expression in apoptosis-resistant cancer cells.

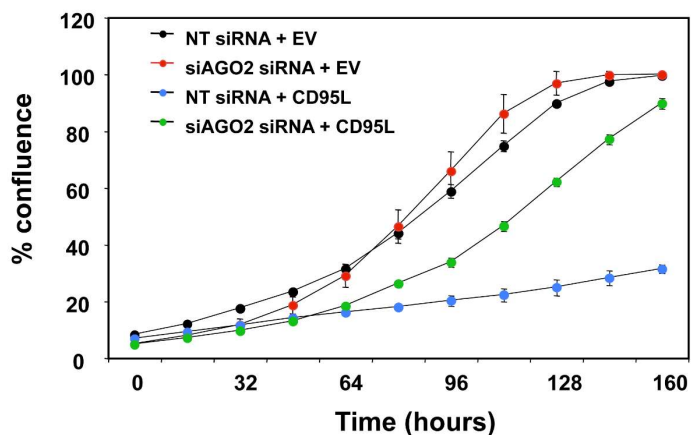


**Figure 4.10 – Knock Down of AGO2 expression attenuates toxicity evoked by CD95L over-expression in CD95 deficient cells.** Percent cell confluence of HeyA8 CD95<sup>-/-</sup> cells transfected with AGO2-targeting siRNA (siAGO2) or siScr (NT; non-targeting) and then infected with pLenti (EV) or pLenti-CD95L virus. Each data point represents the mean  $\pm$  SE of three replicates. Ashley Haluck-Kangas performed experiments for **Figure 4.10**.

Consistently, knock down of AGO2 via siRNAs attenuates the toxicity associated with over-expressing CD95L in HeyA8 CD95<sup>-/-</sup> cells (**Figure 4.10**), which provides strong evidence the apoptosis-independent toxicity evoked by CD95L mRNA is dependent on RNAi.

## Discussion

In chapter 3, we described a novel form of cell death that was induced by expression of si/shRNAs designed from the sequences of CD95/CD95L mRNA. There was a notable enrichment of toxic si/shRNAs derived from those of the CD95L ORF sequence, which pointed toward the CD95L mRNA, itself, having distinct biological importance.

Indeed, in chapter 4, it was shown that expression of full-length CD95L mRNA triggers toxicity that is independent of the protein product and canonical apoptosis. This is intriguing considering a previous study showing transgenic expression of CD95L using viruses killed prostate cancer cells that were treated with an antagonistic CD95 antibody<sup>434</sup>. These results were interpreted as intracellular CD95L triggering apoptosis. However, this work provides an alternate explanation—namely, both the CD95L protein *and* mRNA are toxic to cells by distinct mechanisms. The protein induces apoptosis, and the mRNA induces toxicity through an RNAi-based mechanism. The latter is supported by several lines of evidence: 1) Droscha<sup>-/-</sup> cells are hypersensitive to CD95L mRNA over-expression. 2) Multiple CD95L-derived small RNAs (mostly 19-23 bps) that were bound to AGO proteins in cells over-expressing CD95L mRNA were identified. 3) There is overlap between these AGO-bound small RNA sequences and the shRNA sequences identified as toxic in our previous screen of CD95L-derived shRNAs. 4) Knock down of AGO2 attenuates the CD95L mRNA toxicity.

It is important to note that while the evidence shows many similarities between the toxicity induced from DISE-inducing si/shRNAs and from CD95L mRNA over-expression, it currently cannot be definitively concluded that CD95L mRNA triggers DISE. It is relatively easy to determine whether an individual si/shRNA is targeting genes through their 3' UTRs using RNA-Seq and Sylamer analyses. However, CD95L mRNA gives rise to multiple small AGO-bound RNAs simultaneously, making analysis of likely targets very difficult. Further work is needed to identify how RNAi is involved in the toxicity and what genes are being directly targeted. Furthermore, even in Droscha<sup>-/-</sup> cells, which express less endogenous miRNAs, small RNAs derived from CD95L<sup>MUT</sup>NP in over-expressing cells was still only the 75<sup>th</sup> most abundant AGO-bound

RNA (**Figure 4.4D**). Titration experiments with artificial small RNAs designed on the fragments bound to AGO in CD95L-over-expressing cells will need to be done to determine whether this small amount of small RNA can be toxic.

Dicer and Drosha are not involved in generating the AGO-bound CD95L-derived fragments, and at present the RNA processing machinery involved is unknown. Our results are not consistent with a non-specific degradation of RNAs nor an artifact of the pull-down procedure for the following reasons: 1) Small CD95L-derived fragments were detected using RT-qPCR primers specific for those small RNA sequences. 2) The location of the AGO-bound CD95L-derived sequences (**Figure 4.6B and C**) overlap to some extent with regions of intramolecular secondary structure of the mRNA (**Figure 4.7C**), and we see similar read locations when analyzing small CD95L-derived RNAs in HCT116, HCT116 Drosha<sup>-/-</sup>, and HeyA8 cells, both from total RNA as well as AGO-bound fractions (**Figure 4.6B, C, E and F**). This is all consistent with a model where CD95L mRNA contains specific motifs that are specifically targeted by RNases that are ubiquitously expressed. 3) The distribution of read lengths of CD95L-derived AGO-bound RNA fragments is much narrower compared to the distribution of CD95L-derived RNA fragment lengths found in the total cellular RNA fraction and has a mean length around 19 to 23 nts (**Figure 4.6A**). If this were a non-specific degradation process, this trend would not be observed.

Taken together, the most likely mechanism for generation of these AGO-bound CD95L-derived RNA fragments involves initial targeting of certain secondary structure and/or sequence motifs in the CD95L mRNA by endoribonucleases. Given the differences in length distribution between the cellular versus AGO-bound RNA fragments, it is likely the released CD95L-derived fragment intermediates are then incorporated into the RISC and then trimmed to the appropriate

length by AGO. Indeed, a similar mechanism is known to occur during the maturation of the erythropoietic miRNA-451a, where the pre-miRNA is first cleaved by AGO2 and then trimmed at the 3' end to the final mature form by the exoribonuclease PARN<sup>225</sup>. There are even sources of potential guide RNAs that do not require any pre-processing before RISC incorporation. Indeed, the recently discovered class of agotrons are released as spliced-out introns that get directly incorporated into the RISC, without Drosha or Dicer processing<sup>230</sup>. In a similar way, CD95L mRNA fragments may get directly loaded into the RISC, where AGO and AGO-associated ribonucleases perform the processing necessary to produce the guide RNA of appropriate size. However, identifying the enzymes responsible for producing the initial CD95L fragments will require further experimentation.

Our data provide the first evidence suggesting an overexpressed cDNA to be toxic via an RNAi-dependent mechanism through an mRNA intermediate. It was first shown in plants that overexpressed transgenes can be converted into RNAi-active short RNA sequences<sup>1</sup>. Our data on the effects of overexpressed CD95L mRNA may be the first example of a transgene determining cell fate through RNAi in mammalian cells.

## **Chapter 5: Discussion**

### **DISE was Discovered through a Unique sOTE**

Seed-based OTEs (sOTEs) have been viewed as a major impediment for RNAi—both in the laboratory and clinic. Whether an siRNA's seed sequence will trigger a noticeable and predictable sOTE is difficult to answer since seed matches corresponding to artificial guide RNA

seed sequences may not have been under selective pressure to perform any concerted function. In these cases, it is difficult to predict how seed-based silencing of random genes will interact to produce a concerted cellular response. Indeed, sOTEs are generally viewed as something with no scientific value that should be avoided (**Figure 5.1**).

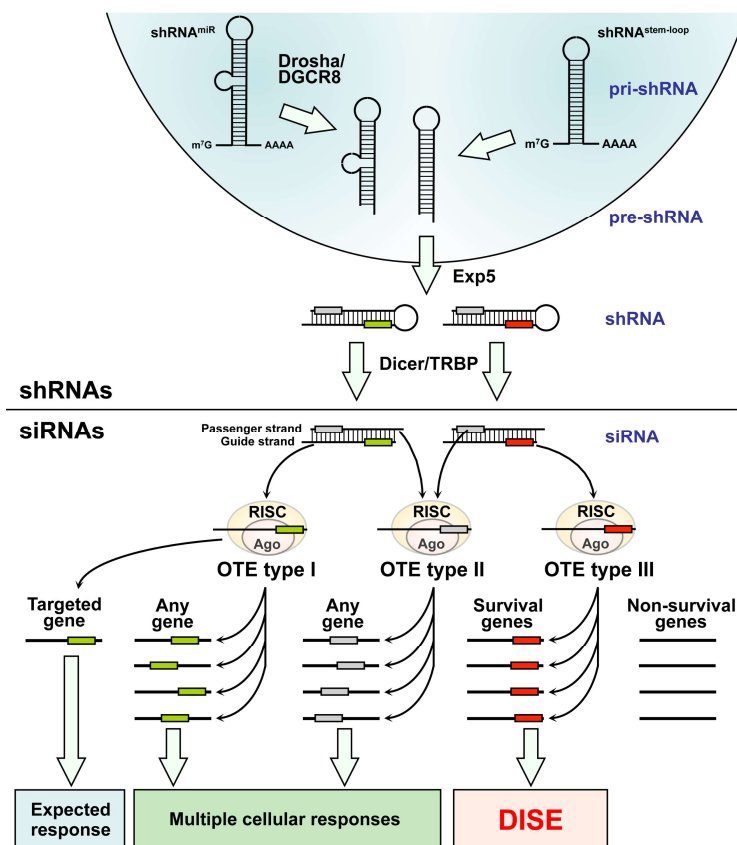


**Figure 5.1 – DISE is distinct from a conventional seed-based off-target effect.** Exogenous shRNAs are processed by the same enzymes as miRNAs, leading to generation of mature siRNAs. These siRNAs inhibit expression of their on-target via extensive base-pairing between the guide strand and the target mRNA, which leads to a predictable on-target response. Besides repressing the intended on-target, siRNAs also repress multiple targets through minimal base pairing between the siRNA's seed sequence and corresponding seed matches in mRNAs. This seed-based targeting can be classified into three groups: (1) In sOTE type I, multiple mRNAs are repressed due to base pairing between seed matches and the seed sequence (green) in the designated guide strand of the siRNA. (2) In sOTE type II, seed-based repression is due to interaction with the seed sequence of the designated passenger strand (grey). Both type I and II sOTEs lead to multiple and unpredictable cellular responses. (3) In sOTE type III, the guide strand seed sequence (red) causes preferential downregulation of survival genes, leading to the recurring and distinct response of DISE activation in cancer cells.

Moreover, even single mutations within the seed sequence can completely change the repertoire of directly targeted genes<sup>108</sup>. Therefore, it might be expected that siRNAs with distinct

seed sequences would produce distinct overt sOTEs. However, the results in this work uncovered a unique behavior of seed-based targeting, which manifested itself as a special kind of sOTE triggered by si/shRNAs derived from CD95/CD95L. This special sOTE is coined DISE (**Figure 5.1**), and it is the first example of RNAi reagents triggering a specific and recurring phenotypic response even though the specific sequences of these reagents, including the seed region, lack congruency and are, in many cases, highly divergent. The DISE phenomenon is characterized as the preferential downregulation of *survival genes* through seed-based targeting, which culminates in simultaneous activation of multiple death pathways in any cancer cell type with distinct morphological/biochemical features<sup>376</sup> (**Figure 5.1**).

Interestingly, inspection of the seed matches corresponding to shL3 in the 10 downregulated survival genes shown in **Figure 3.10B** did not reveal the striking conservation

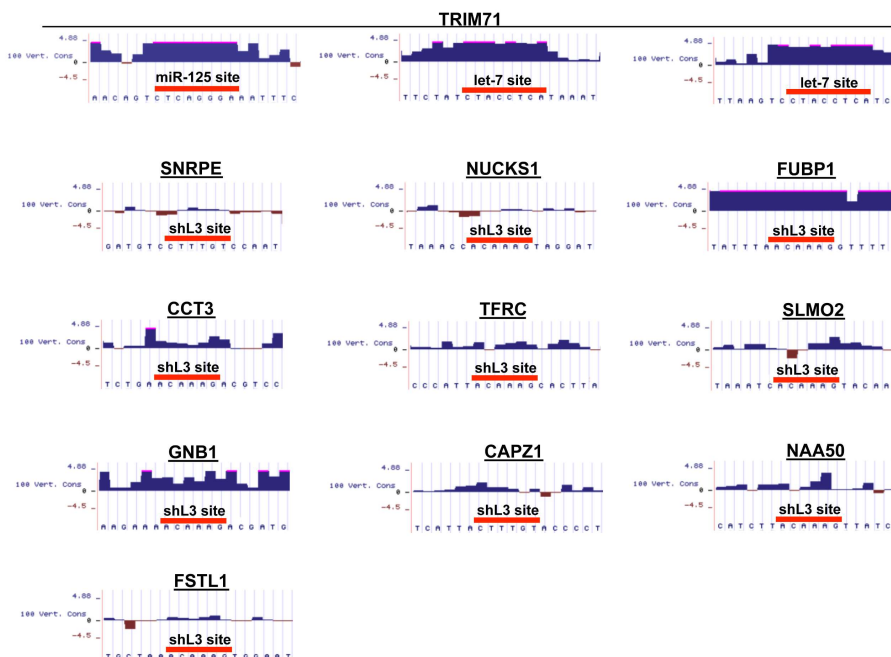


**Figure 5.2 – Lack of seed match conservation in DISE targets.** Conservation landscape of the seed match sequences for the shL3 seed match sites in the 10 downregulated survival genes shown in **Figure 3.10B** and highly conserved let-7 and miRNA-125 seed match sites in the conserved target TRIM71<sup>191</sup>. Conservation landscape generated in the UCSC Genome Browser (<https://genome.ucsc.edu/>) using the PhyloP tract.

pattern like what is often found for highly conserved miRNA seed match targets (**Figure 5.2**). This suggests DISE can be induced in the absence of strong selective pressure reinforcing specific guide RNA-target interactions.

Now, conservation of a miRNA target site often correlates with repressibility/functionality, as selection will retain molecular features conducive to binding, and many miRNA-target pairs show signs of co-evolution<sup>42,111,131,435</sup>. A few well-known examples include the interactions between *lin-4* and *lin-28* and between *let-7* and *lin-41/let-60-RAS*, which play crucial roles in animal development<sup>189,190,192,436</sup>. However, there are also many miRNAs that perform conserved functions in the *absence* of overt seed match conservation in their targets<sup>41,101,112,132,246,437-444</sup>. Although these miRNAs are, themselves, often conserved, their targets' site conservation is, in many cases, only slightly higher than that expected by chance between highly divergent lineages<sup>190,436,445,446</sup>. Now, it is likely some of these nonconserved sites accumulate by chance in genes not co-expressed in the same tissue as their corresponding miRNAs<sup>202</sup>, but nonconserved *de novo* seed matches that appear in co-expressed genes by chance would be eventually selected against due to detrimental targeting by random miRNA-target interactions<sup>447</sup>. This ensures seed matches located in co-expressed target genes, whether conserved or nonconserved, play at least some functional role.

Some of these miRNAs that carry out conserved functions often target the same or similar process(es)/pathways in different organisms through regulating different sets of targets that are, however, all part of that common targeted gene cohort/pathway shared amongst distinct lineages<sup>195,436,448</sup>. A few examples of miRNAs that exhibit this conserved *systems-level* targeting are miRNA-125b<sup>187</sup> and miRNA-8<sup>188,449</sup>, which regulate p53 network dosage and the Wnt

signaling pathways, respectively, in multiple divergent species even though the precise pathway constituents being targeted are different and their seed match sites are not conserved.

The lack of seed match conservation in systems-level miRNA targeting can be attributed to, at least, four factors: (1) The ease with which target sites can be destroyed; a single nt substitution can obliterate the effectivity of the contiguous seed match sequence required by a miRNA to recruit the RISC<sup>450</sup>. (2) The short length of an effective seed match and diversity of sequences in 3' UTRs would cause a high rate of *de novo* site generation<sup>451</sup>. (3) There is a high rate of *de novo* miRNA generation as well<sup>452</sup>, which can decrease the selective pressure on other pre-existing miRNA-target interactions that regulate a function redundantly with the new miRNA-target pairs. (4) There are *multiple* genes regulated in the same pathways/cohorts by any *single* miRNA. Therefore, loss of a seed match site in any single target 3' UTR is negligible<sup>187,443,452,453</sup> to the miRNA's overall functionality.

In this way, genetic drift can continually redefine the target profile of these miRNAs through time, thereby contributing to a high turn-over rate for miRNA seed match sites and preventing specific miRNA-target conservation from being established over the long-run. However, these miRNA will always continue to acquire new targets from the pathway/cohort it is targeting, provided this offers some evolutionary advantage, which contributes to the conservation between the miRNA and the targeted pathway/system<sup>187,454</sup>. In other words, a miRNA can preferentially target a specific cohort of genes, even in the absence of individual overt miRNA-target co-evolution, provided selective pressure is occurring at the systems level. Basically, the conservation is "spread out" or diluted across all the target sites in a single pathway, which lessens the conservation of any individual seed match.



DISE likely represents another example of this conserved systems-level seed-based targeting, as our toxic guide RNA seed sequences can induce DISE in multiple cancer cell types from both human and mouse<sup>376</sup>, which all have different mRNA expression profiles; this suggests functional and systems-level conservation of this process as a cell-autonomous tumor surveillance system regardless of the tissue/organism of origin. The robust nature of DISE as a tumor-killing program can be explained by our data showing toxic guide RNAs derived from CD95/CD95L mRNA sequences repress expression of many different genes from the same cohort of survival genes. Having a certain level of targeted promiscuity permits DISE activation independently of the exact mRNA milieu. This also means mutation of any subset of survival genes' seed matches (or anywhere in any single gene) will not confer resistance in cancer cells, since DISE relies on systems-level targeting through seed-dependent RNAi that represses a *multitude* of genes that harbor seed matches within the survival gene cohort and not on repression of any single survival gene. In other words, even if a cancer cell can adapt to having one or a few survival genes repressed, the systems-level seed-based targeting nature of DISE-inducing guide RNAs ensures many other survival genes will also be repressed, which is a situation cancer cells cannot develop resistance to easily. Finally, survival genes are, by their definition, ubiquitously expressed and therefore, are always targetable, provided a 3' UTR seed match is present. This is consistent with our previously published results showing that knock down of any individual gene or treatment with different pathway inhibitors or any compound from the Preswick library failed to rescue cancer cells from DISE<sup>376</sup>.

### **Basis of Preferential Survival Gene Targeting/Downregulation: Gene Regulatory Network**

This unique gene cohort-specific targeting behavior is unique because these CD95/CD95L-derived si/shRNAs, which all induce the same DISE program in cancer cells with the same morphological and biochemical features by targeting survival genes, all have different sequences with divergent seed regions. If this were a conventional sOTE, each divergent seed sequence would presumably lead to non-recurring changes in gene expression and therefore divergent cell responses. But this is not observed during DISE; it is a recurring and specific cancer cell response ushered in by many non-overlapping guide RNAs (derived from the CD95/CD95L mRNA sequences). This is the consequence of survival and proliferative genes being preferentially targeted both directly by seed-based RNAi and then, indirectly, downstream of the seed match-containing target that resides in the same pathway. This preferential targeting could be the result of the unique and/or altered gene regulatory networks (GRNs) that control expression of survival and proliferative genes in cancer cells. Although these GRNs likely contribute to oncogenesis, we hypothesize they also make the critical genes embedded in these networks more liable to both direct and indirect targeting through RNAi, regardless of the exact seed sequence.

Transcription factors (TFs), miRNAs, and their co-regulated targets are key components of GRNs<sup>455-457</sup>. Four common loop motifs found in GRNs are negative and positive feedback loops (**Figure 5.3A**) and coherent and incoherent feedforward loops (**Figure 5.3B**). These loop motifs exert different regulatory control over the genes embedded in them and play conserved roles in homeostasis<sup>458</sup>, cell fate switches/differentiation<sup>459-463</sup>, cell death<sup>464,465</sup>, and the cell cycle<sup>466-468</sup>. They are often altered/disabled or commandeered in cancer to drive oncogenesis<sup>458,467,469-472</sup>.

Feedback loops (FBLs) are characterized as two factors, such as a TF and miRNA,

mutually regulating each other. In negative FBLs, these two factors regulate the expression of each other in opposite directions, whereas the constituents of a positive FBL mutually regulate each other in the same direction (**Figure 5.3A**; reviewed in <sup>473</sup>). Incoherent feedforward loops (FFLs) involve an apical factor that regulates a target through both direct and indirect regulatory arms in opposite directions. Coherent FFLs are similar, except both the direct and indirect regulatory arms drive expression of the co-target in the same direction (**Figure 5.3B**; reviewed in <sup>473</sup>).

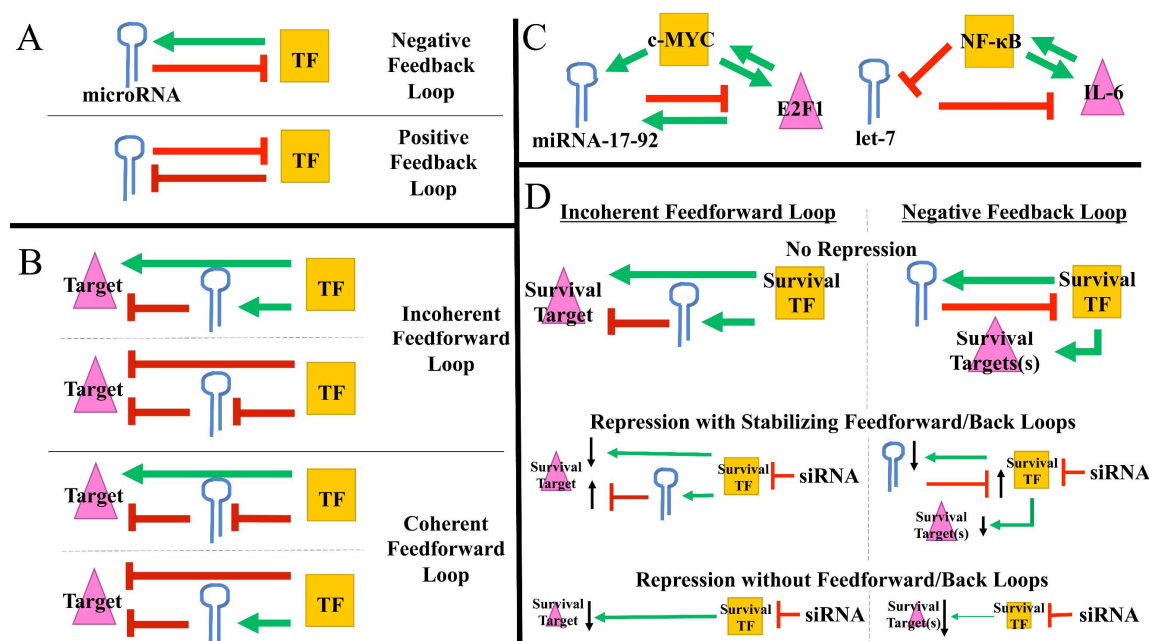


**Figure 5.3 – RNAi seed-based repression of genes embedded in feedforward and feedback loops composed of TFs and miRNAs.** (A) Schematics of negative and positive FBLs between TFs and miRNAs. Green arrow indicates positive regulatory relationship. Red line indicates repressive regulatory relationship. (B) Schematics of incoherent and coherent FFLs, which includes a master TF regulating a target through two arms: a direct arm and an indirect arm that utilizes a miRNA intermediary regulator. (C) The c-MYC/miRNA-17-92/E2F1 and NF-κB/let-7/IL-6 GRN motifs. (D) TFs that positively regulate expression of survival (and proliferative) target genes are, by definition, survival genes (referred to as survival TFs). These TFs can regulate survival target genes through incoherent FFLs and negative FBLs to stabilize gene expression. The counter-balancing regulation afforded by miRNAs in these motifs may dampen repression of target genes or both TFs and downstream target genes in incoherent FFLs and negative FBLs, respectively, mediated by RNAi seed-based targeting of the TFs. In cancers, miRNAs are often downregulated, which would eliminate this regulatory counterbalance and therefore, make target genes and TFs more susceptible to both primary seed-based repression and downstream secondary repression. Size of the triangle or square correlates with the relative expression of target genes and TFs, respectively. Thickness of the arrows and lines indicates the relative intensity of the regulatory relationship. The length and direction of the black arrows indicate whether the alterations in the intensity of the regulatory relationships caused by the introduced siRNA represses (down arrow) or enhances (up arrow) expression of the downstream element that is receiving the regulatory input.

Both tumor suppressive and oncogenic miRNAs exist, and their classification often

depends on their role in GRNs. Consider the c-MYC/miRNA-17-92/E2F1 network depicted in **Figure 5.3C**. It is a composite network that regulates cell cycle entry/progression and is composed of an incoherent FFL with an embedded negative FBL (and a transcription-based positive FBL), which both depend on the miRNA-17-92 cluster<sup>468,474</sup>. As is characteristic of negative FBLs, the mutual regulation between the cell cycle regulator E2F1 and miRNA-17-92 buffers the former from noise produced by extrinsic disturbance or intrinsic stochastic fluctuations in promoter activity by providing a counterbalancing force opposite to the direction<sup>475,476</sup>. This behavior is tumor suppressive, as it prevents tumor progression due to fluctuations in upstream factors or noisy promoter expression that may shift E2F expression toward inducing cell cycle entry<sup>477,478</sup>. Indeed, the miRNA-17-92 cluster is deleted in roughly one fifth of ovarian, melanoma, and breast cancers<sup>479</sup>. Incoherent FFLs also buffer against noise induced by outside perturbation<sup>480</sup>, but in the context of this c-MYC/miRNA-17-92/E2F1 network, the combination of the incoherent FFL and FBLs creates a pulse-like expression profile, which is necessary for accurate timing of E2F1 accumulation needed to drive the cell cycle<sup>467,481</sup>. This composite FFL/FBL motif also limits over-accumulation of E2F1 when oncogenic c-MYC is present, thereby preventing activation of the G<sub>1</sub> checkpoint and apoptosis<sup>481</sup>. In this way, miRNA-17-92 can also function as an oncogene by keeping the E2F1 expression profile within a proliferative range in the presence of oncogenic c-MYC. Indeed, lymphomas will often elevate miRNA-17-92 expression to the cell death that normally accompanies unrestricted cell cycle progression<sup>482,483</sup>. Therefore, miRNA-17-92 can act as either a tumor suppressor or oncogene in the same GRN, depending on the events that drive the oncogenesis of the cancer.

Another composite GRN involved in oncogenesis is the NF- $\kappa$ B/let-7/IL-6 network (**Figure**

5.3C), which is composed of a coherent FFL and positive FBL<sup>472</sup>. In this context, let-7 acts a tumor suppressor by limiting inflammation-driven oncogenic transformation<sup>189,484</sup>. Coherent FFLs function to limit leaky transcription<sup>456,485</sup>. Consistently, let-7 represses expression of the cytokine IL-6, thereby preventing noise-driven induction of an inflammatory response and tumorigenesis. However, in the presence of potent NF- $\kappa$ B activation, both arms of the coherent FFL lead to activation of IL-6, which then positively feeds back on NF- $\kappa$ B<sup>472</sup>. In contrast to negative FBLs, constituents of positive FBLs mutually regulate each other in the same direction, forming a self-reinforcing FBL. Small perturbations to the system are magnified, which permits efficient transition between cell states<sup>486,487</sup>. In this way, activation of NF- $\kappa$ B can overcome the repression of let-7 and induce a potent inflammatory response, which drives oncogenesis<sup>472</sup>.

So clearly, miRNA/TF-mediated GRNs play critical tumor suppressive and oncogenic roles. This is interesting, considering proliferating cells, including cancer cells, tend to globally downregulate miRNAs<sup>379,488,489</sup> and shorten their 3' UTRs to eliminate seed match sites<sup>220,490</sup>. Although some miRNAs that play oncogenic roles, such as miRNA-17-92 (depending on the context), might be preserved to maintain GRNs favorable to tumor progression, many GRN motifs that depend on miRNA constituents would be expected to be disabled or re-wired. This is particularly intriguing considering oncogenes seem to be enriched in predicted miRNA/TF-mediated GRN motifs, particularly in FFL motifs<sup>491</sup>. It is believed cancer cells downregulate miRNA targeting to relieve repression of survival and proliferative genes, which is, otherwise, critical to the maintenance of terminally differentiated cells. In addition to relieving direct miRNA targeting, this downregulation likely also contributes to de-repression of oncogenic survival/proliferative genes by disabling and/or re-wiring miRNA-dependent FFLs and FBLs that would otherwise

dampen their expression, which then drives tumor transformation.

Indeed, survival/proliferative (and housekeeping) genes are already poised to be upregulated in the absence of regulatory miRNAs. Genes fundamental to cell survival are under relatively simple and exclusively positive transcriptional control. Consistently, the upstream promoter sequences of these genes are highly divergent because there are only a handful of conserved TF binding sites, which are bound by a small number of *positive* regulatory TFs<sup>492</sup>. Therefore, in the absence of counterbalancing miRNA-mediated gene regulation, the overall net regulation of these survival and proliferative genes is overwhelmingly positive.

However, this kind of extreme positive regulation may actually make survival and proliferative genes more susceptible to exogenous seed-based targeting through a few potential mechanisms: (1) In the absence of miRNAs, the GRNs that normally stabilize genes against noisy perturbation are no longer there, making them more susceptible to seed-based targeting by exogenous RNAi (**Figure 5.3D**). (2) If certain genes are under nearly exclusively positive transcriptional regulation, then introduction of any repressive agent (e.g. siRNA) into the system will invariably lead to repression within the system.

As mentioned previously, miRNAs function to buffer against intrinsic and outside perturbation as part of incoherent FFLs and negative FBLs by offering a counterbalancing force. These GRNs are fully intact in normal cells since they play important roles in preventing noise-driven disturbances to physiological processes and tumorigenesis. In this context, it can be reasonably expected that outside repression through exogenous siRNAs (or endogenous guide RNAs that do not participate in GRNs such as those locked in mRNAs; see following section **DISE-Inducing Guide RNAs Derived from CD95L mRNAs**) would have minimal repressive

impact on TFs or target genes participating in these GRN motifs or genes regulated downstream, as the endogenous miRNAs that also participate in these motifs would offer a counter-balancing force to the repression (**Figure 5.3D**). Now, cancer cells derive a distinct advantage from disrupting these stabilizing motifs, as the resulting heterogeneity of noisy gene expression may make them more adaptable to different microenvironments<sup>478,493-495</sup>. However, this advantage comes at a price because genes that were formerly part of these stabilizing motifs will presumably become more susceptible to outside perturbation, as that induced by exogenous siRNAs (**Figure 5.3D**), which is consistent with a previous report showing seed-based repression with an exogenous siRNA is strong when endogenous miRNA seed match sites are absent<sup>127</sup>. This creates a distinct weakness for cancer cells compared to normal cells, as gene expression in the former is more unstable, which may also explain our data showing transformed cells are more susceptible to DISE than non-transformed cells<sup>376</sup>.

However, this does not necessarily explain why survival and proliferative genes are *preferentially* targeted during DISE induced by a si/shRNA. An intriguing possibility is that these genes are particularly dependent on these stabilizing networks in normal cells, to prevent neoplastic transformation, compared to other gene cohorts. This is consistent with reports demonstrating (1) enrichment of oncogenes amongst predicted FFLs<sup>491</sup> and (2) that the only recurring phenotypic change in response to shortening 3' UTRs or depleting miRNAs is accelerated growth<sup>148,220,490,496-498</sup>.

Additionally, survival and proliferative genes might be more susceptible to RNAi simply because there are no negative regulatory elements governing expression of these genes. In a mixed network, introduction of repressive elements (e.g. siRNAs) can perturb expression of either

positive or negative regulators, which may, in turn, diminish the overall direction and magnitude of the perturbation. In a completely positive regulatory system (e.g. no miRNAs and only positive regulatory TFs), introduction of any repressive element will invariably lead to inhibition of gene expression because repression of a positive regulatory leads to repression of the downstream element(s).

To determine how miRNA-mediated FFLs or FBLs affect the level of gene deregulation as a result of exogenous seed-based targeting, one could observe how the gene expression profile changes in response to introducing an exogenous RNAi reagent (such as a DISE-inducing siRNA derived from CD95/CD95L) between wild type and either *Dicer*<sup>-/-</sup> or *Drosha*<sup>-/-</sup> cells or in cells where a particular miRNA or cluster of miRNAs is knocked out. Genes that display distinct or similar levels of repressibility between the wild type and knock out cells could then be assessed for the presence/absence of regulatory FFLs/FBLs using bioinformatic methods. It would be expected that mRNAs harboring endogenous 3' UTR seed matches to co-expressed miRNAs would become more repressed in the knock out cells, provided those genes were part of stabilizing FFL/FBL-containing GRN motif that became disabled in the absence of its obligate miRNA. However, the opposite result might be observed if the deregulated genes were part of a positive FBLs, as these motifs function to enhance perturbations to the network (**Figure 5.3A**). Enrichment of survival/proliferative genes (or any GO term) amongst those genes whose repression is enhanced or stabilized upon miRNA depletion in *Drosha*<sup>-/-</sup> and *Dicer*<sup>-/-</sup> compared to wild type cells can then be analyzed. Analysis of how TF/miRNA-based FFLs and FBLs are altered during tumorigenesis could be done by comparing both miRNA and protein-coding gene expression data from matched normal and cancer tissue samples and then mapping TF and miRNA binding sites



using established target prediction methods<sup>131,499</sup>.

In parallel, we can determine whether loop motifs insulate (or enhance) a target gene from seed-based or secondary repression by introducing an exogenous si/shRNA into cells and then performing parallel microarray/RNA-Seq analysis and immunoprecipitation of crosslinked AGO/RNA complexes<sup>123,500</sup>. This would allow identification of mRNAs that are successfully targeted by the RISC through the exogenous RNAi reagent but whose repression remains unchanged, which would be consistent with compensatory gene regulation counteracting the repressive RNAi.

Downregulation of survival genes by DISE-inducing si/shRNAs occurs first through seed-based targeting and then via secondary downregulation of downstream genes, as evidenced by the presence of downregulated survival genes that did not contain seed matches to the introduced si/shRNAs. Inferring the GRNs that regulate survival genes using TF and miRNA target site prediction algorithms/databases and differential gene expression analysis from our RNA-Seq data gathered from cells infected with DISE-inducing shRNAs would allow us to determine how a relatively small number of primary seed-based targeting events leads to global downregulation of survival genes and whether FFLs/FBLs mitigate this permeation.

### **Basis of Preferential Survival Gene Targeting/Downregulation: Seed Base Composition**

Besides the potential role GRN motifs play in making survival genes more vulnerable to direct or indirect seed-based repression, the composition of the seed sequence may also dictate whether a sOTE will manifest as DISE. Although the exact correlation is disputed, several studies showed a statistical enrichment of housekeeping/survival genes in GC-rich isochore regions in the

genome<sup>214-216</sup>. This is consistent with the positive correlation observed between the *in silico* toxicity index and GC content of the seed sequence in **Figure 3.23E**, which supports GC-rich seed sequences are biased toward targeting survival genes with presumably GC-rich 3' UTRs and, therefore, seed matches. It would be interesting to see whether GC enrichment is conserved in certain survival cohorts among multicellular organisms and whether this enrichment is constrained to regions of the 3' UTR that are most amenable to RNAi seed-based targeting (e.g. beginning or end of 3' UTR at least 15 nts away from stop codon<sup>118</sup>), which would be consistent with GC-rich seed matches in these cohorts conferring a fitness advantage.

Beyond general GC content of the seed, it is possible that specific nucleobases are favored at certain positions to trigger DISE. Large-scale libraries consisting of thousands of shRNAs have revealed certain position effects significantly enhance *on-target* potency<sup>501,502</sup>. The Peter lab has recently adapted such an approach to studying DISE; a library of siRNAs containing every possible seed sequence permutation (4096 6mer seed sequences) has now been tested in the lab, and it revealed that certain bases at specific positions favor toxicity. Interestingly, it seems that guanines at the first two positions of the seed (positions two to four of the guide strand) contribute the most to toxicity (**Figure 5.4A**), which is consistent with the current understanding that AGOs first scan the target mRNA using only a few nts in the seed sequence for base pairing<sup>503</sup>.

### **DISE as a Driver of miRNA Evolution**

Although it was discovered using CD95/CD95L-derived si/shRNAs, DISE is a seed-dependent phenomenon, and as such, it is expected any guide RNA with the right seed sequence characteristics can activate the program. This would presumably have drastic effects on the

evolution of new miRNAs. Numerous bioinformatic studies across different organisms suggest that the turn-over of new miRNA species is very high—there is a high “birth rate” of new potential miRNAs followed by rapid loss of most of these candidates, with only a small fraction “surviving” to be a highly expressed miRNA<sup>185,504,505</sup>. This is consistent with the expression of young miRNAs often being much lower than older well-established miRNAs, which is thought to limit deleterious target repression<sup>185,506</sup>. Furthermore, transgenic expression of orthologous miRNAs in related but distinct *Drosophila* species often results in adverse developmental defects<sup>447</sup>, suggesting foreign miRNAs, and likely *de novo* miRNAs, can be toxic to cells.

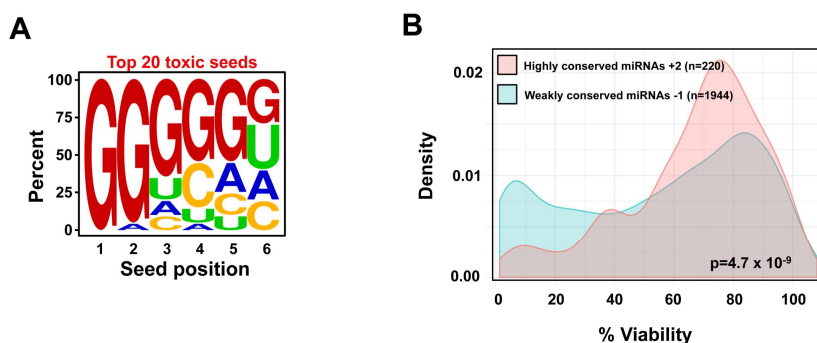


**Figure 5.4 – Nucleotide and evolutionary characteristics of toxic seed sequences.** (A) Nucleotide composition of each position of the seed sequence in the top 20 most toxic siRNAs identified in the arrayed screen of 4096 siRNAs transfected into HeyA8 cells, encompassing every possible 6mer permutation in the seed region. (B) Probability density plots describing the distribution of seed toxicity assigned to the nonconserved and highly conserved seed family miRNAs in the TargetsScan 7.1 human database based on the toxicity identified in the 4096 siRNA screen. Marcus Peter performed analysis for **Figure 5.4A**; Will Putzbach performed analysis for **Figure 5.4B**. Sarah Fazal from the Institute for Genomics and Systems Biology at University of Chicago performed the siRNA screen.

It would be interesting to determine whether this deleterious target repression is a manifestation of DISE and whether it plays any role in the initial selection of miRNAs before established seed/target interactions can be forged by evolution. Specifically, does DISE eliminate or lessen the expression of young potentially deleterious miRNAs through repressive selection? Is there selective pressure to eliminate DISE-inducing seed sequences?

To begin to answer these questions, every miRNA arm in the TargetsScan 7.1 human

database was assigned a toxicity score (sTOX) corresponding to the toxicity induced by the siRNA with the matching seed sequence from the 4096-siRNA screen. Interestingly, there was a striking enrichment of toxic seed sequences in nonconserved seed family miRNA members compared to highly conserved miRNAs (**Figure 5.4B**; p-value =  $5.6 \times 10^{-9}$  according to the Kolmogorov-Smirnov test). Using publicly-available databases of miRNA expression, this analysis could be expanded to determine whether miRNAs with a high sTOX are less expressed or more restrained to specific tissues. Statistical tests for selective neutrality will also allow us to determine the type of selection driving the evolution of miRNAs with toxic versus non-toxic seed sequences. Presumably, if a nonconserved/young miRNA contains a DISE-inducing seed sequence and is expressed, it would be under tremendous negative selection.

### **Relationship between DISE and miRNAs in Cancer**

Besides the elimination or repression of potentially deleterious miRNAs, there are circumstances where maintaining an arsenal of DISE-inducing miRNAs would be beneficial—particularly as tumor suppressors. Oncogenic and tumor suppressive miRNAs both exist, and depending on the cancer type, a miRNA can function in either role. However, there are a handful of miRNAs that act as tumor suppressors regardless of cancer cell type, including miRNAs 34a<sup>507-509</sup>, 15a<sup>510,511</sup>, and 320a<sup>512,513</sup>. It is possible miRNAs like these trigger DISE when upregulated in tumor cells, as DISE is largely independent of the mRNA milieu. The DISE-inducing potential of these miRNAs can be assessed by determining whether over-expression causes preferential downregulation of survival genes and evokes the same morphological/biochemical features associated with DISE such as ROS production, DNA damage, and mitotic catastrophe<sup>376</sup>.

Transformed and cancer stem cells are particularly susceptible to DISE<sup>368,376</sup>. Taken together with our data showing both *Dicer*<sup>-/-</sup> and *Drosha*<sup>-/-</sup> cells are hypersensitive to DISE compared to wild type cells, we propose the following model for why cancer cells would be more sensitive than normal cells: In the absence of most endogenous miRNAs, as in *Drosha*<sup>-/-</sup> and *Dicer*<sup>-/-</sup> cells, there are more unoccupied AGO proteins that can associate with toxic DISE-inducing guide RNAs. Comparison between normal and malignant tissues reveals that cancer cells globally downregulate miRNA expression<sup>379</sup>. However, this downregulation also creates a vulnerability, as there are fewer miRNAs to compete with tumor suppressive guide RNAs. Although studies of *Drosophila* and murine embryonic stem cells have shown absence of guide RNAs decreases AGO stability<sup>433,514</sup>, our results found AGO expression to be unaffected in the absence of *Drosha* or *Dicer* in HCT116 cells. Even so, artificial delivery of DISE-inducing siRNAs into tumor cells would presumably re-stabilize AGO expression.

There is also the intriguing possibility that global downregulation of canonical miRNAs serves as a cell-autonomous tumor suppressive fail-safe by enhancing RISC association with toxic miRNAs that do not rely on the canonical miRNA maturation pathway. For example, mature miRNA-320a is produced independently of *Drosha* processing<sup>60,224</sup>, and as shown in **Figure 4.4D**, becomes the dominant RISC-bound guide RNA in the absence of *Drosha*. Interestingly, *Drosha*<sup>-/-</sup> cells demonstrate a significant growth deficit compared to wild type HCT116 cells in culture (**Figure 3.8E and G**), which is consistent with miRNA-320a operating as a tumor suppressor through DISE. Knocking out miRNA-320a in *Drosha*<sup>-/-</sup> cells should restore the growth potential in these cells if it does, indeed, trigger DISE. More broadly, reconstituting these *Drosha* knock out with highly expressed miRNAs found in the wild type HCT116 cells and/or over-expressing any

non-toxic miRNA to compete with potentially toxic noncanonical miRNAs should also restore their growth rate. This could be extended further by showing that reconstituting cancer cells with miRNAs that were downregulated compared to normal cells could inhibit DISE.

### **DISE-Inducing Guide RNAs Derived from CD95L mRNAs**

It was interesting so many toxic sequences were embedded in the ORF of CD95L, which suggested an important biological function for the mRNA of this gene. This prompted us to determine whether full length CD95L mRNA could be toxic to cells. Our results in chapter four show that expression of mutant CD95L cDNA that produces mRNA, but not full-length protein, induces cell death in a manner independent of apoptosis. Over-expression of these mutant cDNAs causes global downregulation of survival genes as well as morphological/biochemical features consistent with DISE. To unequivocally demonstrate the mRNA is responsible for toxicity, and not the result of residual translation of CD95L-derived peptides, the lab is in the process of determining whether synonymous mutation of every codon in CD95L produces a cDNA whose over-expression is inert or toxic. In this way, the sequence and expression of the protein is preserved but the mRNA sequence/structure is completely altered, thereby allowing us to control for potentially non-specific toxicity associated with over-expressing a protein. If the CD95L mRNA underlies toxicity, then alternate codon usage should completely destroy its toxicity in apoptosis-resistant cells.

Although this study has not conclusively proven over-expression of CD95L mRNA can induce DISE through seed-based RNAi targeting, the results in **Figure 4.6** show the CD95L mRNA can be processed (in a Dicer and Drosha-independent manner; see **Figure 4.4A** and **Figure**

4.7A) into small RNAs that incorporate into the RISC, which has never been shown for any mammalian mRNA. If the guide RNAs released from the CD95L mRNA are functional, then its overexpression should knock down expression of a reporter construct harboring a sequence derived from the CD95L mRNA.

The data in **Figure 4.6** suggest larger CD95L fragments are trimmed either right before incorporation into the RISC or by the RISC itself. A similar mechanism exists for human miRNA-451a<sup>225</sup>, where a combination of AGO2 and PARN cleavage/trimming produces the final mature guide RNA. Loading of larger RNAs into the RISC has also been shown for the new class of agotrons, which are comprised of excised introns that get loaded into the RISC directly without Drosha or Dicer pre-processing<sup>230</sup>.

There is an intriguing possibility that postulates a connection between the CD95L protein and the mRNA in DISE induction. As shown in **Figure 4.9**, co-over-expression of CD95 enhances the expression of over-expressed CD95L protein/mRNA and the toxicity evoked by CD95L over-expression. It is possible this interesting behavior is relevant to DISE. Specifically, interaction between CD95 and CD95L may enhance CD95L mRNA expression and thereby increase the abundance of CD95L mRNA fragments.

Yet the connection may go deeper than just increasing the abundance of CD95L mRNA. The Peter lab has recently shown that CD95L interaction with CD95 at the protein level activates a Type I Interferon response, which maintains the cancer stem cell population in apoptosis-resistant cells<sup>367,368</sup>. However, interferon stimulation also mounts a defense response to things like viral integration, which involves activation of the endoribonuclease RNase-L<sup>515,516</sup>. This endoribonuclease, although not very specific, processes the transcriptome and produces, among

other cleavage products, small dsRNA fragments<sup>284</sup> that then activate double-strand RNA sensors such as MDA5, RIG-1, and IPS-1 in a positive feedback loop<sup>517</sup>. It is conceivable that RNase-L processes mRNAs such as CD95L, which produces the initial fragments that get incorporated into the RISC and execute DISE. In this way, CD95 activation can feed into both the apoptosis pathway and DISE—perhaps as a fail-safe mechanism to induce DISE in apoptosis-resistant cells.

Whether stimulation of CD95 signaling enhances DISE induced by the CD95L mRNA can be assessed by determining whether toxicity induced by CD95L mRNA over-expression in apoptosis-resistance cancer cells is enhanced by addition of recombinant ligand. Involvement of interferon signaling and RNase-L can be determined using conventional pathway inhibition and genetic or RNAi-based perturbation experiments. Alternatively, custom CRISPR or RNAi-based screens targeting annotated ribonucleases may elucidate the constituents involved in processing CD95L mRNA.

Such a system would presumably only operate when cell-autonomous CD95L mRNA and protein are both present with CD95. Indeed, *in vivo* stimulation of CD95 through infiltrating T lymphocytes would likely not induce DISE and would instead enhance cancer stemness in apoptosis-resistant cancer cells since cell-autonomous CD95L mRNA is not expressed. There are, however, numerous situations where cancer cells upregulate cell-autonomous CD95L protein and mRNA in response to stressful stimuli normally encountered during carcinogenesis and metastasis, which is consistent with DISE induced by CD95L-derived guide RNAs playing an endogenous role as an anti-tumor mechanism. Such stimuli include genotoxic stress<sup>518-520</sup>, oxidative stress<sup>521-524</sup>, and detachment from extracellular matrix<sup>525,526</sup>. Chemotherapy has also been shown, albeit in a context-dependent manner, to enhance CD95L mRNA and protein expression<sup>527-530</sup>. Although



cancer cells often develop resistance to the CD95L-induced apoptosis triggered by these stressors<sup>387,531,532</sup>, toxicity mediated by the CD95L mRNA through DISE has never been evaluated. Induction of the DISE program under these conditions can be demonstrated by the occurrence of the characteristic biochemical/morphological features of DISE<sup>376</sup> and by showing that toxicity persists when apoptosis is either genetically or pharmacologically inhibited. Additionally, deep sequencing and AGO pull-down experiments will determine whether CD95L-derived guide RNAs are generated and whether survival genes are downregulated. Involvement of CD95 stimulation, following interaction with cell-autonomous CD95L, in enhancing DISE under these conditions could be determined by assessing differences in toxicity and abundance of CD95L-derived guide RNAs following introduction of a small frameshift mutation in the CD95L gene using CRISPR in cells versus wild type cells that express CD95 but lack the capacity for apoptosis.

### **Evolution of Guide RNAs Derived from mRNAs**

The high abundance of si/shRNAs derived from CD95L (and CD95) that all induce the same form of cancer cell death suggests the same selective pressures operate on all guide RNAs that can be processed from these mRNA sequences. This commonly occurs for miRNAs from the same cluster, particularly polycistronic clusters, as they can perform related and/or interdependent functions even if their seed sequences are different<sup>533-535</sup>. Multiple miRNAs co-expressed at the same time, whether as part of a cluster or even from the same polycistron, are under the same selective pressures and will shift their functionality toward achieving a singular desirable cell state or transition since maintaining expression of miRNAs with inconsistent or competing functions is not conducive to maintaining a stable cellular state or executing a directed

response/transition<sup>456,536,537</sup>. Guide RNAs derived from CD95L mRNA are obviously transcriptionally coupled and, therefore, can be expected to perform the same function in cancer cell death. Indeed, all the molecular changes that happen in a cell upon expression of CD95L (especially in CD95-expressing cells) are shaped by evolution to execute efficient cell death (either through apoptosis or DISE), and there is no reason this would be any different for guide RNAs processed from the CD95L mRNA. Functional redundancy amongst these CD95L-derived guide RNAs would be unlikely to compromise the DISE-inducing capacity of any single CD95L-derived guide RNA since, as discussed above, there is a tremendous fitness advantage conferred by an anti-tumor system that uses an arsenal of different molecules that can target a myriad of distinct survival genes: (1) Different cancer cell types with distinct transcriptome profiles can all be targeted and (2) cancer cells cannot develop resistance<sup>376</sup>.

The sequences of guide RNAs derived from protein-coding mRNAs would be constrained, somewhat, to maintain the optimal primary amino acid sequence<sup>538,539</sup>. This constraint, however, does not necessarily limit their capacity to be selected for during evolution to perform conserved functions. Just consider the evolution of miRNAs, which are selected for based on whether they interact with favorable targets. To achieve this, there needs to be enough sequence diversity to ensure miRNAs that would confer a fitness advantage are generated and, therefore, can be selected. This diversity comes from two sources: (1) mutation/alteration of currently expressed miRNAs and (2) the random hairpin structures in the genome that will eventually give rise to expressed miRNAs. The first source depends on expressed miRNAs, particularly those produced from gene duplication, undergoing alteration that impart new or more specialized functions and can be the result of mutation<sup>115,540</sup>, arm switching or using both miRNA arms for targeting<sup>541-543</sup>, or seed-

shifting<sup>544,545</sup>. The second source already has a diverse set of miRNA sequences in the form of random hairpin structures scattered throughout the genome, many of which can be expressed because of pervasive transcription<sup>452,546-548</sup>. In this way, evolution can select favorable miRNAs either from those generated from alteration of currently expressed miRNAs or by preserving the expression of *de novo* miRNAs that come pre-equipped with a favorable seed sequence.

Similar but distinct mechanisms likely drive mRNA-derived guide RNA evolution. Given the constraint on protein-coding mRNA sequences, it is likely the seed sequence diversity of mRNA-derived guide RNAs occurs through (1) synonymous mutation of the mRNA-embedded precursor guide RNA, similar to how sequence diversity manifests from mutation/alteration of expressed miRNAs, and (2) through a mechanism analogous to *de novo* miRNA generation, where non-overlapping and distinct guide RNA sequences are released from the mRNA through differential and/or promiscuous processing mechanisms. Of course, the latter mechanism would require a fine balance between the processing components' promiscuity, which is needed to generate a diverse range of candidate guide RNAs, and specificity, which would allow the processing of favorable guide RNAs to be preserved by selectively disabling the motifs responsible for generating neutral/unfavorable guide RNAs through synonymous mutations. Such a balance is possible, given the flexibility conferred by differential codon usage. In this way, a mRNA can produce a diverse repertoire of guide RNAs without significantly altering the primary amino acid sequence that is coded. Selection can then preserve processing of the mRNA-derived guide RNAs that confer a fitness advantage.

Consistent with undemanding sequence/motifs being recognized by the machinery that releases mRNA-derived guide RNAs, our AGO pull-down data showed 22 guide RNA clusters in

CD95L (**Figure 4.6B to C and E to F**). Once the enzymes responsible for processing the CD95L mRNA are identified (using the methods mentioned in the previous section), their consensus binding sequences can be identified using conventional “foot-printing” assays or by analyzing sequences of the CD95L mRNA fragments that co-precipitate with the identified components. It can then be determined whether these binding sites are differentially conserved compared to the rest of the CD95L mRNA and where else they occur in the transcriptome, which might be indicative of other mRNAs that can give rise to functionally-relevant mRNA-derived guide RNAs.

It is intriguing that CD95L-derived guide RNAs may perform a conserved function in tumor defense, considering these sequences are normally “locked” into the mRNA, except for the brief instances they are likely to be released to execute cell suicide. Presumably, this window of exposure should be enough to develop the systems-level of conserved functionality described previously. Moreover, sequestering guide RNAs away from the transcriptome under basal conditions might be necessary for maintaining an arsenal of toxic tumor suppressive molecules since this would prevent them from being commandeered as regulators of homeostatic or developmental/differentiation programs, as happens to an expressed miRNA that is continually probing members of the transcriptome and co-evolving with target mRNAs/pathways.

### **Donor Genes as Sources of DISE-Inducing Guide RNAs**

Finally, there is no reason to believe that CD95/CD95L are the only genes that have this peculiar activity. Indeed, the Peter lab recently published a list of genes that contain embedded DISE-inducing sequences<sup>378</sup>. It is possible that activation of DISE *in vivo* involves a general degradation/processing mechanism that releases DISE-inducing guide RNAs from multiple

sources—not only CD95 or CD95L. It makes sense that nature would distribute this mRNA-based DISE-inducing capacity over many genes in the genome to prevent accidentally activating it when any one of those genes is upregulated during normal cellular processes. It is more likely there exists an entire network of *donor* genes that can release toxic small RNAs when the appropriate stimulus is encountered, such as that discussed in the previous section **DISE-Inducing Guide RNAs Derived from CD95L mRNAs (Figure 5.5)**. This also ensures that the highest number and

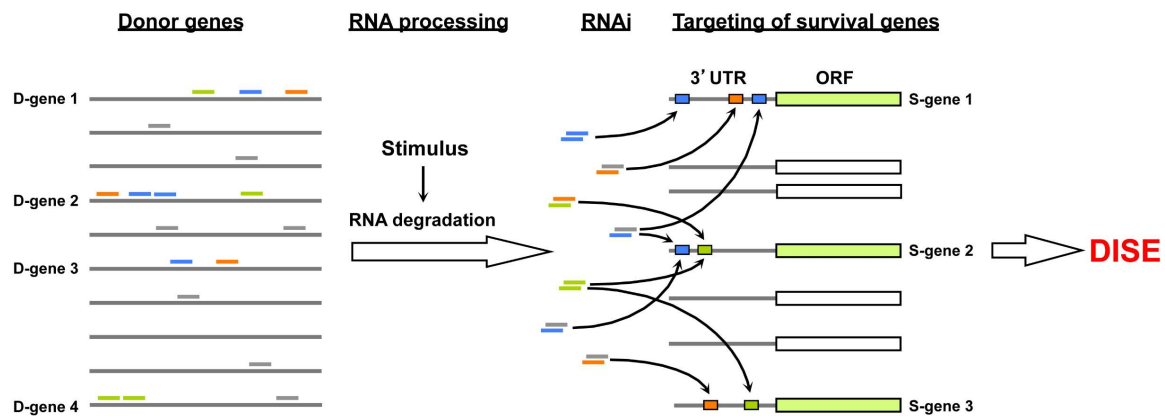


**Figure 5.5 – Triggering DISE *in vivo*.** When a cancer or pre-neoplastic cell encounters the appropriate stimulus, perhaps certain stressors, RNA processing releases guide RNAs from a network of Donor genes (D genes), which include CD95 and CD95L. These endogenous guide RNAs, like the CD95/CD95L-derived si/shRNAs, repress a cohort of survival genes via targeting seed matches located in their 3' UTRs through seed-based targeting, which culminates in DISE cancer cell death.

most diverse set of survival genes are targeted by expanding the diversity of guide RNA sequences released, which would make the opportunity for cancer cell adaption next to impossible. Given the effectivity of DISE as a conserved anti-tumor program in both mouse and human cancer cells, it seems consistent that the stimuli responsible for inducing the release of DISE-inducing guide RNAs from donor genes would be encountered at some point during the oncogenic process—perhaps during times of tumor cell stress, which may cause global destabilization of the transcriptome and the network of donor genes in particular. Future work will be aimed at

identifying this network of donor genes, how they are processed, and the conditions that provide the necessary DISE stimulus.

## References

- 1 Napoli, C., Lemieux, C. & Jorgensen, R. Introduction of a Chimeric Chalcone Synthase Gene into Petunia Results in Reversible Co-Suppression of Homologous Genes in trans. *Plant Cell* **2**, 279-289, doi:10.1105/tpc.2.4.279 (1990).
- 2 Romano, N. & Macino, G. Quelling: transient inactivation of gene expression in *Neurospora crassa* by transformation with homologous sequences. *Mol Microbiol* **6**, 3343-3353 (1992).
- 3 Fire, A., Albertson, D., Harrison, S. W. & Moerman, D. G. Production of antisense RNA leads to effective and specific inhibition of gene expression in *C. elegans* muscle. *Development (Cambridge, England)* **113**, 503-514 (1991).
- 4 Fire, A., Xu, S., Montgomery, M. K., Kostas, S. A., Driver, S. E. & Mello, C. C. Potent and specific genetic interference by double-stranded RNA in *Caenorhabditis elegans*. *Nature* **391**, 806-811, doi:10.1038/35888 (1998).
- 5 Hammond, S. M., Bernstein, E., Beach, D. & Hannon, G. J. An RNA-directed nuclease mediates post-transcriptional gene silencing in *Drosophila* cells. *Nature* **404**, 293-296, doi:10.1038/35005107 (2000).
- 6 Zamore, P. D., Tuschl, T., Sharp, P. A. & Bartel, D. P. RNAi: double-stranded RNA directs the ATP-dependent cleavage of mRNA at 21 to 23 nucleotide intervals. *Cell* **101**, 25-33, doi:10.1016/s0092-8674(00)80620-0 (2000).
- 7 Bernstein, E., Caudy, A. A., Hammond, S. M. & Hannon, G. J. Role for a bidentate ribonuclease in the initiation step of RNA interference. *Nature* **409**, 363-366, doi:10.1038/35053110 (2001).
- 8 Tabara, H., Sarkissian, M., Kelly, W. G., Fleenor, J., Grishok, A., Timmons, L., Fire, A. & Mello, C. C. The *rde-1* gene, RNA interference, and transposon silencing in *C. elegans*. *Cell* **99**, 123-132 (1999).
- 9 Parrish, S. & Fire, A. Distinct roles for RDE-1 and RDE-4 during RNA interference in *Caenorhabditis elegans*. *RNA (New York, N.Y.)* **7**, 1397-1402 (2001).
- 10 Fagard, M., Boutet, S., Morel, J. B., Bellini, C. & Vaucheret, H. AGO1, QDE-2, and RDE-1 are related proteins required for post-transcriptional gene silencing in plants, quelling in fungi, and RNA interference in animals. *Proceedings of the National Academy of Sciences of the United States of America* **97**, 11650-11654, doi:10.1073/pnas.200217597 (2000).
- 11 Cogoni, C. & Macino, G. Isolation of quelling-defective (*qde*) mutants impaired in posttranscriptional transgene-induced gene silencing in *Neurospora crassa*. *Proceedings of the National Academy of Sciences of the United States of America* **94**, 10233-10238 (1997).
- 12 Song, J. J., Smith, S. K., Hannon, G. J. & Joshua-Tor, L. Crystal structure of Argonaute and its implications for RISC slicer activity. *Science (New York, N.Y.)* **305**, 1434-1437, doi:10.1126/science.1102514 (2004).
- 13 Liu, J., Carmell, M. A., Rivas, F. V., Marsden, C. G., Thomson, J. M., Song, J. J., Hammond, S. M., Joshua-Tor, L. & Hannon, G. J. Argonaute2 is the catalytic engine of mammalian RNAi. *Science (New York, N.Y.)* **305**, 1437-1441, doi:10.1126/science.1102513 (2004).
- 14 Elbashir, S. M., Lendeckel, W. & Tuschl, T. RNA interference is mediated by 21- and 22-nucleotide RNAs. *Genes & development* **15**, 188-200 (2001).

- 15 Elbashir, S. M., Harborth, J., Lendeckel, W., Yalcin, A., Weber, K. & Tuschl, T. Duplexes of 21-nucleotide RNAs mediate RNA interference in cultured mammalian cells. *Nature* **411**, 494-498, doi:10.1038/35078107 (2001).
- 16 Brummelkamp, T. R., Bernards, R. & Agami, R. A system for stable expression of short interfering RNAs in mammalian cells. *Science (New York, N.Y.)* **296**, 550-553, doi:10.1126/science.1068999 (2002).
- 17 Moore, C. B., Guthrie, E. H., Huang, M. T. & Taxman, D. J. Short hairpin RNA (shRNA): design, delivery, and assessment of gene knockdown. *Methods in molecular biology (Clifton, N.J.)* **629**, 141-158, doi:10.1007/978-1-60761-657-3\_10 (2010).
- 18 Paddison, P. J., Caudy, A. A., Bernstein, E., Hannon, G. J. & Conklin, D. S. Short hairpin RNAs (shRNAs) induce sequence-specific silencing in mammalian cells. *Genes & development* **16**, 948-958, doi:10.1101/gad.981002 (2002).
- 19 Paddison, P. J., Caudy, A. A., Sachidanandam, R. & Hannon, G. J. Short hairpin activated gene silencing in mammalian cells. *Methods in molecular biology (Clifton, N.J.)* **265**, 85-100, doi:10.1385/1-59259-775-0:085 (2004).
- 20 Paddison, P. J., Silva, J. M., Conklin, D. S., Schlabach, M., Li, M., Aruleba, S., Baliya, V., O'Shaughnessy, A., Gnoj, L., Scobie, K., Chang, K., Westbrook, T., Cleary, M., Sachidanandam, R., McCombie, W. R., Elledge, S. J. & Hannon, G. J. A resource for large-scale RNA-interference-based screens in mammals. *Nature* **428**, 427-431, doi:10.1038/nature02370 (2004).
- 21 Manjunath, N., Wu, H., Subramanya, S. & Shankar, P. Lentiviral delivery of short hairpin RNAs. *Advanced drug delivery reviews* **61**, 732-745, doi:10.1016/j.addr.2009.03.004 (2009).
- 22 Lee, R. C., Feinbaum, R. L. & Ambros, V. The *C. elegans* heterochronic gene *lin-4* encodes small RNAs with antisense complementarity to *lin-14*. *Cell* **75**, 843-854 (1993).
- 23 Griffiths-Jones, S. The microRNA Registry. *Nucleic acids research* **32**, D109-111, doi:10.1093/nar/gkh023 (2004).
- 24 Kozomara, A. & Griffiths-Jones, S. miRBase: annotating high confidence microRNAs using deep sequencing data. *Nucleic acids research* **42**, D68-73, doi:10.1093/nar/gkt1181 (2014).
- 25 Fromm, B., Billipp, T., Peck, L. E., Johansen, M., Tarver, J. E., King, B. L., Newcomb, J. M., Sempere, L. F., Flatmark, K., Hovig, E. & Peterson, K. J. A Uniform System for the Annotation of Vertebrate microRNA Genes and the Evolution of the Human microRNAome. *Annual review of genetics* **49**, 213-242, doi:10.1146/annurev-genet-120213-092023 (2015).
- 26 Lenkala, D., LaCroix, B., Gamazon, E. R., Gleeher, P., Im, H. K. & Huang, R. S. The impact of microRNA expression on cellular proliferation. *Human genetics* **133**, 931-938, doi:10.1007/s00439-014-1434-4 (2014).
- 27 Deng, B., Wang, B., Fang, J., Zhu, X., Cao, Z., Lin, Q., Zhou, L. & Sun, X. MiRNA-203 suppresses cell proliferation, migration and invasion in colorectal cancer via targeting of EIF5A2. *Scientific reports* **6**, 28301, doi:10.1038/srep28301 (2016).
- 28 Liu, L., Cai, X., Liu, E., Tian, X. & Tian, C. MicroRNA-18a promotes proliferation and metastasis in hepatocellular carcinoma via targeting KLF4. *Oncotarget* **8**, 68263-68269, doi:10.18632/oncotarget.19293 (2017).



- 29 Johnnidis, J. B., Harris, M. H., Wheeler, R. T., Stehling-Sun, S., Lam, M. H., Kirak, O., Brummelkamp, T. R., Fleming, M. D. & Camargo, F. D. Regulation of progenitor cell proliferation and granulocyte function by microRNA-223. *Nature* **451**, 1125-1129, doi:10.1038/nature06607 (2008).
- 30 Liu, X., Cheng, Y., Zhang, S., Lin, Y., Yang, J. & Zhang, C. A necessary role of miR-221 and miR-222 in vascular smooth muscle cell proliferation and neointimal hyperplasia. *Circulation research* **104**, 476-487, doi:10.1161/circresaha.108.185363 (2009).
- 31 Geng, L., Zhu, B., Dai, B. H., Sui, C. J., Xu, F., Kan, T., Shen, W. F. & Yang, J. M. A let-7/Fas double-negative feedback loop regulates human colon carcinoma cells sensitivity to Fas-related apoptosis. *Biochemical and biophysical research communications* **408**, 494-499, doi:10.1016/j.bbrc.2011.04.074 (2011).
- 32 Hau, A., Ceppi, P. & Peter, M. E. CD95 is part of a let-7/p53/miR-34 regulatory network. *PLoS one* **7**, e49636, doi:10.1371/journal.pone.0049636 (2012).
- 33 Venkatadri, R., Muni, T., Iyer, A. K., Yakisich, J. S. & Azad, N. Role of apoptosis-related miRNAs in resveratrol-induced breast cancer cell death. *Cell death & disease* **7**, e2104, doi:10.1038/cddis.2016.6 (2016).
- 34 Sherrard, R., Luehr, S., Holzkamp, H., McJunkin, K., Memar, N. & Conradt, B. miRNAs cooperate in apoptosis regulation during *C. elegans* development. *Genes & development* **31**, 209-222, doi:10.1101/gad.288555.116 (2017).
- 35 Makeyev, E. V., Zhang, J., Carrasco, M. A. & Maniatis, T. The MicroRNA miR-124 promotes neuronal differentiation by triggering brain-specific alternative pre-mRNA splicing. *Molecular cell* **27**, 435-448, doi:10.1016/j.molcel.2007.07.015 (2007).
- 36 Naguibneva, I., Ameyar-Zazoua, M., Poleskaya, A., Ait-Si-Ali, S., Groisman, R., Souidi, M., Cuvellier, S. & Harel-Bellan, A. The microRNA miR-181 targets the homeobox protein Hox-A11 during mammalian myoblast differentiation. *Nature cell biology* **8**, 278-284, doi:10.1038/ncb1373 (2006).
- 37 Tsai, D. Y., Hung, K. H., Lin, I. Y., Su, S. T., Wu, S. Y., Chung, C. H., Wang, T. C., Li, W. H., Shih, A. C. & Lin, K. I. Uncovering MicroRNA Regulatory Hubs that Modulate Plasma Cell Differentiation. *Scientific reports* **5**, 17957, doi:10.1038/srep17957 (2015).
- 38 Jung, K. H., McCarthy, R. L., Zhou, C., Uprety, N., Barton, M. C. & Beretta, L. MicroRNA Regulates Hepatocytic Differentiation of Progenitor Cells by Targeting YAP1. *Stem cells (Dayton, Ohio)* **34**, 1284-1296, doi:10.1002/stem.2283 (2016).
- 39 Schratt, G. M., Tuebing, F., Nigh, E. A., Kane, C. G., Sabatini, M. E., Kiebler, M. & Greenberg, M. E. A brain-specific microRNA regulates dendritic spine development. *Nature* **439**, 283-289, doi:10.1038/nature04367 (2006).
- 40 Chen, J. F., Murchison, E. P., Tang, R., Callis, T. E., Tatsuguchi, M., Deng, Z., Rojas, M., Hammond, S. M., Schneider, M. D., Selzman, C. H., Meissner, G., Patterson, C., Hannon, G. J. & Wang, D. Z. Targeted deletion of Dicer in the heart leads to dilated cardiomyopathy and heart failure. *Proceedings of the National Academy of Sciences of the United States of America* **105**, 2111-2116, doi:10.1073/pnas.0710228105 (2008).
- 41 Sokol, N. S. & Ambros, V. Mesodermally expressed *Drosophila* microRNA-1 is regulated by Twist and is required in muscles during larval growth. *Genes & development* **19**, 2343-2354, doi:10.1101/gad.1356105 (2005).

- 42 Friedman, R. C., Farh, K. K., Burge, C. B. & Bartel, D. P. Most mammalian mRNAs are conserved targets of microRNAs. *Genome research* **19**, 92-105, doi:10.1101/gr.082701.108 (2009).
- 43 Lee, Y., Kim, M., Han, J., Yeom, K. H., Lee, S., Baek, S. H. & Kim, V. N. MicroRNA genes are transcribed by RNA polymerase II. *The EMBO journal* **23**, 4051-4060, doi:10.1038/sj.emboj.7600385 (2004).
- 44 Lee, Y., Jeon, K., Lee, J. T., Kim, S. & Kim, V. N. MicroRNA maturation: stepwise processing and subcellular localization. *The EMBO journal* **21**, 4663-4670 (2002).
- 45 He, L., Thomson, J. M., Hemann, M. T., Hernando-Monge, E., Mu, D., Goodson, S., Powers, S., Cordon-Cardo, C., Lowe, S. W., Hannon, G. J. & Hammond, S. M. A microRNA polycistron as a potential human oncogene. *Nature* **435**, 828-833, doi:10.1038/nature03552 (2005).
- 46 Lee, Y., Ahn, C., Han, J., Choi, H., Kim, J., Yim, J., Lee, J., Provost, P., Radmark, O., Kim, S. & Kim, V. N. The nuclear RNase III Drosha initiates microRNA processing. *Nature* **425**, 415-419, doi:10.1038/nature01957 (2003).
- 47 Lagos-Quintana, M., Rauhut, R., Lendeckel, W. & Tuschl, T. Identification of novel genes coding for small expressed RNAs. *Science (New York, N.Y.)* **294**, 853-858, doi:10.1126/science.1064921 (2001).
- 48 Lau, N. C., Lim, L. P., Weinstein, E. G. & Bartel, D. P. An abundant class of tiny RNAs with probable regulatory roles in *Caenorhabditis elegans*. *Science (New York, N.Y.)* **294**, 858-862, doi:10.1126/science.1065062 (2001).
- 49 Han, J., Lee, Y., Yeom, K. H., Nam, J. W., Heo, I., Rhee, J. K., Sohn, S. Y., Cho, Y., Zhang, B. T. & Kim, V. N. Molecular basis for the recognition of primary microRNAs by the Drosha-DGCR8 complex. *Cell* **125**, 887-901, doi:10.1016/j.cell.2006.03.043 (2006).
- 50 Han, J., Lee, Y., Yeom, K. H., Kim, Y. K., Jin, H. & Kim, V. N. The Drosha-DGCR8 complex in primary microRNA processing. *Genes & development* **18**, 3016-3027, doi:10.1101/gad.1262504 (2004).
- 51 Blaszczyk, J., Tropea, J. E., Bubunencko, M., Routzahn, K. M., Waugh, D. S., Court, D. L. & Ji, X. Crystallographic and modeling studies of RNase III suggest a mechanism for double-stranded RNA cleavage. *Structure (London, England : 1993)* **9**, 1225-1236 (2001).
- 52 Partin, A. C., Ngo, T. D., Herrell, E., Jeong, B. C., Hon, G. & Nam, Y. Heme enables proper positioning of Drosha and DGCR8 on primary microRNAs. *Nature communications* **8**, 1737, doi:10.1038/s41467-017-01713-y (2017).
- 53 Ma, H., Wu, Y., Choi, J. G. & Wu, H. Lower and upper stem-single-stranded RNA junctions together determine the Drosha cleavage site. *Proceedings of the National Academy of Sciences of the United States of America* **110**, 20687-20692, doi:10.1073/pnas.1311639110 (2013).
- 54 Gregory, R. I., Yan, K. P., Amuthan, G., Chendrimada, T., Doratotaj, B., Cooch, N. & Shiekhattar, R. The Microprocessor complex mediates the genesis of microRNAs. *Nature* **432**, 235-240, doi:10.1038/nature03120 (2004).
- 55 Denli, A. M., Tops, B. B., Plasterk, R. H., Ketting, R. F. & Hannon, G. J. Processing of primary microRNAs by the Microprocessor complex. *Nature* **432**, 231-235, doi:10.1038/nature03049 (2004).

- 56 Zeng, Y. & Cullen, B. R. Efficient processing of primary microRNA hairpins by Drosha requires flanking nonstructured RNA sequences. *The Journal of biological chemistry* **280**, 27595-27603, doi:10.1074/jbc.M504714200 (2005).
- 57 Auyeung, V. C., Ulitsky, I., McGeary, S. E. & Bartel, D. P. Beyond secondary structure: primary-sequence determinants license pri-miRNA hairpins for processing. *Cell* **152**, 844-858, doi:10.1016/j.cell.2013.01.031 (2013).
- 58 Yi, R., Qin, Y., Macara, I. G. & Cullen, B. R. Exportin-5 mediates the nuclear export of pre-microRNAs and short hairpin RNAs. *Genes & development* **17**, 3011-3016, doi:10.1101/gad.1158803 (2003).
- 59 Martinez, I., Hayes, K. E., Barr, J. A., Harold, A. D., Xie, M., Bukhari, S. I. A., Vasudevan, S., Steitz, J. A. & DiMaio, D. An Exportin-1-dependent microRNA biogenesis pathway during human cell quiescence. *Proceedings of the National Academy of Sciences of the United States of America* **114**, E4961-e4970, doi:10.1073/pnas.1618732114 (2017).
- 60 Kim, Y. K., Kim, B. & Kim, V. N. Re-evaluation of the roles of DROSHA, Exportin 5, and DICER in microRNA biogenesis. *Proceedings of the National Academy of Sciences of the United States of America* **113**, E1881-1889, doi:10.1073/pnas.1602532113 (2016).
- 61 Hutvagner, G., McLachlan, J., Pasquinelli, A. E., Balint, E., Tuschl, T. & Zamore, P. D. A cellular function for the RNA-interference enzyme Dicer in the maturation of the let-7 small temporal RNA. *Science (New York, N.Y.)* **293**, 834-838, doi:10.1126/science.1062961 (2001).
- 62 Macrae, I. J., Zhou, K., Li, F., Repic, A., Brooks, A. N., Cande, W. Z., Adams, P. D. & Doudna, J. A. Structural basis for double-stranded RNA processing by Dicer. *Science (New York, N.Y.)* **311**, 195-198, doi:10.1126/science.1121638 (2006).
- 63 Watanabe, T., Totoki, Y., Toyoda, A., Kaneda, M., Kuramochi-Miyagawa, S., Obata, Y., Chiba, H., Kohara, Y., Kono, T., Nakano, T., Surani, M. A., Sakaki, Y. & Sasaki, H. Endogenous siRNAs from naturally formed dsRNAs regulate transcripts in mouse oocytes. *Nature* **453**, 539-543, doi:10.1038/nature06908 (2008).
- 64 Tam, O. H., Aravin, A. A., Stein, P., Girard, A., Murchison, E. P., Cheloufi, S., Hodges, E., Anger, M., Sachidanandam, R., Schultz, R. M. & Hannon, G. J. Pseudogene-derived small interfering RNAs regulate gene expression in mouse oocytes. *Nature* **453**, 534-538, doi:10.1038/nature06904 (2008).
- 65 Ghildiyal, M., Seitz, H., Horwich, M. D., Li, C., Du, T., Lee, S., Xu, J., Kittler, E. L., Zapp, M. L., Weng, Z. & Zamore, P. D. Endogenous siRNAs derived from transposons and mRNAs in *Drosophila* somatic cells. *Science (New York, N.Y.)* **320**, 1077-1081, doi:10.1126/science.1157396 (2008).
- 66 Siolas, D., Lerner, C., Burchard, J., Ge, W., Linsley, P. S., Paddison, P. J., Hannon, G. J. & Cleary, M. A. Synthetic shRNAs as potent RNAi triggers. *Nature biotechnology* **23**, 227-231, doi:10.1038/nbt1052 (2005).
- 67 Wilson, R. C., Tambe, A., Kidwell, M. A., Noland, C. L., Schneider, C. P. & Doudna, J. A. Dicer-TRBP complex formation ensures accurate mammalian microRNA biogenesis. *Molecular cell* **57**, 397-407, doi:10.1016/j.molcel.2014.11.030 (2015).
- 68 Fareh, M., Yeom, K. H., Haagsma, A. C., Chauhan, S., Heo, I. & Joo, C. TRBP ensures efficient Dicer processing of precursor microRNA in RNA-crowded environments. *Nature communications* **7**, 13694, doi:10.1038/ncomms13694 (2016).

- 69 Ma, J. B., Ye, K. & Patel, D. J. Structural basis for overhang-specific small interfering RNA recognition by the PAZ domain. *Nature* **429**, 318-322, doi:10.1038/nature02519 (2004).
- 70 MacRae, I. J., Zhou, K. & Doudna, J. A. Structural determinants of RNA recognition and cleavage by Dicer. *Nature structural & molecular biology* **14**, 934-940, doi:10.1038/nsmb1293 (2007).
- 71 Park, J. E., Heo, I., Tian, Y., Simanshu, D. K., Chang, H., Jee, D., Patel, D. J. & Kim, V. N. Dicer recognizes the 5' end of RNA for efficient and accurate processing. *Nature* **475**, 201-205, doi:10.1038/nature10198 (2011).
- 72 Gu, S., Jin, L., Zhang, Y., Huang, Y., Zhang, F., Valdmanis, P. N. & Kay, M. A. The loop position of shRNAs and pre-miRNAs is critical for the accuracy of dicer processing in vivo. *Cell* **151**, 900-911, doi:10.1016/j.cell.2012.09.042 (2012).
- 73 Schirle, N. T. & MacRae, I. J. The crystal structure of human Argonaute2. *Science (New York, N.Y.)* **336**, 1037-1040, doi:10.1126/science.1221551 (2012).
- 74 Elkayam, E., Kuhn, C. D., Tocilj, A., Haase, A. D., Greene, E. M., Hannon, G. J. & Joshua-Tor, L. The structure of human argonaute-2 in complex with miR-20a. *Cell* **150**, 100-110, doi:10.1016/j.cell.2012.05.017 (2012).
- 75 Nakanishi, K., Weinberg, D. E., Bartel, D. P. & Patel, D. J. Structure of yeast Argonaute with guide RNA. *Nature* **486**, 368-374, doi:10.1038/nature11211 (2012).
- 76 Wang, Y., Sheng, G., Juranek, S., Tuschl, T. & Patel, D. J. Structure of the guide-strand-containing argonaute silencing complex. *Nature* **456**, 209-213, doi:10.1038/nature07315 (2008).
- 77 Iwasaki, S., Kobayashi, M., Yoda, M., Sakaguchi, Y., Katsuma, S., Suzuki, T. & Tomari, Y. Hsc70/Hsp90 chaperone machinery mediates ATP-dependent RISC loading of small RNA duplexes. *Molecular cell* **39**, 292-299, doi:10.1016/j.molcel.2010.05.015 (2010).
- 78 Leuschner, P. J., Ameres, S. L., Kueng, S. & Martinez, J. Cleavage of the siRNA passenger strand during RISC assembly in human cells. *EMBO reports* **7**, 314-320, doi:10.1038/sj.embor.7400637 (2006).
- 79 Park, J. H. & Shin, C. Slicer-independent mechanism drives small-RNA strand separation during human RISC assembly. *Nucleic acids research* **43**, 9418-9433, doi:10.1093/nar/gkv937 (2015).
- 80 Lingel, A., Simon, B., Izaurralde, E. & Sattler, M. Nucleic acid 3'-end recognition by the Argonaute2 PAZ domain. *Nature structural & molecular biology* **11**, 576-577, doi:10.1038/nsmb777 (2004).
- 81 Boland, A., Tritschler, F., Heimstadt, S., Izaurralde, E. & Weichenrieder, O. Crystal structure and ligand binding of the MID domain of a eukaryotic Argonaute protein. *EMBO reports* **11**, 522-527, doi:10.1038/embor.2010.81 (2010).
- 82 Wang, Y., Juranek, S., Li, H., Sheng, G., Tuschl, T. & Patel, D. J. Structure of an argonaute silencing complex with a seed-containing guide DNA and target RNA duplex. *Nature* **456**, 921-926, doi:10.1038/nature07666 (2008).
- 83 Wang, Y., Juranek, S., Li, H., Sheng, G., Wardle, G. S., Tuschl, T. & Patel, D. J. Nucleation, propagation and cleavage of target RNAs in Ago silencing complexes. *Nature* **461**, 754-761, doi:10.1038/nature08434 (2009).

- 84 Parker, J. S., Roe, S. M. & Barford, D. Crystal structure of a PIWI protein suggests mechanisms for siRNA recognition and slicer activity. *The EMBO journal* **23**, 4727-4737, doi:10.1038/sj.emboj.7600488 (2004).
- 85 Schirle, N. T., Sheu-Gruttadauria, J. & MacRae, I. J. Structural basis for microRNA targeting. *Science (New York, N.Y.)* **346**, 608-613, doi:10.1126/science.1258040 (2014).
- 86 Hauptmann, J., Dueck, A., Harlander, S., Pfaff, J., Merkl, R. & Meister, G. Turning catalytically inactive human Argonaute proteins into active slicer enzymes. *Nature structural & molecular biology* **20**, 814-817, doi:10.1038/nsmb.2577 (2013).
- 87 Faehnle, C. R., Elkayam, E., Haase, A. D., Hannon, G. J. & Joshua-Tor, L. The making of a slicer: activation of human Argonaute-1. *Cell reports* **3**, 1901-1909, doi:10.1016/j.celrep.2013.05.033 (2013).
- 88 Lian, S. L., Li, S., Abadal, G. X., Pauley, B. A., Fritzler, M. J. & Chan, E. K. The C-terminal half of human Ago2 binds to multiple GW-rich regions of GW182 and requires GW182 to mediate silencing. *RNA (New York, N.Y.)* **15**, 804-813, doi:10.1261/rna.1229409 (2009).
- 89 Eulalio, A., Huntzinger, E. & Izaurralde, E. GW182 interaction with Argonaute is essential for miRNA-mediated translational repression and mRNA decay. *Nature structural & molecular biology* **15**, 346-353, doi:10.1038/nsmb.1405 (2008).
- 90 Jinek, M., Fabian, M. R., Coyle, S. M., Sonenberg, N. & Doudna, J. A. Structural insights into the human GW182-PABC interaction in microRNA-mediated deadenylation. *Nature structural & molecular biology* **17**, 238-240, doi:10.1038/nsmb.1768 (2010).
- 91 Fabian, M. R., Cieplak, M. K., Frank, F., Morita, M., Green, J., Srikumar, T., Nagar, B., Yamamoto, T., Raught, B., Duchaine, T. F. & Sonenberg, N. miRNA-mediated deadenylation is orchestrated by GW182 through two conserved motifs that interact with CCR4-NOT. *Nature structural & molecular biology* **18**, 1211-1217, doi:10.1038/nsmb.2149 (2011).
- 92 Behm-Ansmant, I., Rehwinkel, J., Doerks, T., Stark, A., Bork, P. & Izaurralde, E. mRNA degradation by miRNAs and GW182 requires both CCR4:NOT deadenylase and DCP1:DCP2 decapping complexes. *Genes & development* **20**, 1885-1898, doi:10.1101/gad.1424106 (2006).
- 93 Chen, C. Y., Zheng, D., Xia, Z. & Shyu, A. B. Ago-TNRC6 triggers microRNA-mediated decay by promoting two deadenylation steps. *Nature structural & molecular biology* **16**, 1160-1166, doi:10.1038/nsmb.1709 (2009).
- 94 Zekri, L., Kuzuoglu-Ozturk, D. & Izaurralde, E. GW182 proteins cause PABP dissociation from silenced miRNA targets in the absence of deadenylation. *The EMBO journal* **32**, 1052-1065, doi:10.1038/emboj.2013.44 (2013).
- 95 Huntzinger, E., Braun, J. E., Heimstadt, S., Zekri, L. & Izaurralde, E. Two PABPC1-binding sites in GW182 proteins promote miRNA-mediated gene silencing. *The EMBO journal* **29**, 4146-4160, doi:10.1038/emboj.2010.274 (2010).
- 96 Zekri, L., Huntzinger, E., Heimstadt, S. & Izaurralde, E. The silencing domain of GW182 interacts with PABPC1 to promote translational repression and degradation of microRNA targets and is required for target release. *Molecular and cellular biology* **29**, 6220-6231, doi:10.1128/mcb.01081-09 (2009).

- 97 Carthew, R. W. & Sontheimer, E. J. Origins and Mechanisms of miRNAs and siRNAs. *Cell* **136**, 642-655, doi:10.1016/j.cell.2009.01.035 (2009).
- 98 Haley, B. & Zamore, P. D. Kinetic analysis of the RNAi enzyme complex. *Nature structural & molecular biology* **11**, 599-606, doi:10.1038/nsmb780 (2004).
- 99 Doench, J. G., Petersen, C. P. & Sharp, P. A. siRNAs can function as miRNAs. *Genes & development* **17**, 438-442, doi:10.1101/gad.1064703 (2003).
- 100 Bagga, S., Bracht, J., Hunter, S., Massirer, K., Holtz, J., Eachus, R. & Pasquinelli, A. E. Regulation by let-7 and lin-4 miRNAs results in target mRNA degradation. *Cell* **122**, 553-563, doi:10.1016/j.cell.2005.07.031 (2005).
- 101 Lewis, B. P., Burge, C. B. & Bartel, D. P. Conserved seed pairing, often flanked by adenosines, indicates that thousands of human genes are microRNA targets. *Cell* **120**, 15-20, doi:10.1016/j.cell.2004.12.035 (2005).
- 102 Zeng, Y., Yi, R. & Cullen, B. R. MicroRNAs and small interfering RNAs can inhibit mRNA expression by similar mechanisms. *Proceedings of the National Academy of Sciences of the United States of America* **100**, 9779-9784, doi:10.1073/pnas.1630797100 (2003).
- 103 Doench, J. G. & Sharp, P. A. Specificity of microRNA target selection in translational repression. *Genes & development* **18**, 504-511, doi:10.1101/gad.1184404 (2004).
- 104 Lim, L. P., Lau, N. C., Garrett-Engele, P., Grimson, A., Schelter, J. M., Castle, J., Bartel, D. P., Linsley, P. S. & Johnson, J. M. Microarray analysis shows that some microRNAs downregulate large numbers of target mRNAs. *Nature* **433**, 769-773, doi:10.1038/nature03315 (2005).
- 105 Nielsen, C. B., Shomron, N., Sandberg, R., Hornstein, E., Kitzman, J. & Burge, C. B. Determinants of targeting by endogenous and exogenous microRNAs and siRNAs. *RNA (New York, N.Y.)* **13**, 1894-1910, doi:10.1261/rna.768207 (2007).
- 106 Kamola, P. J., Nakano, Y., Takahashi, T., Wilson, P. A. & Ui-Tei, K. The siRNA Non-seed Region and Its Target Sequences Are Auxiliary Determinants of Off-Target Effects. *PLoS computational biology* **11**, e1004656, doi:10.1371/journal.pcbi.1004656 (2015).
- 107 Lewis, B. P., Shih, I. H., Jones-Rhoades, M. W., Bartel, D. P. & Burge, C. B. Prediction of mammalian microRNA targets. *Cell* **115**, 787-798 (2003).
- 108 Jackson, A. L., Burchard, J., Schelter, J., Chau, B. N., Cleary, M., Lim, L. & Linsley, P. S. Widespread siRNA "off-target" transcript silencing mediated by seed region sequence complementarity. *RNA (New York, N.Y.)* **12**, 1179-1187, doi:10.1261/rna.25706 (2006).
- 109 Birmingham, A., Anderson, E. M., Reynolds, A., Ilesley-Tyree, D., Leake, D., Fedorov, Y., Baskerville, S., Maksimova, E., Robinson, K., Karpilow, J., Marshall, W. S. & Khvorova, A. 3' UTR seed matches, but not overall identity, are associated with RNAi off-targets. *Nature methods* **3**, 199-204, doi:10.1038/nmeth854 (2006).
- 110 Wei, N., Zhang, L., Huang, H., Chen, Y., Zheng, J., Zhou, X., Yi, F., Du, Q. & Liang, Z. siRNA has greatly elevated mismatch tolerance at 3'-UTR sites. *PloS one* **7**, e49309, doi:10.1371/journal.pone.0049309 (2012).
- 111 Selbach, M., Schwanhausser, B., Thierfelder, N., Fang, Z., Khanin, R. & Rajewsky, N. Widespread changes in protein synthesis induced by microRNAs. *Nature* **455**, 58-63, doi:10.1038/nature07228 (2008).

- 112 Baek, D., Villen, J., Shin, C., Camargo, F. D., Gygi, S. P. & Bartel, D. P. The impact of  
microRNAs on protein output. *Nature* **455**, 64-71, doi:10.1038/nature07242 (2008).
- 113 Lai, C. F., Chen, C. Y. & Au, L. C. Comparison between the repression potency of siRNA  
targeting the coding region and the 3'-untranslated region of mRNA. *BioMed research  
international* **2013**, 637850, doi:10.1155/2013/637850 (2013).
- 114 Gu, S., Jin, L., Zhang, F., Sarnow, P. & Kay, M. A. Biological basis for restriction of  
microRNA targets to the 3' untranslated region in mammalian mRNAs. *Nature structural  
& molecular biology* **16**, 144-150, doi:10.1038/nsmb.1552 (2009).
- 115 Lim, L. P., Lau, N. C., Weinstein, E. G., Abdelhakim, A., Yekta, S., Rhoades, M. W.,  
Burge, C. B. & Bartel, D. P. The microRNAs of *Caenorhabditis elegans*. *Genes &  
development* **17**, 991-1008, doi:10.1101/gad.1074403 (2003).
- 116 Llave, C., Xie, Z., Kasschau, K. D. & Carrington, J. C. Cleavage of Scarecrow-like mRNA  
targets directed by a class of Arabidopsis miRNA. *Science (New York, N.Y.)* **297**, 2053-  
2056, doi:10.1126/science.1076311 (2002).
- 117 Zhang, H., Artiles, K. L. & Fire, A. Z. Functional relevance of "seed" and "non-seed"  
sequences in microRNA-mediated promotion of *C. elegans* developmental progression.  
*RNA (New York, N.Y.)* **21**, 1980-1992, doi:10.1261/rna.053793.115 (2015).
- 118 Grimson, A., Farh, K. K., Johnston, W. K., Garrett-Engle, P., Lim, L. P. & Bartel, D. P.  
MicroRNA targeting specificity in mammals: determinants beyond seed pairing.  
*Molecular cell* **27**, 91-105, doi:10.1016/j.molcel.2007.06.017 (2007).
- 119 Rhoades, M. W., Reinhart, B. J., Lim, L. P., Burge, C. B., Bartel, B. & Bartel, D. P.  
Prediction of plant microRNA targets. *Cell* **110**, 513-520 (2002).
- 120 Parizotto, E. A., Dunoyer, P., Rahm, N., Himber, C. & Voinnet, O. In vivo investigation  
of the transcription, processing, endonucleolytic activity, and functional relevance of the  
spatial distribution of a plant miRNA. *Genes & development* **18**, 2237-2242,  
doi:10.1101/gad.307804 (2004).
- 121 Brodersen, P., Sakvarelidze-Achard, L., Bruun-Rasmussen, M., Dunoyer, P., Yamamoto,  
Y. Y., Sieburth, L. & Voinnet, O. Widespread translational inhibition by plant miRNAs  
and siRNAs. *Science (New York, N.Y.)* **320**, 1185-1190, doi:10.1126/science.1159151  
(2008).
- 122 Hafner, M., Landthaler, M., Burger, L., Khorshid, M., Hausser, J., Berninger, P.,  
Rothballer, A., Ascano, M., Jr., Jungkamp, A. C., Munschauer, M., Ulrich, A., Wardle, G.  
S., Dewell, S., Zavolan, M. & Tuschl, T. Transcriptome-wide identification of RNA-  
binding protein and microRNA target sites by PAR-CLIP. *Cell* **141**, 129-141,  
doi:10.1016/j.cell.2010.03.009 (2010).
- 123 Helwak, A., Kudla, G., Dudnakova, T. & Tollervey, D. Mapping the human miRNA  
interactome by CLASH reveals frequent noncanonical binding. *Cell* **153**, 654-665,  
doi:10.1016/j.cell.2013.03.043 (2013).
- 124 Huang, H., Qiao, R., Zhao, D., Zhang, T., Li, Y., Yi, F., Lai, F., Hong, J., Ding, X., Yang,  
Z., Zhang, L., Du, Q. & Liang, Z. Profiling of mismatch discrimination in RNAi enabled  
rational design of allele-specific siRNAs. *Nucleic acids research* **37**, 7560-7569,  
doi:10.1093/nar/gkp835 (2009).

- 125 De, N., Young, L., Lau, P. W., Meisner, N. C., Morrissey, D. V. & MacRae, I. J. Highly complementary target RNAs promote release of guide RNAs from human Argonaute2. *Molecular cell* **50**, 344-355, doi:10.1016/j.molcel.2013.04.001 (2013).
- 126 van Dongen, S., Abreu-Goodger, C. & Enright, A. J. Detecting microRNA binding and siRNA off-target effects from expression data. *Nature methods* **5**, 1023-1025, doi:10.1038/nmeth.1267 (2008).
- 127 Khan, A. A., Betel, D., Miller, M. L., Sander, C., Leslie, C. S. & Marks, D. S. Transfection of small RNAs globally perturbs gene regulation by endogenous microRNAs. *Nature biotechnology* **27**, 549-555, doi:10.1038/nbt.1543 (2009).
- 128 Wee, L. M., Flores-Jasso, C. F., Salomon, W. E. & Zamore, P. D. Argonaute divides its RNA guide into domains with distinct functions and RNA-binding properties. *Cell* **151**, 1055-1067, doi:10.1016/j.cell.2012.10.036 (2012).
- 129 Elkayam, E., Parmar, R., Brown, C. R., Willoughby, J. L., Theile, C. S., Manoharan, M. & Joshua-Tor, L. siRNA carrying an (E)-vinylphosphonate moiety at the 5' end of the guide strand augments gene silencing by enhanced binding to human Argonaute-2. *Nucleic acids research* **45**, 3528-3536, doi:10.1093/nar/gkw1171 (2017).
- 130 Elkayam, E., Faehnle, C. R., Morales, M., Sun, J., Li, H. & Joshua-Tor, L. Multivalent Recruitment of Human Argonaute by GW182. *Molecular cell* **67**, 646-658.e643, doi:10.1016/j.molcel.2017.07.007 (2017).
- 131 Agarwal, V., Bell, G. W., Nam, J. W. & Bartel, D. P. Predicting effective microRNA target sites in mammalian mRNAs. *eLife* **4**, doi:10.7554/eLife.05005 (2015).
- 132 Krek, A., Grun, D., Poy, M. N., Wolf, R., Rosenberg, L., Epstein, E. J., MacMenamin, P., da Piedade, I., Gunsalus, K. C., Stoffel, M. & Rajewsky, N. Combinatorial microRNA target predictions. *Nature genetics* **37**, 495-500, doi:10.1038/ng1536 (2005).
- 133 John, B., Enright, A. J., Aravin, A., Tuschl, T., Sander, C. & Marks, D. S. Human MicroRNA targets. *PLoS biology* **2**, e363, doi:10.1371/journal.pbio.0020363 (2004).
- 134 Schirle, N. T., Sheu-Gruttadauria, J., Chandradoss, S. D., Joo, C. & MacRae, I. J. Water-mediated recognition of t1-adenosine anchors Argonaute2 to microRNA targets. *eLife* **4**, doi:10.7554/eLife.07646 (2015).
- 135 Broughton, J. P., Lovci, M. T., Huang, J. L., Yeo, G. W. & Pasquinelli, A. E. Pairing beyond the Seed Supports MicroRNA Targeting Specificity. *Molecular cell* **64**, 320-333, doi:10.1016/j.molcel.2016.09.004 (2016).
- 136 Moore, M. J., Scheel, T. K., Luna, J. M., Park, C. Y., Fak, J. J., Nishiuchi, E., Rice, C. M. & Darnell, R. B. miRNA-target chimeras reveal miRNA 3'-end pairing as a major determinant of Argonaute target specificity. *Nature communications* **6**, 8864, doi:10.1038/ncomms9864 (2015).
- 137 Ui-Tei, K., Nishi, K., Takahashi, T. & Nagasawa, T. Thermodynamic Control of Small RNA-Mediated Gene Silencing. *Frontiers in genetics* **3**, 101, doi:10.3389/fgene.2012.00101 (2012).
- 138 Gu, S., Zhang, Y., Jin, L., Huang, Y., Zhang, F., Bassik, M. C., Kampmann, M. & Kay, M. A. Weak base pairing in both seed and 3' regions reduces RNAi off-targets and enhances si/shRNA designs. *Nucleic acids research* **42**, 12169-12176, doi:10.1093/nar/gku854 (2014).



- 139 Kertesz, M., Iovino, N., Unnerstall, U., Gaul, U. & Segal, E. The role of site accessibility in microRNA target recognition. *Nature genetics* **39**, 1278-1284, doi:10.1038/ng2135 (2007).
- 140 Kedde, M., Strasser, M. J., Boldajipour, B., Oude Vrielink, J. A., Slanchev, K., le Sage, C., Nagel, R., Voorhoeve, P. M., van Duijse, J., Orom, U. A., Lund, A. H., Perrakis, A., Raz, E. & Agami, R. RNA-binding protein Dnd1 inhibits microRNA access to target mRNA. *Cell* **131**, 1273-1286, doi:10.1016/j.cell.2007.11.034 (2007).
- 141 Bhattacharyya, S. N., Habermacher, R., Martine, U., Closs, E. I. & Filipowicz, W. Relief of microRNA-mediated translational repression in human cells subjected to stress. *Cell* **125**, 1111-1124, doi:10.1016/j.cell.2006.04.031 (2006).
- 142 Plass, M., Rasmussen, S. H. & Krogh, A. Highly accessible AU-rich regions in 3' untranslated regions are hotspots for binding of regulatory factors. *PLoS computational biology* **13**, e1005460, doi:10.1371/journal.pcbi.1005460 (2017).
- 143 Tominaga, K., Srikantan, S., Lee, E. K., Subaran, S. S., Martindale, J. L., Abdelmohsen, K. & Gorospe, M. Competitive regulation of nucleolin expression by HuR and miR-494. *Molecular and cellular biology* **31**, 4219-4231, doi:10.1128/mcb.05955-11 (2011).
- 144 Mukherjee, N., Corcoran, D. L., Nusbaum, J. D., Reid, D. W., Georgiev, S., Hafner, M., Ascano, M., Jr., Tuschl, T., Ohler, U. & Keene, J. D. Integrative regulatory mapping indicates that the RNA-binding protein HuR couples pre-mRNA processing and mRNA stability. *Molecular cell* **43**, 327-339, doi:10.1016/j.molcel.2011.06.007 (2011).
- 145 Galgano, A., Forrer, M., Jaskiewicz, L., Kanitz, A., Zavolan, M. & Gerber, A. P. Comparative analysis of mRNA targets for human PUF-family proteins suggests extensive interaction with the miRNA regulatory system. *PloS one* **3**, e3164, doi:10.1371/journal.pone.0003164 (2008).
- 146 Kim, H. H., Kuwano, Y., Srikantan, S., Lee, E. K., Martindale, J. L. & Gorospe, M. HuR recruits let-7/RISC to repress c-Myc expression. *Genes & development* **23**, 1743-1748, doi:10.1101/gad.1812509 (2009).
- 147 Glorian, V., Maillot, G., Poles, S., Iacovoni, J. S., Favre, G. & Vagner, S. HuR-dependent loading of miRNA RISC to the mRNA encoding the Ras-related small GTPase RhoB controls its translation during UV-induced apoptosis. *Cell death and differentiation* **18**, 1692-1701, doi:10.1038/cdd.2011.35 (2011).
- 148 Hoffman, Y., Bublik, D. R., Ugalde, A. P., Elkon, R., Biniashvili, T., Agami, R., Oren, M. & Pilpel, Y. 3'UTR Shortening Potentiates MicroRNA-Based Repression of Proliferation Genes in Proliferating Human Cells. *PLoS genetics* **12**, e1005879, doi:10.1371/journal.pgen.1005879 (2016).
- 149 Judge, A. D., Sood, V., Shaw, J. R., Fang, D., McClintock, K. & MacLachlan, I. Sequence-dependent stimulation of the mammalian innate immune response by synthetic siRNA. *Nature biotechnology* **23**, 457-462, doi:10.1038/nbt1081 (2005).
- 150 Manche, L., Green, S. R., Schmedt, C. & Mathews, M. B. Interactions between double-stranded RNA regulators and the protein kinase DAI. *Molecular and cellular biology* **12**, 5238-5248 (1992).
- 151 Minks, M. A., West, D. K., Benveniste, S. & Baglioni, C. Structural requirements of double-stranded RNA for the activation of 2',5'-oligo(A) polymerase and protein kinase of

- interferon-treated HeLa cells. *The Journal of biological chemistry* **254**, 10180-10183 (1979).
- 152 Sioud, M. Induction of inflammatory cytokines and interferon responses by double-stranded and single-stranded siRNAs is sequence-dependent and requires endosomal localization. *Journal of molecular biology* **348**, 1079-1090, doi:10.1016/j.jmb.2005.03.013 (2005).
- 153 Sledz, C. A., Holko, M., de Veer, M. J., Silverman, R. H. & Williams, B. R. Activation of the interferon system by short-interfering RNAs. *Nature cell biology* **5**, 834-839, doi:10.1038/ncb1038 (2003).
- 154 Kariko, K., Bhuyan, P., Capodici, J. & Weissman, D. Small interfering RNAs mediate sequence-independent gene suppression and induce immune activation by signaling through toll-like receptor 3. *Journal of immunology (Baltimore, Md. : 1950)* **172**, 6545-6549 (2004).
- 155 Heil, F., Hemmi, H., Hochrein, H., Ampenberger, F., Kirschning, C., Akira, S., Lipford, G., Wagner, H. & Bauer, S. Species-specific recognition of single-stranded RNA via toll-like receptor 7 and 8. *Science (New York, N.Y.)* **303**, 1526-1529, doi:10.1126/science.1093620 (2004).
- 156 Reynolds, A., Anderson, E. M., Vermeulen, A., Fedorov, Y., Robinson, K., Leake, D., Karpilow, J., Marshall, W. S. & Khvorovova, A. Induction of the interferon response by siRNA is cell type- and duplex length-dependent. *RNA (New York, N.Y.)* **12**, 988-993, doi:10.1261/rna.2340906 (2006).
- 157 Zamanian-Daryoush, M., Marques, J. T., Gantier, M. P., Behlke, M. A., John, M., Rayman, P., Finke, J. & Williams, B. R. Determinants of cytokine induction by small interfering RNA in human peripheral blood mononuclear cells. *Journal of interferon & cytokine research : the official journal of the International Society for Interferon and Cytokine Research* **28**, 221-233, doi:10.1089/jir.2007.0090 (2008).
- 158 Broering, R., Real, C. I., John, M. J., Jahn-Hofmann, K., Ickenstein, L. M., Kleinehr, K., Paul, A., Gibbert, K., Dittmer, U., Gerken, G. & Schlaak, J. F. Chemical modifications on siRNAs avoid Toll-like-receptor-mediated activation of the hepatic immune system in vivo and in vitro. *International immunology* **26**, 35-46, doi:10.1093/intimm/dxt040 (2014).
- 159 Judge, A. D., Bola, G., Lee, A. C. & MacLachlan, I. Design of noninflammatory synthetic siRNA mediating potent gene silencing in vivo. *Molecular therapy : the journal of the American Society of Gene Therapy* **13**, 494-505, doi:10.1016/j.ymthe.2005.11.002 (2006).
- 160 Eberle, F., Giessler, K., Deck, C., Heeg, K., Peter, M., Richert, C. & Dalpke, A. H. Modifications in small interfering RNA that separate immunostimulation from RNA interference. *Journal of immunology (Baltimore, Md. : 1950)* **180**, 3229-3237 (2008).
- 161 Nguyen, D. N., Chen, S. C., Lu, J., Goldberg, M., Kim, P., Sprague, A., Novobrantseva, T., Sherman, J., Shulga-Morskaya, S., de Fougerolles, A., Chen, J., Langer, R. & Anderson, D. G. Drug delivery-mediated control of RNA immunostimulation. *Molecular therapy : the journal of the American Society of Gene Therapy* **17**, 1555-1562, doi:10.1038/mt.2009.147 (2009).
- 162 Grimm, D., Streetz, K. L., Jopling, C. L., Storm, T. A., Pandey, K., Davis, C. R., Marion, P., Salazar, F. & Kay, M. A. Fatality in mice due to oversaturation of cellular

- microRNA/short hairpin RNA pathways. *Nature* **441**, 537-541, doi:10.1038/nature04791 (2006).
- 163 Beer, S., Bellovin, D. I., Lee, J. S., Komatsubara, K., Wang, L. S., Koh, H., Borner, K., Storm, T. A., Davis, C. R., Kay, M. A., Felsher, D. W. & Grimm, D. Low-level shRNA cytotoxicity can contribute to MYC-induced hepatocellular carcinoma in adult mice. *Molecular therapy : the journal of the American Society of Gene Therapy* **18**, 161-170, doi:10.1038/mt.2009.222 (2010).
- 164 Martin, J. N., Wolken, N., Brown, T., Dauer, W. T., Ehrlich, M. E. & Gonzalez-Alegre, P. Lethal toxicity caused by expression of shRNA in the mouse striatum: implications for therapeutic design. *Gene therapy* **18**, 666-673, doi:10.1038/gt.2011.10 (2011).
- 165 Baek, S. T., Kerjan, G., Bielas, S. L., Lee, J. E., Fenstermaker, A. G., Novarino, G. & Gleeson, J. G. Off-target effect of doublecortin family shRNA on neuronal migration associated with endogenous microRNA dysregulation. *Neuron* **82**, 1255-1262, doi:10.1016/j.neuron.2014.04.036 (2014).
- 166 Liang, X. H., Hart, C. E. & Crooke, S. T. Transfection of siRNAs can alter miRNA levels and trigger non-specific protein degradation in mammalian cells. *Biochimica et biophysica acta* **1829**, 455-468, doi:10.1016/j.bbagr.2013.01.011 (2013).
- 167 Ui-Tei, K., Naito, Y., Takahashi, F., Haraguchi, T., Ohki-Hamazaki, H., Juni, A., Ueda, R. & Saigo, K. Guidelines for the selection of highly effective siRNA sequences for mammalian and chick RNA interference. *Nucleic acids research* **32**, 936-948, doi:10.1093/nar/gkh247 (2004).
- 168 Jackson, A. L., Bartz, S. R., Schelter, J., Kobayashi, S. V., Burchard, J., Mao, M., Li, B., Cavet, G. & Linsley, P. S. Expression profiling reveals off-target gene regulation by RNAi. *Nature biotechnology* **21**, 635-637, doi:10.1038/nbt831 (2003).
- 169 Lin, X., Ruan, X., Anderson, M. G., McDowell, J. A., Kroeger, P. E., Fesik, S. W. & Shen, Y. siRNA-mediated off-target gene silencing triggered by a 7 nt complementation. *Nucleic acids research* **33**, 4527-4535, doi:10.1093/nar/gki762 (2005).
- 170 Cullen, B. R. Enhancing and confirming the specificity of RNAi experiments. *Nature methods* **3**, 677-681, doi:10.1038/nmeth913 (2006).
- 171 Puri, N., Wang, X., Varma, R., Burnett, C., Beauchamp, L., Batten, D. M., Young, M., Sule, V., Latham, K., Sendera, T., Echeverri, C., Sachse, C. & Magdaleno, S. LNA incorporated siRNAs exhibit lower off-target effects compared to 2'-OMethoxy in cell phenotypic assays and microarray analysis. *Nucleic acids symposium series (2004)*, 25-26, doi:10.1093/nass/nrn013 (2008).
- 172 Jackson, A. L., Burchard, J., Leake, D., Reynolds, A., Schelter, J., Guo, J., Johnson, J. M., Lim, L., Karpilow, J., Nichols, K., Marshall, W., Khvorova, A. & Linsley, P. S. Position-specific chemical modification of siRNAs reduces "off-target" transcript silencing. *RNA (New York, N.Y.)* **12**, 1197-1205, doi:10.1261/rna.30706 (2006).
- 173 Iribe, H., Miyamoto, K., Takahashi, T., Kobayashi, Y., Leo, J., Aida, M. & Ui-Tei, K. Chemical Modification of the siRNA Seed Region Suppresses Off-Target Effects by Steric Hindrance to Base-Pairing with Targets. *ACS Omega* **2**, 2055-2064, doi:10.1021/acsomega.7b00291 (2017).
- 174 Naito, Y. & Ui-Tei, K. siRNA Design Software for a Target Gene-Specific RNA Interference. *Frontiers in genetics* **3**, 102, doi:10.3389/fgene.2012.00102 (2012).

- 175 Ui-Tei, K., Naito, Y., Nishi, K., Juni, A. & Saigo, K. Thermodynamic stability and Watson-Crick base pairing in the seed duplex are major determinants of the efficiency of the siRNA-based off-target effect. *Nucleic acids research* **36**, 7100-7109, doi:10.1093/nar/gkn902 (2008).
- 176 Zhang, J., Zheng, J., Lu, C., Du, Q., Liang, Z. & Xi, Z. Modification of the siRNA passenger strand by 5-nitroindole dramatically reduces its off-target effects. *Chembiochem : a European journal of chemical biology* **13**, 1940-1945, doi:10.1002/cbic.201200349 (2012).
- 177 Ui-Tei, K., Naito, Y., Zenno, S., Nishi, K., Yamato, K., Takahashi, F., Juni, A. & Saigo, K. Functional dissection of siRNA sequence by systematic DNA substitution: modified siRNA with a DNA seed arm is a powerful tool for mammalian gene silencing with significantly reduced off-target effect. *Nucleic acids research* **36**, 2136-2151, doi:10.1093/nar/gkn042 (2008).
- 178 Khvorova, A., Reynolds, A. & Jayasena, S. D. Functional siRNAs and miRNAs exhibit strand bias. *Cell* **115**, 209-216 (2003).
- 179 Schwarz, D. S., Hutvagner, G., Du, T., Xu, Z., Aronin, N. & Zamore, P. D. Asymmetry in the assembly of the RNAi enzyme complex. *Cell* **115**, 199-208 (2003).
- 180 Amarzguioui, M. & Prydz, H. An algorithm for selection of functional siRNA sequences. *Biochemical and biophysical research communications* **316**, 1050-1058, doi:10.1016/j.bbrc.2004.02.157 (2004).
- 181 Suzuki, H. I., Katsura, A., Yasuda, T., Ueno, T., Mano, H., Sugimoto, K. & Miyazono, K. Small-RNA asymmetry is directly driven by mammalian Argonautes. *Nature structural & molecular biology* **22**, 512-521, doi:10.1038/nsmb.3050 (2015).
- 182 Starega-Roslan, J., Witkos, T. M., Galka-Marciniak, P. & Krzyzosiak, W. J. Sequence features of Drosha and Dicer cleavage sites affect the complexity of isomiRs. *International journal of molecular sciences* **16**, 8110-8127, doi:10.3390/ijms16048110 (2015).
- 183 Sheng, Y., Engstrom, P. G. & Lenhard, B. Mammalian microRNA prediction through a support vector machine model of sequence and structure. *PloS one* **2**, e946, doi:10.1371/journal.pone.0000946 (2007).
- 184 Pasquinelli, A. E., Reinhart, B. J., Slack, F., Martindale, M. Q., Kuroda, M. I., Maller, B., Hayward, D. C., Ball, E. E., Degan, B., Muller, P., Spring, J., Srinivasan, A., Fishman, M., Finnerty, J., Corbo, J., Levine, M., Leahy, P., Davidson, E. & Ruvkun, G. Conservation of the sequence and temporal expression of let-7 heterochronic regulatory RNA. *Nature* **408**, 86-89, doi:10.1038/35040556 (2000).
- 185 Meunier, J., Lemoine, F., Soumillon, M., Liechti, A., Weier, M., Guschanski, K., Hu, H., Khaitovich, P. & Kaessmann, H. Birth and expression evolution of mammalian microRNA genes. *Genome research* **23**, 34-45, doi:10.1101/gr.140269.112 (2013).
- 186 Hertel, J., Lindemeyer, M., Missal, K., Fried, C., Tanzer, A., Flamm, C., Hofacker, I. L. & Stadler, P. F. The expansion of the metazoan microRNA repertoire. *BMC genomics* **7**, 25, doi:10.1186/1471-2164-7-25 (2006).
- 187 Le, M. T., Shyh-Chang, N., Khaw, S. L., Chin, L., Teh, C., Tay, J., O'Day, E., Korzh, V., Yang, H., Lal, A., Lieberman, J., Lodish, H. F. & Lim, B. Conserved regulation of p53 network dosage by microRNA-125b occurs through evolving miRNA-target gene pairs. *PLoS genetics* **7**, e1002242, doi:10.1371/journal.pgen.1002242 (2011).

- 188 Kennell, J. A., Gerin, I., MacDougald, O. A. & Cadigan, K. M. The microRNA miR-8 is a conserved negative regulator of Wnt signaling. *Proceedings of the National Academy of Sciences of the United States of America* **105**, 15417-15422, doi:10.1073/pnas.0807763105 (2008).
- 189 Johnson, S. M., Grosshans, H., Shingara, J., Byrom, M., Jarvis, R., Cheng, A., Labourier, E., Reinert, K. L., Brown, D. & Slack, F. J. RAS is regulated by the let-7 microRNA family. *Cell* **120**, 635-647, doi:10.1016/j.cell.2005.01.014 (2005).
- 190 Chen, K. & Rajewsky, N. Deep conservation of microRNA-target relationships and 3'UTR motifs in vertebrates, flies, and nematodes. *Cold Spring Harbor symposia on quantitative biology* **71**, 149-156, doi:10.1101/sqb.2006.71.039 (2006).
- 191 Schulman, B. R., Esquela-Kerscher, A. & Slack, F. J. Reciprocal expression of lin-41 and the microRNAs let-7 and mir-125 during mouse embryogenesis. *Developmental dynamics : an official publication of the American Association of Anatomists* **234**, 1046-1054, doi:10.1002/dvdy.20599 (2005).
- 192 Moss, E. G. & Tang, L. Conservation of the heterochronic regulator Lin-28, its developmental expression and microRNA complementary sites. *Developmental biology* **258**, 432-442 (2003).
- 193 Chen, K. & Rajewsky, N. Natural selection on human microRNA binding sites inferred from SNP data. *Nature genetics* **38**, 1452-1456, doi:10.1038/ng1910 (2006).
- 194 Tsang, J. S., Ebert, M. S. & van Oudenaarden, A. Genome-wide dissection of microRNA functions and cotargeting networks using gene set signatures. *Molecular cell* **38**, 140-153, doi:10.1016/j.molcel.2010.03.007 (2010).
- 195 Sass, S., Dietmann, S., Burk, U. C., Brabletz, S., Lutter, D., Kowarsch, A., Mayer, K. F., Brabletz, T., Ruepp, A., Theis, F. J. & Wang, Y. MicroRNAs coordinately regulate protein complexes. *BMC systems biology* **5**, 136, doi:10.1186/1752-0509-5-136 (2011).
- 196 Lall, S., Grun, D., Krek, A., Chen, K., Wang, Y. L., Dewey, C. N., Sood, P., Colombo, T., Bray, N., Macmenamin, P., Kao, H. L., Gunsalus, K. C., Pachter, L., Piano, F. & Rajewsky, N. A genome-wide map of conserved microRNA targets in *C. elegans*. *Current biology : CB* **16**, 460-471, doi:10.1016/j.cub.2006.01.050 (2006).
- 197 Landgraf, P., Rusu, M., Sheridan, R., Sewer, A., Iovino, N., Aravin, A., Pfeffer, S., Rice, A., Kamphorst, A. O., Landthaler, M., Lin, C., Succi, N. D., Hermida, L., Fulci, V., Chiaretti, S., Foa, R., Schliwka, J., Fuchs, U., Novosel, A., Muller, R. U., Schermer, B., Bissels, U., Inman, J., Phan, Q., Chien, M., Weir, D. B., Choksi, R., De Vita, G., Frezzetti, D., Trompeter, H. I., Hornung, V., Teng, G., Hartmann, G., Palkovits, M., Di Lauro, R., Wernet, P., Macino, G., Rogler, C. E., Nagle, J. W., Ju, J., Papavasiliou, F. N., Benzing, T., Lichter, P., Tam, W., Brownstein, M. J., Bosio, A., Borkhardt, A., Russo, J. J., Sander, C., Zavolan, M. & Tuschl, T. A mammalian microRNA expression atlas based on small RNA library sequencing. *Cell* **129**, 1401-1414, doi:10.1016/j.cell.2007.04.040 (2007).
- 198 Gurtan, A. M. & Sharp, P. A. The role of miRNAs in regulating gene expression networks. *Journal of molecular biology* **425**, 3582-3600, doi:10.1016/j.jmb.2013.03.007 (2013).
- 199 Gusev, Y., Schmittgen, T. D., Lerner, M., Postier, R. & Brackett, D. Computational analysis of biological functions and pathways collectively targeted by co-expressed microRNAs in cancer. *BMC bioinformatics* **8 Suppl 7**, S16, doi:10.1186/1471-2105-8-s7-s16 (2007).

- 200 Zhang, L., Hammell, M., Kudlow, B. A., Ambros, V. & Han, M. Systematic analysis of dynamic miRNA-target interactions during *C. elegans* development. *Development (Cambridge, England)* **136**, 3043-3055, doi:10.1242/dev.039008 (2009).
- 201 Stark, A., Brennecke, J., Bushati, N., Russell, R. B. & Cohen, S. M. Animal MicroRNAs confer robustness to gene expression and have a significant impact on 3'UTR evolution. *Cell* **123**, 1133-1146, doi:10.1016/j.cell.2005.11.023 (2005).
- 202 Farh, K. K., Grimson, A., Jan, C., Lewis, B. P., Johnston, W. K., Lim, L. P., Burge, C. B. & Bartel, D. P. The widespread impact of mammalian MicroRNAs on mRNA repression and evolution. *Science (New York, N.Y.)* **310**, 1817-1821, doi:10.1126/science.1121158 (2005).
- 203 Zare, H., Khodursky, A. & Sartorelli, V. An evolutionarily biased distribution of miRNA sites toward regulatory genes with high promoter-driven intrinsic transcriptional noise. *BMC evolutionary biology* **14**, 74, doi:10.1186/1471-2148-14-74 (2014).
- 204 Dassi, E., Zuccotti, P., Leo, S., Provenzani, A., Assfalg, M., D'Onofrio, M., Riva, P. & Quattrone, A. Hyper conserved elements in vertebrate mRNA 3'-UTRs reveal a translational network of RNA-binding proteins controlled by HuR. *Nucleic acids research* **41**, 3201-3216, doi:10.1093/nar/gkt017 (2013).
- 205 Winter, J., Roepcke, S., Krause, S., Muller, E. C., Otto, A., Vingron, M. & Schweiger, S. Comparative 3'UTR analysis allows identification of regulatory clusters that drive Eph/ephrin expression in cancer cell lines. *PloS one* **3**, e2780, doi:10.1371/journal.pone.0002780 (2008).
- 206 Larizza, A., Makalowski, W., Pesole, G. & Saccone, C. Evolutionary dynamics of mammalian mRNA untranslated regions by comparative analysis of orthologous human, artiodactyl and rodent gene pairs. *Computers & chemistry* **26**, 479-490 (2002).
- 207 Makalowski, W. & Boguski, M. S. Evolutionary parameters of the transcribed mammalian genome: an analysis of 2,820 orthologous rodent and human sequences. *Proceedings of the National Academy of Sciences of the United States of America* **95**, 9407-9412 (1998).
- 208 Schultz, N., Marenstein, D. R., De Angelis, D. A., Wang, W. Q., Nelander, S., Jacobsen, A., Marks, D. S., Massague, J. & Sander, C. Off-target effects dominate a large-scale RNAi screen for modulators of the TGF-beta pathway and reveal microRNA regulation of TGFBR2. *Silence* **2**, 3, doi:10.1186/1758-907x-2-3 (2011).
- 209 Gumienny, R. & Zavolan, M. Accurate transcriptome-wide prediction of microRNA targets and small interfering RNA off-targets with MIRZA-G. *Nucleic acids research* **43**, 9095, doi:10.1093/nar/gkv924 (2015).
- 210 Buehler, E., Khan, A. A., Marine, S., Rajaram, M., Bahl, A., Burchard, J. & Ferrer, M. siRNA off-target effects in genome-wide screens identify signaling pathway members. *Scientific reports* **2**, 428, doi:10.1038/srep00428 (2012).
- 211 Riba, A., Emmenlauer, M., Chen, A., Sigoillot, F., Cong, F., Dehio, C., Jenkins, J. & Zavolan, M. Explicit Modeling of siRNA-Dependent On- and Off-Target Repression Improves the Interpretation of Screening Results. *Cell systems* **4**, 182-193.e184, doi:10.1016/j.cels.2017.01.011 (2017).
- 212 Lin, X., Morgan-Lappe, S., Huang, X., Li, L., Zakula, D. M., Verneti, L. A., Fesik, S. W. & Shen, Y. 'Seed' analysis of off-target siRNAs reveals an essential role of Mcl-1 in

- resistance to the small-molecule Bcl-2/Bcl-XL inhibitor ABT-737. *Oncogene* **26**, 3972-3979, doi:10.1038/sj.onc.1210166 (2007).
- 213 Arvey, A., Larsson, E., Sander, C., Leslie, C. S. & Marks, D. S. Target mRNA abundance dilutes microRNA and siRNA activity. *Molecular systems biology* **6**, 363, doi:10.1038/msb.2010.24 (2010).
- 214 Vinogradov, A. E. Isochores and tissue-specificity. *Nucleic acids research* **31**, 5212-5220 (2003).
- 215 Semon, M., Mouchiroud, D. & Duret, L. Relationship between gene expression and GC-content in mammals: statistical significance and biological relevance. *Human molecular genetics* **14**, 421-427, doi:10.1093/hmg/ddi038 (2005).
- 216 Lercher, M. J., Urrutia, A. O., Pavlicek, A. & Hurst, L. D. A unification of mosaic structures in the human genome. *Human molecular genetics* **12**, 2411-2415, doi:10.1093/hmg/ddg251 (2003).
- 217 Lianoglou, S., Garg, V., Yang, J. L., Leslie, C. S. & Mayr, C. Ubiquitously transcribed genes use alternative polyadenylation to achieve tissue-specific expression. *Genes & development* **27**, 2380-2396, doi:10.1101/gad.229328.113 (2013).
- 218 Eisenberg, E. & Levanon, E. Y. Human housekeeping genes are compact. *Trends in genetics : TIG* **19**, 362-365, doi:10.1016/s0168-9525(03)00140-9 (2003).
- 219 Blazie, S. M., Geissel, H. C., Wilky, H., Joshi, R., Newbern, J. & Mangone, M. Alternative Polyadenylation Directs Tissue-Specific miRNA Targeting in *Caenorhabditis elegans* Somatic Tissues. *Genetics* **206**, 757-774, doi:10.1534/genetics.116.196774 (2017).
- 220 Mayr, C. & Bartel, D. P. Widespread shortening of 3'UTRs by alternative cleavage and polyadenylation activates oncogenes in cancer cells. *Cell* **138**, 673-684, doi:10.1016/j.cell.2009.06.016 (2009).
- 221 Heo, I., Ha, M., Lim, J., Yoon, M. J., Park, J. E., Kwon, S. C., Chang, H. & Kim, V. N. Mono-uridylation of pre-microRNA as a key step in the biogenesis of group II let-7 microRNAs. *Cell* **151**, 521-532, doi:10.1016/j.cell.2012.09.022 (2012).
- 222 Babiarz, J. E., Ruby, J. G., Wang, Y., Bartel, D. P. & Blelloch, R. Mouse ES cells express endogenous shRNAs, siRNAs, and other Microprocessor-independent, Dicer-dependent small RNAs. *Genes & development* **22**, 2773-2785, doi:10.1101/gad.1705308 (2008).
- 223 Chong, M. M., Zhang, G., Cheloufi, S., Neubert, T. A., Hannon, G. J. & Littman, D. R. Canonical and alternate functions of the microRNA biogenesis machinery. *Genes & development* **24**, 1951-1960, doi:10.1101/gad.1953310 (2010).
- 224 Xie, M., Li, M., Vilborg, A., Lee, N., Shu, M. D., Yartseva, V., Sestan, N. & Steitz, J. A. Mammalian 5'-capped microRNA precursors that generate a single microRNA. *Cell* **155**, 1568-1580, doi:10.1016/j.cell.2013.11.027 (2013).
- 225 Yoda, M., Cifuentes, D., Izumi, N., Sakaguchi, Y., Suzuki, T., Giraldez, A. J. & Tomari, Y. Poly(A)-specific ribonuclease mediates 3'-end trimming of Argonaute2-cleaved precursor microRNAs. *Cell reports* **5**, 715-726, doi:10.1016/j.celrep.2013.09.029 (2013).
- 226 Schamberger, A., Sarkadi, B. & Orban, T. I. Human mirtrons can express functional microRNAs simultaneously from both arms in a flanking exon-independent manner. *RNA biology* **9**, 1177-1185, doi:10.4161/rna.21359 (2012).
- 227 Berezikov, E., Chung, W. J., Willis, J., Cuppen, E. & Lai, E. C. Mammalian mirtron genes. *Molecular cell* **28**, 328-336, doi:10.1016/j.molcel.2007.09.028 (2007).

- 228 Ruby, J. G., Jan, C. H. & Bartel, D. P. Intronic microRNA precursors that bypass Drosha processing. *Nature* **448**, 83-86, doi:10.1038/nature05983 (2007).
- 229 Butkyte, S., Ciupas, L., Jakubauskiene, E., Vilys, L., Mocevicius, P., Kanopka, A. & Vilkaitis, G. Splicing-dependent expression of microRNAs of mirtron origin in human digestive and excretory system cancer cells. *Clinical epigenetics* **8**, 33, doi:10.1186/s13148-016-0200-y (2016).
- 230 Hansen, T. B., Veno, M. T., Jensen, T. I., Schaefer, A., Damgaard, C. K. & Kjems, J. Argonaute-associated short introns are a novel class of gene regulators. *Nature communications* **7**, 11538, doi:10.1038/ncomms11538 (2016).
- 231 Helm, M., Giege, R. & Florentz, C. A Watson-Crick base-pair-disrupting methyl group (m1A9) is sufficient for cloverleaf folding of human mitochondrial tRNA<sup>Lys</sup>. *Biochemistry* **38**, 13338-13346 (1999).
- 232 Schimmel, P. The emerging complexity of the tRNA world: mammalian tRNAs beyond protein synthesis. *Nature reviews. Molecular cell biology* **19**, 45-58, doi:10.1038/nrm.2017.77 (2018).
- 233 Thompson, D. M., Lu, C., Green, P. J. & Parker, R. tRNA cleavage is a conserved response to oxidative stress in eukaryotes. *RNA (New York, N.Y.)* **14**, 2095-2103, doi:10.1261/rna.1232808 (2008).
- 234 Ivanov, P., Emara, M. M., Villen, J., Gygi, S. P. & Anderson, P. Angiogenin-induced tRNA fragments inhibit translation initiation. *Molecular cell* **43**, 613-623, doi:10.1016/j.molcel.2011.06.022 (2011).
- 235 Gebetsberger, J., Zywicki, M., Kunzi, A. & Polacek, N. tRNA-derived fragments target the ribosome and function as regulatory non-coding RNA in *Haloferax volcanii*. *Archaea (Vancouver, B.C.)* **2012**, 260909, doi:10.1155/2012/260909 (2012).
- 236 Sobala, A. & Hutvagner, G. Small RNAs derived from the 5' end of tRNA can inhibit protein translation in human cells. *RNA biology* **10**, 553-563, doi:10.4161/rna.24285 (2013).
- 237 Kumar, P., Anaya, J., Mudunuri, S. B. & Dutta, A. Meta-analysis of tRNA derived RNA fragments reveals that they are evolutionarily conserved and associate with AGO proteins to recognize specific RNA targets. *BMC biology* **12**, 78, doi:10.1186/s12915-014-0078-0 (2014).
- 238 Gebetsberger, J., Wyss, L., Mleczko, A. M., Reuther, J. & Polacek, N. A tRNA-derived fragment competes with mRNA for ribosome binding and regulates translation during stress. *RNA biology* **14**, 1364-1373, doi:10.1080/15476286.2016.1257470 (2017).
- 239 Cole, C., Sobala, A., Lu, C., Thatcher, S. R., Bowman, A., Brown, J. W., Green, P. J., Barton, G. J. & Hutvagner, G. Filtering of deep sequencing data reveals the existence of abundant Dicer-dependent small RNAs derived from tRNAs. *RNA (New York, N.Y.)* **15**, 2147-2160, doi:10.1261/rna.1738409 (2009).
- 240 Fu, H., Feng, J., Liu, Q., Sun, F., Tie, Y., Zhu, J., Xing, R., Sun, Z. & Zheng, X. Stress induces tRNA cleavage by angiogenin in mammalian cells. *FEBS letters* **583**, 437-442, doi:10.1016/j.febslet.2008.12.043 (2009).
- 241 Haussecker, D., Huang, Y., Lau, A., Parameswaran, P., Fire, A. Z. & Kay, M. A. Human tRNA-derived small RNAs in the global regulation of RNA silencing. *RNA (New York, N.Y.)* **16**, 673-695, doi:10.1261/rna.2000810 (2010).



- 242 Yeung, M. L., Bennasser, Y., Watashi, K., Le, S. Y., Houzet, L. & Jeang, K. T. Pyrosequencing of small non-coding RNAs in HIV-1 infected cells: evidence for the processing of a viral-cellular double-stranded RNA hybrid. *Nucleic acids research* **37**, 6575-6586, doi:10.1093/nar/gkp707 (2009).
- 243 Wang, Q., Lee, I., Ren, J., Ajay, S. S., Lee, Y. S. & Bao, X. Identification and functional characterization of tRNA-derived RNA fragments (tRFs) in respiratory syncytial virus infection. *Molecular therapy : the journal of the American Society of Gene Therapy* **21**, 368-379, doi:10.1038/mt.2012.237 (2013).
- 244 Maute, R. L., Schneider, C., Sumazin, P., Holmes, A., Califano, A., Basso, K. & Dalla-Favera, R. tRNA-derived microRNA modulates proliferation and the DNA damage response and is down-regulated in B cell lymphoma. *Proceedings of the National Academy of Sciences of the United States of America* **110**, 1404-1409, doi:10.1073/pnas.1206761110 (2013).
- 245 Erhard, F., Dolken, L., Jaskiewicz, L. & Zimmer, R. PARma: identification of microRNA target sites in AGO-PAR-CLIP data. *Genome biology* **14**, R79, doi:10.1186/gb-2013-14-7-r79 (2013).
- 246 Grosswendt, S., Filipchyk, A., Manzano, M., Klironomos, F., Schilling, M., Herzog, M., Gottwein, E. & Rajewsky, N. Unambiguous identification of miRNA:target site interactions by different types of ligation reactions. *Molecular cell* **54**, 1042-1054, doi:10.1016/j.molcel.2014.03.049 (2014).
- 247 Wise, J. A. & Weiner, A. M. Dictyostelium small nuclear RNA D2 is homologous to rat nucleolar RNA U3 and is encoded by a dispersed multigene family. *Cell* **22**, 109-118 (1980).
- 248 Parker, K. A. & Steitz, J. A. Structural analysis of the human U3 ribonucleoprotein particle reveal a conserved sequence available for base pairing with pre-rRNA. *Molecular and cellular biology* **7**, 2899-2913 (1987).
- 249 Porter, G. L., Brennwald, P. J., Holm, K. A. & Wise, J. A. The sequence of U3 from *Schizosaccharomyces pombe* suggests structural divergence of this snRNA between metazoans and unicellular eukaryotes. *Nucleic acids research* **16**, 10131-10152 (1988).
- 250 Jeppesen, C., Stebbins-Boaz, B. & Gerbi, S. A. Nucleotide sequence determination and secondary structure of *Xenopus* U3 snRNA. *Nucleic acids research* **16**, 2127-2148 (1988).
- 251 Mereau, A., Fournier, R., Gregoire, A., Mouglin, A., Fabrizio, P., Luhrmann, R. & Branlant, C. An in vivo and in vitro structure-function analysis of the *Saccharomyces cerevisiae* U3A snoRNP: protein-RNA contacts and base-pair interaction with the pre-ribosomal RNA. *Journal of molecular biology* **273**, 552-571, doi:10.1006/jmbi.1997.1320 (1997).
- 252 Wormsley, S., Samarsky, D. A., Fournier, M. J. & Baserga, S. J. An unexpected, conserved element of the U3 snoRNA is required for Mpp10p association. *RNA (New York, N.Y.)* **7**, 904-919 (2001).
- 253 Tyc, K. & Steitz, J. A. U3, U8 and U13 comprise a new class of mammalian snRNPs localized in the cell nucleolus. *The EMBO journal* **8**, 3113-3119 (1989).
- 254 Watkins, N. J., Segault, V., Charpentier, B., Nottrott, S., Fabrizio, P., Bachi, A., Wilm, M., Rosbash, M., Branlant, C. & Luhrmann, R. A common core RNP structure shared between the small nucleolar box C/D RNPs and the spliceosomal U4 snRNP. *Cell* **103**, 457-466 (2000).

- 255 Vidovic, I., Nottrott, S., Hartmuth, K., Luhrmann, R. & Ficner, R. Crystal structure of the spliceosomal 15.5kD protein bound to a U4 snRNA fragment. *Molecular cell* **6**, 1331-1342 (2000).
- 256 Balakin, A. G., Smith, L. & Fournier, M. J. The RNA world of the nucleolus: two major families of small RNAs defined by different box elements with related functions. *Cell* **86**, 823-834 (1996).
- 257 Ganot, P., Caizergues-Ferrer, M. & Kiss, T. The family of box ACA small nucleolar RNAs is defined by an evolutionarily conserved secondary structure and ubiquitous sequence elements essential for RNA accumulation. *Genes & development* **11**, 941-956 (1997).
- 258 Kiss-Laszlo, Z., Henry, Y., Bachellerie, J. P., Caizergues-Ferrer, M. & Kiss, T. Site-specific ribose methylation of preribosomal RNA: a novel function for small nucleolar RNAs. *Cell* **85**, 1077-1088 (1996).
- 259 Ganot, P., Bortolin, M. L. & Kiss, T. Site-specific pseudouridine formation in preribosomal RNA is guided by small nucleolar RNAs. *Cell* **89**, 799-809 (1997).
- 260 Dupuis-Sandoval, F., Poirier, M. & Scott, M. S. The emerging landscape of small nucleolar RNAs in cell biology. *Wiley interdisciplinary reviews. RNA* **6**, 381-397, doi:10.1002/wrna.1284 (2015).
- 261 Hoepfner, M. P., White, S., Jeffares, D. C. & Poole, A. M. Evolutionarily stable association of intronic snoRNAs and microRNAs with their host genes. *Genome biology and evolution* **1**, 420-428, doi:10.1093/gbe/evp045 (2009).
- 262 Qu, G., Kruszka, K., Plewka, P., Yang, S. Y., Chiou, T. J., Jarmolowski, A., Szweykowska-Kulinska, Z., Echeverria, M. & Karlowski, W. M. Promoter-based identification of novel non-coding RNAs reveals the presence of dicistronic snoRNA-miRNA genes in *Arabidopsis thaliana*. *BMC genomics* **16**, 1009, doi:10.1186/s12864-015-2221-x (2015).
- 263 Kuhn, J. F., Tran, E. J. & Maxwell, E. S. Archaeal ribosomal protein L7 is a functional homolog of the eukaryotic 15.5kD/Snu13p snoRNP core protein. *Nucleic acids research* **30**, 931-941 (2002).
- 264 Omer, A. D., Lowe, T. M., Russell, A. G., Ebhardt, H., Eddy, S. R. & Dennis, P. P. Homologs of small nucleolar RNAs in Archaea. *Science (New York, N.Y.)* **288**, 517-522 (2000).
- 265 Scott, M. S. & Ono, M. From snoRNA to miRNA: Dual function regulatory non-coding RNAs. *Biochimie* **93**, 1987-1992, doi:10.1016/j.biochi.2011.05.026 (2011).
- 266 Scott, M. S., Avolio, F., Ono, M., Lamond, A. I. & Barton, G. J. Human miRNA precursors with box H/ACA snoRNA features. *PLoS computational biology* **5**, e1000507, doi:10.1371/journal.pcbi.1000507 (2009).
- 267 Li, W., Saraiya, A. A. & Wang, C. C. Gene regulation in *Giardia lamblia* involves a putative microRNA derived from a small nucleolar RNA. *PLoS neglected tropical diseases* **5**, e1338, doi:10.1371/journal.pntd.0001338 (2011).
- 268 Ono, M., Scott, M. S., Yamada, K., Avolio, F., Barton, G. J. & Lamond, A. I. Identification of human miRNA precursors that resemble box C/D snoRNAs. *Nucleic acids research* **39**, 3879-3891, doi:10.1093/nar/gkq1355 (2011).
- 269 Ender, C., Krek, A., Friedlander, M. R., Beitzinger, M., Weinmann, L., Chen, W., Pfeffer, S., Rajewsky, N. & Meister, G. A human snoRNA with microRNA-like functions. *Molecular cell* **32**, 519-528, doi:10.1016/j.molcel.2008.10.017 (2008).

- 270 Taft, R. J., Glazov, E. A., Lassmann, T., Hayashizaki, Y., Carninci, P. & Mattick, J. S. Small RNAs derived from snoRNAs. *RNA (New York, N.Y.)* **15**, 1233-1240, doi:10.1261/rna.1528909 (2009).
- 271 Brameier, M., Herwig, A., Reinhardt, R., Walter, L. & Gruber, J. Human box C/D snoRNAs with miRNA like functions: expanding the range of regulatory RNAs. *Nucleic acids research* **39**, 675-686, doi:10.1093/nar/gkq776 (2011).
- 272 Thomson, D. W., Pillman, K. A., Anderson, M. L., Lawrence, D. M., Toubia, J., Goodall, G. J. & Bracken, C. P. Assessing the gene regulatory properties of Argonaute-bound small RNAs of diverse genomic origin. *Nucleic acids research* **43**, 470-481, doi:10.1093/nar/gku1242 (2015).
- 273 Son, D. J., Kumar, S., Takabe, W., Kim, C. W., Ni, C. W., Alberts-Grill, N., Jang, I. H., Kim, S., Kim, W., Won Kang, S., Baker, A. H., Woong Seo, J., Ferrara, K. W. & Jo, H. The atypical mechanosensitive microRNA-712 derived from pre-ribosomal RNA induces endothelial inflammation and atherosclerosis. *Nature communications* **4**, 3000, doi:10.1038/ncomms4000 (2013).
- 274 Yoshikawa, M. & Fujii, Y. R. Human Ribosomal RNA-Derived Resident MicroRNAs as the Transmitter of Information upon the Cytoplasmic Cancer Stress. *BioMed research international* **2016**, 7562085, doi:10.1155/2016/7562085 (2016).
- 275 Borsani, O., Zhu, J., Verslues, P. E., Sunkar, R. & Zhu, J. K. Endogenous siRNAs derived from a pair of natural cis-antisense transcripts regulate salt tolerance in Arabidopsis. *Cell* **123**, 1279-1291, doi:10.1016/j.cell.2005.11.035 (2005).
- 276 Lareau, L. F., Hite, D. H., Hogan, G. J. & Brown, P. O. Distinct stages of the translation elongation cycle revealed by sequencing ribosome-protected mRNA fragments. *eLife* **3**, e01257, doi:10.7554/eLife.01257 (2014).
- 277 Schueler, M., Munschauer, M., Gregersen, L. H., Finzel, A., Loewer, A., Chen, W., Landthaler, M. & Dieterich, C. Differential protein occupancy profiling of the mRNA transcriptome. *Genome biology* **15**, R15, doi:10.1186/gb-2014-15-1-r15 (2014).
- 278 Baltz, A. G., Munschauer, M., Schwanhauser, B., Vasile, A., Murakawa, Y., Schueler, M., Youngs, N., Penfold-Brown, D., Drew, K., Milek, M., Wyler, E., Bonneau, R., Selbach, M., Dieterich, C. & Landthaler, M. The mRNA-bound proteome and its global occupancy profile on protein-coding transcripts. *Molecular cell* **46**, 674-690, doi:10.1016/j.molcel.2012.05.021 (2012).
- 279 Lipardi, C., Wei, Q. & Paterson, B. M. RNAi as random degradative PCR: siRNA primers convert mRNA into dsRNAs that are degraded to generate new siRNAs. *Cell* **107**, 297-307 (2001).
- 280 Smardon, A., Spoerke, J. M., Stacey, S. C., Klein, M. E., Mackin, N. & Maine, E. M. EGO-1 is related to RNA-directed RNA polymerase and functions in germ-line development and RNA interference in *C. elegans*. *Current biology : CB* **10**, 169-178 (2000).
- 281 Lee, H. C., Aalto, A. P., Yang, Q., Chang, S. S., Huang, G., Fisher, D., Cha, J., Poranen, M. M., Bamford, D. H. & Liu, Y. The DNA/RNA-dependent RNA polymerase QDE-1 generates aberrant RNA and dsRNA for RNAi in a process requiring replication protein A and a DNA helicase. *PLoS biology* **8**, doi:10.1371/journal.pbio.1000496 (2010).

- 282 Forrest, E. C., Cogoni, C. & Macino, G. The RNA-dependent RNA polymerase, QDE-1, is a rate-limiting factor in post-transcriptional gene silencing in *Neurospora crassa*. *Nucleic acids research* **32**, 2123-2128, doi:10.1093/nar/gkh530 (2004).
- 283 Dalmay, T., Hamilton, A., Rudd, S., Angell, S. & Baulcombe, D. C. An RNA-dependent RNA polymerase gene in *Arabidopsis* is required for posttranscriptional gene silencing mediated by a transgene but not by a virus. *Cell* **101**, 543-553 (2000).
- 284 Siddiqui, M. A., Mukherjee, S., Manivannan, P. & Malathi, K. RNase L Cleavage Products Promote Switch from Autophagy to Apoptosis by Caspase-Mediated Cleavage of Beclin-1. *International journal of molecular sciences* **16**, 17611-17636, doi:10.3390/ijms160817611 (2015).
- 285 Nilsen, T. W., Maroney, P. A. & Baglioni, C. Double-stranded RNA causes synthesis of 2',5'-oligo(A) and degradation of messenger RNA in interferon-treated cells. *The Journal of biological chemistry* **256**, 7806-7811 (1981).
- 286 Wreschner, D. H., McCauley, J. W., Skehel, J. J. & Kerr, I. M. Interferon action--sequence specificity of the ppp(A2'p)nA-dependent ribonuclease. *Nature* **289**, 414-417 (1981).
- 287 Thomas, M. P., Liu, X., Whangbo, J., McCrossan, G., Sanborn, K. B., Basar, E., Walch, M. & Lieberman, J. Apoptosis Triggers Specific, Rapid, and Global mRNA Decay with 3' Uridylated Intermediates Degraded by DIS3L2. *Cell reports* **11**, 1079-1089, doi:10.1016/j.celrep.2015.04.026 (2015).
- 288 Tokmakov, A. A., Iguchi, S., Iwasaki, T., Fukami, Y. & Sato, K. I. Global decay of mRNA is a hallmark of apoptosis in aging *Xenopus* eggs. *RNA biology* **14**, 339-346, doi:10.1080/15476286.2016.1276695 (2017).
- 289 Gaglia, M. M., Rycroft, C. H. & Glaunsinger, B. A. Transcriptome-Wide Cleavage Site Mapping on Cellular mRNAs Reveals Features Underlying Sequence-Specific Cleavage by the Viral Ribonuclease SOX. *PLoS pathogens* **11**, e1005305, doi:10.1371/journal.ppat.1005305 (2015).
- 290 Oehm, A., Behrmann, I., Falk, W., Pawlita, M., Maier, G., Klas, C., Li-Weber, M., Richards, S., Dhein, J., Trauth, B. C. & et al. Purification and molecular cloning of the APO-1 cell surface antigen, a member of the tumor necrosis factor/nerve growth factor receptor superfamily. Sequence identity with the Fas antigen. *The Journal of biological chemistry* **267**, 10709-10715 (1992).
- 291 Suda, T., Takahashi, T., Golstein, P. & Nagata, S. Molecular cloning and expression of the Fas ligand, a novel member of the tumor necrosis factor family. *Cell* **75**, 1169-1178 (1993).
- 292 Kakinuma, C., Takagaki, K., Yatomi, T., Nakamura, N., Nagata, S., Uemura, A. & Shibutani, Y. Acute toxicity of an anti-Fas antibody in mice. *Toxicologic pathology* **27**, 412-420, doi:10.1177/019262339902700404 (1999).
- 293 Ogasawara, J., Watanabe-Fukunaga, R., Adachi, M., Matsuzawa, A., Kasugai, T., Kitamura, Y., Itoh, N., Suda, T. & Nagata, S. Lethal effect of the anti-Fas antibody in mice. *Nature* **364**, 806-809, doi:10.1038/364806a0 (1993).
- 294 Watanabe-Fukunaga, R., Brannan, C. I., Itoh, N., Yonehara, S., Copeland, N. G., Jenkins, N. A. & Nagata, S. The cDNA structure, expression, and chromosomal assignment of the mouse Fas antigen. *Journal of immunology (Baltimore, Md. : 1950)* **148**, 1274-1279 (1992).

- 295 Griffith, T. S., Brunner, T., Fletcher, S. M., Green, D. R. & Ferguson, T. A. Fas ligand-induced apoptosis as a mechanism of immune privilege. *Science (New York, N.Y.)* **270**, 1189-1192 (1995).
- 296 Xerri, L., Devilard, E., Hassoun, J., Mawas, C. & Birg, F. Fas ligand is not only expressed in immune privileged human organs but is also coexpressed with Fas in various epithelial tissues. *Molecular pathology : MP* **50**, 87-91 (1997).
- 297 Suda, T., Okazaki, T., Naito, Y., Yokota, T., Arai, N., Ozaki, S., Nakao, K. & Nagata, S. Expression of the Fas ligand in cells of T cell lineage. *Journal of immunology (Baltimore, Md. : 1950)* **154**, 3806-3813 (1995).
- 298 Ettinger, R., Panka, D. J., Wang, J. K., Stanger, B. Z., Ju, S. T. & Marshak-Rothstein, A. Fas ligand-mediated cytotoxicity is directly responsible for apoptosis of normal CD4+ T cells responding to a bacterial superantigen. *Journal of immunology (Baltimore, Md. : 1950)* **154**, 4302-4308 (1995).
- 299 Singer, G. G. & Abbas, A. K. The fas antigen is involved in peripheral but not thymic deletion of T lymphocytes in T cell receptor transgenic mice. *Immunity* **1**, 365-371 (1994).
- 300 Stranges, P. B., Watson, J., Cooper, C. J., Choisy-Rossi, C. M., Stonebraker, A. C., Beighton, R. A., Hartig, H., Sundberg, J. P., Servick, S., Kaufmann, G., Fink, P. J. & Chervonsky, A. V. Elimination of antigen-presenting cells and autoreactive T cells by Fas contributes to prevention of autoimmunity. *Immunity* **26**, 629-641, doi:10.1016/j.immuni.2007.03.016 (2007).
- 301 Brunner, T., Mogil, R. J., LaFace, D., Yoo, N. J., Mahboubi, A., Echeverri, F., Martin, S. J., Force, W. R., Lynch, D. H., Ware, C. F. & et al. Cell-autonomous Fas (CD95)/Fas-ligand interaction mediates activation-induced apoptosis in T-cell hybridomas. *Nature* **373**, 441-444, doi:10.1038/373441a0 (1995).
- 302 Jabs, D. A. & Prendergast, R. A. Reactive lymphocytes in lacrimal gland and vasculitic renal lesions of autoimmune MRL/lpr mice express L3T4. *The Journal of experimental medicine* **166**, 1198-1203 (1987).
- 303 Hoffman, R. W., Alspaugh, M. A., Waggie, K. S., Durham, J. B. & Walker, S. E. Sjogren's syndrome in MRL/l and MRL/n mice. *Arthritis and rheumatism* **27**, 157-165 (1984).
- 304 Theofilopoulos, A. N. & Dixon, F. J. Murine models of systemic lupus erythematosus. *Advances in immunology* **37**, 269-390 (1985).
- 305 Sunderrajan, E. V., McKenzie, W. N., Lieske, T. R., Kavanaugh, J. L., Braun, S. R. & Walker, S. E. Pulmonary inflammation in autoimmune MRL/Mp-lpr/lpr mice. Histopathology and bronchoalveolar lavage evaluation. *The American journal of pathology* **124**, 353-362 (1986).
- 306 Watanabe-Fukunaga, R., Brannan, C. I., Copeland, N. G., Jenkins, N. A. & Nagata, S. Lymphoproliferation disorder in mice explained by defects in Fas antigen that mediates apoptosis. *Nature* **356**, 314-317, doi:10.1038/356314a0 (1992).
- 307 Roths, J. B., Murphy, E. D. & Eicher, E. M. A new mutation, gld, that produces lymphoproliferation and autoimmunity in C3H/HeJ mice. *The Journal of experimental medicine* **159**, 1-20 (1984).
- 308 Seldin, M. F., Morse, H. C., 3rd, Reeves, J. P., Scribner, C. L., LeBoeuf, R. C. & Steinberg, A. D. Genetic analysis of autoimmune gld mice. I. Identification of a restriction fragment

- length polymorphism closely linked to the gld mutation within a conserved linkage group. *The Journal of experimental medicine* **167**, 688-693 (1988).
- 309 Lynch, D. H., Watson, M. L., Alderson, M. R., Baum, P. R., Miller, R. E., Tough, T., Gibson, M., Davis-Smith, T., Smith, C. A., Hunter, K. & et al. The mouse Fas-ligand gene is mutated in gld mice and is part of a TNF family gene cluster. *Immunity* **1**, 131-136 (1994).
- 310 Li, H., Zhu, H., Xu, C. J. & Yuan, J. Cleavage of BID by caspase 8 mediates the mitochondrial damage in the Fas pathway of apoptosis. *Cell* **94**, 491-501 (1998).
- 311 Lovell, J. F., Billen, L. P., Bindner, S., Shamas-Din, A., Fradin, C., Leber, B. & Andrews, D. W. Membrane binding by tBid initiates an ordered series of events culminating in membrane permeabilization by Bax. *Cell* **135**, 1074-1084, doi:10.1016/j.cell.2008.11.010 (2008).
- 312 Li, P., Nijhawan, D., Budihardjo, I., Srinivasula, S. M., Ahmad, M., Alnemri, E. S. & Wang, X. Cytochrome c and dATP-dependent formation of Apaf-1/caspase-9 complex initiates an apoptotic protease cascade. *Cell* **91**, 479-489 (1997).
- 313 Rodriguez, J. & Lazebnik, Y. Caspase-9 and APAF-1 form an active holoenzyme. *Genes & development* **13**, 3179-3184 (1999).
- 314 Schneider, P., Holler, N., Bodmer, J. L., Hahne, M., Frei, K., Fontana, A. & Tschopp, J. Conversion of membrane-bound Fas(CD95) ligand to its soluble form is associated with downregulation of its proapoptotic activity and loss of liver toxicity. *The Journal of experimental medicine* **187**, 1205-1213 (1998).
- 315 Holler, N., Tardivel, A., Kovacsovics-Bankowski, M., Hertig, S., Gaide, O., Martinon, F., Tinel, A., Deperthes, D., Calderara, S., Schulthess, T., Engel, J., Schneider, P. & Tschopp, J. Two adjacent trimeric Fas ligands are required for Fas signaling and formation of a death-inducing signaling complex. *Molecular and cellular biology* **23**, 1428-1440 (2003).
- 316 Lavrik, I. N., Golks, A., Riess, D., Bentele, M., Eils, R. & Krammer, P. H. Analysis of CD95 threshold signaling: triggering of CD95 (FAS/APO-1) at low concentrations primarily results in survival signaling. *The Journal of biological chemistry* **282**, 13664-13671, doi:10.1074/jbc.M700434200 (2007).
- 317 Ishikawa, T., Yamada, H., Oyamada, A., Goshima, F., Nishiyama, Y. & Yoshikai, Y. Protective role of Fas-FasL signaling in lethal infection with herpes simplex virus type 2 in mice. *Journal of virology* **83**, 11777-11783, doi:10.1128/jvi.01006-09 (2009).
- 318 Shrestha, B. & Diamond, M. S. Fas ligand interactions contribute to CD8<sup>+</sup> T-cell-mediated control of West Nile virus infection in the central nervous system. *Journal of virology* **81**, 11749-11757, doi:10.1128/jvi.01136-07 (2007).
- 319 Malyshkina, A., Littwitz-Salomon, E., Sutter, K., Zelinsky, G., Windmann, S., Schimmer, S., Paschen, A., Streeck, H., Hasenkrug, K. J. & Dittmer, U. Fas Ligand-mediated cytotoxicity of CD4<sup>+</sup> T cells during chronic retrovirus infection. *Scientific reports* **7**, 7785, doi:10.1038/s41598-017-08578-7 (2017).
- 320 Tsutsui, H., Nakanishi, K., Matsui, K., Higashino, K., Okamura, H., Miyazawa, Y. & Kaneda, K. IFN-gamma-inducing factor up-regulates Fas ligand-mediated cytotoxic activity of murine natural killer cell clones. *Journal of immunology (Baltimore, Md. : 1950)* **157**, 3967-3973 (1996).

- 321 Okazaki, A., Hiraga, N., Imamura, M., Hayes, C. N., Tsuge, M., Takahashi, S., Aikata, H., Abe, H., Miki, D., Ochi, H., Tateno, C., Yoshizato, K., Ohdan, H. & Chayama, K. Severe necroinflammatory reaction caused by natural killer cell-mediated Fas/Fas ligand interaction and dendritic cells in human hepatocyte chimeric mouse. *Hepatology (Baltimore, Md.)* **56**, 555-566, doi:10.1002/hep.25651 (2012).
- 322 Afshar-Sterle, S., Zotos, D., Bernard, N. J., Scherger, A. K., Rodling, L., Alsop, A. E., Walker, J., Masson, F., Belz, G. T., Corcoran, L. M., O'Reilly, L. A., Strasser, A., Smyth, M. J., Johnstone, R., Tarlinton, D. M., Nutt, S. L. & Kallies, A. Fas ligand-mediated immune surveillance by T cells is essential for the control of spontaneous B cell lymphomas. *Nature medicine* **20**, 283-290, doi:10.1038/nm.3442 (2014).
- 323 Davidson, W. F., Giese, T. & Fredrickson, T. N. Spontaneous Development of Plasmacytoid Tumors in Mice with Defective Fas–Fas Ligand Interactions. *The Journal of experimental medicine* **187**, 1825-1838, doi:10.1084/jem.187.11.1825 (1998).
- 324 Kagi, D., Vignaux, F., Ledermann, B., Burki, K., Depraetere, V., Nagata, S., Hengartner, H. & Golstein, P. Fas and perforin pathways as major mechanisms of T cell-mediated cytotoxicity. *Science (New York, N.Y.)* **265**, 528-530, doi:10.1126/science.7518614 (1994).
- 325 Nisihara, T., Ushio, Y., Higuchi, H., Kayagaki, N., Yamaguchi, N., Soejima, K., Matsuo, S., Maeda, H., Eda, Y., Okumura, K. & Yagita, H. Humanization and epitope mapping of neutralizing anti-human Fas ligand monoclonal antibodies: structural insights into Fas/Fas ligand interaction. *Journal of immunology (Baltimore, Md. : 1950)* **167**, 3266-3275 (2001).
- 326 Schneider, P., Bodmer, J. L., Holler, N., Mattmann, C., Scuderi, P., Terskikh, A., Peitsch, M. C. & Tschoop, J. Characterization of Fas (Apo-1, CD95)-Fas ligand interaction. *The Journal of biological chemistry* **272**, 18827-18833 (1997).
- 327 Fu, Q., Fu, T. M., Cruz, A. C., Sengupta, P., Thomas, S. K., Wang, S., Siegel, R. M., Wu, H. & Chou, J. J. Structural Basis and Functional Role of Intramembrane Trimerization of the Fas/CD95 Death Receptor. *Molecular cell* **61**, 602-613, doi:10.1016/j.molcel.2016.01.009 (2016).
- 328 Papoff, G., Hausler, P., Eramo, A., Pagano, M. G., Di Leve, G., Signore, A. & Ruberti, G. Identification and characterization of a ligand-independent oligomerization domain in the extracellular region of the CD95 death receptor. *The Journal of biological chemistry* **274**, 38241-38250 (1999).
- 329 Algeciras-Schimnich, A., Shen, L., Barnhart, B. C., Murmann, A. E., Burkhardt, J. K. & Peter, M. E. Molecular ordering of the initial signaling events of CD95. *Molecular and cellular biology* **22**, 207-220 (2002).
- 330 Feig, C., Tchikov, V., Schutze, S. & Peter, M. E. Palmitoylation of CD95 facilitates formation of SDS-stable receptor aggregates that initiate apoptosis signaling. *The EMBO journal* **26**, 221-231, doi:10.1038/sj.emboj.7601460 (2007).
- 331 Kischkel, F. C., Hellbardt, S., Behrmann, I., Germer, M., Pawlita, M., Krammer, P. H. & Peter, M. E. Cytotoxicity-dependent APO-1 (Fas/CD95)-associated proteins form a death-inducing signaling complex (DISC) with the receptor. *The EMBO journal* **14**, 5579-5588 (1995).
- 332 Boldin, M. P., Goncharov, T. M., Goltsev, Y. V. & Wallach, D. Involvement of MACH, a novel MORT1/FADD-interacting protease, in Fas/APO-1- and TNF receptor-induced cell death. *Cell* **85**, 803-815 (1996).

- 333 Fernandes-Alnemri, T., Armstrong, R. C., Krebs, J., Srinivasula, S. M., Wang, L., Bullrich, F., Fritz, L. C., Trapani, J. A., Tomaselli, K. J., Litwack, G. & Alnemri, E. S. In vitro activation of CPP32 and Mch3 by Mch4, a novel human apoptotic cysteine protease containing two FADD-like domains. *Proceedings of the National Academy of Sciences of the United States of America* **93**, 7464-7469 (1996).
- 334 Muzio, M., Chinnaiyan, A. M., Kischkel, F. C., O'Rourke, K., Shevchenko, A., Ni, J., Scaffidi, C., Bretz, J. D., Zhang, M., Gentz, R., Mann, M., Krammer, P. H., Peter, M. E. & Dixit, V. M. FLICE, a novel FADD-homologous ICE/CED-3-like protease, is recruited to the CD95 (Fas/APO-1) death-inducing signaling complex. *Cell* **85**, 817-827 (1996).
- 335 Sprick, M. R., Rieser, E., Stahl, H., Grosse-Wilde, A., Weigand, M. A. & Walczak, H. Caspase-10 is recruited to and activated at the native TRAIL and CD95 death-inducing signalling complexes in a FADD-dependent manner but can not functionally substitute caspase-8. *The EMBO journal* **21**, 4520-4530 (2002).
- 336 Muzio, M., Stockwell, B. R., Stennicke, H. R., Salvesen, G. S. & Dixit, V. M. An induced proximity model for caspase-8 activation. *The Journal of biological chemistry* **273**, 2926-2930 (1998).
- 337 Yang, X., Chang, H. Y. & Baltimore, D. Autoproteolytic activation of pro-caspases by oligomerization. *Molecular cell* **1**, 319-325 (1998).
- 338 Chai, J., Wu, Q., Shiozaki, E., Srinivasula, S. M., Alnemri, E. S. & Shi, Y. Crystal structure of a procaspase-7 zymogen: mechanisms of activation and substrate binding. *Cell* **107**, 399-407 (2001).
- 339 Riedl, S. J., Fuentes-Prior, P., Renatus, M., Kairies, N., Krapp, S., Huber, R., Salvesen, G. S. & Bode, W. Structural basis for the activation of human procaspase-7. *Proceedings of the National Academy of Sciences of the United States of America* **98**, 14790-14795, doi:10.1073/pnas.221580098 (2001).
- 340 Liu, X., Kim, C. N., Yang, J., Jemmerson, R. & Wang, X. Induction of apoptotic program in cell-free extracts: requirement for dATP and cytochrome c. *Cell* **86**, 147-157 (1996).
- 341 Kluck, R. M., Bossy-Wetzel, E., Green, D. R. & Newmeyer, D. D. The release of cytochrome c from mitochondria: a primary site for Bcl-2 regulation of apoptosis. *Science (New York, N.Y.)* **275**, 1132-1136 (1997).
- 342 Kuwana, T., Mackey, M. R., Perkins, G., Ellisman, M. H., Latterich, M., Schneider, R., Green, D. R. & Newmeyer, D. D. Bid, Bax, and lipids cooperate to form supramolecular openings in the outer mitochondrial membrane. *Cell* **111**, 331-342 (2002).
- 343 Janicke, R. U., Sprengart, M. L., Wati, M. R. & Porter, A. G. Caspase-3 is required for DNA fragmentation and morphological changes associated with apoptosis. *The Journal of biological chemistry* **273**, 9357-9360 (1998).
- 344 Woo, M., Hakem, R., Soengas, M. S., Duncan, G. S., Shahinian, A., Kagi, D., Hakem, A., McCurrach, M., Khoo, W., Kaufman, S. A., Senaldi, G., Howard, T., Lowe, S. W. & Mak, T. W. Essential contribution of caspase 3/CPP32 to apoptosis and its associated nuclear changes. *Genes & development* **12**, 806-819 (1998).
- 345 Janicke, R. U., Ng, P., Sprengart, M. L. & Porter, A. G. Caspase-3 is required for alpha-fodrin cleavage but dispensable for cleavage of other death substrates in apoptosis. *The Journal of biological chemistry* **273**, 15540-15545 (1998).



- 346 Kothakota, S., Azuma, T., Reinhard, C., Klippel, A., Tang, J., Chu, K., McGarry, T. J., Kirschner, M. W., Koths, K., Kwiatkowski, D. J. & Williams, L. T. Caspase-3-generated fragment of gelsolin: effector of morphological change in apoptosis. *Science (New York, N.Y.)* **278**, 294-298 (1997).
- 347 Rudel, T. & Bokoch, G. M. Membrane and morphological changes in apoptotic cells regulated by caspase-mediated activation of PAK2. *Science (New York, N.Y.)* **276**, 1571-1574 (1997).
- 348 Desbarats, J., Birge, R. B., Mimouni-Rongy, M., Weinstein, D. E., Palerme, J. S. & Newell, M. K. Fas engagement induces neurite growth through ERK activation and p35 upregulation. *Nature cell biology* **5**, 118-125, doi:10.1038/ncb916 (2003).
- 349 Paulsen, M., Valentin, S., Mathew, B., Adam-Klages, S., Bertsch, U., Lavrik, I., Krammer, P. H., Kabelitz, D. & Janssen, O. Modulation of CD4+ T-cell activation by CD95 costimulation. *Cell death and differentiation* **18**, 619-631, doi:10.1038/cdd.2010.134 (2011).
- 350 Alderson, M. R., Armitage, R. J., Maraskovsky, E., Tough, T. W., Roux, E., Schooley, K., Ramsdell, F. & Lynch, D. H. Fas transduces activation signals in normal human T lymphocytes. *The Journal of experimental medicine* **178**, 2231-2235 (1993).
- 351 Desbarats, J. & Newell, M. K. Fas engagement accelerates liver regeneration after partial hepatectomy. *Nature medicine* **6**, 920-923, doi:10.1038/78688 (2000).
- 352 Letellier, E., Kumar, S., Sancho-Martinez, I., Krauth, S., Funke-Kaiser, A., Laudenklos, S., Konecki, K., Klussmann, S., Corsini, N. S., Kleber, S., Drost, N., Neumann, A., Levi-Strauss, M., Brors, B., Gretz, N., Edler, L., Fischer, C., Hill, O., Thiemann, M., Biglari, B., Karray, S. & Martin-Villalba, A. CD95-ligand on peripheral myeloid cells activates Syk kinase to trigger their recruitment to the inflammatory site. *Immunity* **32**, 240-252, doi:10.1016/j.immuni.2010.01.011 (2010).
- 353 Poissonnier, A., Sanseau, D., Le Gallo, M., Malleter, M., Levoine, N., Viel, R., Morere, L., Penna, A., Blanco, P., Dupuy, A., Poizeau, F., Fautrel, A., Seneschal, J., Jouan, F., Ritz, J., Forcade, E., Rioux, N., Contin-Bordes, C., Ducret, T., Vacher, A. M., Barrow, P. A., Flynn, R. J., Vacher, P. & Legembre, P. CD95-Mediated Calcium Signaling Promotes T Helper 17 Trafficking to Inflamed Organs in Lupus-Prone Mice. *Immunity* **45**, 209-223, doi:10.1016/j.immuni.2016.06.028 (2016).
- 354 Hofmann, T. G., Moller, A., Hehner, S. P., Welsch, D., Droge, W. & Schmitz, M. L. CD95-induced JNK activation signals are transmitted by the death-inducing signaling complex (DISC), but not by Daxx. *International journal of cancer* **93**, 185-191, doi:10.1002/ijc.1316 (2001).
- 355 Lee, S. M., Kim, E. J., Suk, K. & Lee, W. H. Stimulation of Fas (CD95) induces production of pro-inflammatory mediators through ERK/JNK-dependent activation of NF-kappaB in THP-1 cells. *Cellular immunology* **271**, 157-162, doi:10.1016/j.cellimm.2011.06.019 (2011).
- 356 Legembre, P., Barnhart, B. C., Zheng, L., Vijayan, S., Straus, S. E., Puck, J., Dale, J. K., Lenardo, M. & Peter, M. E. Induction of apoptosis and activation of NF-kappaB by CD95 require different signalling thresholds. *EMBO reports* **5**, 1084-1089, doi:10.1038/sj.embor.7400280 (2004).
- 357 Tauzin, S., Chaigne-Delalande, B., Selva, E., Khadra, N., Daburon, S., Contin-Bordes, C., Blanco, P., Le Seyec, J., Ducret, T., Counillon, L., Moreau, J. F., Hofman, P., Vacher, P.

- & Legembre, P. The naturally processed CD95L elicits a c-src/calcium/PI3K-driven cell migration pathway. *PLoS biology* **9**, e1001090, doi:10.1371/journal.pbio.1001090 (2011).
- 358 Kleber, S., Sancho-Martinez, I., Wiestler, B., Beisel, A., Gieffers, C., Hill, O., Thiemann, M., Mueller, W., Sykora, J., Kuhn, A., Schreglmann, N., Letellier, E., Zuliani, C., Klussmann, S., Teodorczyk, M., Grone, H. J., Ganten, T. M., Sultmann, H., Tuttenberg, J., von Deimling, A., Regnier-Vigouroux, A., Herold-Mende, C. & Martin-Villalba, A. Yes and PI3K bind CD95 to signal invasion of glioblastoma. *Cancer cell* **13**, 235-248, doi:10.1016/j.ccr.2008.02.003 (2008).
- 359 Steller, E. J., Ritsma, L., Raats, D. A., Hoogwater, F. J., Emmink, B. L., Govaert, K. M., Laoukili, J., Rinkes, I. H., van Rheenen, J. & Kranenburg, O. The death receptor CD95 activates the cofilin pathway to stimulate tumour cell invasion. *EMBO reports* **12**, 931-937, doi:10.1038/embor.2011.129 (2011).
- 360 Trauth, B. C., Klas, C., Peters, A. M., Matzku, S., Moller, P., Falk, W., Debatin, K. M. & Krammer, P. H. Monoclonal antibody-mediated tumor regression by induction of apoptosis. *Science (New York, N.Y.)* **245**, 301-305 (1989).
- 361 Teodorczyk, M., Kleber, S., Wollny, D., Sefrin, J. P., Aykut, B., Mateos, A., Herhaus, P., Sancho-Martinez, I., Hill, O., Gieffers, C., Sykora, J., Weichert, W., Eisen, C., Trumpp, A., Sprick, M. R., Bergmann, F., Welsch, T. & Martin-Villalba, A. CD95 promotes metastatic spread via Sck in pancreatic ductal adenocarcinoma. *Cell death and differentiation* **22**, 1192-1202, doi:10.1038/cdd.2014.217 (2015).
- 362 Keane, M. M., Ettenberg, S. A., Lowrey, G. A., Russell, E. K. & Lipkowitz, S. Fas expression and function in normal and malignant breast cell lines. *Cancer research* **56**, 4791-4798 (1996).
- 363 Algeciras-Schimmich, A., Pietras, E. M., Barnhart, B. C., Legembre, P., Vijayan, S., Holbeck, S. L. & Peter, M. E. Two CD95 tumor classes with different sensitivities to antitumor drugs. *Proceedings of the National Academy of Sciences of the United States of America* **100**, 11445-11450, doi:10.1073/pnas.2034995100 (2003).
- 364 Chen, L., Park, S. M., Tumanov, A. V., Hau, A., Sawada, K., Feig, C., Turner, J. R., Fu, Y. X., Romero, I. L., Lengyel, E. & Peter, M. E. CD95 promotes tumour growth. *Nature* **465**, 492-496, doi:10.1038/nature09075 (2010).
- 365 Arscott, P. L., Stokes, T., Myc, A., Giordano, T. J., Thompson, N. W. & Baker, J. R., Jr. Fas (CD95) expression is up-regulated on papillary thyroid carcinoma. *The Journal of clinical endocrinology and metabolism* **84**, 4246-4252, doi:10.1210/jcem.84.11.6139 (1999).
- 366 Barnhart, B. C., Legembre, P., Pietras, E., Bubici, C., Franzoso, G. & Peter, M. E. CD95 ligand induces motility and invasiveness of apoptosis-resistant tumor cells. *The EMBO journal* **23**, 3175-3185, doi:10.1038/sj.emboj.7600325 (2004).
- 367 Qadir, A. S., Ceppi, P., Brockway, S., Law, C., Mu, L., Khodarev, N. N., Kim, J., Zhao, J. C., Putzbach, W., Murmann, A. E., Chen, Z., Chen, W., Liu, X., Salomon, A. R., Liu, H., Weichselbaum, R. R., Yu, J. & Peter, M. E. CD95/Fas Increases Stemness in Cancer Cells by Inducing a STAT1-Dependent Type I Interferon Response. *Cell reports* **18**, 2373-2386, doi:10.1016/j.celrep.2017.02.037 (2017).

- 368 Ceppi, P., Hadji, A., Kohlhapp, F. J., Pattanayak, A., Hau, A., Liu, X., Liu, H., Murmann, A. E. & Peter, M. E. CD95 and CD95L promote and protect cancer stem cells. *Nature communications* **5**, 5238, doi:10.1038/ncomms6238 (2014).
- 369 Hoogwater, F. J., Nijkamp, M. W., Smakman, N., Steller, E. J., Emmink, B. L., Westendorp, B. F., Raats, D. A., Sprick, M. R., Schaefer, U., Van Houdt, W. J., De Bruijn, M. T., Schackmann, R. C., Derksen, P. W., Medema, J. P., Walczak, H., Borel Rinkes, I. H. & Kranenburg, O. Oncogenic K-Ras turns death receptors into metastasis-promoting receptors in human and mouse colorectal cancer cells. *Gastroenterology* **138**, 2357-2367, doi:10.1053/j.gastro.2010.02.046 (2010).
- 370 Mitsiades, C. S., Poulaki, V., Fanourakis, G., Sozopoulos, E., McMillin, D., Wen, Z., Voutsinas, G., Tseleni-Balafouta, S. & Mitsiades, N. Fas signaling in thyroid carcinomas is diverted from apoptosis to proliferation. *Clinical cancer research : an official journal of the American Association for Cancer Research* **12**, 3705-3712, doi:10.1158/1078-0432.ccr-05-2493 (2006).
- 371 Peter, M. E., Hadji, A., Murmann, A. E., Brockway, S., Putzbach, W., Pattanayak, A. & Ceppi, P. The role of CD95 and CD95 ligand in cancer. *Cell death and differentiation* **22**, 549-559, doi:10.1038/cdd.2015.3 (2015).
- 372 Fouque, A., Lepvrier, E., Debure, L., Gouriou, Y., Malleter, M., Delcroix, V., Ovize, M., Ducret, T., Li, C., Hammadi, M., Vacher, P. & Legembre, P. The apoptotic members CD95, BclxL, and Bcl-2 cooperate to promote cell migration by inducing Ca(2+) flux from the endoplasmic reticulum to mitochondria. *Cell death and differentiation* **23**, 1702-1716, doi:10.1038/cdd.2016.61 (2016).
- 373 Kataoka, T., Budd, R. C., Holler, N., Thome, M., Martinon, F., Irmeler, M., Burns, K., Hahne, M., Kennedy, N., Kovacsovics, M. & Tschopp, J. The caspase-8 inhibitor FLIP promotes activation of NF-kappaB and Erk signaling pathways. *Current biology : CB* **10**, 640-648 (2000).
- 374 Xiao, S., Jodo, S., Sung, S. S., Marshak-Rothstein, A. & Ju, S. T. A novel signaling mechanism for soluble CD95 ligand. Synergy with anti-CD95 monoclonal antibodies for apoptosis and NF-kappaB nuclear translocation. *The Journal of biological chemistry* **277**, 50907-50913, doi:10.1074/jbc.M206093200 (2002).
- 375 Schleich, K., Warnken, U., Fricker, N., Ozturk, S., Richter, P., Kammerer, K., Schnolzer, M., Krammer, P. H. & Lavrik, I. N. Stoichiometry of the CD95 death-inducing signaling complex: experimental and modeling evidence for a death effector domain chain model. *Molecular cell* **47**, 306-319, doi:10.1016/j.molcel.2012.05.006 (2012).
- 376 Hadji, A., Ceppi, P., Murmann, A. E., Brockway, S., Pattanayak, A., Bhinder, B., Hau, A., De Chant, S., Parimi, V., Kolesza, P., Richards, J., Chandel, N., Djaballah, H. & Peter, M. E. Death induced by CD95 or CD95 ligand elimination. *Cell reports* **7**, 208-222, doi:10.1016/j.celrep.2014.02.035 (2014).
- 377 Cowley, G. S., Weir, B. A., Vazquez, F., Tamayo, P., Scott, J. A., Rusin, S., East-Seletsky, A., Ali, L. D., Gerath, W. F., Pantel, S. E., Lizotte, P. H., Jiang, G., Hsiao, J., Tsherniak, A., Dwinell, E., Aoyama, S., Okamoto, M., Harrington, W., Gelfand, E., Green, T. M., Tomko, M. J., Gopal, S., Wong, T. C., Li, H., Howell, S., Stransky, N., Liefeld, T., Jang, D., Bistline, J., Hill Meyers, B., Armstrong, S. A., Anderson, K. C., Stegmaier, K., Reich, M., Pellman, D., Boehm, J. S., Mesirov, J. P., Golub, T. R., Root, D. E. & Hahn, W. C.

- Parallel genome-scale loss of function screens in 216 cancer cell lines for the identification of context-specific genetic dependencies. *Scientific data* **1**, 140035, doi:10.1038/sdata.2014.35 (2014).
- 378 Patel, M. & Peter, M. E. Identification of DISE-inducing shRNAs by monitoring cellular responses. *Cell cycle (Georgetown, Tex.)*, 0, doi:10.1080/15384101.2017.1383576 (2017).
- 379 Lu, J., Getz, G., Miska, E. A., Alvarez-Saavedra, E., Lamb, J., Peck, D., Sweet-Cordero, A., Ebert, B. L., Mak, R. H., Ferrando, A. A., Downing, J. R., Jacks, T., Horvitz, H. R. & Golub, T. R. MicroRNA expression profiles classify human cancers. *Nature* **435**, 834-838, doi:10.1038/nature03702 (2005).
- 380 Diaz-Garcia, C. V., Agudo-Lopez, A., Perez, C., Lopez-Martin, J. A., Rodriguez-Peralto, J. L., de Castro, J., Cortijo, A., Martinez-Villanueva, M., Iglesias, L., Garcia-Carbonero, R., Fresno Vara, J. A., Gamez-Pozo, A., Palacios, J., Cortes-Funes, H., Paz-Ares, L. & Agullo-Ortuno, M. T. DICER1, DROSHA and miRNAs in patients with non-small cell lung cancer: implications for outcomes and histologic classification. *Carcinogenesis* **34**, 1031-1038, doi:10.1093/carcin/bgt022 (2013).
- 381 Murmann, A. E., McMahan, K. M., Haluck-Kangas, A., Ravindran, N., Patel, M., Law, C. Y., Brockway, S., Wei, J. J., Thaxton, C. S. & Peter, M. E. Induction of DISE in ovarian cancer cells in vivo. *Oncotarget* **8**, 84643-84658, doi:10.18632/oncotarget.21471 (2017).
- 382 Aoki, K., Kurooka, M., Chen, J. J., Petryniak, J., Nabel, E. G. & Nabel, G. J. Extracellular matrix interacts with soluble CD95L: retention and enhancement of cytotoxicity. *Nature immunology* **2**, 333-337, doi:10.1038/86336 (2001).
- 383 Dow, L. E., Premsrirut, P. K., Zuber, J., Fellmann, C., McJunkin, K., Miething, C., Park, Y., Dickins, R. A., Hannon, G. J. & Lowe, S. W. A pipeline for the generation of shRNA transgenic mice. *Nature protocols* **7**, 374-393, doi:10.1038/nprot.2011.446 (2012).
- 384 Mali, P., Yang, L., Esvelt, K. M., Aach, J., Guell, M., DiCarlo, J. E., Norville, J. E. & Church, G. M. RNA-guided human genome engineering via Cas9. *Science (New York, N.Y.)* **339**, 823-826, doi:10.1126/science.1232033 (2013).
- 385 Jinek, M., East, A., Cheng, A., Lin, S., Ma, E. & Doudna, J. RNA-programmed genome editing in human cells. *eLife* **2**, e00471, doi:10.7554/eLife.00471 (2013).
- 386 Nakamura, M., Suzuki, A., Akada, J., Yarimizu, T., Iwakiri, R., Hoshida, H. & Akada, R. A Novel Terminator Primer and Enhancer Reagents for Direct Expression of PCR-Amplified Genes in Mammalian Cells. *Molecular biotechnology* **57**, 767-780, doi:10.1007/s12033-015-9870-5 (2015).
- 387 Fiandalo, M. V., Schwarze, S. R. & Kyprianou, N. Proteasomal regulation of caspase-8 in cancer cell apoptosis. *Apoptosis : an international journal on programmed cell death* **18**, 766-776, doi:10.1007/s10495-013-0821-y (2013).
- 388 Love, M. I., Huber, W. & Anders, S. Moderated estimation of fold change and dispersion for RNA-seq data with DESeq2. *Genome biology* **15**, 550, doi:10.1186/s13059-014-0550-8 (2014).
- 389 Hauptmann, J., Schraivogel, D., Bruckmann, A., Manickavel, S., Jakob, L., Eichner, N., Pfaff, J., Urban, M., Sprunck, S., Hafner, M., Tuschl, T., Deutzmann, R. & Meister, G. Biochemical isolation of Argonaute protein complexes by Ago-APP. *Proceedings of the National Academy of Sciences of the United States of America* **112**, 11841-11845, doi:10.1073/pnas.1506116112 (2015).

- 390 Hafner, M., Renwick, N., Farazi, T. A., Mihailovic, A., Pena, J. T. & Tuschl, T. Barcoded cDNA library preparation for small RNA profiling by next-generation sequencing. *Methods* **58**, 164-170, doi:10.1016/j.ymeth.2012.07.030 (2012).
- 391 Pham, D. H., Moretti, P. A., Goodall, G. J. & Pitson, S. M. Attenuation of leakiness in doxycycline-inducible expression via incorporation of 3' AU-rich mRNA destabilizing elements. *BioTechniques* **45**, 155-156, 158, 160 passim, doi:10.2144/000112896 (2008).
- 392 Murmann, A. E., Gao, Q. Q., Putzbach, W. E., Patel, M., Bartom, E. T., Law, C. Y., Bridgeman, B., Chen, S., McMahon, K. M., Thaxton, C. S. & Peter, M. E. Small interfering RNAs based on huntingtin trinucleotide repeats are highly toxic to cancer cells. *EMBO reports* **19**, doi:10.15252/embr.201745336 (2018).
- 393 Bramsen, J. B., Laursen, M. B., Nielsen, A. F., Hansen, T. B., Bus, C., Langkjaer, N., Babu, B. R., Hojland, T., Abramov, M., Van Aerschot, A., Odadzic, D., Smicius, R., Haas, J., Andree, C., Barman, J., Wenska, M., Srivastava, P., Zhou, C., Honcharenko, D., Hess, S., Muller, E., Bobkov, G. V., Mikhailov, S. N., Fava, E., Meyer, T. F., Chattopadhyaya, J., Zerial, M., Engels, J. W., Herdewijn, P., Wengel, J. & Kjems, J. A large-scale chemical modification screen identifies design rules to generate siRNAs with high activity, high stability and low toxicity. *Nucleic acids research* **37**, 2867-2881, doi:10.1093/nar/gkp106 (2009).
- 394 Wang, T., Wei, J. J., Sabatini, D. M. & Lander, E. S. Genetic screens in human cells using the CRISPR-Cas9 system. *Science (New York, N.Y.)* **343**, 80-84, doi:10.1126/science.1246981 (2014).
- 395 Morgulis, A., Gertz, E. M., Schaffer, A. A. & Agarwala, R. A fast and symmetric DUST implementation to mask low-complexity DNA sequences. *Journal of computational biology : a journal of computational molecular cell biology* **13**, 1028-1040, doi:10.1089/cmb.2006.13.1028 (2006).
- 396 Medina-Rivera, A., Defrance, M., Sand, O., Herrmann, C., Castro-Mondragon, J. A., Delerce, J., Jaeger, S., Blanchet, C., Vincens, P., Caron, C., Staines, D. M., Contreras-Moreira, B., Artufel, M., Charbonnier-Khamvongsa, L., Hernandez, C., Thieffry, D., Thomas-Chollier, M. & van Helden, J. RSAT 2015: Regulatory Sequence Analysis Tools. *Nucleic acids research* **43**, W50-56, doi:10.1093/nar/gkv362 (2015).
- 397 De Paepe, M. E., Rubin, L. P., Jude, C., Lesieur-Brooks, A. M., Mills, D. R. & Luks, F. I. Fas ligand expression coincides with alveolar cell apoptosis in late-gestation fetal lung development. *American journal of physiology. Lung cellular and molecular physiology* **279**, L967-976, doi:10.1152/ajplung.2000.279.5.L967 (2000).
- 398 Nat, R., Radu, E., Regalia, T. & Popescu, L. M. Apoptosis in human embryo development: 3. Fas-induced apoptosis in brain primary cultures. *Journal of cellular and molecular medicine* **5**, 417-428 (2001).
- 399 Kim, D. H., Behlke, M. A., Rose, S. D., Chang, M. S., Choi, S. & Rossi, J. J. Synthetic dsRNA Dicer substrates enhance RNAi potency and efficacy. *Nature biotechnology* **23**, 222-226, doi:10.1038/nbt1051 (2005).
- 400 Snead, N. M., Wu, X., Li, A., Cui, Q., Sakurai, K., Burnett, J. C. & Rossi, J. J. Molecular basis for improved gene silencing by Dicer substrate interfering RNA compared with other siRNA variants. *Nucleic acids research* **41**, 6209-6221, doi:10.1093/nar/gkt200 (2013).

- 401 Bauer, M., Kinkl, N., Meixner, A., Kremmer, E., Riemenschneider, M., Forstl, H., Gasser, T. & Ueffing, M. Prevention of interferon-stimulated gene expression using microRNA-designed hairpins. *Gene therapy* **16**, 142-147, doi:10.1038/gt.2008.123 (2009).
- 402 Morgens, D. W., Deans, R. M., Li, A. & Bassik, M. C. Systematic comparison of CRISPR/Cas9 and RNAi screens for essential genes. *Nature biotechnology* **34**, 634-636, doi:10.1038/nbt.3567 (2016).
- 403 Caffrey, D. R., Zhao, J., Song, Z., Schaffer, M. E., Haney, S. A., Subramanian, R. R., Seymour, A. B. & Hughes, J. D. siRNA off-target effects can be reduced at concentrations that match their individual potency. *PloS one* **6**, e21503, doi:10.1371/journal.pone.0021503 (2011).
- 404 Teitz, T., Wei, T., Valentine, M. B., Vanin, E. F., Grenet, J., Valentine, V. A., Behm, F. G., Look, A. T., Lahti, J. M. & Kidd, V. J. Caspase 8 is deleted or silenced preferentially in childhood neuroblastomas with amplification of MYCN. *Nature medicine* **6**, 529-535, doi:10.1038/75007 (2000).
- 405 Ghosh, P., Dullea, R., Fischer, J. E., Turi, T. G., Sarver, R. W., Zhang, C., Basu, K., Das, S. K. & Poland, B. W. Comparing 2-nt 3' overhangs against blunt-ended siRNAs: a systems biology based study. *BMC genomics* **10 Suppl 1**, S17, doi:10.1186/1471-2164-10-s1-s17 (2009).
- 406 Parmar, R., Willoughby, J. L., Liu, J., Foster, D. J., Brigham, B., Theile, C. S., Charisse, K., Akinc, A., Guidry, E., Pei, Y., Strapps, W., Cancelli, M., Stanton, M. G., Rajeev, K. G., Sepp-Lorenzino, L., Manoharan, M., Meyers, R., Maier, M. A. & Jadhav, V. 5'-(E)-Vinylphosphonate: A Stable Phosphate Mimic Can Improve the RNAi Activity of siRNA-GalNAc Conjugates. *Chembiochem : a European journal of chemical biology* **17**, 985-989, doi:10.1002/cbic.201600130 (2016).
- 407 Blomen, V. A., Majek, P., Jae, L. T., Bigenzahn, J. W., Nieuwenhuis, J., Staring, J., Sacco, R., van Diemen, F. R., Olk, N., Stukalov, A., Marceau, C., Janssen, H., Carette, J. E., Bennett, K. L., Colinge, J., Superti-Furga, G. & Brummelkamp, T. R. Gene essentiality and synthetic lethality in haploid human cells. *Science (New York, N.Y.)* **350**, 1092-1096, doi:10.1126/science.aac7557 (2015).
- 408 Wang, T., Birsoy, K., Hughes, N. W., Krupczak, K. M., Post, Y., Wei, J. J., Lander, E. S. & Sabatini, D. M. Identification and characterization of essential genes in the human genome. *Science (New York, N.Y.)* **350**, 1096-1101, doi:10.1126/science.aac7041 (2015).
- 409 Mi, N., Chen, Y., Wang, S., Chen, M., Zhao, M., Yang, G., Ma, M., Su, Q., Luo, S., Shi, J., Xu, J., Guo, Q., Gao, N., Sun, Y., Chen, Z. & Yu, L. CapZ regulates autophagosomal membrane shaping by promoting actin assembly inside the isolation membrane. *Nature cell biology* **17**, 1112-1123, doi:10.1038/ncb3215 (2015).
- 410 Sun, D., Zhou, M., Kowolik, C. M., Trisal, V., Huang, Q., Kernstine, K. H., Lian, F. & Shen, B. Differential expression patterns of capping protein, protein phosphatase 1, and casein kinase 1 may serve as diagnostic markers for malignant melanoma. *Melanoma research* **21**, 335-343, doi:10.1097/CMR.0b013e328346b715 (2011).
- 411 Zhang, Y., Wang, Y., Wei, Y., Wu, J., Zhang, P., Shen, S., Saiyin, H., Wumaier, R., Yang, X., Wang, C. & Yu, L. Molecular chaperone CCT3 supports proper mitotic progression and cell proliferation in hepatocellular carcinoma cells. *Cancer letters* **372**, 101-109, doi:10.1016/j.canlet.2015.12.029 (2016).

- 412 Bae, K., Park, K. E., Han, J., Kim, J., Kim, K. & Yoon, K. A. Mitotic cell death caused by follistatin-like 1 inhibition is associated with up-regulated Bim by inactivated Erk1/2 in human lung cancer cells. *Oncotarget* **7**, 18076-18084, doi:10.18632/oncotarget.6729 (2016).
- 413 Yoo, J. K., Choi, S. J. & Kim, J. K. Expression profiles of subtracted mRNAs during cellular senescence in human mesenchymal stem cells derived from bone marrow. *Experimental gerontology* **48**, 464-471, doi:10.1016/j.exger.2013.02.022 (2013).
- 414 Rabenhorst, U., Thalheimer, F. B., Gerlach, K., Kijonka, M., Bohm, S., Krause, D. S., Vauti, F., Arnold, H. H., Schroeder, T., Schnutgen, F., von Melchner, H., Rieger, M. A. & Zornig, M. Single-Stranded DNA-Binding Transcriptional Regulator FUBP1 Is Essential for Fetal and Adult Hematopoietic Stem Cell Self-Renewal. *Cell reports* **11**, 1847-1855, doi:10.1016/j.celrep.2015.05.038 (2015).
- 415 Jang, M., Park, B. C., Kang, S., Chi, S. W., Cho, S., Chung, S. J., Lee, S. C., Bae, K. H. & Park, S. G. Far upstream element-binding protein-1, a novel caspase substrate, acts as a cross-talker between apoptosis and the c-myc oncogene. *Oncogene* **28**, 1529-1536, doi:10.1038/onc.2009.11 (2009).
- 416 Baumgarten, P., Harter, P. N., Tonjes, M., Capper, D., Blank, A. E., Sahm, F., von Deimling, A., Kolluru, V., Schwamb, B., Rabenhorst, U., Starzetz, T., Kogel, D., Rieker, R. J., Plate, K. H., Ohgaki, H., Radlwimmer, B., Zornig, M. & Mittelbronn, M. Loss of FUBP1 expression in gliomas predicts FUBP1 mutation and is associated with oligodendroglial differentiation, IDH1 mutation and 1p/19q loss of heterozygosity. *Neuropathology and applied neurobiology* **40**, 205-216, doi:10.1111/nan.12088 (2014).
- 417 Wazir, U., Jiang, W. G., Sharma, A. K. & Mokbel, K. Guanine nucleotide binding protein beta 1: a novel transduction protein with a possible role in human breast cancer. *Cancer genomics & proteomics* **10**, 69-73 (2013).
- 418 Sancho, M., Diani, E., Beato, M. & Jordan, A. Depletion of human histone H1 variants uncovers specific roles in gene expression and cell growth. *PLoS genetics* **4**, e1000227, doi:10.1371/journal.pgen.1000227 (2008).
- 419 Hou, F., Chu, C. W., Kong, X., Yokomori, K. & Zou, H. The acetyltransferase activity of San stabilizes the mitotic cohesin at the centromeres in a shugoshin-independent manner. *The Journal of cell biology* **177**, 587-597, doi:10.1083/jcb.200701043 (2007).
- 420 Parpys, A. C., Zhao, W., Sharma, N., Groesser, T., Liang, F., Maranon, D. G., Leung, S. G., Grundt, K., Dray, E., Idate, R., Ostvold, A. C., Schild, D., Sung, P. & Wiese, C. NUCKS1 is a novel RAD51AP1 paralog important for homologous recombination and genome stability. *Nucleic acids research* **43**, 9817-9834, doi:10.1093/nar/gkv859 (2015).
- 421 Quidville, V., Alsafadi, S., Goubar, A., Commo, F., Scott, V., Pioche-Durieu, C., Girault, I., Bacconnais, S., Le Cam, E., Lazar, V., Delalogue, S., Saghatchian, M., Pautier, P., Morice, P., Dessen, P., Vagner, S. & Andre, F. Targeting the deregulated spliceosome core machinery in cancer cells triggers mTOR blockade and autophagy. *Cancer research* **73**, 2247-2258, doi:10.1158/0008-5472.can-12-2501 (2013).
- 422 Pham, D. H., Powell, J. A., Gliddon, B. L., Moretti, P. A., Tsykin, A., Van der Hoek, M., Kenyon, R., Goodall, G. J. & Pitson, S. M. Enhanced expression of transferrin receptor 1 contributes to oncogenic signalling by sphingosine kinase 1. *Oncogene* **33**, 5559-5568, doi:10.1038/onc.2013.502 (2014).

- 423 Chan, K. T., Choi, M. Y., Lai, K. K., Tan, W., Tung, L. N., Lam, H. Y., Tong, D. K., Lee, N. P. & Law, S. Overexpression of transferrin receptor CD71 and its tumorigenic properties in esophageal squamous cell carcinoma. *Oncology reports* **31**, 1296-1304, doi:10.3892/or.2014.2981 (2014).
- 424 Mantei, A., Rutz, S., Janke, M., Kirchhoff, D., Jung, U., Patzel, V., Vogel, U., Rudel, T., Andreou, I., Weber, M. & Scheffold, A. siRNA stabilization prolongs gene knockdown in primary T lymphocytes. *European journal of immunology* **38**, 2616-2625, doi:10.1002/eji.200738075 (2008).
- 425 Cerami, E., Gao, J., Dogrusoz, U., Gross, B. E., Sumer, S. O., Aksoy, B. A., Jacobsen, A., Byrne, C. J., Heuer, M. L., Larsson, E., Antipin, Y., Reva, B., Goldberg, A. P., Sander, C. & Schultz, N. The cBio cancer genomics portal: an open platform for exploring multidimensional cancer genomics data. *Cancer discovery* **2**, 401-404, doi:10.1158/2159-8290.cd-12-0095 (2012).
- 426 Gao, J., Aksoy, B. A., Dogrusoz, U., Dresdner, G., Gross, B., Sumer, S. O., Sun, Y., Jacobsen, A., Sinha, R., Larsson, E., Cerami, E., Sander, C. & Schultz, N. Integrative analysis of complex cancer genomics and clinical profiles using the cBioPortal. *Science signaling* **6**, p11, doi:10.1126/scisignal.2004088 (2013).
- 427 Lin, X., Yang, J., Chen, J., Gunasekera, A., Fesik, S. W. & Shen, Y. Development of a tightly regulated U6 promoter for shRNA expression. *FEBS letters* **577**, 376-380, doi:10.1016/j.febslet.2004.10.033 (2004).
- 428 Burchard, J., Jackson, A. L., Malkov, V., Needham, R. H., Tan, Y., Bartz, S. R., Dai, H., Sachs, A. B. & Linsley, P. S. MicroRNA-like off-target transcript regulation by siRNAs is species specific. *RNA (New York, N.Y.)* **15**, 308-315, doi:10.1261/rna.1326809 (2009).
- 429 Fedorov, Y., Anderson, E. M., Birmingham, A., Reynolds, A., Karpilow, J., Robinson, K., Leake, D., Marshall, W. S. & Khvorova, A. Off-target effects by siRNA can induce toxic phenotype. *RNA (New York, N.Y.)* **12**, 1188-1196, doi:10.1261/rna.28106 (2006).
- 430 Robbins, M. A., Li, M., Leung, I., Li, H., Boyer, D. V., Song, Y., Behlke, M. A. & Rossi, J. J. Stable expression of shRNAs in human CD34+ progenitor cells can avoid induction of interferon responses to siRNAs in vitro. *Nature biotechnology* **24**, 566-571, doi:10.1038/nbt1206 (2006).
- 431 Kawasaki, M., Kuwano, K., Nakanishi, Y., Hagimoto, N., Takayama, K., Pei, X. H., Maeyama, T., Yoshimi, M. & Hara, N. Analysis of Fas and Fas ligand expression and function in lung cancer cell lines. *European journal of cancer (Oxford, England : 1990)* **36**, 656-663 (2000).
- 432 Kuo, H. C., Lee, H. J., Hu, C. C., Shun, H. I. & Tseng, T. H. Enhancement of esculetin on Taxol-induced apoptosis in human hepatoma HepG2 cells. *Toxicol Appl Pharmacol* **210**, 55-62, doi:10.1016/j.taap.2005.06.020 (2006).
- 433 Martinez, N. J. & Gregory, R. I. Argonaute2 expression is post-transcriptionally coupled to microRNA abundance. *RNA (New York, N.Y.)* **19**, 605-612, doi:10.1261/rna.036434.112 (2013).
- 434 Hyer, M. L., Voelkel-Johnson, C., Rubinchik, S., Dong, J.-y. & Norris, J. S. Intracellular Fas Ligand Expression Causes Fas-Mediated Apoptosis in Human Prostate Cancer Cells Resistant to Monoclonal Antibody-Induced Apoptosis. *Molecular Therapy* **2**, 348-358, doi:10.1006/mthe.2000.0139.



- 435 Clark, A. M., Goldstein, L. D., Tevlin, M., Tavare, S., Shaham, S. & Miska, E. A. The microRNA miR-124 controls gene expression in the sensory nervous system of *Caenorhabditis elegans*. *Nucleic acids research* **38**, 3780-3793, doi:10.1093/nar/gkq083 (2010).
- 436 Grun, D., Wang, Y. L., Langenberger, D., Gunsalus, K. C. & Rajewsky, N. microRNA target predictions across seven *Drosophila* species and comparison to mammalian targets. *PLoS computational biology* **1**, e13, doi:10.1371/journal.pcbi.0010013 (2005).
- 437 Qi, X. The role of miR-9 during neuron differentiation of mouse retinal stem cells. *Artificial cells, nanomedicine, and biotechnology* **44**, 1883-1890, doi:10.3109/21691401.2015.1111231 (2016).
- 438 Coolen, M., Thieffry, D., Drivenes, O., Becker, T. S. & Bally-Cuif, L. miR-9 controls the timing of neurogenesis through the direct inhibition of antagonistic factors. *Developmental cell* **22**, 1052-1064, doi:10.1016/j.devcel.2012.03.003 (2012).
- 439 Leucht, C., Stigloher, C., Wizenmann, A., Klafke, R., Folchert, A. & Bally-Cuif, L. MicroRNA-9 directs late organizer activity of the midbrain-hindbrain boundary. *Nature neuroscience* **11**, 641-648, doi:10.1038/nn.2115 (2008).
- 440 Garaffo, G., Conte, D., Provero, P., Tomaiuolo, D., Luo, Z., Pinciroli, P., Peano, C., D'Atri, I., Gitton, Y., Etzion, T., Gothilf, Y., Gays, D., Santoro, M. M. & Merlo, G. R. The *Dlx5* and *Foxg1* transcription factors, linked via miRNA-9 and -200, are required for the development of the olfactory and GnRH system. *Molecular and cellular neurosciences* **68**, 103-119, doi:10.1016/j.mcn.2015.04.007 (2015).
- 441 Cohen, S. M., Brennecke, J. & Stark, A. Denoising feedback loops by thresholding--a new role for microRNAs. *Genes & development* **20**, 2769-2772, doi:10.1101/gad.1484606 (2006).
- 442 Mishima, Y., Abreu-Goodger, C., Staton, A. A., Stahlhut, C., Shou, C., Cheng, C., Gerstein, M., Enright, A. J. & Giraldez, A. J. Zebrafish miR-1 and miR-133 shape muscle gene expression and regulate sarcomeric actin organization. *Genes & development* **23**, 619-632, doi:10.1101/gad.1760209 (2009).
- 443 Wu, C. I., Shen, Y. & Tang, T. Evolution under canalization and the dual roles of microRNAs: a hypothesis. *Genome research* **19**, 734-743, doi:10.1101/gr.084640.108 (2009).
- 444 Betel, D., Koppal, A., Agius, P., Sander, C. & Leslie, C. Comprehensive modeling of microRNA targets predicts functional non-conserved and non-canonical sites. *Genome biology* **11**, R90, doi:10.1186/gb-2010-11-8-r90 (2010).
- 445 Chan, C. S., Elemento, O. & Tavazoie, S. Revealing posttranscriptional regulatory elements through network-level conservation. *PLoS computational biology* **1**, e69, doi:10.1371/journal.pcbi.0010069 (2005).
- 446 Wang, X. & El Naqa, I. M. Prediction of both conserved and nonconserved microRNA targets in animals. *Bioinformatics (Oxford, England)* **24**, 325-332, doi:10.1093/bioinformatics/btm595 (2008).
- 447 Tang, T., Kumar, S., Shen, Y., Lu, J., Wu, M. L., Shi, S., Li, W. H. & Wu, C. I. Adverse interactions between micro-RNAs and target genes from different species. *Proceedings of the National Academy of Sciences of the United States of America* **107**, 12935-12940, doi:10.1073/pnas.1007591107 (2010).

- 448 Linsley, P. S., Schelter, J., Burchard, J., Kibukawa, M., Martin, M. M., Bartz, S. R.,  
Johnson, J. M., Cummins, J. M., Raymond, C. K., Dai, H., Chau, N., Cleary, M., Jackson,  
A. L., Carleton, M. & Lim, L. Transcripts targeted by the microRNA-16 family  
cooperatively regulate cell cycle progression. *Molecular and cellular biology* **27**, 2240-  
2252, doi:10.1128/mcb.02005-06 (2007).
- 449 Su, J., Zhang, A., Shi, Z., Ma, F., Pu, P., Wang, T., Zhang, J., Kang, C. & Zhang, Q.  
MicroRNA-200a suppresses the Wnt/beta-catenin signaling pathway by interacting with  
beta-catenin. *International journal of oncology* **40**, 1162-1170, doi:10.3892/ijo.2011.1322  
(2012).
- 450 Kirino, Y. & Mourelatos, Z. Site-specific crosslinking of human microRNPs to RNA  
targets. *RNA (New York, N.Y.)* **14**, 2254-2259, doi:10.1261/rna.1133808 (2008).
- 451 Durrett, R. & Schmidt, D. Waiting for two mutations: with applications to regulatory  
sequence evolution and the limits of Darwinian evolution. *Genetics* **180**, 1501-1509,  
doi:10.1534/genetics.107.082610 (2008).
- 452 Bentwich, I., Avniel, A., Karov, Y., Aharonov, R., Gilad, S., Barad, O., Barzilai, A., Einat,  
P., Einav, U., Meiri, E., Sharon, E., Spector, Y. & Bentwich, Z. Identification of hundreds  
of conserved and nonconserved human microRNAs. *Nature genetics* **37**, 766-770,  
doi:10.1038/ng1590 (2005).
- 453 Ciliberti, S., Martin, O. C. & Wagner, A. Robustness can evolve gradually in complex  
regulatory gene networks with varying topology. *PLoS computational biology* **3**, e15,  
doi:10.1371/journal.pcbi.0030015 (2007).
- 454 Ciliberti, S., Martin, O. C. & Wagner, A. Innovation and robustness in complex regulatory  
gene networks. *Proceedings of the National Academy of Sciences of the United States of  
America* **104**, 13591-13596, doi:10.1073/pnas.0705396104 (2007).
- 455 Martinez, N. J., Ow, M. C., Barrasa, M. I., Hammell, M., Sequerra, R., Doucette-Stamm,  
L., Roth, F. P., Ambros, V. R. & Walhout, A. J. A C. elegans genome-scale microRNA  
network contains composite feedback motifs with high flux capacity. *Genes &  
development* **22**, 2535-2549, doi:10.1101/gad.1678608 (2008).
- 456 Tsang, J., Zhu, J. & van Oudenaarden, A. MicroRNA-mediated feedback and feedforward  
loops are recurrent network motifs in mammals. *Molecular cell* **26**, 753-767,  
doi:10.1016/j.molcel.2007.05.018 (2007).
- 457 Ebert, M. S. & Sharp, P. A. Roles for microRNAs in conferring robustness to biological  
processes. *Cell* **149**, 515-524, doi:10.1016/j.cell.2012.04.005 (2012).
- 458 Bu, P., Wang, L., Chen, K. Y., Srinivasan, T., Murthy, P. K., Tung, K. L., Varanko, A. K.,  
Chen, H. J., Ai, Y., King, S., Lipkin, S. M. & Shen, X. A miR-34a-Numb Feedforward  
Loop Triggered by Inflammation Regulates Asymmetric Stem Cell Division in Intestine  
and Colon Cancer. *Cell stem cell* **18**, 189-202, doi:10.1016/j.stem.2016.01.006 (2016).
- 459 Lu, M., Jolly, M. K., Levine, H., Onuchic, J. N. & Ben-Jacob, E. MicroRNA-based  
regulation of epithelial-hybrid-mesenchymal fate determination. *Proceedings of the  
National Academy of Sciences of the United States of America* **110**, 18144-18149,  
doi:10.1073/pnas.1318192110 (2013).
- 460 Tian, X. J., Zhang, H. & Xing, J. Coupled reversible and irreversible bistable switches  
underlying TGFbeta-induced epithelial to mesenchymal transition. *Biophysical journal*  
**105**, 1079-1089, doi:10.1016/j.bpj.2013.07.011 (2013).

- 461 Li, X., Cassidy, J. J., Reinke, C. A., Fischboeck, S. & Carthew, R. W. A microRNA imparts robustness against environmental fluctuation during development. *Cell* **137**, 273-282, doi:10.1016/j.cell.2009.01.058 (2009).
- 462 Fazi, F., Rosa, A., Fatica, A., Gelmetti, V., De Marchis, M. L., Nervi, C. & Bozzoni, I. A minicircuitry comprised of microRNA-223 and transcription factors NFI-A and C/EBPalpha regulates human granulopoiesis. *Cell* **123**, 819-831, doi:10.1016/j.cell.2005.09.023 (2005).
- 463 Luo, W., Li, G., Yi, Z., Nie, Q. & Zhang, X. E2F1-miR-20a-5p/20b-5p auto-regulatory feedback loop involved in myoblast proliferation and differentiation. *Scientific reports* **6**, 27904, doi:10.1038/srep27904 (2016).
- 464 Zhang, Z., Zha, Y., Hu, W., Huang, Z., Gao, Z., Zang, Y., Chen, J., Dong, L. & Zhang, J. The autoregulatory feedback loop of microRNA-21/programmed cell death protein 4/activation protein-1 (MiR-21/PDCD4/AP-1) as a driving force for hepatic fibrosis development. *The Journal of biological chemistry* **288**, 37082-37093, doi:10.1074/jbc.M113.517953 (2013).
- 465 Cho, C. Y., Huang, J. S., Shiah, S. G., Chung, S. Y., Lay, J. D., Yang, Y. Y., Lai, G. M., Cheng, A. L., Chen, L. T. & Chuang, S. E. Negative feedback regulation of AXL by miR-34a modulates apoptosis in lung cancer cells. *RNA (New York, N.Y.)* **22**, 303-315, doi:10.1261/rna.052571.115 (2016).
- 466 Cohen, E. E., Zhu, H., Lingen, M. W., Martin, L. E., Kuo, W. L., Choi, E. A., Kocherginsky, M., Parker, J. S., Chung, C. H. & Rosner, M. R. A feed-forward loop involving protein kinase Calpha and microRNAs regulates tumor cell cycle. *Cancer research* **69**, 65-74, doi:10.1158/0008-5472.can-08-0377 (2009).
- 467 Aguda, B. D., Kim, Y., Piper-Hunter, M. G., Friedman, A. & Marsh, C. B. MicroRNA regulation of a cancer network: consequences of the feedback loops involving miR-17-92, E2F, and Myc. *Proceedings of the National Academy of Sciences of the United States of America* **105**, 19678-19683, doi:10.1073/pnas.0811166106 (2008).
- 468 Sylvestre, Y., De Guire, V., Querido, E., Mukhopadhyay, U. K., Bourdeau, V., Major, F., Ferbeyre, G. & Chartrand, P. An E2F/miR-20a autoregulatory feedback loop. *The Journal of biological chemistry* **282**, 2135-2143, doi:10.1074/jbc.M608939200 (2007).
- 469 Si, W., Shen, J., Du, C., Chen, D., Gu, X., Li, C., Yao, M., Pan, J., Cheng, J., Jiang, D., Xu, L., Bao, C., Fu, P. & Fan, W. A miR-20a/MAPK1/c-Myc regulatory feedback loop regulates breast carcinogenesis and chemoresistance. *Cell death and differentiation* **25**, 406-420, doi:10.1038/cdd.2017.176 (2018).
- 470 Jiang, W., Mitra, R., Lin, C. C., Wang, Q., Cheng, F. & Zhao, Z. Systematic dissection of dysregulated transcription factor-miRNA feed-forward loops across tumor types. *Briefings in bioinformatics* **17**, 996-1008, doi:10.1093/bib/bbv107 (2016).
- 471 Brabletz, S., Bajdak, K., Meidhof, S., Burk, U., Niedermann, G., Firat, E., Wellner, U., Dimmler, A., Faller, G., Schubert, J. & Brabletz, T. The ZEB1/miR-200 feedback loop controls Notch signalling in cancer cells. *The EMBO journal* **30**, 770-782, doi:10.1038/emboj.2010.349 (2011).
- 472 Iliopoulos, D., Hirsch, H. A. & Struhl, K. An epigenetic switch involving NF-kappaB, Lin28, Let-7 MicroRNA, and IL6 links inflammation to cell transformation. *Cell* **139**, 693-706, doi:10.1016/j.cell.2009.10.014 (2009).

- 473 Lai, X., Wolkenhauer, O. & Vera, J. Understanding microRNA-mediated gene regulatory networks through mathematical modelling. *Nucleic acids research* **44**, 6019-6035, doi:10.1093/nar/gkw550 (2016).
- 474 O'Donnell, K. A., Wentzel, E. A., Zeller, K. I., Dang, C. V. & Mendell, J. T. c-Myc-regulated microRNAs modulate E2F1 expression. *Nature* **435**, 839-843, doi:10.1038/nature03677 (2005).
- 475 Siciliano, V., Garzilli, I., Fracassi, C., Criscuolo, S., Ventre, S. & di Bernardo, D. MiRNAs confer phenotypic robustness to gene networks by suppressing biological noise. *Nature communications* **4**, 2364, doi:10.1038/ncomms3364 (2013).
- 476 Rosenfeld, N., Young, J. W., Alon, U., Swain, P. S. & Elowitz, M. B. Accurate prediction of gene feedback circuit behavior from component properties. *Molecular systems biology* **3**, 143, doi:10.1038/msb4100185 (2007).
- 477 Li, L., Shi, B., Chen, J., Li, C., Wang, S., Wang, Z. & Zhu, G. An E2F1/MiR-17-92 Negative Feedback Loop mediates proliferation of Mouse Palatal Mesenchymal Cells. *Scientific reports* **7**, 5148, doi:10.1038/s41598-017-05479-7 (2017).
- 478 Blum, W., Henzi, T., Schwaller, B. & Pecze, L. Biological noise and positional effects influence cell stemness. *The Journal of biological chemistry*, doi:10.1074/jbc.RA117.001643 (2018).
- 479 Zhang, L., Huang, J., Yang, N., Greshock, J., Megraw, M. S., Giannakakis, A., Liang, S., Naylor, T. L., Barchetti, A., Ward, M. R., Yao, G., Medina, A., O'Brien-Jenkins, A., Katsaros, D., Hatzigeorgiou, A., Gimotty, P. A., Weber, B. L. & Coukos, G. microRNAs exhibit high frequency genomic alterations in human cancer. *Proceedings of the National Academy of Sciences of the United States of America* **103**, 9136-9141, doi:10.1073/pnas.0508889103 (2006).
- 480 Osella, M., Bosia, C., Cora, D. & Caselle, M. The role of incoherent microRNA-mediated feedforward loops in noise buffering. *PLoS computational biology* **7**, e1001101, doi:10.1371/journal.pcbi.1001101 (2011).
- 481 Pickering, M. T., Stadler, B. M. & Kowalik, T. F. miR-17 and miR-20a temper an E2F1-induced G1 checkpoint to regulate cell cycle progression. *Oncogene* **28**, 140-145, doi:10.1038/onc.2008.372 (2009).
- 482 Mu, P., Han, Y. C., Betel, D., Yao, E., Squatrito, M., Ogdowski, P., de Stanchina, E., D'Andrea, A., Sander, C. & Ventura, A. Genetic dissection of the miR-17~92 cluster of microRNAs in Myc-induced B-cell lymphomas. *Genes & development* **23**, 2806-2811, doi:10.1101/gad.1872909 (2009).
- 483 Robaina, M. C., Faccion, R. S., Mazzoccoli, L., Rezende, L. M., Queiroga, E., Bacchi, C. E., Thomas-Tikhonenko, A. & Klumb, C. E. miR-17-92 cluster components analysis in Burkitt lymphoma: overexpression of miR-17 is associated with poor prognosis. *Annals of hematology* **95**, 881-891, doi:10.1007/s00277-016-2653-7 (2016).
- 484 Kumar, M. S., Erkeland, S. J., Pester, R. E., Chen, C. Y., Ebert, M. S., Sharp, P. A. & Jacks, T. Suppression of non-small cell lung tumor development by the let-7 microRNA family. *Proceedings of the National Academy of Sciences of the United States of America* **105**, 3903-3908, doi:10.1073/pnas.0712321105 (2008).
- 485 Riba, A., Bosia, C., El Baroudi, M., Ollino, L. & Caselle, M. A combination of transcriptional and microRNA regulation improves the stability of the relative

- concentrations of target genes. *PLoS computational biology* **10**, e1003490, doi:10.1371/journal.pcbi.1003490 (2014).
- 486 Xiong, W. & Ferrell, J. E., Jr. A positive-feedback-based bistable 'memory module' that governs a cell fate decision. *Nature* **426**, 460-465, doi:10.1038/nature02089 (2003).
- 487 Li, Y., Li, Y., Zhang, H. & Chen, Y. MicroRNA-mediated positive feedback loop and optimized bistable switch in a cancer network Involving miR-17-92. *PloS one* **6**, e26302, doi:10.1371/journal.pone.0026302 (2011).
- 488 Pampalakis, G., Diamandis, E. P., Katsaros, D. & Sotiropoulou, G. Down-regulation of dicer expression in ovarian cancer tissues. *Clinical biochemistry* **43**, 324-327, doi:10.1016/j.clinbiochem.2009.09.014 (2010).
- 489 Dedes, K. J., Natrajan, R., Lambros, M. B., Geyer, F. C., Lopez-Garcia, M. A., Savage, K., Jones, R. L. & Reis-Filho, J. S. Down-regulation of the miRNA master regulators Droscha and Dicer is associated with specific subgroups of breast cancer. *European journal of cancer (Oxford, England : 1990)* **47**, 138-150, doi:10.1016/j.ejca.2010.08.007 (2011).
- 490 Sandberg, R., Neilson, J. R., Sarma, A., Sharp, P. A. & Burge, C. B. Proliferating cells express mRNAs with shortened 3' untranslated regions and fewer microRNA target sites. *Science (New York, N.Y.)* **320**, 1643-1647, doi:10.1126/science.1155390 (2008).
- 491 Re, A., Cora, D., Taverna, D. & Caselle, M. Genome-wide survey of microRNA-transcription factor feed-forward regulatory circuits in human. *Molecular bioSystems* **5**, 854-867, doi:10.1039/b900177h (2009).
- 492 Farre, D., Bellora, N., Mularoni, L., Messeguer, X. & Alba, M. M. Housekeeping genes tend to show reduced upstream sequence conservation. *Genome biology* **8**, R140, doi:10.1186/gb-2007-8-7-r140 (2007).
- 493 Spencer, S. L., Gaudet, S., Albeck, J. G., Burke, J. M. & Sorger, P. K. Non-genetic origins of cell-to-cell variability in TRAIL-induced apoptosis. *Nature* **459**, 428-432, doi:10.1038/nature08012 (2009).
- 494 Hill, R. P., Chambers, A. F., Ling, V. & Harris, J. F. Dynamic heterogeneity: rapid generation of metastatic variants in mouse B16 melanoma cells. *Science (New York, N.Y.)* **224**, 998-1001 (1984).
- 495 Li, Q., Wennborg, A., Aurell, E., Dekel, E., Zou, J. Z., Xu, Y., Huang, S. & Ernberg, I. Dynamics inside the cancer cell attractor reveal cell heterogeneity, limits of stability, and escape. *Proceedings of the National Academy of Sciences of the United States of America* **113**, 2672-2677, doi:10.1073/pnas.1519210113 (2016).
- 496 Kumar, M. S., Lu, J., Mercer, K. L., Golub, T. R. & Jacks, T. Impaired microRNA processing enhances cellular transformation and tumorigenesis. *Nature genetics* **39**, 673-677, doi:10.1038/ng2003 (2007).
- 497 Kumar, M. S., Pester, R. E., Chen, C. Y., Lane, K., Chin, C., Lu, J., Kirsch, D. G., Golub, T. R. & Jacks, T. Dicer1 functions as a haploinsufficient tumor suppressor. *Genes & development* **23**, 2700-2704, doi:10.1101/gad.1848209 (2009).
- 498 Akman, H. B., Oyken, M., Tuncer, T., Can, T. & Erson-Bensan, A. E. 3'UTR shortening and EGF signaling: implications for breast cancer. *Human molecular genetics* **24**, 6910-6920, doi:10.1093/hmg/ddv391 (2015).

- 499 Messeguer, X., Escudero, R., Farre, D., Nunez, O., Martinez, J. & Alba, M. M. PROMO: detection of known transcription regulatory elements using species-tailored searches. *Bioinformatics (Oxford, England)* **18**, 333-334 (2002).
- 500 Chi, S. W., Zang, J. B., Mele, A. & Darnell, R. B. Argonaute HITS-CLIP decodes microRNA-mRNA interaction maps. *Nature* **460**, 479-486, doi:10.1038/nature08170 (2009).
- 501 Knott, S. R. V., Maceli, A., Erard, N., Chang, K., Marran, K., Zhou, X., Gordon, A., Demerdash, O. E., Wagenblast, E., Kim, S., Fellmann, C. & Hannon, G. J. A computational algorithm to predict shRNA potency. *Molecular cell* **56**, 796-807, doi:10.1016/j.molcel.2014.10.025 (2014).
- 502 Fellmann, C., Zuber, J., McJunkin, K., Chang, K., Malone, C. D., Dickins, R. A., Xu, Q., Hengartner, M. O., Elledge, S. J., Hannon, G. J. & Lowe, S. W. Functional identification of optimized RNAi triggers using a massively parallel sensor assay. *Molecular cell* **41**, 733-746, doi:10.1016/j.molcel.2011.02.008 (2011).
- 503 Chandradoss, S. D., Schirle, N. T., Szczepaniak, M., MacRae, I. J. & Joo, C. A Dynamic Search Process Underlies MicroRNA Targeting. *Cell* **162**, 96-107, doi:10.1016/j.cell.2015.06.032 (2015).
- 504 Lyu, Y., Shen, Y., Li, H., Chen, Y., Guo, L., Zhao, Y., Hungate, E., Shi, S., Wu, C. I. & Tang, T. New microRNAs in Drosophila--birth, death and cycles of adaptive evolution. *PLoS genetics* **10**, e1004096, doi:10.1371/journal.pgen.1004096 (2014).
- 505 Lu, J., Shen, Y., Wu, Q., Kumar, S., He, B., Shi, S., Carthew, R. W., Wang, S. M. & Wu, C. I. The birth and death of microRNA genes in Drosophila. *Nature genetics* **40**, 351-355, doi:10.1038/ng.73 (2008).
- 506 Nozawa, M., Fujimi, M., Iwamoto, C., Onizuka, K., Fukuda, N., Ikeo, K. & Gojobori, T. Evolutionary Transitions of MicroRNA-Target Pairs. *Genome biology and evolution* **8**, 1621-1633, doi:10.1093/gbe/evw092 (2016).
- 507 Ito, Y., Inoue, A., Seers, T., Hato, Y., Igarashi, A., Toyama, T., Taganov, K. D., Boldin, M. P. & Asahara, H. Identification of targets of tumor suppressor microRNA-34a using a reporter library system. *Proceedings of the National Academy of Sciences of the United States of America* **114**, 3927-3932, doi:10.1073/pnas.1620019114 (2017).
- 508 Yin, D., Ogawa, S., Kawamata, N., Leiter, A., Ham, M., Li, D., Doan, N. B., Said, J. W., Black, K. L. & Phillip Koeffler, H. miR-34a functions as a tumor suppressor modulating EGFR in glioblastoma multiforme. *Oncogene* **32**, 1155-1163, doi:10.1038/onc.2012.132 (2013).
- 509 Tivnan, A., Tracey, L., Buckley, P. G., Alcock, L. C., Davidoff, A. M. & Stallings, R. L. MicroRNA-34a is a potent tumor suppressor molecule in vivo in neuroblastoma. *BMC cancer* **11**, 33, doi:10.1186/1471-2407-11-33 (2011).
- 510 Tian, X., Zhang, J., Yan, L., Dong, J. M. & Guo, Q. MiRNA-15a inhibits proliferation, migration and invasion by targeting TNFAIP1 in human osteosarcoma cells. *International journal of clinical and experimental pathology* **8**, 6442-6449 (2015).
- 511 Kang, W., Tong, J. H., Lung, R. W., Dong, Y., Zhao, J., Liang, Q., Zhang, L., Pan, Y., Yang, W., Pang, J. C., Cheng, A. S., Yu, J. & To, K. F. Targeting of YAP1 by microRNA-15a and microRNA-16-1 exerts tumor suppressor function in gastric adenocarcinoma. *Molecular cancer* **14**, 52, doi:10.1186/s12943-015-0323-3 (2015).

- 512 Xie, F., Yuan, Y., Xie, L., Ran, P., Xiang, X., Huang, Q., Qi, G., Guo, X., Xiao, C. & Zheng, S. miRNA-320a inhibits tumor proliferation and invasion by targeting c-Myc in human hepatocellular carcinoma. *OncoTargets and therapy* **10**, 885-894, doi:10.2147/ott.s122992 (2017).
- 513 Xishan, Z., Ziyang, L., Jing, D. & Gang, L. MicroRNA-320a acts as a tumor suppressor by targeting BCR/ABL oncogene in chronic myeloid leukemia. *Scientific reports* **5**, 12460, doi:10.1038/srep12460 (2015).
- 514 Smibert, P., Yang, J. S., Azzam, G., Liu, J. L. & Lai, E. C. Homeostatic control of Argonaute stability by microRNA availability. *Nature structural & molecular biology* **20**, 789-795, doi:10.1038/nsmb.2606 (2013).
- 515 Chakrabarti, A., Banerjee, S., Franchi, L., Loo, Y. M., Gale, M., Jr., Nunez, G. & Silverman, R. H. RNase L activates the NLRP3 inflammasome during viral infections. *Cell host & microbe* **17**, 466-477, doi:10.1016/j.chom.2015.02.010 (2015).
- 516 Li, X. L., Blackford, J. A. & Hassel, B. A. RNase L mediates the antiviral effect of interferon through a selective reduction in viral RNA during encephalomyocarditis virus infection. *Journal of virology* **72**, 2752-2759 (1998).
- 517 Malathi, K., Dong, B., Gale, M., Jr. & Silverman, R. H. Small self-RNA generated by RNase L amplifies antiviral innate immunity. *Nature* **448**, 816-819, doi:10.1038/nature06042 (2007).
- 518 Santamaria, A. B., Davis, D. W., Nghiem, D. X., McConkey, D. J., Ullrich, S. E., Kapoor, M., Lozano, G. & Ananthaswamy, H. N. p53 and Fas ligand are required for psoralen and UVA-induced apoptosis in mouse epidermal cells. *Cell death and differentiation* **9**, 549-560, doi:10.1038/sj/cdd/4401007 (2002).
- 519 Faris, M., Latinis, K. M., Kempiak, S. J., Koretzky, G. A. & Nel, A. Stress-induced Fas ligand expression in T cells is mediated through a MEK kinase 1-regulated response element in the Fas ligand promoter. *Molecular and cellular biology* **18**, 5414-5424 (1998).
- 520 Mo, Y. Y. & Beck, W. T. DNA damage signals induction of fas ligand in tumor cells. *Molecular pharmacology* **55**, 216-222 (1999).
- 521 Caricchio, R., Kovalenko, D., Kaufmann, W. K. & Cohen, P. L. Apoptosis provoked by the oxidative stress inducer menadione (Vitamin K(3)) is mediated by the Fas/Fas ligand system. *Clinical immunology (Orlando, Fla.)* **93**, 65-74, doi:10.1006/clim.1999.4757 (1999).
- 522 Denning, T. L., Takaishi, H., Crowe, S. E., Boldogh, I., Jevnikar, A. & Ernst, P. B. Oxidative stress induces the expression of Fas and Fas ligand and apoptosis in murine intestinal epithelial cells. *Free radical biology & medicine* **33**, 1641-1650 (2002).
- 523 Okamoto, K., Toyokuni, S., Uchida, K., Ogawa, O., Takenawa, J., Kakehi, Y., Kinoshita, H., Hattori-Nakakuki, Y., Hiai, H. & Yoshida, O. Formation of 8-hydroxy-2'-deoxyguanosine and 4-hydroxy-2-nonenal-modified proteins in human renal-cell carcinoma. *International journal of cancer* **58**, 825-829 (1994).
- 524 Hileman, E. O., Liu, J., Albitar, M., Keating, M. J. & Huang, P. Intrinsic oxidative stress in cancer cells: a biochemical basis for therapeutic selectivity. *Cancer chemotherapy and pharmacology* **53**, 209-219, doi:10.1007/s00280-003-0726-5 (2004).

- 525 Thangaraju, M., Kaufmann, S. H. & Couch, F. J. BRCA1 facilitates stress-induced apoptosis in breast and ovarian cancer cell lines. *The Journal of biological chemistry* **275**, 33487-33496, doi:10.1074/jbc.M005824200 (2000).
- 526 Mawji, I. A., Simpson, C. D., Hurren, R., Gronda, M., Williams, M. A., Filmus, J., Jonkman, J., Da Costa, R. S., Wilson, B. C., Thomas, M. P., Reed, J. C., Glinsky, G. V. & Schimmer, A. D. Critical role for Fas-associated death domain-like interleukin-1-converting enzyme-like inhibitory protein in anoikis resistance and distant tumor formation. *Journal of the National Cancer Institute* **99**, 811-822, doi:10.1093/jnci/djk182 (2007).
- 527 Stumm, S., Meyer, A., Lindner, M., Bastert, G., Wallwiener, D. & Guckel, B. Paclitaxel treatment of breast cancer cell lines modulates Fas/Fas ligand expression and induces apoptosis which can be inhibited through the CD40 receptor. *Oncology* **66**, 101-111, doi:10.1159/000077435 (2004).
- 528 Schneiderman, D., Kim, J. M., Senterman, M. & Tsang, B. K. Sustained suppression of Fas ligand expression in cisplatin-resistant human ovarian surface epithelial cancer cells. *Apoptosis : an international journal on programmed cell death* **4**, 271-281 (1999).
- 529 Kasibhatla, S., Brunner, T., Genestier, L., Echeverri, F., Mahboubi, A. & Green, D. R. DNA damaging agents induce expression of Fas ligand and subsequent apoptosis in T lymphocytes via the activation of NF-kappa B and AP-1. *Molecular cell* **1**, 543-551 (1998).
- 530 Kang, Y. H., Lee, K. A., Ryu, C. J., Lee, H. G., Lim, J. S., Park, S. N., Paik, S. G. & Yoon, D. Y. Mitomycin C induces apoptosis via Fas/FasL dependent pathway and suppression of IL-18 in cervical carcinoma cells. *Cancer letters* **237**, 33-44, doi:10.1016/j.canlet.2005.05.043 (2006).
- 531 Hu, X., Bardhan, K., Paschall, A. V., Yang, D., Waller, J. L., Park, M. A., Nayak-Kapoor, A., Samuel, T. A., Abrams, S. I. & Liu, K. Deregulation of apoptotic factors Bcl-xL and Bax confers apoptotic resistance to myeloid-derived suppressor cells and contributes to their persistence in cancer. *The Journal of biological chemistry* **288**, 19103-19115, doi:10.1074/jbc.M112.434530 (2013).
- 532 Rao-Bindal, K., Rao, C. K., Yu, L. & Kleinerman, E. S. Expression of c-FLIP in pulmonary metastases in osteosarcoma patients and human xenografts. *Pediatric blood & cancer* **60**, 575-579, doi:10.1002/pbc.24412 (2013).
- 533 Wang, Y., Luo, J., Zhang, H. & Lu, J. microRNAs in the Same Clusters Evolve to Coordinately Regulate Functionally Related Genes. *Molecular biology and evolution* **33**, 2232-2247, doi:10.1093/molbev/msw089 (2016).
- 534 Sakai, A., Saitow, F., Maruyama, M., Miyake, N., Miyake, K., Shimada, T., Okada, T. & Suzuki, H. MicroRNA cluster miR-17-92 regulates multiple functionally related voltage-gated potassium channels in chronic neuropathic pain. *Nature communications* **8**, 16079, doi:10.1038/ncomms16079 (2017).
- 535 Hayashita, Y., Osada, H., Tatematsu, Y., Yamada, H., Yanagisawa, K., Tomida, S., Yatabe, Y., Kawahara, K., Sekido, Y. & Takahashi, T. A polycistronic microRNA cluster, miR-17-92, is overexpressed in human lung cancers and enhances cell proliferation. *Cancer research* **65**, 9628-9632, doi:10.1158/0008-5472.can-05-2352 (2005).
- 536 Gennarino, V. A., D'Angelo, G., Dharmalingam, G., Fernandez, S., Russolillo, G., Sanges, R., Mutarelli, M., Belcastro, V., Ballabio, A., Verde, P., Sardiello, M. & Banfi, S.



- Identification of microRNA-regulated gene networks by expression analysis of target genes. *Genome research* **22**, 1163-1172, doi:10.1101/gr.130435.111 (2012).
- 537 Liao, M., Jiang, W., Chen, X., Lian, B., Li, W., Lv, Y., Wang, Y., Wang, S. & Li, X. Systematic analysis of regulation and functions of co-expressed microRNAs in humans. *Molecular bioSystems* **6**, 1863-1872, doi:10.1039/b926947a (2010).
- 538 Miyata, T., Yasunaga, T. & Nishida, T. Nucleotide sequence divergence and functional constraint in mRNA evolution. *Proceedings of the National Academy of Sciences of the United States of America* **77**, 7328-7332 (1980).
- 539 Carninci, P., Kasukawa, T., Katayama, S., Gough, J., Frith, M. C., Maeda, N., Oyama, R., Ravasi, T., Lenhard, B., Wells, C., Kodzius, R., Shimokawa, K., Bajic, V. B., Brenner, S. E., Batalov, S., Forrest, A. R., Zavolan, M., Davis, M. J., Wilming, L. G., Aidinis, V., Allen, J. E., Ambesi-Impiombato, A., Apweiler, R., Aturaliya, R. N., Bailey, T. L., Bansal, M., Baxter, L., Beisel, K. W., Bersano, T., Bono, H., Chalk, A. M., Chiu, K. P., Choudhary, V., Christoffels, A., Clutterbuck, D. R., Crowe, M. L., Dalla, E., Dalrymple, B. P., de Bono, B., Della Gatta, G., di Bernardo, D., Down, T., Engstrom, P., Fagiolini, M., Faulkner, G., Fletcher, C. F., Fukushima, T., Furuno, M., Futaki, S., Gariboldi, M., Georgii-Hemming, P., Gingeras, T. R., Gojobori, T., Green, R. E., Gustincich, S., Harbers, M., Hayashi, Y., Hensch, T. K., Hirokawa, N., Hill, D., Huminiecki, L., Iacono, M., Ikeo, K., Iwama, A., Ishikawa, T., Jakt, M., Kanapin, A., Katoh, M., Kawasawa, Y., Kelso, J., Kitamura, H., Kitano, H., Kollias, G., Krishnan, S. P., Kruger, A., Kummerfeld, S. K., Kurochkin, I. V., Lareau, L. F., Lazarevic, D., Lipovich, L., Liu, J., Liuni, S., McWilliam, S., Madan Babu, M., Madera, M., Marchionni, L., Matsuda, H., Matsuzawa, S., Miki, H., Mignone, F., Miyake, S., Morris, K., Mottagui-Tabar, S., Mulder, N., Nakano, N., Nakauchi, H., Ng, P., Nilsson, R., Nishiguchi, S., Nishikawa, S., Nori, F., Ohara, O., Okazaki, Y., Orlando, V., Pang, K. C., Pavan, W. J., Pavesi, G., Pesole, G., Petrovsky, N., Piazza, S., Reed, J., Reid, J. F., Ring, B. Z., Ringwald, M., Rost, B., Ruan, Y., Salzberg, S. L., Sandelin, A., Schneider, C., Schonbach, C., Sekiguchi, K., Sempile, C. A., Seno, S., Sessa, L., Sheng, Y., Shibata, Y., Shimada, H., Shimada, K., Silva, D., Sinclair, B., Sperling, S., Stupka, E., Sugiura, K., Sultana, R., Takenaka, Y., Taki, K., Tammoja, K., Tan, S. L., Tang, S., Taylor, M. S., Tegner, J., Teichmann, S. A., Ueda, H. R., van Nimwegen, E., Verardo, R., Wei, C. L., Yagi, K., Yamanishi, H., Zabarovsky, E., Zhu, S., Zimmer, A., Hide, W., Bult, C., Grimmond, S. M., Teasdale, R. D., Liu, E. T., Brusica, V., Quackenbush, J., Wahlestedt, C., Mattick, J. S., Hume, D. A., Kai, C., Sasaki, D., Tomaru, Y., Fukuda, S., Kanamori-Katayama, M., Suzuki, M., Aoki, J., Arakawa, T., Iida, J., Imamura, K., Itoh, M., Kato, T., Kawaji, H., Kawagashira, N., Kawashima, T., Kojima, M., Kondo, S., Konno, H., Nakano, K., Ninomiya, N., Nishio, T., Okada, M., Plessy, C., Shibata, K., Shiraki, T., Suzuki, S., Tagami, M., Waki, K., Watahiki, A., Okamura-Oho, Y., Suzuki, H., Kawai, J. & Hayashizaki, Y. The transcriptional landscape of the mammalian genome. *Science (New York, N.Y.)* **309**, 1559-1563, doi:10.1126/science.1112014 (2005).
- 540 Mohammed, J., Siepel, A. & Lai, E. C. Diverse modes of evolutionary emergence and flux of conserved microRNA clusters. *RNA (New York, N.Y.)* **20**, 1850-1863, doi:10.1261/rna.046805.114 (2014).
- 541 Okamura, K., Phillips, M. D., Tyler, D. M., Duan, H., Chou, Y. T. & Lai, E. C. The regulatory activity of microRNA\* species has substantial influence on microRNA and 3'

- UTR evolution. *Nature structural & molecular biology* **15**, 354-363, doi:10.1038/nsmb.1409 (2008).
- 542 Lai, E. C., Wiel, C. & Rubin, G. M. Complementary miRNA pairs suggest a regulatory  
role for miRNA:miRNA duplexes. *RNA (New York, N.Y.)* **10**, 171-175 (2004).
- 543 Griffiths-Jones, S., Hui, J. H., Marco, A. & Ronshaugen, M. MicroRNA evolution by arm  
switching. *EMBO reports* **12**, 172-177, doi:10.1038/embor.2010.191 (2011).
- 544 Ruby, J. G., Stark, A., Johnston, W. K., Kellis, M., Bartel, D. P. & Lai, E. C. Evolution,  
biogenesis, expression, and target predictions of a substantially expanded set of *Drosophila*  
microRNAs. *Genome research* **17**, 1850-1864, doi:10.1101/gr.6597907 (2007).
- 545 Liu, N., Okamura, K., Tyler, D. M., Phillips, M. D., Chung, W. J. & Lai, E. C. The  
evolution and functional diversification of animal microRNA genes. *Cell research* **18**, 985-  
996, doi:10.1038/cr.2008.278 (2008).
- 546 Lai, E. C., Tomancak, P., Williams, R. W. & Rubin, G. M. Computational identification of  
*Drosophila* microRNA genes. *Genome biology* **4**, R42, doi:10.1186/gb-2003-4-7-r42  
(2003).
- 547 Friedlander, M. R., Lizano, E., Houben, A. J., Bezdan, D., Banez-Coronel, M., Kudla, G.,  
Mateu-Huertas, E., Kagerbauer, B., Gonzalez, J., Chen, K. C., LeProust, E. M., Marti, E.  
& Estivill, X. Evidence for the biogenesis of more than 1,000 novel human microRNAs.  
*Genome biology* **15**, R57, doi:10.1186/gb-2014-15-4-r57 (2014).
- 548 Kapranov, P., Cheng, J., Dike, S., Nix, D. A., Dutttagupta, R., Willingham, A. T., Stadler,  
P. F., Hertel, J., Hackermuller, J., Hofacker, I. L., Bell, I., Cheung, E., Drenkow, J.,  
Dumais, E., Patel, S., Helt, G., Ganesh, M., Ghosh, S., Piccolboni, A., Sementchenko, V.,  
Tammana, H. & Gingeras, T. R. RNA maps reveal new RNA classes and a possible  
function for pervasive transcription. *Science (New York, N.Y.)* **316**, 1484-1488,  
doi:10.1126/science.1138341 (2007).

**Vita**

Name: William Edward Putzbach

Place of Birth: Arlington Heights, IL

Date of Birth: December 23, 1989

Education:

<b>Northwestern University</b>	Chicago, IL
Ph.D. in Life Science, Cancer Biology cluster in Driskill Graduate Program	Sept 2012 to
Title of thesis:	June 2018
Toxicity Mediated by Seed-Dependent Off-Target Effects in RNA Interference	

<b>Benedictine University</b>	Lisle, IL
B.S., Biology	2008-2012

Research Experience:

<b>Northwestern University</b>	Chicago, IL
Graduate Student Researcher	2013 – 2018
Advisor: Marcus Peter, Ph.D.	

- Investigating novel mode of cancer cell death induced by RNAi through a novel type of seed-based off-target effect that selectively targets survival genes (referred to as Death Induced by Survival Gene Elimination or DISE)
- Investigating the existence of toxic siRNA sequences embedded in the CD95L mRNA transcripts
- Developed shRNA-based lethality lentiviral library
- Adapted protocol for generating knockout clones using CRISPR for lab

<b>Benedictine University</b>	Lisle, IL
Undergraduate Research Assistant	2011
Advisor: Niina Ronkainen, Ph.D.	

- Researching current trends in nanomaterial-based biosensors

<b>University of Tennessee</b>	Knoxville, TN
Undergraduate Research Assistant	2011
Advisor: Albrecht von Arnim, Ph.D.	

- Optimization of Bioluminescence Resonant Energy Transfer (BRET) in *Arabidopsis*
- Investigated the use of antioxidants to stabilize BRET substrate coelenterazine

### **Narchem Corporation**

Organic Synthesis Technician

Chicago, IL

2010

- Designing and carrying out custom bromine-based organic syntheses

Skills:

### **Molecular Biology**

- DNA isolation, RNA isolation, PCR, plasmid-based cloning, genomic and plasmid DNA isolation, qPCR, flow cytometry, fluorescent microscopy, design and construction of lentiviral-based shRNA pools, shRNA lethality screens

### **Genetics**

- Deletion of whole gene or gene segments using CRISPR, generation of protein KO clones using CRISPR

### **Biochemistry**

- Western blotting, recombinant protein expression/isolation from *E. coli*, *in vitro* actin binding assay, pull-down of Argonaute protein/small RNA complex

### **Cell Biology**

- Cell line maintenance for diverse cell types, lentivirus production, plasmid and siRNA transfection, lentivirus infection to deliver shRNAs or cDNAs, propidium iodide staining, sphere formation assay, immunofluorescence staining, cell culture drug treatments

### **Data Analysis**

- Statistics using R and SPSS software, basic bioinformatic script writing in R and Python, Gene Set Enrichment Analysis

Publications:

Murmann AE, Gao QQ, **Putzbach W**, Patel M, Bartom E, Law C, Bridgeman B, Chen S, McMahon KM, Thaxton CS, and Peter ME. Small interfering RNAs based on huntingtin trinucleotide repeats are highly toxic to cancer cells. *EMBO Reports*. 2018. In Press.

**Putzbach W**, Gao QQ, Patel M, Haluck-Kangas A, Murmann AE, and Marcus E. Peter ME. DISE: A seed-dependent RNAi off-Target effect that kills cancer cells. *Trends in Cancer*. 2017. In Press.

**Putzbach W**, Gao QQ, Patel M, van Dongen S, Haluck-Kangas A, Sarshad AA, Bartom ET, Kim KA, Scholtens DM, Hafner M, Zhao JC, Murmann AE, and Peter ME. Many si/shRNAs can kill cancer cells by targeting multiple survival genes through an off-target mechanism. *Elife*. 2017 Oct 24;6. pii: e29702. doi: 10.7554/eLife.29702.

Qadir AS, Ceppi P, Brockway S, Law C, Mu L, Khodarev NN, Kim J, Zhao JC, **Putzbach W**, Murmann AE, Chen Z, Chen W, Liu X, Salomon AR, Liu H, Weichselbaum RR, Yu J, Peter ME. CD95/Fas Increases Stemness in Cancer Cells by Inducing a STAT1-Dependent Type I Interferon Response. *Cell Rep*. 2017 Mar 7;18(10):2373-2386.

Peter ME, Hadji A, Murmann AE, Brockway S, **Putzbach W**, Pattanayak A, and Ceppi P. The role of CD95 and CD95 ligand in cancer. *Cell Death Differ*. 2015 Apr;22(4):549-559.

Werner ME, Mitchell JW, **Putzbach W**, Bacon E, Kim SK, and Mitchell BJ. Radial intercalation is regulated by the Par complex and the microtubule-stabilizing protein CLAMP/Spf1. *J Cell Biol*. 2014 Aug 4;206(3):367-376.

**Putzbach W** and Ronkainen NJ. Immobilization techniques in the fabrication of nanomaterial-based electrochemical biosensors: a review. *Sensors (Basel)*. 2013 Apr 11;13(4):4811-4840.